Optimization of the Design of Flexible Pavements with Unbound Bases Reinforced with Geogrids using APT

Subramanian Sankaranarayanan,
Jorge G. Zornberg, and
G. Hossein Roodi

https://library.ctr.utexas.edu/ctr-publications/0-6834-1.pdf

Technical Report Documentation Page

1. Report No. FHWA/TX-23/0-6834-1	2. Government Accession No.	3. Recipient's Catalog No.
4. Title and Subtitle Evaluation of the Performance of Geosynthetic-stabilized Unbound Bases using Accelerated Pavement Testing		5. Report Date August 2018
		6. Performing Organization Code
7. Author(s) Sankaranarayanan, Subramanian, Jorge G. Zornberg, and G. Hossein Roodi		8. Performing Organization Report No. 0-6834-1
9. Performing Organization Name and Address Center for Transportation Research The University of Texas at Austin 3925 W. Braker Lane, 4th floor Austin, TX 78759		10. Work Unit No. (TRAIS)
		11. Contract or Grant No. 0-6834
12. Sponsoring Agency Name and Address Texas Department of Transportation Research and Technology Implementation Division P.O. Box 5080 Austin, TX 78763-5080		13. Type of Report and Period Covered Technical Report September 2015 – August 2018
		14. Sponsoring Agency Code
15. Supplementary Notes Project performed in cooperation with the Texas Department of Transportation.		

16. Abstract

The design of flexible pavements with geosynthetic-stabilized unbound base layers is evaluated using accelerated pavement testing. The evaluation also assesses use of K_{SGI} as a parameter governing the performance of the pavement system. The major components of this project include: (i) Field monitoring of geosynthetic-stabilized and control pavement sections in relation to the long-term performance under traffic loads; (ii) Experimental evaluation of the performance of geogrid-reinforced pavement sections using reduced-scale Accelerated Pavement Testing (APT) program; and (iii) Development of tools for the design of geosynthetic-stabilized pavements (GSPs).

17. Key Words Geosynthetics, geogrids, stabilization, flexible pavements, accelerated pavement testing, unbound base		18. Distribution Statement No restrictions. This document is available to the public through the National Technical Information Service, Springfield, Virginia 22161; www.ntis.gov.	
19. Security Classif. (of report) Unclassified	20. Security Classif. (of this page) Unclassified	21. No. of pages TBD	22. Price

Form DOT F 1700.7 (8-72) Reproduction of completed page authorized

THE UNIVERSITY OF TEXAS AT AUSTIN
CENTER FOR TRANSPORTATION RESEARCH

Evaluation of the Performance of Geosynthetic-stabilized Unbound Bases using Accelerated Pavement Testing

Sankaranarayanan, Subramanian,
Jorge G. Zornberg, and
G. Hossein Roodi

Center for Transportation Research
The University of Texas at Austin
3925 W. Braker Lane, 4th Floor
Austin, TX 78759

http://ctr.utexas.edu/

Disclaimers

Author's Disclaimer: The contents of this report reflect the views of the authors, who are responsible for the facts and the accuracy of the data presented herein. The contents do not necessarily reflect the official view or policies of the Federal Highway Administration or the Texas Department of Transportation (TxDOT). This report does not constitute a standard, specification, or regulation.

Patent Disclaimer: There was no invention or discovery conceived or first actually reduced to practice in the course of or under this contract, including any art, method, process, machine manufacture, design or composition of matter, or any new useful improvement thereof, or any variety of plant, which is or may be patentable under the patent laws of the United States of America or any foreign country.

Engineering Disclaimer

NOT INTENDED FOR CONSTRUCTION, BIDDING, OR PERMIT PURPOSES.

Project Engineer: Jorge G. Zornberg, Ph.D., P.E., F.ASCE
Professional Engineer License State and Number: California No. C 056325
P.E. Designation: Research Supervisor

TABLE OF CONTENTS

LIST OF FIGURES

LIST OF TABLES

1. INTRODUCTION

1.1 BACKGROUND

Geogrids have long been used by Department of Transportations (DOTs) within the base or as a subgrade/base interface layer as a means for enhancing the performance of flexible and rigid pavements. The enhancement in performance of the pavements is often observed under both traffic and environmental loading. While there has been significant use, particularly in Texas, of geogrid-reinforced pavements (GRPs), limited research has dealt with methodologies of quantifying their influence on pavement performance. The current design method for flexible pavements, adopted by the Texas Department of Transportation (TxDOT), which is compiled in FPS-21, does not accommodate the presence of geogrid reinforcement layers within the base. Thus, a comprehensive design method that accommodates geogrid-reinforced base layers, will result in significant benefits to TxDOT.

Further, the proliferation of geogrid products and aggressive marketing from manufacturers has made the selection of geogrids (amongst the variety of products available in the market) to be used in GRPs a difficult process. Geogrid reinforcements, traditionally nationwide, are often selected based on manufacturer's recommendations without a validated test method to evaluate the efficiency of the reinforcements for different conditions and designs. Specification established by DOTs, nationwide, to select geogrids involves the conventional characteristics of geosynthetics which are treated in isolation (i.e., without involvement of surrounding soil) or for failure conditions (i.e., large displacements). However, in the case of pavements, large deformations are not allowed, and the pavement is declared to have failed under such deformations. Thus, the performance of GRPs is governed by interaction between the geogrid and the surrounding soil under small displacements which is the focus of TxDOT projects 0-4829 and 5-4829. The index parameter developed, K_{SGC} addresses the in-soil performance of geogrids under small displacements. Project 5-4829 provided clear evidence that the index K_{SGC} is positively correlated to the performance of GRPs under environmental loading. Further validation of this evidence needs to be conducted under traffic loading, to establish the geogrid selection guideline based on actual mechanisms involved in geogrid-reinforced base-layers.

This project TxDOT 0-6834 addresses the design of flexible pavements with geogrid-reinforced base-layer and the validation of the use of K_{SGC} as the geogrid selection index parameter. The project consists of three major components.

  i. Field monitoring of geogrid-reinforced and control pavement sections in relation to the long-term performance under traffic loads.
 ii. Experimental evaluation of the performance of geogrid-reinforced pavement sections using reduced-scale Accelerated Pavement Testing (APT) program.
iii. Development of tools for the design of geogrid-reinforced pavements (GRPs).

1.2 ROLE OF GEOGRIDS WITHIN BASE IN FLEXIBLE PAVEMENTS

The stresses experienced within a flexible pavement structure has primarily two origins: (a) traffic induced stresses, and (ii) environment induced stresses. The stresses induced by traffic are cyclic in nature and act over a short duration. For simplicity, traffic loads are modelled as static vertical circular loads on the surface of the pavement. The associated induced stress in the pavement is expected to reduce in intensity with the depth of the pavement. Further, the repeated traffic loading causes accumulation of strains in the pavement leading to its permanent deformation. There are

three critical points of stress within the pavement. Kerkhoven and Dormon (1953) first suggested the use of vertical compressive strain on the surface of subgrade as a failure criterion to reduce permanent deformation; Saal and Pell (1960) recommended the use of horizontal tensile strain at the bottom of the asphalt layer to minimize fatigue cracking. The use of vertical compressive strain to control permanent deformation is because plastic strains after N cycles of loading are proportional to elastic strains in paving materials (the basis of transfer functions in MEPDG analysis). Thus, by limiting the elastic strains on top of the subgrade, and in other layers above the subgrade, the magnitude of permanent deformation on the pavement surface can be controlled. If the subgrade is weak and unable to resist this load, the top layers of pavement need to be made stiffer. The strategy adopted would be to strengthen the top layer to minimize the stress transferred to the bottom. This can be achieved by replacing the top layer materials with ones that have a higher modulus or by increasing the thickness of the top layers. Both these approaches result in more expensive designs. In such a case, the geogrid can be used as an additional reinforcement material to resist these loads and prevent growth of interface shear stresses, without having to replace the materials or increase their thickness.

The stresses from environmental factors are due to variation of temperature and moisture in the various layers of the pavements. While temperature changes affect the HMA layers, moisture changes affect the response of the aggregate layers, specifically the subgrade. The seasonal variation of temperature and rainfall at a site can lead to a change in subgrade moisture. Further, the edges of the pavement are prone to moisture variation as compared to the center of the pavement, which tends to remain at constant moisture or as compacted moisture level. If the subgrade below the pavement is expansive in nature, the soil would shrink and swell with the moisture variation causing additional stress on the pavement surface. The primary result of this moisture variation below the pavement is the formation of longitudinal cracks that are found predominantly on the edges of the pavement. To remedy this situation, some measures that have been suggested are lime or cement treatment of the soil, construction of trenches along the edge of pavement, and providing proper drainage to avoid ponding of the rainwater. Recently, geosynthetics have been also used successfully to prevent the propagation of the micro cracks upward from the subgrade.

1.3   RESEARCH OBJECTIVES

The specific objectives of this study are to:

- Conduct a comprehensive review of literature in relation to geosynthetics in pavement systems, APTs, instrumentation in flexible pavements and design guidelines on flexible pavement systems.
- Evaluate the long-term performance of reinforced and control sections under traffic loads in the field and quantify the benefits of reinforced base-layers in flexible pavements.
- Perform reduced-scale APT of control and geogrid-reinforced pavements under various testing conditions.
- Evaluate the performance of geogrid-reinforced pavements under the reduced-scale APTs and quantify the benefits of using geogrids under various conditions.
- Translate the findings of this research into design tools and approaches to the design of flexible pavements with geogrid-reinforced base-layers.
- Validate the use of the index K_{SGI} as the geogrid selection criterion for GRPs.
- Develop a full-scale APT program to establish the design tools for the design of GRPs.

2. BACKGROUND

Base reinforcement results from the addition of a geogrid at the bottom or within a base course to increase the structural or load-carrying capacity of a pavement system. While there is clear evidence that geosynthetic reinforcements can lead to improved pavement performance, the identification and quantification of the parameters that contribute to such improvement has remained, at best, unclear. In addition, pavement structures deteriorate under the combined effects of traffic loading and environmental conditions. The effect of environmental changes, especially in locations with expansive clays, has been studied in detail in earlier TxDOT Projects (0-4829 and 5-4829). Consequently, this research focuses on the benefits of using geogrids on the pavement structural response under traffic loads. To fully understand the significance of the research, an overview is provided herein on key components of this study: (i) Geogrids, (ii) Mechanisms of Geogrid-reinforcements in pavements, (iii) Specification and Design Procedures of GRPs, (iv) Recent TxDOT Projects on GRPs, (v) APT of GRPs. Then, the problems encountered when designing these pavements under current specifications are addressed.

2.1 GEOGRIDS

Geosynthetics can be defined as planar products manufactured from polymeric material, which are used with soil, rock, or other geotechnical engineering related material as an integral part of a man-made project, structure, or system (ASTM 1995). Geosynthetics are widely used in many geotechnical and transportation applications. The geosynthetics market is strong and rapidly increasing due to the continued use of geosynthetics in well-established applications and particularly, due to the increasing number of new applications which make use of these products.

Geogrids constitute a category of geosynthetic materials that have an open grid-like appearance (Figure 2.1). These products are distinguished by the regular network of tensile elements that form openings that are large enough to interlock with the surrounding soil matrix.

Figure 2.1 Various types of Geogrids: (a) Homogenous; (b) Coated Yarn; (c) Welded

Geogrids are categorized by three different manufacturing processes.

2.1.1 PUNCHED AND DRAWN GEOGRIDS

"Punched and Drawn" (or "Extruded" or "Homogenous" or "Unitized") geogrids are manufactured by punching out holes in polymer sheets on a regular grid pattern and then heat and stretch them in one or two directions (Figure 2.1a).
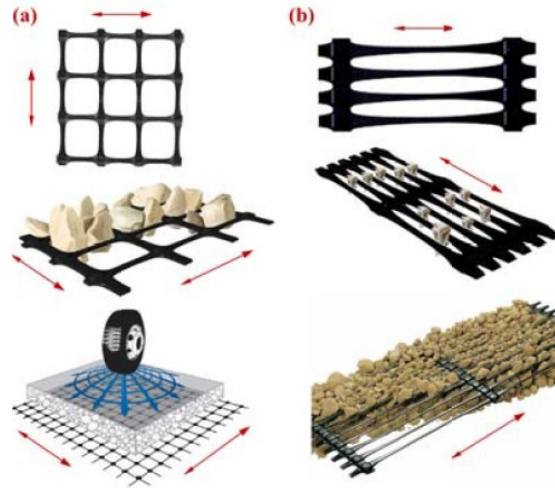
Figure 2.2 (a) Biaxial Geogrids; (b) Uniaxial Geogrids

2.1.2 WOVEN GEOGRIDS

"Woven" (or "Knitted" or "Coated Yarn") geogrids are manufactured by weaving polymer yarns into transverse or longitudinal ribs with large open spaces in between. The junctions are linking by knitting or intertwining of the crossed-over yarns. To provide additional protection, the entire unit is coated with PVC, latex, or Bitumen material (Figure 2.1b).

2.1.3 BONDED GEOGRIDS

"Bonded" (or "Welded" or "Rod" or "Strap") geogrids are manufactured by bonding mutually perpendicular rods or straps in a grid-like pattern. The junctions are bonded by laser or ultrasonic welding (Figure 2.1c)

Geogrids are composed of "Longitudinal" and Transverse" ribs with the opening between the adjacent ribs which are called "Apertures." The key feature for the effectiveness of geogrids is that the apertures should be large enough to allow for the soil to be interlocked from one side of the geogrid to the other side, thereby increasing the interaction between the geogrid and the surround soil. As illustrated in Figure 2.2, geogrids are often manufactured in two forms: "Uniaxially Oriented" or "Biaxially Oriented". Uniaxial geogrids are mainly used for wall and slope reinforcement where the direction of major principal stress is known. On the other hand, biaxial geogrids are used in the areas where direction of the major principal stress is unknown, such as pavement, base, and foundation reinforcement. A more recent group of geogrid product features triangular apertures intended to provide more effective stress distribution. This group is referred as "Triaxial Geogrids"

2.2 MECHANISMS IN GEOGRID-REINFORCED PAVEMENTS

Over the past decades, geogrids have found numerous applications in transportation projects (Zornberg and Christopher, 2000). Their cast applications have been expanded from the improvement of the foundation of unpaved roads founded on weak subgrades, to the enhancement of the performance of low to moderate volume road with thin asphalt layer, to reducing the base course rutting and improving the fatigue performance of the surface layer in flexible airport pavements, and to balancing differential settlement and heaving in roads founded on expansive subgrades induced by environmental conditions.

Application of geogrids for unbound base course reinforcement involves addition of geogrid layer at the bottom or within a base course to increase the structural or load-carrying capacity of a pavement system by the transfer of load to the geosynthetic material. The mechanisms by which geosynthetics provide reinforcement include the following.

2.2.1 LATERAL RESTRAINT

Lateral restraint or confinement is a pavement reinforcement mechanism, the components of which can include: (i) restrain of lateral movement of base, or subbase, aggregate (confinement); (ii) increase in modulus of base aggregate due to confinement; (iii) improved vertical stress distribution on subgrade due to increased base modulus; and (iv) reduced shear strain along the top of the subgrade (Bender and Barenberg 1978)
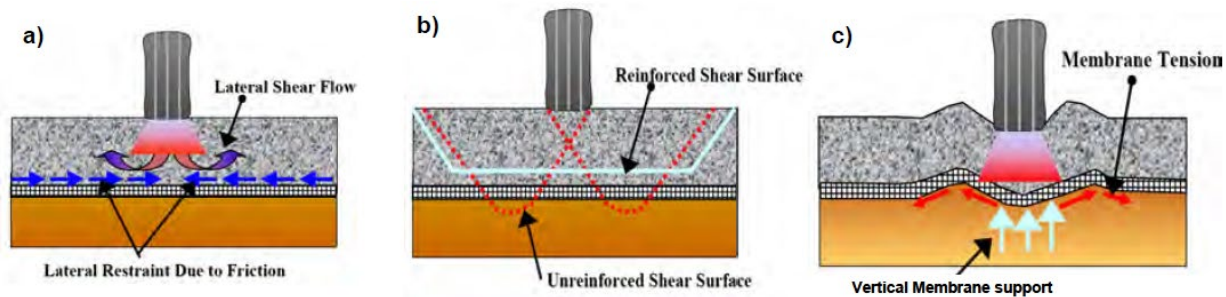
Figure 2.3 Reinforcement Mechanisms induced by geosynthetics (Holtz et al. 1998): (a) Lateral Restraint; (b) Increased Bearing Capacity; (c) Membrane support

2.2.2 INCREASE IN SUBGRADE BEARING CAPACITY

As illustrated in Figure 2.3 b, the increased bearing capacity mechanism leads to layer reinforcement when the presence of a geosynthetic imposes the development of an alternate failure surface. This new alternate plane provides higher bearing capacity. The geosynthetic reinforcement can decrease the shear stresses transferred to the subgrade and provide vertical confinement outside the loaded area. The bearing failure mode of the subgrade is expected to change from punching failure without reinforcement to general failure with reinforcement.

2.2.3 TENSILE MEMBRANE SUPPORT

The geosynthetic can also be assumed to act as a tensioned membrane, which supports the wheel loads (Figure 2.3c). In this case, the reinforcement provides a vertical reaction component to the applied wheel load. This tensioned-membrane effect is induced by vertical deformations, leading to a concave shape in the geosynthetic. The tension developed in the geosynthetic contributes to support the wheel load and reduces the vertical stress on the subgrade. However, significant deformations are necessary to realize this effect.

The aforementioned mechanisms required different magnitudes of deformation in the pavement system to be mobilized. The "increased bearing capacity" and "tensioned membrane support" mechanisms would be activated when significant rutting is allowed (e.g., in unpaved roads). For the case of surfaced pavements, "lateral restraint," which can be mobilized in relatively smaller deformations, is considered to contribute the most to the improved performance of geosynthetic-reinforced pavements.

2.3 SPECIFICATIONS AND DESIGN PROCEDURES OF GRPS

Geosynthetics have numerous material properties with many of them being important in the manufacture and quality control of geosynthetics, and many others being important in engineering design. The material properties related to the manufacturing and quality control of geosynthetics are generally referred to as index properties and those related to the design as design or performance properties (Zornberg and Christopher 2007). Studies have aimed at establishing correlations between geogrid properties and their field performance. These properties included the rib strength, junction strength, aperture size, wide-width tensile strength, tensile modulus, tensile strength at 2% and 5%, and flexural rigidity (e.g., Christopher et al. (2008)). While almost all these properties are determined in isolated condition (i.e., without involvement of surrounding soil), numerous studies have concluded that the actual performance of geogrid reinforced systems should be determined by the interaction between the geogrid and the surrounding soil (Archer and Wayne 2012). Specifically, the performance of the geogrid-reinforced pavements is governed by the soil-geosynthetic interface properties under small displacements, which is not considered in any of the conventional geosynthetic testing. However, the current state of the practice of most of the DOTs including TxDOT is to select the geogrid reinforcement based on conventional index or performance properties. For example, TxDOT DMS-6420 specifications for geogrid products include both index properties (e.g., aperture size, % open area) and performance properties (e.g., Tensile modulus, junction efficiency, ultimate strength in machine and cross-machine direction). However, TxDOT Project 5-4829 has identified the new parameter as K_{SGI} which allows characterization of soil-geosynthetic interaction under confined (in-soil) conditions.

Table 2.1 Current state of practice for design of geogrid base-reinforced pavements using improvement ratios

Design for extension of performance periods (The pavement geometry does not differ from the unreinforced construction option.)	Design with a TBR	$(W_{18})_R = W_{18} \times TBR$ $(Years\ before\ rehabilitation)_R = \dfrac{(W_{18})_R}{ESALs\,/\,Year}$
	Design with an LCR (not recommended)	$(SN)_R = a_1 D_1 + LCR \times a_2 D_2 + a_3 D_3$ With base course thickness (D_2) held constant, SN increases with which leads to an extended service life of the pavement comparing to the unreinforced option.
Design for reduction of aggregate base thickness (The performance period does not differ from the unreinforced construction option)	Design with a BCR ratio	$(D_2)_R = (D_2)_{Unreinf} \times (1 - BCR)$ (without subsase)
	Design with a TBR	$(W_{18})_R = W_{18} \times TBR$ Then find adjusted structural number $((SN)_R)$ using $(W_{18})_R$. $(D_2)_R = \dfrac{(SN)_R - a_1 D_1}{a_2}$
	Design with an LCR	$(D_2)_R = \dfrac{SN - a_1 D_1 - a_3 D_3}{LCR \times a_2}$
Design for combination of some extension of performance period and some reduction of aggregate base thickness.		1) Select a base course thickness greater than $(D_2)_R$ and less than (D_2) 2) Use the selected base course thickness to find the performance period which is something between reinforced and unreinforced case

2.3.1 IMPROVEMENT RATIOS

The current state of practice for design of unbound geosynthetic reinforced pavements is modifying the design of unreinforced pavement by applying modification factors. To do this, the pavement is designed according to the well-known AASHTO 1993 empirical design guide assuming no reinforcement exist. Then, the improvement to the pavement system provided by geosynthetic reinforcement is taken into account by the following improvement ratios:

2.3.1.1 Traffic Benefit Ratio (TBR)

A ratio of the number of load cycles on a reinforced section to reach a defined failure state to the number of load cycles on an unreinforced section, with the same geometry and material constituents, to each the same defined failure state. TBE is sometimes termed Traffic Improvement Factor (TIF).

2.3.1.2 Base Course Reduction (BCR)

The percent reduction in the reinforced base, or subbase, thickness from the unreinforced thickness, with the same material constituents, to each the same defined failure state in the same number of load cycles.

2.3.1.3 Layer Coefficient Ratio (LCR)

A modifier applied to the layer coefficient of the aggregate. This value is back calculated, based upon the number of load cycles on a reinforced section to reach a defined failure state to the number of load cycles on an unreinforced section, with the same geometry, to reach the same defined failure state.

Table 2.1 summarizes the design approaches based on the improvement ratios.

To this date, a generally accepted mechanistic-empirical approach for design of geosynthetic base-reinforced pavements has not been established. A major attempt made by Perkins et al. (2009) to develop a mechanistic-empirical model for geosynthetic base-reinforced flexible pavement is based upon the models and procedures developed in NCHRP Project 1-37A for unreinforced pavements. However, in their model Perkins et al. (2009) introduced several new components associated with reinforcements which require further validations.

2.3.2 TEXAS FLEXIBLE PAVEMENT (DESIGN) SYSTEM (FPS-21)

FPS-21 is a software program developed to run on the Windows operating system for the design of flexible pavements by TxDOT (Liu and Scullion, 2001). It incorporates a full linear elastic analysis package to compute stress and strains and deflections in pavement structures. As such it is similar to other software packages such as CHEVRON, ELSYM5 and BISAR but has been simplified to address specific structures as used in Texas comprising asphalt concrete pavement, granular flexible base, asphalt stabilized base/subbase, subgrade layers and used defined pavement layers. It also provides a module for the design of asphalt overlays.

Pavement structures are designed as multiple linear elastic layers defined in terms of Young's modulus and Poisson's ratio. A total thickness criterion is used to allocate thicknesses to the individual layers making up the structure to satisfy design criteria in terms of allowable maximum horizontal tensile stress beneath the asphalt layer (to prevent fatigue cracking) and allowable maximum vertical compressive stress on top of the subgrade (to prevent permanent deformation). Results of Texas Triaxial tests are also used to negate shear failure in the subgrade layer. In addition to the mechanistic functions, FPS21 incorporates basic life cycle cost and performance prediction algorithms.

Heavily stabilized bases cannot be designed with the current versions FPS21, primarily because of the non-linear failure mechanisms associated with these types of structures. Geogrid-reinforced base layers can also not be modeled in FPS21 primarily owing to the complex behavior of the soil-geosynthetic composite.

2.4 TxDOT Projects on GRPs

Comprehensive studies on the evaluation of geogrid-reinforced pavements in Texas have been conducted as a part of TxDOT Projects No. 0-4829 and 5-4829. The primary purpose of these projects was to provide insight into the controversial issue of pavement performance enhancement using geosynthetic reinforcements. In the field study part of Project 0-4829, which has been considered as the largest long-term field-testing program in the United States, 32 test sections were constructed in FM2 road, Grimes County, TX, USA (Figure 2.4)

Figure 2.4 FM2 field study conducted by UT Austin

Three different types of geosynthetics (2 geogrids and 1 geotextile) were used to reinforce the base of the road. The performance of the reinforced sections under actual traffic and environmental conditions was compared to the performance of control sections, which were constructed without reinforcement. The comparison was based on a comprehensive monitoring program over the course of 7 years (Jan 2006 to Dec 2012) performed by the University of Texas at Austin with collaboration of TxDOT.

The monitoring program included (1) Performing nondestructive tests including Rolling Dynamic Deflectometer (RDD) and Falling Weight Deflectometer (FWD) to evaluate changes in the mechanical properties of pavements layers; (2) Installing moisture sensors in horizontal and vertical arrays to study the moisture migration pattern under the pavement; (3) Monitoring environmental conditions including precipitation, humidity and temperature; and (4) Periodic condition surveys to identify and quantify the distresses involved in sections and determine pavement surface condition.

The final evaluation of the performance of the test sections was presented in the closing report of the project, which was submitted to TxDOT in Feb 2013. In the final report, the results of the 20 condition surveys were used to evaluate the performance of geogrid-reinforced sections in mitigation of environmentally induced longitudinal cracks. Seasonal change in the moisture content of the expansive subgrade, which is induced by cycles of wet and dry seasons in the area, leads to cycles of swelling and shrinkage of the subgrade soil and develops deep longitudinal cracking in the road.
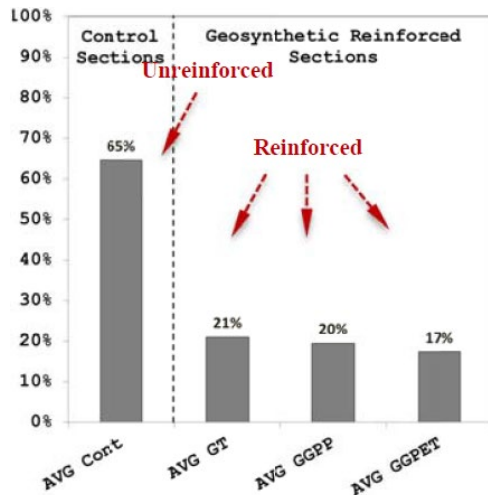
Figure 2.5 Performance of FM2 sections at the end
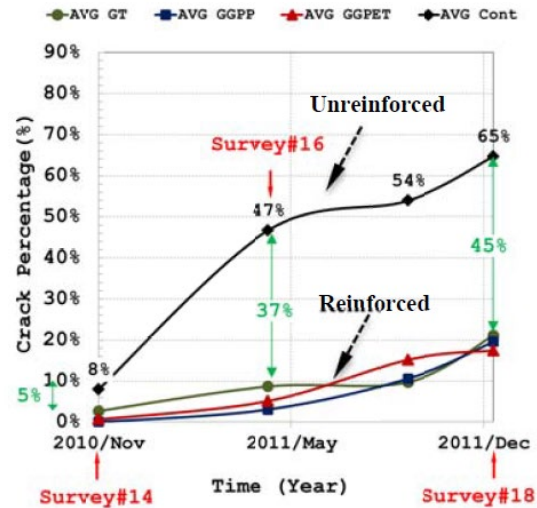
Figure 2.6 Performance of FM2 sections over time

Figure 2.5 presents the final performance of the test sections at the end of Project 5-4829. The horizontal axis of this chart represents various groups of test sections, and the vertical axis shows the percentage of longitudinal cracks length as compared to the total length of the sections in each group. As seen in this figure, all geosynthetic-reinforced test sections show a significantly lower percentage of cracking than the control sections. The average percentage crack was 17% and 20% for the geogrid reinforced sections GG PET and GG PP, respectively, and was 21% for the geotextile reinforced sections GT. However, the average percentage crack for the control sections was 65%.
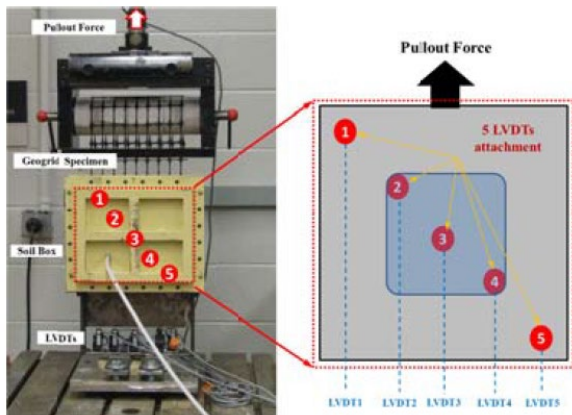
Figure 2.7 The SGI Test device developed at UT Austin
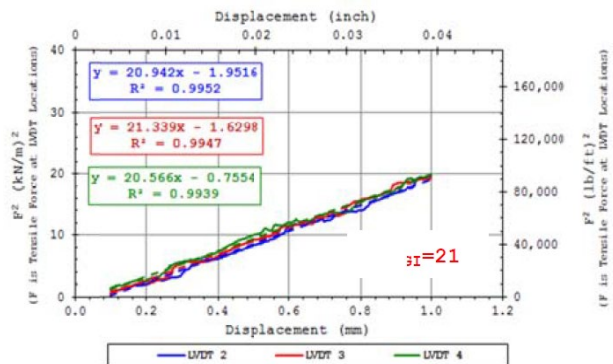
Figure 2.8 Sample results obtained from the SGI test to identify KSGI

The results of the condition surveys were also compiled to compare the performance of the test sections over time. Figure 2.6 compares the percentage of cracking from Survey #14 to #18. This figure emphasized that all geosynthetic reinforced sections indubitably improved the performance of the road. The three types of geosynthetics, i.e., GG PET, GG PP, and GT, show every similar performance over the lifetime of the project, whereas the control sections clearly show consistently a higher percentage of cracking.

9
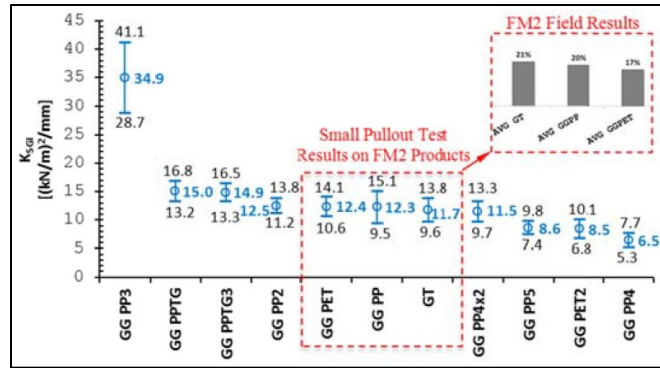
Figure 2.9 SGI Test Vs. FM2 Results

As part of Project 0-4829, a new testing technique, referred to as the "Soil-Geosynthetic Interaction Test (SGI Test)" was developed at the University of Texas at Austin (Figure 2.7). The main purpose of the SGI test is the characterization of the confined stiffness in geosynthetic reinforcements. Most of the parameters used in the design of geosynthetic reinforced systems consider the characterization of the ultimate failure; and/or they are obtained under unconfined conditions. However, the actual performance of pavement reinforced systems is governed by the interaction between the surrounding soil and the geogrid under small-displacement conditions. The SGI test quantifies the stiffness of the soil-reinforcement interface under low strains, referred to as K_{SGI}, which is a pertinent property for evaluating the confined performance of geosynthetic products in base-reinforced pavements. As shown in Figure 2.8, K_{SGI} is defined as the slope of the Unit Tension Square vs. Displacement (F_2-w) curve obtained from SGI test results. A recommendation has been made for developing this test procedure as an ASTM standard because of its ability to characterize the soil-geosynthetic interaction under small displacements.

Under Project 5-4829, a comprehensive study was conducted to verify the repeatability of the results of the small pullout test and to correspond the results to the in-situ performance of the geogrids in the field. To achieve this objective, 11 different geosynthetic products, including those geosynthetics used in the FM2 field experiment, were tested in the SGI test. Over 5 repeat tests were performed for each geosynthetic products, and the K_{SGI} results were analyzed. As shown in Figure 2.9, the results proved to be reasonably reliable with 95 percent of confidence interval in classifying the geosynthetic products. In addition, for the geosynthetic products used in FM2, the obtained small pullout test results show a surprising consistency with the observed performance in the field. (Compare field results versus lab results for GG PET, GG PP, and GT in Figure 2.9).

Additional field test sections are currently being monitored to further validate the SGI test result predictions. These sections include (1) two geogrid sections and four control sections in FM1644, Robertson County, (2) 5.6 miles of geogrid reinforced sections on State Highway (SH21) north of Highway 290, and (3) eight geogrid/geotextile-reinforced sections in SH21 south of Highway 290.

In addition, significant experimental studies have been conducted across the US and worldwide on the performance of geogrid reinforced pavements. Among the most important ones are the studies conducted by US Army Corp of Engineers, Arkansas DOT, Pennsylvania State University, and the research programs performed in Norway, Germany, and Brazil. However, to this date there is no generally accepted design procedure to account for the contribution of geogrids in performance of the flexible pavements.

2.5 USE OF APTS TO EVALUATE THE PERFORMANCE OF GRPS

2.5.1 ACCELERATED PAVEMENT TESTING (APT)

APT is defined as the controlled application of wheel loading to pavements structures for simulating the effects of long-term in-service loading conditions in a compressed time period. A large volume of knowledge exists globally in the field of APT that has been systematically and concisely synthetized in three studies by Metcalf (1996), Hugo (2004) and Steyn (2012) spanning work done in this field over the last 40 years. As shown in Figure 2.10, APT is one of several different disciplines used in pavement engineering to understand the response of pavement structure and materials to traffic loading and the environment. APT serves to bridge the knowledge gap between laboratory testing and pavement performance studies.
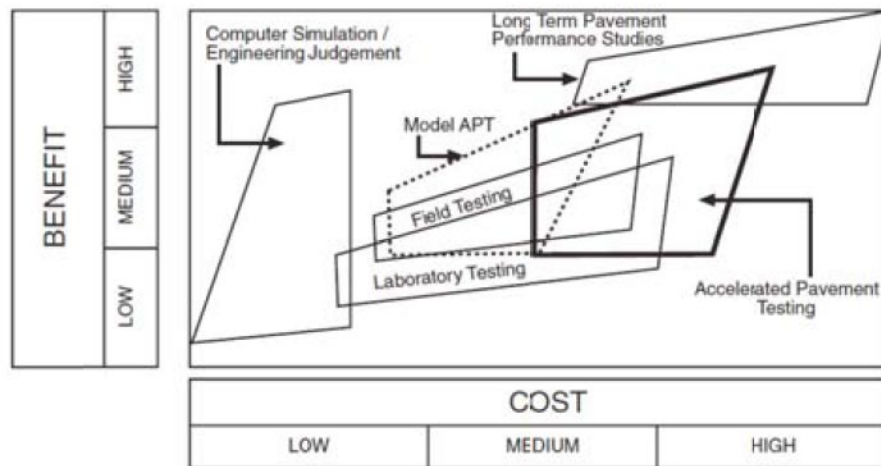
Figure 2.10 Benefit derived from pavement engineering knowledge vs. cost

Ultimately long-term pavement performance studies (LTPP) provide performance of real pavements under real traffic and climate conditions but are cost prohibitive, require many years of data collection and are often difficult to interpret give the very large number of influence factors impacting performance over time. APT testing done under controlled loading and environmental conditions provides a better understanding of the mechanisms influencing the performance of pavements but at a cost. A number of DOTs in the US and abroad sponsor APT programs and the major emphasis in recent years has been justifying this cost against expected benefits. As Steyn (2012) indicates, researchers are now forced to prove the benefit of their research and identify, analyze, and quantify the direct and indirect benefits obtained from full-scale APT. The majority of ongoing programs are still only conducting benefit-cost ratio (BCR) analyses after the research has been completed. Estimates of BCRs from Steyn's survey respondents ranged broadly between 1.4 and 11.6, with some as high as and greater than 30. The model mobile load simulator (MMLS), shown in Figure 2.11, was developed specifically to maximize the cost benefit ratio of APT studies. It is a scaled down version that is inexpensive to maintain and operate and provides a number of advantages over full-scale testing. The use of scaled APT compared to full-scale APT is more prevalent throughout the US and abroad with as many as 21 MMLS devices in operation by DOTs and research organizations worldwide. Two aspects are critical in the evaluation of MMLS tests. First it is important to recognize that small scale testing of pavement structure and materials provides an alternative means for preliminary indicator or ranking tests prior to, or in place of expensive full-scale APT. Second, in order to carry out scaled tests effectively, dimensional

analysis considerations need to be met. This requires that the laws of similitude be observed. In particular, scaled down pavement layers need to be subjected to the same stresses and strains as the full-scale pavement under equivalent loading and environmental conditions. Moreover, the materials properties of the scaled-down layer must be equivalent to the full-scale materials.

Figure 2.11 MMLS at UT Austin

The immediate benefit of scaled APT using MMLS3 is that testing can be done at a fraction of the cost of full-scale APT. Moreover, testing can be done on laboratory scale under controlled environmental and testing conditions. This allows many of the variables impacting pavement systems to be controlled directly such as base moisture content and trafficking load and speed. These factors have a direct influence on the stiffness of the base layers and hence the response of the materials and layers under loading. Controlling these variables eliminates uncertainties often associated with the development of APT performance models, typically exacerbated under full-scale conditions. In the development of APT performance models, a significant number of performance tests are required to evaluate impact factors, and this has necessitated finding means whereby it would be possible to expedite the testing of the different variables prior to conducting full-scale APT. Accelerated testing on laboratory scale is favored as a cost efficient, yet effective means of doing this.

2.5.2 SCALING CONSIDERATIONS

Scaled prototype studies of large civil engineering problems are widely used and accepted as a sound and cost-efficient solution. In fact, the same scaling laws applied to structural and hydrology engineering are applied to the scaling of pavement structures. The theory is simple. If one assumes an elastic pavement response, then the fundamental principle underlying model testing is that a pavement's structural composition, when scaled down, is subject to the same stresses and strains as a full-scale pavement under equivalent loading and assuming the same material properties i.e., modulus and Poisson's ratio. The scaling factor is then calculated as the square root of the ratio of the full-scale loading force to the scaled loading forced provided the load contact pressure of the scaled-down vehicle is the same as the full-scale vehicle. Under these conditions the rate of loading is negated, and the laws of similitude dictate that all physical dimensions be scaled by the appropriate scaling factor. Figure 2.12 illustrates these concepts by comparing a full-scale and

scaled down pavement structure subjected to full-scale and reduced scale loading. A scaling factor of N is applied.

Applying laws of similitude, it can easily be shown that stresses and strain within the full-scale and scaled down pavements shown in Figure 2.12 are identical. The MMLS repeatedly applied a single wheel load to a scaled down pavement structure. The wheel load in the MMLS is in the order of 2.5 kN (560 lbf.). This may be compared to either a super-single or dual tire wheel load of 9000 lbf being one-half of a standard axle wheel load i.e., 18 kips. This translates to a scaling factor of 4. In effect therefore, an 18-inch base layer may be scaled down to a thickness of 4.5 inches in a scaled pavement when using the MMLS. It should be noted that although scaling of the structure is required to ensure response equivalency, scaling of materials is not required if the dimensions of the materials do not influence the structural response in terms of compaction, densification under traffic, etc.
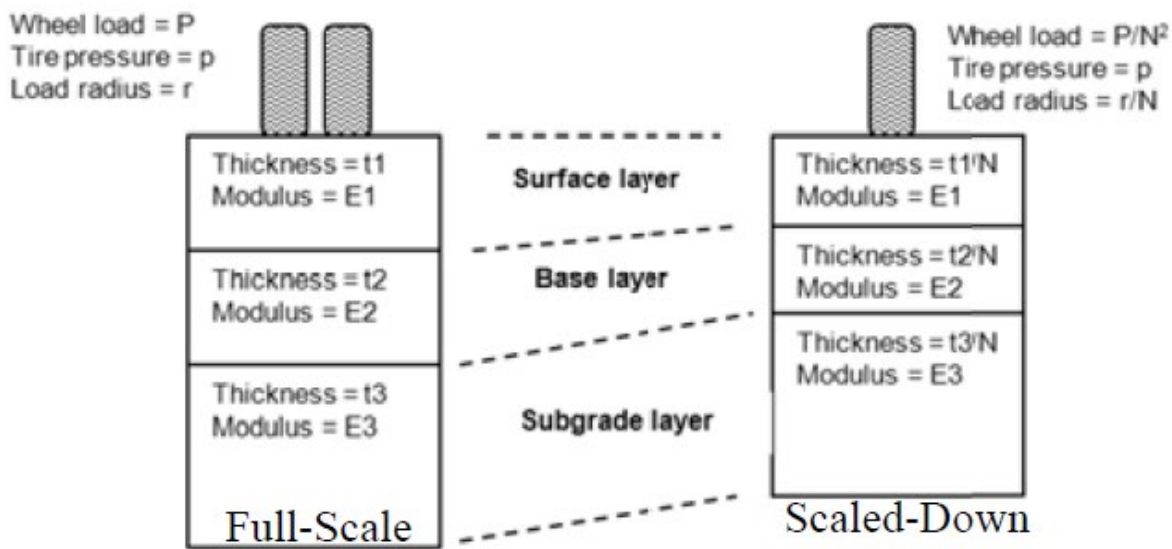
Figure 2.12 Full-scale and scaled-down pavement structure equivalency

Scaling down technique proved particularly effective when compared to full-scale performance data. For example, TxDOT has sponsored three main MMLS projects performed in Jacksboro TX, WesTrack NV and in NCAT Test Track. The focus of these projects was to establish and validate the predictive capability of the MMLS in reliably predicting rutting performance of pavement sections.

3. LITERATURE REVIEW

A comprehensive literature survey of all domestic and foreign literatures on geosynthetic-reinforced pavement systems and accelerated pavement testing is completed as a part of this project. The project demanded the understanding of accelerated pavement testing methods, scaling down of pavements sections for controlled laboratory testing, index (and interface) properties of the geosynthetics (with the soil) relevant to the reinforcement of unbound bases, the mechanisms associated with the reinforcement of soil with geogrids and the types of sensors needed to measure the relevant data from a scaled-down reinforced pavement section trafficked using an accelerated vehicle simulator (such as MMLS3). The multi-disciplinary nature of the study needed a thorough literature review of the various fields involved to get an overall picture of where the current research stands, in the various fields. This allowed the research to have a comprehensive approach to ratifying the existing ideas, identifying the areas that need further research and developing a more integral solution to the problem. The literature review done in this task aided in learning and building up from the previous work in the various areas. The following objectives are met as part of the technical literature review for this project.

- Collection, review, and assessment of relevant domestic and foreign literature on geosynthetic-reinforced pavement systems, with emphasis on the experimental, field validation and design components.
- Analyses of the field performance data from geosynthetic-reinforced pavements constructed in Texas and verification of any relevant proposed reinforcement mechanisms.
- Compilation of APT data from relevant unreinforced and geosynthetic-reinforced pavements studies and identification of any relevant strategies to use APT programs to evaluate the performance of GRPs.
- Identification of relevant results from the small pull-out box testing program.

3.1 GEOSYNTHETICS IN PAVEMENT SYSTEMS

There are different types of geosynthetics (geo-membranes, geo-cells, geo-nets, etc.) specializing in different functions (separation, filtration, drainage, etc.). One of the chief functions of geosynthetics is providing reinforcement. The geosynthetics that specialize in reinforcement are of three types namely, geogrids, geocells and geotextiles. Of these, the geosynthetics that are chiefly used for reinforcing unbound base course in pavement structures are geogrids. Geogrids constitute a category of geosynthetic materials that have an open grid-like appearance forming a regular network of tensile elements that form large enough openings to interlock with the surrounding soil matrix.

3.1.1 HISTORICAL EVOLUTION OF THE USE OF GEOSYNTHETICS IN PAVEMENTS

The research on the use of reinforcements in asphalt concrete dates to the 1950's. However, it was limited by the fact that asphalt concretes are relatively stiff materials, hence reinforcements essentially needed stiffer materials which were relatively scarce in the earlier days. However, with the advent of polymeric geosynthetics, this limitation was overcome. The use of geosynthetic reinforcements in asphalt concrete layers began in the early 1980's, as a solution to address the problem of reflective cracking in asphalt overlays on flexible and rigid pavements. It was found that the geosynthetics provided the necessary reinforcement, strain relief and undersealing required to retard the reflective cracking and further deterioration of the lower pavement layers (Lytton 1989, Austin & Gilchrist 1996, Khodaii et al. 2009). In 1981, research on the benefits of using

geogrids for asphalt reinforcement with respect to surface deformation control, reflective cracking and fatigue life of pavement was carried out at the University of Nottingham, UK (Brown et al. 1985a, b). The first commercial use of stiff biaxial geogrids was in 1982 at Canvey Island, near London, England where approximately 10,000 m^2 of geogrid was used to control reflective cracking over a cracked concrete pavement (Austin & Gilchrist 1996). Since then, numerous research have been carried out to identify and quantify the benefits of using geosynthetic reinforcements in pavement systems. A number of those studies primarily focus on the incorporation of geosynthetics (geogrids, in particular) in the unbound base course of the pavement structure to improve the performance of the pavement system.

3.1.2 RELEVANT LITERATURE

The wide spectrum of geosynthetic material available alongside the significant difference in their index properties and functions opens numerous combinations of geosynthetics embedded in the various unbound layers of the pavement structure. Watn et al. (2005) summarized the functions served by the various geosynthetic materials in the different unbound pavement layers as shown in Figure 3.1.
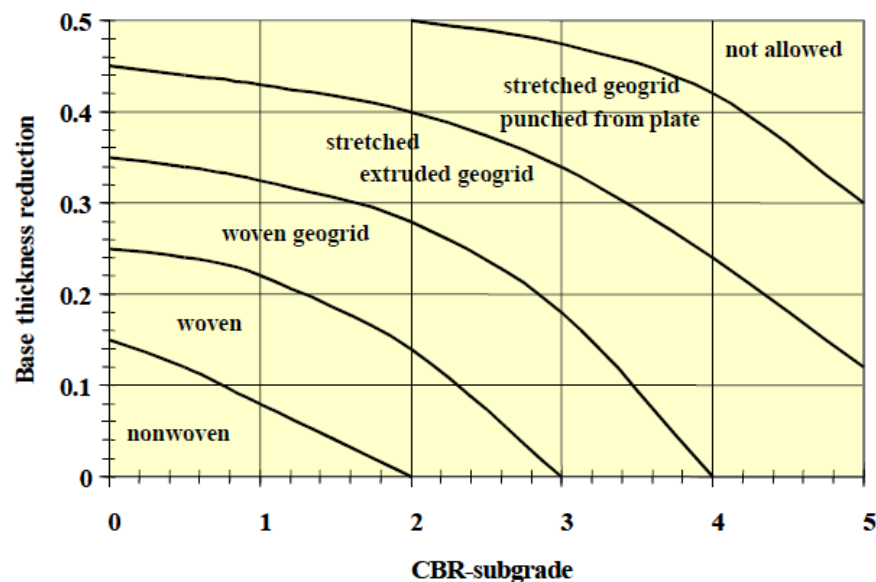
Figure 3.1. Benefits of geosynthetics in unbound layers in terms of reduced base thickness

It can be seen from Figure 3.1 that the predominant candidate for the reinforcement of an unbound base layer in a pavement structure is polymer grid or geogrid. This notion is further reinforced by the fact that geogrids offer the maximum reduction in base thickness without compromise in performance for a pavement section. This is illustrated from Figure 3.1. **Benefits of geosynthetics in unbound layers in terms of reduced base thickness** which shows the range of base thickness reduction for various geosynthetics as a function of the California Bearing Ratio of the Subgrade. It is seen that, for a given subgrade CBR, geogrids provide better base thickness reduction than the geotextiles. Watn et al. (2005) also describe two case studies namely Test Road in Hitra, Norway and Test Trial in Germany. Their critical observation was that the mechanism of reinforcement and the aggregate-reinforcement interaction is not fully understood and that very few national standards recognize the benefits of designing with geosynthetic reinforcement showing a lack of understanding in the field.

15

Table 3.1. Function, Location and Type of Reinforcement in Unbound Layers (Watn et al. 2005)

Function	Base Course	Subbase Course	Capping Layer	Stabilised Subgrade
Avoidance of Rutting	Polymer grids Steel fabrics Composite polymer grids/geotextiles.	Polymer grids Composite polymer grids/geotextiles. Geotextiles	Polymer grids Composite polymer grids/geotextiles. Geotextiles	Polymer grids Composite polymer grids/geotextiles. Geotextiles
Increase of Bearing Capacity	Polymer grids Steel fabrics Composite polymer grids/geotextiles. Geotextiles	Polymer grids Steel fabrics Composite polymer grids/geotextiles. Geotextiles	Polymer grids Composite polymer grids/geotextiles. Geotextiles	Polymer grids Composite polymer grids/geotextiles. Geotextiles
Avoidance of Cracking due to Frost Heave	Steel fabrics Polymer grids	Steel fabrics Polymer grids		
Avoidance of Reflective Cracking in areas of road widening	Polymer grids Steel fabrics Composite polymer grids/geotextiles. Geotextiles	Polymer grids Steel fabrics Composite polymer grids/geotextiles. Geotextiles	Polymer grids Steel fabrics Composite polymer grids/geotextiles. Geotextiles	
Avoidance of Fatigue Cracking	Polymer grids Steel fabrics Composite polymer grids/geotextiles. Geotextiles	Polymer grids Steel fabrics Composite polymer grids/geotextiles. Geotextiles	Polymer grids Composite polymer grids/geotextiles. Geotextiles	
Control of Subgrade Deformation		Polymer grids Composite polymer grids/geotextiles.	Polymer grids Composite polymer grids/geotextiles.	Polymer grids Composite polymer grids/geotextiles.
Bridging over Voids		Polymer grids Steel fabrics Composite polymer grids/geotextiles. Geotextiles	Polymer grids Steel fabrics Composite polymer grids/geotextiles. Geotextiles	Polymer grids Steel fabrics Composite polymer grids/geotextiles. Geotextiles
Construction Platform	Not normally a base layer	Polymer grids Composite polymer grids/geotextiles. Geotextiles	Polymer grids Composite polymer grids/geotextiles. Geotextiles	Polymer grids Composite polymer grids/geotextiles. Geotextiles

Tingle and Webster (2005) reviewed the U.S. Army Corps of Engineers design procedure to validate the existing criteria for geotextile-reinforced unpaved roads and to modify the criteria for the addition of stiff biaxial geogrids. They used previously unpublished results from historical test

16

sections to validate the empirical bearing-capacity factors used for unreinforced and geotextile-reinforced base materials. They developed empirical bearing-capacity factors for geogrid reinforced base materials to modify the existing design procedure for use with geogrid reinforcements. The test sections comprised of a subgrade of the high-plasticity (CH) Vicksburg Buckshot clay (CH), which was relatively immune to the influence of moisture content on the shear strength. Crushed limestone was used for the base-layer. The geosynthetic products (2 Geotextiles and 1 Geogrid) were placed directly on the subgrade to act as reinforcements in the subgrade-base layer interface. The sections were loaded using an M923 5-ton military truck loaded to a gross vehicle weight of 43.5 kips. The calculated bearing capacity factors for the various sections studied are shown in Table 3.2.

Table 3.2. Calculation of Subgrade Bearing-Capacity Factor (Tingle and Webster 2005)

Test Section Item	Base Thickness in. (Design)	Effective Subgrade Bearing Capacity[1] CN_c, psi (Figure 3)	Average Subgrade Strength[2] CBR, % (Table 3)	Equivalent Shear Strength C, psi (Figure 4)	Calculated Bearing Capacity Factor[3] N_c
1	20	9.3	0.7	3.6	2.6
2	15	13	0.7	3.6	3.6
3	15	13	0.7	3.6	3.6
4	10	21	0.7	3.6	5.8

Tingle & Jersey (2009) studied the performance of geosynthetic reinforced aggregate road sections. They constructed and trafficked eight instrumented full-scale aggregate road sections with marginal base materials over a typical subgrade. To quantify the benefits of reinforcement, the mechanistic response and permanent surface deformation of each test section was monitored periodically during trafficking and the traffic benefit ratios were calculated and tabulated in Table 3.3. It was found that the mobilization of the geosynthetic reinforcement takes place only after the initial densification phase of the trafficking. Thus, the benefits of reinforcement were identified to be predominant after this phase and any difference in performance before this initial densification is mainly due to the aggregate gradation, packing, etc. The post densification results showed improved load response for the reinforced sections, compared to their unreinforced counterparts. It is noted that initial pavement stiffness should not be used to evaluate reinforcement effectiveness.

Table 3.3. Traffic Benefit Ratio Comparisons (Tingle & Jersey 2009)

Performance Factor	Test Item	12-mm Deformation	25-mm Deformation	38-mm Deformation	50-mm Deformation	75-mm Deformation
Traffic benefit ratio	Item 1—crushed aggregate control	1	1	1	1	1
	Item 2—clay gravel control	1	1	1	1	1
	Item 3—crushed limestone control	1	1	1	1	1
	Item 4—crushed limestone w/GT	3	9	17	32	15+
	Item 5—crushed limestone w/GT-GG	3	217	169+	71+	15+
	Item 6—crushed limestone w/GG	2	98	161	71+	15+
	Item 7—clay gravel w/GG	0	1	1	1	1
	Item 8—crushed aggregate w/GG	2	8	18	29	27

The Texas Farm-to-Market Road No.2 or FM2 project (0-4829-1) is one of the most relevant GRP fields studies in the US. The project located in Grimes County included the evaluation of the performance of 32 field test sections comprising control portions, three different types of geosynthetic reinforcements, sections with lime-treatment and multiple repeats of each section type. The data was collected over a period of nine years (January 2006 to January 2015). The results of the project were mainly used to assess the long-term performance of the various sections under the effects of environmental loads (e.g., longitudinal cracks). The geosynthetics used were geogrids GG PET, GG PP, and a geotextile GT. More details on the materials used are available in Report No. FHWA/TX-08/0-4829-1.

The authors found two main gaps in the current TxDOT specification for geogrids. One, there is no test to quantify the reinforcement function of the geogrids. Two, the relevant property measured by flexural rigidity test is not clear. Further, they have also noted that while all the testing of geogrids is done under unconfined conditions, the application of those geogrids is under confined conditions. This makes the whole testing procedure more of a geosynthetic property, whereas the parameter of interest is the soil-geosynthetic interaction property. The authors recommend the development of an index property based on confined monotonic tests for quantifying the confinement effect of the geosynthetic which is the principal effect of reinforcements in flexible pavements. The authors have hypothesized that the confined stiffness of the soil-geosynthetic system under low strains would be a relevant parameter to quantify the benefits of geosynthetics in pavement. To determine the confined stiffness of the soil-geosynthetic system, the authors had developed a new test setup called the soil-geosynthetic interaction (SGI) test.

The research indicated adequate field evidence that geogrid reinforcement provides benefits by stabilizing pavement over clays of high plasticity. Based on the laboratory and field studies, it was demonstrated that the principal effect of the geosynthetics was to provide lateral confinement to the aggregate or base course layer of the pavement. The evaluation of benefits from reinforcement was done based on the confined stiffness of the reinforcement in the SGI test. It was found that the junction strength of the geogrids played a major role in determining the confined stiffness of the geogrids and eventually in the enhancement of performance of the pavement structure. Other factors that contributed to the differential performance of the geosynthetics were identified to be sensitivity to installation damage, high manufacturing variability and low friction coefficient.

The second full-scale field section reinforced with geogrids under the purview of the research team is the Texas Farm-to-Market Road No. 1644 (5-4829-01-2). The project included six experimental geogrid-reinforced and control sections treated with cement constructed in Robertson County. Geogrid was used to reinforce the two reinforced sections. The sections were constructed in 2010 and monitored data is available for 2 years. The results of the project were ratified by testing the same geogrid products in the small pull-out box assembly. It was found that the results of the field performance were found to be reasonably consistent with the experimental testing program using the SGI test.

The SGI test was developed as part of the Projects 0-4829 and 5-4829 at the University of Texas at Austin. A complete description of the apparatus and its working principles can be found in Report No. FHWA/TX-08/0-4829-1 and Report No. FHWA/TX-13/5-4829-01-2. One of the significant findings of 5-4829-01-2 was the repeatability of small pullout test results along with the various sources of errors in the testing setup namely uneven torque on the clamping assembly, inconsistency in the tie wires for the extensometers, variations in the dry density of the compacted

soil, material variations of the geosynthetic product and inconsistency of the analog air pressure gauge. Given considerable control over these factors, the authors were able to obtain repeatable results from the testing apparatus. 11 different types of geosynthetics (10 Geogrids and 1 Woven Geotextile) were tested against a standard soil and the results obtained were with an estimated error ranging from 10 to 20 % with a 95% confidence level.

Further comparison of the results across the various geosynthetic products reinforced the suggestion by Brown et al. (2008) that the product with the aperture width (W) to mean diameter of soil particles (D_{50}) ratio closest to the optimal value of 1.4 exhibited maximum confined stiffness values. Also, it was noted that the tests with geogrids of same aperture size, but different stiffness values showed improved performance of stiffer geogrids at higher confining pressures (Brown et al. 2007). The authors noted that the trends and rankings of geosynthetic products obtained from unconfined tensile tests were significantly different than those obtained using stiffness results from the proposed small pull-out box tests, highlighting the relevance of characterizing the stiffness under confined applications in pavement projects involving geosynthetic reinforcements.

The Texas State Highway 21 (SH 21) is an ongoing project involving the performance evaluation of GRPs located in SH21 (Austin District). The project involved the experimental rehabilitation of a section of SH21 to enhance the mechanical and hydraulic performance of the road. The experimental stretch was divided into eight sections. Each section typically comprised of two layers of biaxial geogrids in the base layer to improve the mechanical property and one layer of geotextile at the subgrade-base interface to improve the hydraulic property. Four different types of geotextiles were used. It was envisioned that while nonwoven GT would provide only separation, the woven GTs would provide separation as well as reinforcement of pavement layers. The superior product was identified to be the GT with wicking fibers, as it had enhanced lateral drainage capacity along with the separation and reinforcement functions. The project is ongoing, and it is expected to provide comprehensive comparison between effects of reinforcement, separation, and drainage functions of the geosynthetics on the pavement performance.

The placement of the geosynthetic reinforcement, particularly geogrids, has been confined to the base-subgrade interface. However recent research suggests a more nuanced approach to this placement. For instance, Kuo & Hsu (2003) used the ABAQUS finite element program to model geogrid-reinforced asphalt overlays on the old PCC pavement with joints/cracks. They concluded that placing the geogrid at one-third depth of asphalt overlay thickness from the bottom had the minimum tensile strain. After this, placing the geogrid at the mid-depth reduced the tensile stress above the geogrid compared to placing the geogrid at the bottom of the specimen. This observation is further reinforced in the dynamic creep tests conducted by Khodaii et al. (2009) which showed similar results where the sample with the reinforcement at one-third depth showing the best performance. Also, Correia & Zornberg (2014) also note that moving the geogrid closer to the surface from the bottom of the asphalt layer would provide better performance. These research emphasize the need for understanding the effect of the depth of placement of the reinforcement below the surface layer on the performance enhancement due to the reinforcements.

3.1.3 CONCLUDING REMARKS

Some of the key lessons learnt from the comprehensive literature survey relevant to geosynthetic reinforcements in full-scale field pavements systems are

- The use of geosynthetics to reinforce an unbound base layer in a pavement structure enhances the performance of pavements.
- The predominant candidate for the reinforcement of an unbound base layer in a pavement structure is polymer grid or geogrid.
- The benefits of reinforcing the unbound base layer of a pavement system are evident only after the initial densification phase, by which stage, the reinforcements are mobilized to influence the performance of the pavement. Thus, benefits from reinforcing a base layer must be quantified after this initial densification phase.
- The principal effect of reinforcing an unbound base layer using geogrids is an increase in lateral confinement of the base layer resulting in enhancement in mechanical properties such as modulus of the base layer, etc.
- TxDOT specification for testing geogrids DMS 6240 does not have a test for measuring the reinforcement function of the geogrids rather it only uses the properties of the geogrid in isolation.
- Material properties obtained by testing geosynthetic products in isolation do not correlate well with the quantification of benefits effected by using them as reinforcement in pavement structures.
- The confined stiffness of the geogrid which is a soil-geosynthetic interaction property was found to be a more appropriate parameter and it depended on the junction strength of the geogrids, sensitivity to installation damage, manufacturing variability and friction coefficient.
- The results of the field performance were found to be reasonably consistent with the experimental testing program using the small pullout device.
- The K_{SGI} coefficient, a parameter obtained from the small pullout box test, can be used as an index property for testing geosynthetics to be used in base course reinforcement.
- Historically the placement of geosynthetics has been at the base-subgrade interface of pavement structure. However recent research challenges this idea by introducing a position dependent performance analysis.

3.2 ACCELERATED PAVEMENT TESTING

Accelerated Pavement Testing (APT) is defined as the controlled application of wheel loading in pavement structure for simulating the effects of long-term in-service loading conditions in a compressed time. APT is one of the several different disciplines used in pavement engineering to understand the response of pavement structures and materials to traffic loading and the environment. One of the chief advantages of using APT programs is that they are cost effective, and they take a significantly less time when compared to the full-scale field sections. Long term pavement performance (LTPP) studies provide performance of real pavements under real traffic and climate conditions but are cost prohibitive, requiring many years of data collection and are often difficult to interpret given the very large number of factors influencing performance over time. APT done under controlled loading and environmental conditions provide a better understanding of the mechanisms influencing the performance of pavement.

3.2.1 MODEL MOBILE LOAD SIMULATOR (MMLS3)

Model Mobile Load Simulator (Figure 3.2) is an APT device that is one-fourth scale of a full-scale APT device. A scaled-down version of the load simulator cuts down costs in terms of equipment, construction of pavement section and operation. It also facilitates testing on a laboratory scale

under controlled environment and testing conditions. The use of scaled APT to full-scale APT is becoming increasingly popular with as many as 21 MMLS devises in operation by DOTs and research organizations worldwide. Two aspects are critical in the evaluation of MMLS tests. First it is important to recognize that small scale testing of pavement structures and materials provides an alternative means for preliminary indicator or ranking tests prior to, or in place of expensive full-scale APT. Second, to carry out scaled tests effectively, dimensional analysis considerations need to be met, i.e., laws of similitude must be observed. This essentially ensures the scaled-down pavement sections are subjected to the same stresses and strains as the full-scale pavement under equivalent loading and environmental conditions, with the material properties being equivalent to full-scale materials. Figure 3.3 shows the schematic of the MMLS3 one-third scale APT device. Relevant Literature on APT

Figure 3.2. UT's MMLS in the field

A large volume of knowledge exists globally in the field of full-scale APT that has been systematically and concisely synthesized in three studies by Metcalf (1996), Hugo & Epps (2004) and Steyn (2012) spanning work done in this field over the last 40 years. Metcalf (1996) noted that there were 35 full-scale APT devices in the world, of which 19 of them were active. Since then, there has been a significant increase in the number of full-scale APT devices in the US and around the world. Brown et al. (2004) attributes this to the quick and cost-effective solution to emerging pavement issues. Steyn (2012) elaborates that much of the benefit from full-scale APT has been derived from comparison studies of known materials and configurations against new and innovative materials and configurations where some equivalency between the tow has provided sufficient confidence to apply the novel solution. This short-term pay-off has been complemented by progress in the understanding of material behavior and pavement performance.

When scaled models are used, caution must be addressed to the level of load on the pavement. The stresses must be determined by the laws of similitude and corresponding wheel load and tire inflation pressure must be determined so that the stresses applied are representative. Alabaster et al. (2004a, b) demonstrated that vertical surface deformation or rutting follow a power law as function of the applied stress with exponents varying from 2 to 9, depending on the pavement type and end of pavement life definition.

Similarly, tire inflation pressure determines the shape of the contact area between the tire and the surface layer. Since the contact area does not have a uniform stress distribution, this in-turn

determines the maximum vertical and shear stresses applied onto the surface under the determined loading. Several researchers (De Beer et al. 2004, Prozzi and Luo 2005, Machemehl et al. 2005, Wang and Machemehl 2006a, b) have found that this is directly related to the tensile stresses at the bottom of the surface layer and thereby having a direct effect on the performance of the pavement structure.

Table 3.4. Technical Specification of the MMLS3 as provided by the manufacturer

No. of bogies	4	
No. of axles per bogie	1	
Wheels per axle	1	
Wheel diameter	300	mm
Tire width	80	mm
Lateral spread of tracks from centerline	0 to 80	mm
Maximum tracking width	240	mm
Tire footprint area	34	cm^2
Tire contact pressure	560-800	kPa
Nominal load per wheel	1900-2700	N
Load setting	Load cell calibration	
Load control	Automatic	
Nominal speed	2.5	m/s
Nominal wheel load application per hour	7200	
Nominal motor supply voltage	220 V AC single phase	
Power consumption	1500	Watt (max)
Dimensions:		
Length	2400	mm
Width	600	mm
Height	1150	mm
Weight	800	kg

Wheel wander was observed to produce reduced levels of rutting in the pavement in case of unidirectional loading such as in case of MMLS3 (Tia et al. 2003). Significant stresses are developed both on the pavement surface and on the wheel. Hence consistency in the use of wheel wandering across the different test sections is advised to facilitate unbiased comparison of section performances.
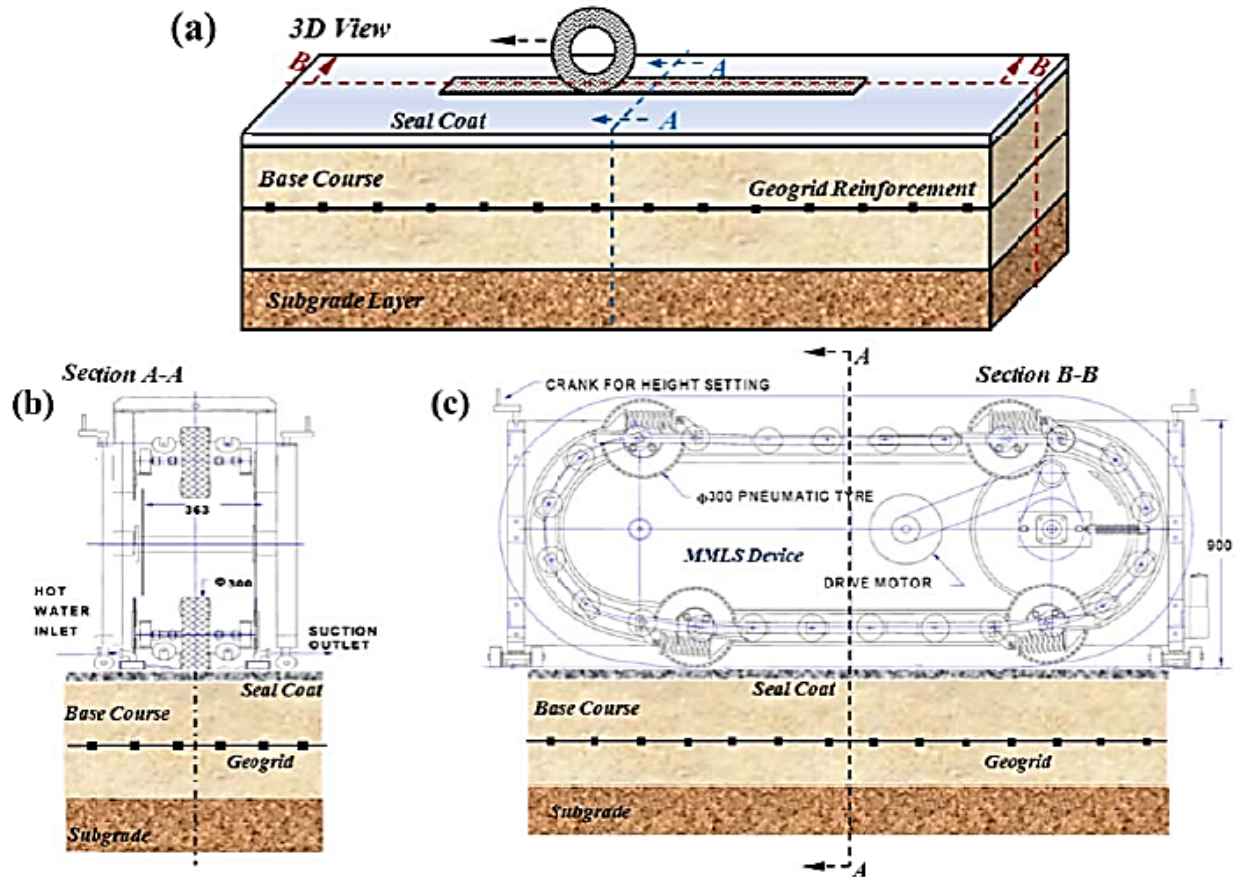
Figure 3.3. Pavement in APT program: (a) Schematic View (b) Cross-section (c) Longitudinal Section.

Smit et al. (1999) outlined three accelerated pavement tests completed on US 281 in Jacksboro, Texas using the one-third scale Model Mobile Load Simulator (MMLS3). The MMLS3 testing was used to investigate and compare the relative rutting of the one-third scale MMLS3 against that of the full-scale TxMLS. Figure 3.4 shows the comparison between the rutting performance under MMLS3 and TxMLS loading. Figure 3.5 shows the relationship between the rut depths. From these figures, it is perceivable that the rate of TxMLS rutting depth relative to MMLS3 was low (2.9) under lower traffic volume and with increase in traffic volume this relative increased to a value of 12.6. The authors attribute to this delayed increase in rutting rate to deep-seated consolidation and shear deformation of asphalt concrete layers under higher wheel loads. Note that MMLS3 is a one-third scale APT device and the laws of similitude as discussed earlier are not followed in this study. This results in extraneous rutting as reinforced by the observations of Alabaster et al. (2006a, b) discussed earlier.

The authors also give an alternative explanation for stark difference in performance under the two mechanisms. They attribute the cause of the difference to the configuration of the wheel. While MMLS3 uses a single wheel load, TxMLS uses a dual wheel configuration. This distinctly affects the stress distribution beyond the point superposition of the stresses from the two wheels as illustrated in Figure 3.6.

23
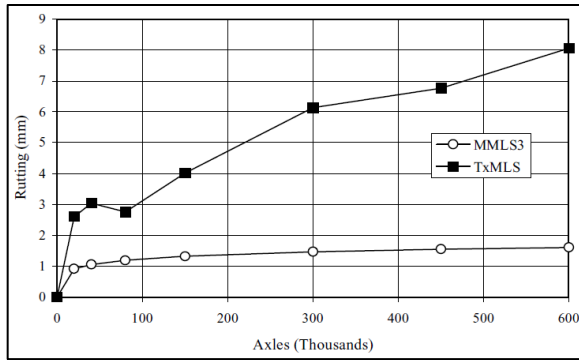
Figure 3.4 . TxMLS vs. MMLS3 rutting (Smit et al. 1999)
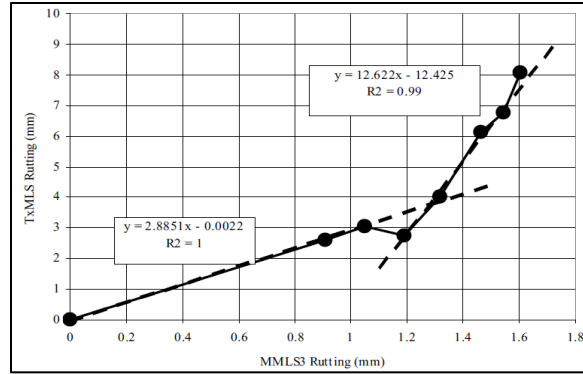
Figure 3.5 . Relationship between TxMLS and MMLS3 rutting (Smit et al. 1999)
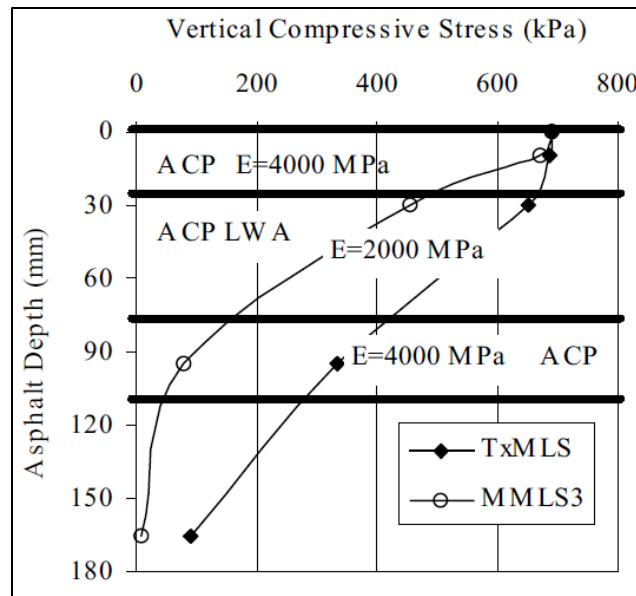
Figure 3.6 . Model tests in the field for composite layered structure (Smit et al. 1999)

The authors observed that rutting TxMLS had three mechanically different causes namely, consolidation, viscous flow, and shear failure (plastic flow). The viscous flow component was similar to that under the MMLS3, although magnitude of stresses caused a differential rutting performance. Thus, the scale of loads applied to pavements determines the mechanisms of rutting activated in the pavement system.

Epps et al. (2001) conducted five MMLS3 tests on four pavement sections at WesTrack to establish a relationship between the existing field performance, material properties and MMLS3 test results. The authors compared measured performance under full-scale loading and performance predicted from laboratory tests with performance predicted using MMLS3. The researchers found that the MMLS3 successfully ranked the relative rutting performance of four independently trafficked sections, however the rutting depths were dependent on the analysis method. The authors recommend the standardization of the rutting depth analysis method to ensure uniformity. The method favored by the author was the Reference Method. A comprehensive quantitative performance prediction methodology was developed to predict rutting performance under full-scale trafficking after conducting an MMLS3 test and a theoretical stress analysis that accounts for

24

all factors affecting performance (identified as an improved rutting depth analysis, lateral wander effects, tire contact stresses, future traffic, prevailing environmental conditions, and material properties).

Smit et al. (2003) performed one-third scale, dry & wet-heated model mobile load simulator testing on five sections at the National Center for Asphalt Technology Test Track. They compared the rutting performance of the sections under the MMLS3 with that under full-scale truck loading. Cores were extracted from the sections, both under and outside the wheel path and laboratory tests such as wet and dry Hamburg wheel testing, Superpave shear tester frequency sweep and semi-circular bending strength testing were performed.

Table 3.5 shows the NCAT tack sections tested using the MMLS3, the order in which the tests were done, and the type of test. No lateral wandering of the wheel was applied during testing. In addition to the tests listed in the testing matrix, several cores were taken from untrafficked regions of the sections for wet Hamburg and SCB strength testing. Additional cores were taken from the wheel path (trafficked region) for SCB strength testing.

Table 3.5 . MMLS3 Test matrix and Rutting Results

Test No.	Date	NCAT Section	Dry/ Wet	Axles, k	Total Rut, mm	Down Rut, mm
1	03/04/2002	S9	Dry	44	2.2	1.4
2	03/11/2002	S10	Dry	109	3.4	2.2
3	03/18/2002	E2	Dry	112	4.1	3.1
4	03/25/2002	S9	Dry	94	2.7	2.0
5	04/02/2002	E6	Wet	85	3.0	1.9
6	04/15/2002	E2	Dry	107	3.4	2.7
7	04/15/2002	E2	Wet	103	3.8	2.9
8	04/22/2002	E8	Dry	106	4.6	3.5
9	04/22/2002	E8	Wet	106	4.0	2.9

Table 3.6 the results and ranking of the various test sections subject to laboratory and field tests. The results indicated that the ranking of the sections remained consistent independent of the testing method between the full-scale rutting performance of the truck sections and compared to the MMLS3 sections. As far as the results from the laboratory tests are concerned, they do not agree with full or one-third scale wheel loading methods. The procedure to predict the performance of a section under full-scale loading from the performance under MMLS3 loading was developed by Epps et al. (2001). This procedure was used in the current study and the results of the comparative analysis were presented. The authors found that the rutting prediction ratio, PR was approximately equal to 1 for most sections (except E2 and E8). The authors indicated that estimation of full-scale loading rut depth from MMLS3 loading rut depth may lead to overestimation. However, they recommended this area must be further examined before any conclusions can be drawn from the same. As a concluding remark, the authors found that the project validated the rut prediction approach developed to compare MMLS3 and full-scale rutting performance based on vertical compressive stress potentials and influence factors. It was observed that the primary factors influencing the comparison between MMLS3, and full-scale truck rutting performance were temperature, frequency, traffic wander and effective volume of traffic.

Table 3.6. Ranking of Mix Rutting Performance based on Laboratory and Field Tests

Rank	Trucks[1]	APA (NCAT)[2]	Hamburg (NCAT)[2]	Hamburg (TxDOT)[3]	MMLS3[4]
1	S9 (2.7 mm)	S9 (2.2 mm)	E6 (2.7 mm)	E2 (3.2 mm)	S9 (2.7 mm)
2	E6 (4.0 mm)	E6 (2.3 mm)	E2 (2.8 mm)	S9 (3.8 mm)	E6 (3.0 mm)
3	E8 (4.0 mm)	E2 (2.3 mm)	E8 (3.0 mm)	E6 (4.0 mm)	S10 (3.2 mm)
4	S10 (4.1 mm)	S10 (2.6 mm)	S10 (3.5 mm)	S10 (4.2 mm)	E2 (3.8 mm)
5	E2 (5.1 mm)	E8 (4.6 mm)	S9 (3.7 mm)	E8 (4.6 mm)	E8 (4.0 mm)

[1] Dipstick rutting after 8.5 million ESALs
[2] Dry at 64°C after application of 8,000 cycles
[3] Wet at 50°C after application of 20,000 cycles
[4] Total rutting at 100,000 axles (interpolated/extrapolated)

3.2.2 CONCLUDING REMARKS

Some of the key lessons learnt from the comprehensive literature survey of those literatures relevant to Accelerated Pavement Testing of pavements systems are as follows.

- The use of scaled-APT programs warrants attention to considerations of dimensional analysis i.e., laws of similitude. However, scaling of materials is not required if the dimensions of the materials do not influence the structural response in terms of compaction, densification under traffic, etc.

- APT programs are more commonly used in case of studies that involve comparison between two or more sections with different materials or configurations with all other parameters remaining constant. APT has the advantage of allowing the operator to control all the parameters with respect to the testing. Thus, APT programs are predominantly used to demonstrate equivalency of sections.

- Scaling of the loads between full-scale and reduced-scale sections becomes mandatory when rutting performance of the pavement sections are considered, as the rutting depths correlate exponentially with the applied stress levels. This is in-turn increases the estimated error in the analysis, even in the case of comparison studies.

- Improper scaling of loads results in variable relative rates of rutting across the various test sections thus introducing an error in the comparison of the relevant data.

- Improper scaling of loads results in activation of different or unexpected mechanisms of rutting. Hence caution must be exercised to ensure that the loads are scaled in accordance with the laws of similitude.

- Variation in the tire inflation pressure affects the contact area and maximum vertical and shear stresses that come on the contact surface. This is found to be directly related to the tensile stresses at the bottom of the surface layer. Hence caution must be exercised to ensure that the tire inflation pressure is set to the manufacturer recommended value to obtain the desired contact area.

- Wheel wander affects the level of rutting significantly. Hence care must be taken to ensure that the wheel wander is accounted for uniformly across the various test sections.

- Rutting depth measured with respect to an initial non-trafficked profile is more reliable.

- Prediction of rutting performance under full-scale loading from that under reduced scale may lead to overestimation.

- Laboratory torture tests such as the Hamburg wheel tests have poor predictability both qualitatively (ranking) and quantitatively.

3.3 INSTRUMENTATION

Understanding the mechanisms involved in reinforcements of unbound bases requires extensive data collected from highly instrumented sections subject to trafficking. Some of the common parameters that are to be measured to develop a mechanistic-empirical pavement design model, include strains, stresses, deflections, moisture, and temperature (Weinmann 2004). In situ measurements during full-scale APT allow for the development of accurate performance models and the calibration of mechanistic pavement design approaches (Steyn 2012).

3.3.1 INSTRUMENTATION OF FULL–SCALE FIELD SECTION

Sargand et al. (1997) identified the most important parameters or material properties required to develop and validate a numerical model such as FEM, FDM, BEM of the pavement design which is essential for developing an empirical mechanistic design method. They identified two sets of input parameters for these models. The first set consisted of material properties of the various layers in the pavement system, namely the stiffness, Poisson's ratio, strength, and nature of the failure limits (brittle or ductile). The second set consisted of parameters that would be needed to calibrate such a model such as pressure between the layers, deflection of the layers, strain in the pavement, joint discontinuities, temperature distribution, etc. Since then, any attempt at developing an empirical mechanistic model has involved instrumentation of test sections to determine these parameters.

Brandon et al. (1996) discussed the construction and instrumentation of geosynthetic reinforced secondary road test sections in Southeast Virginia. The test road consisted of nine instrumented, control and geosynthetic reinforced test sections of varying base and surface HMA layer thicknesses. The geosynthetics used were a geogrid and a geotextile which had been characterized by Smith et al. (1995).

Two types of Earth Pressure Cells (EPCs) were used in the study, namely the hydraulic pressure type Carlson TP 101 and the diaphragm type Kullite Type 0234. They were used to measure dynamic traffic loading. It was found that maximum registration ratio was observed when the EPCs were flush with the surface of the respective soil layer. This ensured minimum disturbance between the subsequent layers. The EPCs were placed at mid-depth of the base layer and at the base-subgrade interface. Carlson JO-1 Soil Horizontal Strain Gauge was used to measure strain in the soil layers and near the base-subgrade interface just below the EPCs. Kyowa KM HMA Horizontal Strain Gauge was used to measure the strains at the bottom of the HMA wearing surface layer. Measurements Group N2A 06 40 CBY 120 Foil type strain gauge was used to measure the strains at the bottom of the geotextile. Texas Measurements FLK-6-1L Foil type Strain Gauge was used to measure the strain at the bottom of the geogrid. Further, T Type thermocouple for temperature sensing, Gypsum Block Moisture sensor and piezometric polymer traffic sensor were used in the study.

Table 3.7. Instrument Survivability after 8 Months

Gage Type	Number Installed	Number Survived	Percent Survived
Kulite earth pressure cells	6	3	50%
Carlson earth pressure cells	21	16	76%
HMA strain gages	35	26	74%
Geotextile strain gages	18	1	6%
Geogrid strain gages	18	5	28%
Soil strain gages	6	5	83%
Thermocouples	17	15	88%
Gypsum blocks	18	18	100%
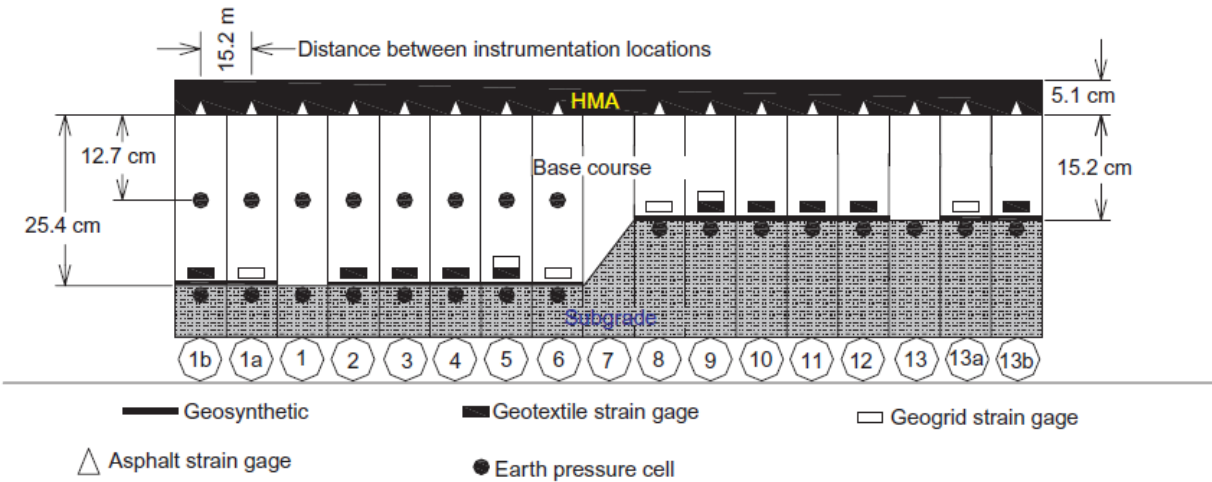
Figure 3.7. Profile View of the test sections

The authors also conducted a gauge survivability analysis by determining the percentage of sensors still active in the sections, 8 months after construction and traffic. They also observed that the critical period for gauge survivability is during construction and the failure rate of sensors beyond the very first month of trafficking is very low. Thus, to ensure maximum functionality of the gauges, care must be exercised primarily during the construction phase of the project.

One of the pioneering works done, in terms of instrumentation of a full-scale field pavement section is the project that was part of a research initiative conducted by the Arkansas State Highway and Transportation Department (Warren and Howard 2007). The project involved the construction of 17 highly instrumented sections (Figure 3.7) of full-scale geosynthetic reinforced flexible pavement at Marked Tree, Northeast Arkansas. Two geogrids, three woven geotextiles, and one nonwoven geotextile were utilized in this study and were placed at the subgrade-base layer interface for all the test sections. The end goal of the project was to determine the benefits of geosynthetic inclusions and collect dynamic response data from traffic loads to support a mechanistic-empirical pavement design procedure. They provided with the details and recommendations for the use of sensors in full-scale projects.

28

Geokon 3500 hydraulic earth pressure cells were used to measure the vertical stresses in the soil. The earth pressure cells were installed in the subgrade, approximately 2 cm form the subgrade surface and mid-depth (sections 1-6) in the 25.4 cm thick base coarse layer. The idea behind the position of the earth pressure cells was that those cells positioned at the surface of the subgrade would measure any relief in stress at the subgrade level because of the geosynthetic and those cells positioned at mid-depth in the base course would measure the stress distribution within the aggregate mix thus evaluating the confining effect from the geosynthetic. The instrumentation was in the outside wheel path in the center of each test section (longitudinally). Vishay Micro-Measurement foil strain gauges were utilized to measure strain on the geosynthetics. EP-08-19CDZ-350 was utilized for the geotextiles (48.3 mm in length), EP-08-500GC-350 (12.7 mm long) for the polyester geogrid and EP-08-230DS-120 (5.8 mm long) for the biaxial polypropylene geogrid. CTL Group ASG-152, H-type Asphalt Strain Gauge is embedded at the bottom of the asphalt surface layer. Omega TMQSS-125G-6 T-type thermocouples (rated 220° C) were placed in the base course and subgrade layers to create a temperature profile. Three T-type thermocouples were placed at the bottom of the asphalt-concrete layer, since the surface layer was only 5.1 cm thick. For this purpose, the Omega CPSS-14G-12-NHX T-type thermocouples (rated 650° C) were used. Decagon EC-20 capacitance type moisture content probe was used to measure moisture content variation in this study. Geokon 3400 piezometers were installed outside the wheel paths in section 7 to monitor the existence of static pore pressures at the surface of the subgrade and mid-depth in the base course.

All 17 active earth pressure cells installed in the subgrade and all eight earth pressure cells in the base course showed signal presence and stability upon pre-traffic evaluation. All 17 active asphalt strain gauges installed were found to be working satisfactorily. Out of the 16 active geosynthetic gauges, 3 gauges malfunctioned thus showing an 81 % survivability rate, post-construction, for geosynthetic foil type strain gauges. In summary, out of the 56 active structural gauges, 94 % provided functional signal post-construction. Of the 11 thermocouples installed, five were not satisfactory. All five moisture content probes and both piezometers were satisfactory. Approximately 77 % of the active environmental sensors provided functional signal post-construction. The authors finally produced some installation recommendations for the sensor. They recommended that the gauges must be oriented in a direction that will maximize gauge survivability. This means, for pavement structures, the gauges aligned horizontal (perpendicular to applied load) survived better than those aligned vertical. Wherever possible, backup gauges must be installed to reinforce the instrumentation configuration. The functionality of the gauges and the quality of the signal were to be checked before the burying of cable lines in the conduit system. This facilitated repairs and ensured near 100% functionality before trafficking. The authors recommended the calibration of all sensors (or at least validation of the calibration factors) in a controlled environment using the full-scale data acquisition system prior to the field installation. This is especially necessary of foil type strain gauges, where the modulus of the material used to attach the gauges to the materials will probably be higher than the stiffness of the material. Signal noise from the test configuration must be evaluated prior to the implementation of the network of sensors, rather than doing it as a part of the implementation program. Prior knowledge of on-site noise and any other problems in the signal helps in saving a lot of time during the implementation. The authors recommend the use of wire extensometers and conductance coils to measure the global displacement in the geosynthetics as against the use of strain gauges. The research team at UT Austin also has very good experience with the use of extensometers to measure the strains in the geosynthetics from the small pull-out box test program. They also

recommend developing a repeatable gauge evaluation procedure to be performed regularly during testing to evaluate gauge performance over time.
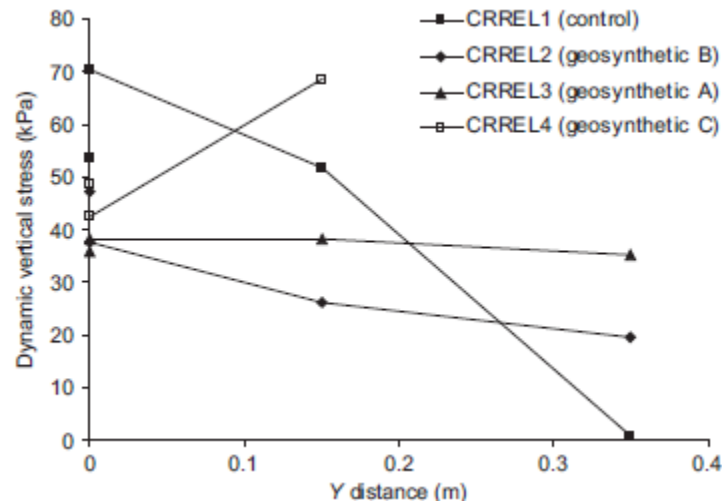
Figure 3.8. Distribution of Stresses in the transverse direction

3.3.2 INSTRUMENTATION OF LABORATORY SECTIONS UNDER APTS

Perkins & Cortez (2005) conducted full-scale APTs on four test sections reinforced with geosynthetics including a control section at the US Army Corp of Engineers Engineering Research and Development Center, Cold Region Research and Engineering Laboratory. They constructed four full scale test sections in the laboratory and used DynaTest Mark IV heavy vehicle simulator to traffic the same. The geosynthetics used were Amoco Propex 2006 woven geotextile, Tensar BX 1100 geogrid and Tensar BX 1200 geogrid.

To measure the vertical dynamic stress within the pavement layers due to the wheel load, DynaTest Stress cells were used. The calibration procedure for the same can be obtained from Selig et al. (1997). These stress cells are placed at a depth of 0.46 m below the pavement surface at the base-subgrade interface below the geosynthetic directly below the center wheel path and at 0.15 m and 0.35 m offsets from the wheel path. The idea behind this placement of the stress cells was that they would shed light into the aspect of the load distribution beneath the wheel load under cases of with and without reinforcement as illustrated in Figure 3.8.

35 EMU Strain coils under various configurations were embedded into the pavement system. These were electromagnetic coils, 100 mm diameter that worked in transmitter-receiver pairs. They measured strains (dynamic and permanent) in the soil in terms of change in voltage across the coils.

3.3.3 CONCLUDING REMARKS

A comprehensive list of all instrumentation used in pavement sections in previous studies is listed as follows.

Profilometer	Forensic Trenching
Portable Seismic Pavement Analyzer (P-SPA)	GeoGrid Strain Gauge (Foil type)
Light Weight Deflectometer	Soil Strain Gauge
LVDT to measure surface deflection	Earth Pressure cells

Extensometers	HMA Strain Gauge
Settlement plates at different depths	Pore Pressures

Some of the key lessons learnt from the comprehensive literature survey of those literatures relevant to instrumentation of pavements systems are as follows.

- For the development of accurate performance models and calibration of mechanistic pavement design approaches, it is advised to make use of in-situ measurements of relevant parameters.
- The input parameters for the development of an empirical mechanistic model are the material properties of the various layers in the pavement system such as stiffness, Poisson's ratio, strength, and nature of failure.
- The input parameters for the calibration and validation of an empirical mechanistic model include parameters such as pressure between the layers, deflection of the layers, strain in the pavement, joint openings, temperature distribution, frost depth characteristics, etc.
- When measuring properties that are to be correlated to each other, such as stress and strain, it is advisable to align the appropriate sensors vertically so that the response measured is not phase delayed.
- The alignment of the gauges inside the pavement section is an important property that determines the survivability of the gauge. As far as possible, gauges must be aligned horizontal, perpendicular to the traffic loads as far as to maximize survivability.
- Use of back-up gauges is highly recommended in the case of field sections, as replacement of faulty gauges is difficult without disturbing the in-situ state of the system.
- One of the critical measurements to develop a mechanistic-empirical model of GSR pavements is the stress at the surface of the subgrade, so EPC measurements are mandatory in this case and backup gauges are highly recommended.
- Ideal locations of the EPCs were found to be at the mid-depth of the base layer and at the base-subgrade interface.
- The calibration of all sensors is recommended to be done using the same data acquisition system as that to be used during the monitoring of the pavement section.
- The use of extensometers with LVDTs is preferred over the use of foil-type strain gauges in measuring the strains in a geosynthetic. This is a more popular observation made by several researchers (Warren & Howard 2007, Zornberg et al. 2008, Brandon et al. 1996).
- Most of the instrument failures occur either during construction or the first few weeks of operation. Hence caution must be primarily observed during this phase of the project for both field and laboratory scale sections.

3.4 ACCELERATED PAVEMENT TESTING OF GRPS

Numerous studies have been carried out in the use of full-scale and reduced-scale APT on Geo-Synthetic Reinforced Pavements. This is primarily due to the unique advantage APT programs have to offer in terms of demonstrating equivalency of two or more test configurations. APT tests have been predominantly used to demonstrate equivalency in terms of increase in traffic benefit ratio, effect on the modulus of the base material, effect on the reduced equivalent thickness of the base material, etc. Since they are cost effective at reduced scales and require a very short amount of time to obtain the results, they make comparisons between several experimental configurations much easier and thus readily favored by the researchers.

3.4.1 RELEVANT LITERATURE

The Brazilian experience in the field of APTs encompasses 12 years of APT programs. While several parallel studies were run, it is of more relevance to this task to focus on the one involving geosynthetics. The purpose of the study was to comparatively evaluate the performances of asphalt overlays on cracked pavements with and without using paving fabrics. Two kinds of geotextiles (named as G 150 and G 150-TF) were used as intermediate layers in a test section loaded by the traffic simulator UFRGS-DAER/RS. The system composed of AC overlay and geotextile G 150 remarkably delayed cracking reflection and outperformed the system of AC overlay with no fabric by a factor of two. Reflection cracking on the AC over G 150-TF was significantly lower (60%) than on the AC with no fabric. However, the results obtained in an in-service road with similar reinforcement configurations were not so conclusive. There, AC overlays with or without paving fabric performed similarly. Some fabric installation problems were identified as having affected the performance of a given zone with geotextile G 150. And that reinforced the idea that paving fabrics installation procedures are critical.

Tang et al. (2008) studied the mechanical and physical properties of geogrids that are critical to their effectiveness in the stabilization of pavement subgrade. Geogrid properties were correlated with bench-scale interface test results such as direct shear, pull-out and accelerated pavement testing results. The performance was evaluated in terms of surface rutting with trafficking levels. Four different types of Geogrids were used in the study and designated as A, B, C and D. Grids A and D were composed of high tenacity polyester multifilament yarns and coated with a proprietary polymer and polyvinyl chloride coating, respectively. Grid B was made of woven polypropylene yarns. Gird C is made of extruded polypropylene sheets. Grids A, B and D were flexible geogrids and gird C was a stiff geogrid. The subgrade soil was silty sand (SW-SM). Base course aggregate comprised of dense-graded crushed stone with a standard proctor maximum dry density of 2329 kg/m^3 at an optimum moisture content of 3.9%. The surface layer used in the study was an HMA layer with a theoretical maximum specific gravity of 2.510 (G_{mm}).

Table 3.8. Tested index properties of the geogrids (Chehab et al. 2007)

Index property	Test method	Grid A MD*	Grid A TD**	Grid B MD	Grid B TD	Grid C MD	Grid C TD	Grid D MD	Grid D TD
Aperture size (mm)	Calipers	27.18	28.96	35.05	41.15	25.65	36.58	25.65	26.42
Rib thickness (mm)	Calipers	0.76	1.12	1.98	1.09	0.76	1.07	1.42	2.03
Junction thickness (mm)	ASTM D5199	1.17		2.29		3.94		1.55	
Mass per unit area (g/m²)	ASTM D5261	298.37		252.26		319.06		350.93	
Tensile strength at 2% strain (kN/m)		7.5	10.1	14.8	15.0	9.8	15.6	10.3	11.2
Tensile strength at 5% strain (kN/m)	ASTM D6637	13.1	14.1	30.1	30.0	16.8	29.2	18.1	17.4
Ultimate tensile strength (kN/m)		33.3	57.8	36.5	35.7	23.9	32.9	39.5	52.8
Elongation at break (%)		10.5	14.0	7.1	6.7	20.6	10.9	10.5	12.0
Junction strength (kN/m)	GRI GG2	6.1	7.6	10.2	4.3	17.7	28.1	7.4	7.1
Flexural rigidity (mg cm)	ASTM D1388, modified	146,119		271,509		1,429,355		452,671	
Torsional stiffness (cm kg/deg)	COE/GRI GG9	3.47		3.97		7.50		3.43	

*MD, machine direction; **TD, transverse/cross-machine direction.

The index properties of the geogrids such as the aperture size, tensile strength, etc. were determined by a series of tests conducted as per the ASTM standards and standards set forth by the Geosynthetic Research Institute (GRI). A summary of the test results is provided in Table 3.8.

The bench-scale tests, namely, direct shear test and pull-out box test, were done to characterize the interaction properties of the several types of geogrids installed between the subgrade and the aggregates used in the aggregate base layer. The results of these tests are shown in Table 3.9.

Table 3.9. Results of the direct shear and pull-out tests

Property	Grid A	Grid B	Grid C	Grid D	Control
Friction angle, δ_{peak} (deg)	28.6	44.0	48.0	32.7	44.2
Efficiency factor, E_{ϕ}	0.56	0.99	1.14	0.66	N/A
Adhesion, c (kN/m^2)	1.72	0.00	0.00	3.69	0
Interaction coefficient, C_i	0.86	1.00	0.82	0.62	N/A

As for the accelerated pavement testing, the tests were conducted by applying wheel loads from MMLS3 onto the laboratory-fabricated slabs for the four types of geogrid products. Two phases of testing were conducted. APT I with subgrade CBR = 3 and APT II with subgrade = 1.5. The unidirectional trafficking to the pavement was applied by MMLS3 in the controlled laboratory experiment. Testing was conducted at room temperature under dry conditions with no wandering i.e., channelized trafficking.

From the direct shear test results, the authors have found that geogrids with larger aperture size resulted in higher interface efficiency factor for the types of materials used in this study. They also noted that there is no correlation between the rib thickness and the interface efficiency factor, whereas the combination of the junction strength and the tensile strength at 2% strain in the machine direction had a strong correlation with the interface efficiency factor. It was also seen that junction thickness as an indicator of the junction strength also showed a good correlation with the interface efficiency factor

They identified that for pavement applications, evaluating the load-displacement relationship at small displacements was more meaningful to the pull-out behavior compared to the coefficient of interaction derived from a single value of the maximum pull-out load. Therefore, from the pull-out tests, they have found that an insignificant correlation existed between the increase in aperture area and flexural rigidity and an increase in the pull-out force measured at 5 mm (small strain) while stronger correlations were observed for tensile strength at 2% strain and efficiency factor from direct shear.

The authors exemplified the fact that the coefficient of interaction being a large strain property had no evident correlation with the index properties of the geogrids. However, one key aspect was observed about the importance of aperture size to aggregate size ratio. It was found that maximum interaction efforts can be achieved when the grain size was similar to that of the geogrid aperture size, as this facilitates an optimum between interlocking and contact area of the geogrid with the granular aggregate.

A summary of the results and the associated trends are tabulated into Table 3.10. The trends are indicated as a function of the increasing index properties.

Table 3.10 Relationship between selected index and bench-scale properties with subgrade rutting from accelerated testing

Property	Correlation and observed trend				
	Efficiency factor	Pull-out @ 5 mm	Coefficient of interaction	Rutting @ 1.5 CBR	Rutting @ 3.0 CBR
Aperture area	I	I	I	D	I
Junction strength	I	I	N	D	I
Tensile strength at 2% strain	I	I	N	N	N
Ultimate strength	N	I	N	N	N
Flexural rigidity	N	I	N	D	I
Efficiency factor		I	N	N	I
Pull-out force @ 5 mm				N	N
Coefficient of interaction				N	N

I, increasing trend; D, decreasing trend; N, no observed trend.

3.4.2 CONCLUDING REMARKS

Some of the key lessons learnt from the comprehensive literature survey of those literatures relevant to Accelerated Pavement Testing of GSR pavements sections are as follows.

- Although APT program results show considerable difference in performance of pavement sections with different configurations, one must be wary of the fact a number of factors including but not exclusive to environmental factors, installation conditions, etc. affect the in-field performance of these test sections.
- In the case of geogrid reinforced pavement sections, the aperture size is one of the crucial factors determining the degree of mobilization of the reinforcement.
- For pavement application, evaluation of load-displacement relationship at small displacements correlated well with the pavement performance.
- The choice of aperture size of the geogrid depended on the grain size of the particle such that when the aperture size and grain size are similar, maximum interlocking is expected, which in turn produces better performance.

3.5 SUMMARY AND CONCLUSION

3.5.1 SUMMARY

- A brief background of study was provided with emphasis on the expertise needed in the various areas that would contribute to the study. The objectives of this technical memorandum were listed out, followed by brief description of the layout of the technical memorandum
- The material, geosynthetics, was introduced with brief discussion on the different types and functions of the various geosynthetics. Particular emphasis was placed on geogrids and a historical account of the usage of geogrids in the pavement industry was provided.
- The various geosynthetics used in the previous studies were discussed along with their intended functions and geogrids were identified to be ideal in providing reinforcement to pavement systems. Relevant literature along with lessons learnt from these literatures were neatly outlined.
- A pavement testing technique, namely Accelerated Pavement Testing was introduced. The advantages and disadvantages of using APT for testing pavement sections were outlined. The cost benefits and scaling limitations with respect to the use of a reduced scale APT

program were discussed. One such reduced scale APT device, namely MMLS3 available with UT Austin was described.

- Relevant literature with respect to APT systems, and their use in full-scale field and reduced-scale laboratory pavement sections was reviewed along with the lessons learnt about the advantages, shortcomings, and sources of errors from these systems.

- The need for instrumentation in order to determine the various material properties and input parameters that are identified to be required for developing the empirical mechanistic multi-layer pavement model was outlined.

- The instrumentation used in previous studies for pavement systems in full-scale field sections and in pavement sections subjected to APT in the laboratory was discussed and the relevant lessons learnt were outlined.

- Finally, a few literatures on the use of accelerated pavement testing systems on pavement sections reinforced with geosynthetics were reviewed in order to breed familiarity with the workings of these programs and identify any particular issues with the testing procedures.

3.5.2 CONCLUSION

Relevant domestic and foreign literature on geosynthetic-reinforced pavement systems, with particular emphasis on the experimental, field validation and design components of the study were collected, reviewed, assessed, and summarized into the Technical Memorandum 1. The field performance data from geosynthetic-reinforced pavements constructed in Texas were analyzed and the relevant proposed reinforcement mechanisms were noted. The APT data from relevant unreinforced and geosynthetic-reinforced pavements studies were presented and the relevant strategies to use APT programs to evaluate the performance of GRPs were identified. The relevance of the results from the small pull-out box testing program was determined and the parameters of interest from the testing program were identified. All the objectives set out for the Technical Memorandum I was completed.

4.   FIELD PERFORMANCE UNDER TRAFFIC LOADS

The long-term performance under traffic loads of geosynthetic-reinforced and control pavement sections constructed by TxDOT in FM2 is characterized as a part of this project. The scope of the project includes evaluation of the performance of 32 field test sections comprising control portions, three different types of geosynthetic reinforcements, sections with lime-treatment, and multiple repeats of each section type. In addition, continued condition surveys have been conducted for nine years (2006 to 2015). Results of this project have provided the Research Team with a unique database of the long-term performance of the reinforced and unreinforced field sections. While the data analysis has focused on the impacts of environmental loads for 0-4829, which has been characterized by evaluation of longitudinal cracks, further analysis of the raw data has been done for the effects of traffic loads in this project. In particular, rutting measurements and alligator cracking data, which was available in the form of raw data, is processed. It was found that alligator cracking was negligible in most parts of the road. Therefore, the focus of the evaluation has been on characterization of rutting data.

An additional condition survey was also conducted in 2015 as part of this project. As part of this survey, various types of pavement surface distresses and rut depth were characterized with the careful protocols previously established as part of TxDOT Projects 0-4829 and 5-4829. The information collected during this survey is integrated into the database of previous field performance data collected through December 2015. The new rut data is incorporated into the evaluation and synthesis of rut depth information.

4.1   PROJECT DESCRIPTION

FM 2 starts from 2 miles west of Highway 6 at Courtney eastward to FM 362 in Grimes County, Texas. The total distance is about 6.4 miles. Major problems with ride quality and different types of distresses, particularly in the form of longitudinal cracks, had been reported for the section between Highway 6 and FM 362. Following the falling weight deflectometer (FWD) and rolling dynamic deflectometer (RDD) tests in this portion of the road, a major rehabilitation plan was designed in 2006. The length of this section is about 4.4 miles (Figure 4.1).
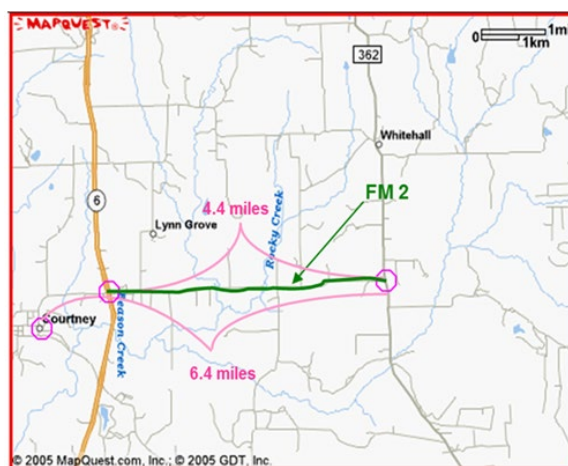
Figure 4.1 Location of FM2 road and the rehabilitation area

4.1.1 TEST SECTIONS DESIGN AND LAYOUT

FM 2 is a two-lane light traffic road with trucks being the major traffic on the road. The speed limit is 55 mph. Four pavement cores were obtained from FM2 road in summer 2003 by TxDOT, which indicated a light pavement structure consisted of one-inch asphalt concrete layer as the top cover of the road and up to 15-inch iron ore base course (Figure 4.2). The rehabilitation design in 2006 involved 10-inch scarification and remix of the old base course and construction of a new 7-inch base layer. As part of rehabilitation plan, 32 test sections were designed at two sections of the road as illustrated in Figure 4.3. Four different repair schemes (with multiple replicates for each scheme) were designed for the test sections that include (1) control sections, (2) sections with lime-treated subbase, (3) sections with geosynthetic reinforcement in base course, and (4) sections with geosynthetic reinforcement in base course and lime-treated subbase (Figure 4.4).
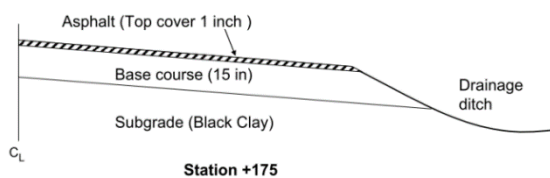
Figure 4.2 Pavement system structure in FM2 before reconstruction

Figure 4.3 Location of test sections in FM2

Scheme (1) (Control sections) was designed as the baseline for comparative evaluation of the performance of the lime-treated and geosynthetic-reinforced sections. In Schemes (2) and (4) the 10-inch scarified old base was treated and stabilized with 4 to 6 percent lime. In Schemes (3) and (4) one layer of geosynthetic reinforcement was placed at the interface between the 10-inch scarified old base course and the 7-inch new base course. Three different types of geosynthetic reinforcements were used including two geogrids, referred to as GGPP and GGPET, and one geotextile, referred to as GT.
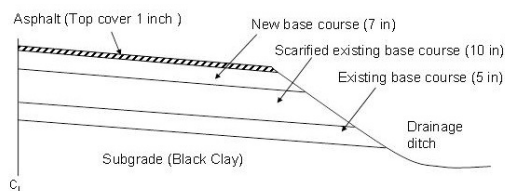
Unreinforced without lime stabilization
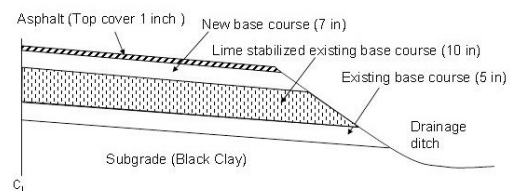
Unreinforced with lime stabilization
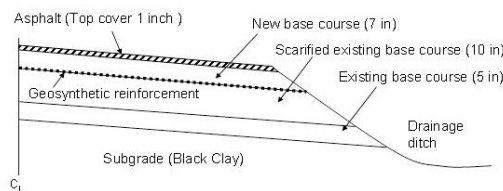
Reinforced without lime stabilization
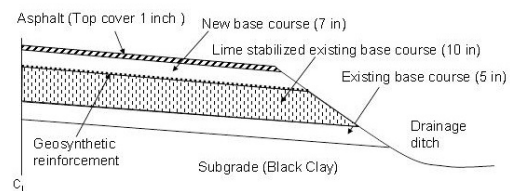
Reinforced with lime stabilization

Figure 4.4 Four repair schemes constructed in FM2 rehabilitation project

4.2   MATERIAL CHARACTERIZATION

Pavement materials, subgrade soil properties, and properties of geosynthetic products used in this study are discussed in this section.

4.2.1   SUBGRADE SOIL PROPERTIES

The subgrade soil in FM2, referred to as "FM2 Clay", was sampled from the construction site in May 2005. The clay was excavated with a backhoe from a depth of approximately 5 feet near Station 184 close to K6 lane. The clay was transported to the laboratory at the University of Texas in two 55-gallon plastic drums. It was dried by placing it on metal trays in a temperature-controlled room at a temperature of 914° F (490° C) for 48 hours. The dried soil was then broken down with a hammer and passed through a soil crushing machine (Chipmunk Jaw Crusher model VD 67, Bico Inc., Burbank, CA). The soil was then sieved and particles passing the #10 sieve were set aside for testing. Particles not passing the #10 sieve were reprocessed using the soil crushing machine until the material passed the #10 sieve.

Classification tests, including Specific Gravity Test, Grain Size Distribution Test, Atterberg Limits Test, Compaction Test, and Hydraulic Conductivity Test, were conducted on the collected soil sample. The soil was categorized as gray high-plastic clay with high dry strength, high toughness, and no dilatancy. The average specific gravity (Gs) of FM2 Clay was obtained as 2.70. Using standard sieve analysis procedure (ASTM D 422), 2000 grams of FM2 clay were used to determine the grain size distribution. The results are presented in Table 4.1 and further illustrated in Figure 4.5. Values for D_{10}, D_{30}, and D_{60}, in addition to the uniformity coefficient and the coefficient of gradation, are also presented in Table 4.1.

Table 4.1 Detailed characterization of a FM2 clay sample

Test	Parameter	Results	ASTM Standard
Specific Gravity	G_s	2.7	D 845
Particle Size Analysis	Fine content, %	60 %	D 422
	D_{10}, mm	0.1	
	D_{30}, mm	0.3	
	D_{60}, mm	0.7	
	Uniformity coefficient, C_u	7.0	
	Coefficient of gradation, C_c	1.3	
Standard Proctor Compaction	Optimum Water Content, %	32	D 698
	Maximum Dry Unit Weight, γ_d, kN/m^3	15.5	
Atterberg Limits	Liquid Limit (LL)	72	D 4318
	Plastic Limit (PL)	33	
	Plasticity Index (PI)	39	
Soil Classifications	CH		D 2487
Hydraulic Conductivity of Saturated Soil	@ w = 23 % and γ = 13 kN/m^3	4.0 x 10^{-7}cm/s	
	@ w = 27.6 % and γ = 13.5 kN/m^3	4.0 x 10^{-7}cm/s	
	@ w = 29 % and γ = 15 kN/m^3	7.0 x 10^{-8}cm/s	
	@ w = 32 % and γ = 15 kN/m^3	2.0 x 10^{-9}cm/s	
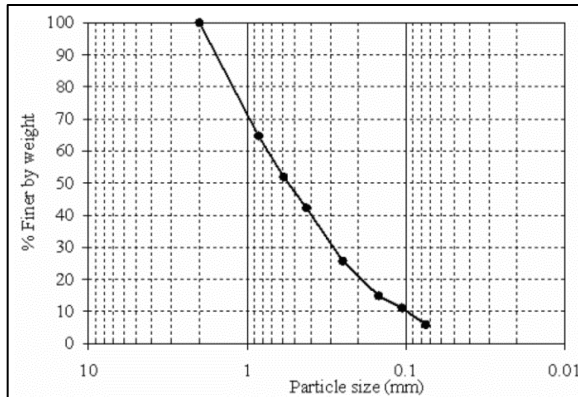
Figure 4.5 Grain Size Distribution curve for FM2 clay sample
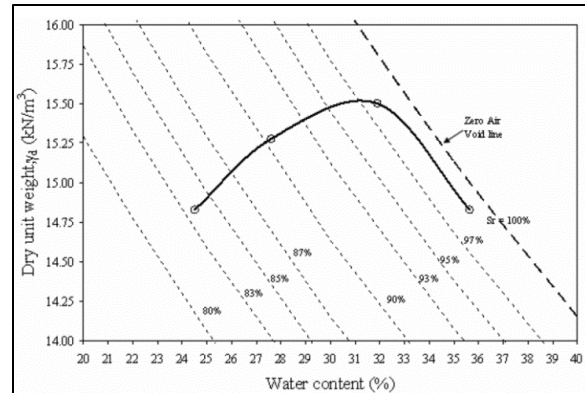
Figure 4.6 Result of compaction test on FM2 clay sample

Atterberg limits were determined according to ASTM D 4318 for FM2 Clay. The values for the plastic limit and the liquid limit were measured as 33 and 72, respectively. Therefore, the plasticity index was found to be 39, which classifies FM2 Clay as high expansive soil. Using the plasticity chart and ASTM D 2487, FM 2 Clay was classified as clay of high plasticity (CH).

Standard proctor compaction tests (ASTM D 698) were performed on FM2 Clay. Results obtained from tests performed using the standard proctor procedures are summarized in Table 4.1. The curve corresponding to the procedure was plotted in Figure 4.6. The optimum water content, in addition to the corresponding maximum dry density, are presented in Table 4.1.

Hydraulic conductivity test on FM 2 Clay specimens prepared using standard proctor test was conducted using flexible wall permeameter. The results obtained are as listed in Table 4.1. The hydraulic conductivity of FM 2 Clay varied with compaction water content as shown in Figure 4.7.
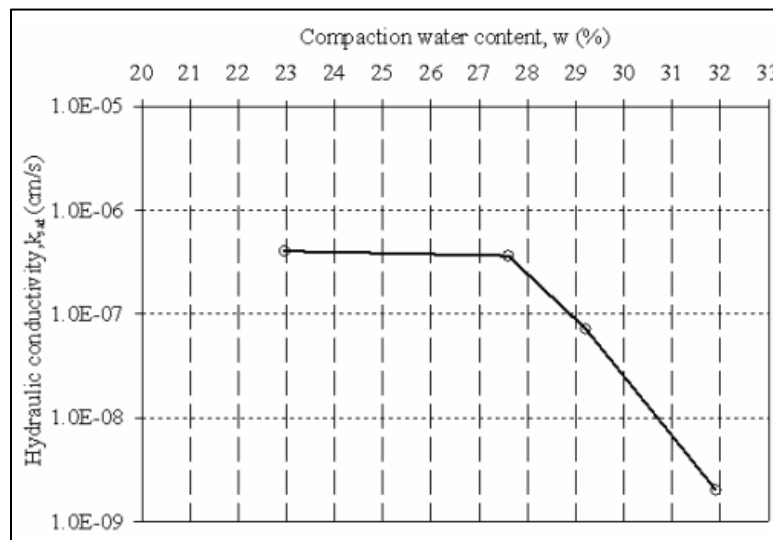
Figure 4.7 Result of hydraulic conductivity test on FM2 clay sample

4.2.2 BASE COURSE MATERIAL PROPERTIES

Base course sample was collected from the Fuqua contractor's yard in Navasota, Texas, which was the base course provider for this project. This material was consistent with the requirements of TxDOT Item 247, Flexible Base, type "A" Grade 1. The base course was transported from the contractor's yard to the geotechnical testing laboratory at UT Austin in two plastic drums of 55 gallon each and characterized by Specific Gravity Test, Grain Size Distribution Test, and Compaction Test, with the results illustrated in Table 4.2, Figure 4.8, and Figure 4.9.

The average specific gravity (G_s) of this material was obtained as 2.68. Using a standard sieve analysis procedure (ASTM D 422), 2000 grams of base course were used to determine the grain size distribution as shown in Figure 8. Values for D_{10}, D_{30}, D_{60}, in addition to the uniformity coefficient (C_u) and the coefficient of gradation (C_c), are shown in Table 2. As per ASTM D 2487, the base course was then classified as silty gravel with sand (GM-ML).

Table 4.2 Characterization of FM2 base course material

Test	Parameter	Results	ASTM Standard
Specific Gravity	G_s	2.68	D 845
Particle Size Analysis	Fine content, %	10 %	D 422
	D_{10}, mm	0.6	
	D_{30}, mm	6.0	
	D_{60}, mm	10.8	
	Uniformity coefficient, C_u	18.0	
	Coefficient of gradation, C_c	5.6	
Standard Proctor Compaction	Optimum Water Content, %	7.5	D 698
	Maximum Dry Unit Weight, γ_d, kN/m^3	22.0	
Soil Classifications	GM-ML		D 2487
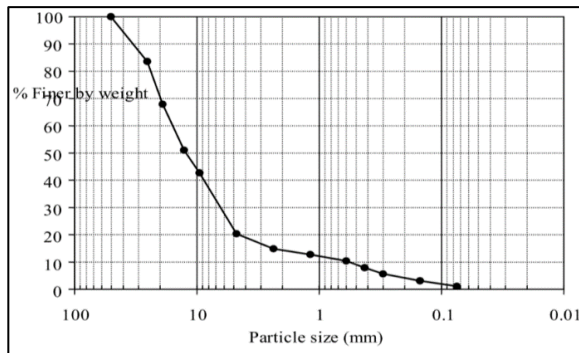
Figure 4.8 Grain Size Distribution curve for base course material used in FM2 project
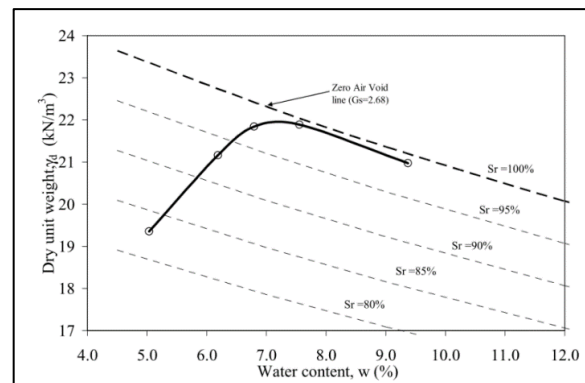
Figure 4.9 Result of compaction test on FM2 base course material

Standard proctor compaction tests (ASTM D 698) were performed on the collected sample from base course materials. The results obtained from tests performed using the standard proctor procedures are summarized in Table 4.2. The curve obtained using the procedure is as shown in Figure 4.9. The optimum water content was found to be 7.5 % and the corresponding maximum dry density was found to be 22 kN/m^3.

4.2.3 GEOSYNTHETIC PRODUCTS PROPERTIES

Three geosynthetic products were used in FM2 project including BX1100 (a biaxial geogrid from polypropylene material manufactured by Tensar Corporation), BasXgrid 11 (a biaxial geogrid from polyester material manufactured by Tencate Mirafi), and HP570 (a woven geotextile from polypropylene material manufactured by Tencate Mirafi). In this project, these products are referred to as GGPP, GGPET, and GT, respectively.

One roll of each geosynthetic product was obtained from the construction site and their index properties (including percent open area, rib thickness, single rib tensile strength, wide width tensile strength, and junction efficiency) were characterized according to TxDOT specifications. Table 4.3 illustrates the results of index testing of geosynthetic specimens as compared to the specifications provided by manufacturers. It was found that most of the property values obtained from index testing are larger or reasonably close to the values provided by manufacturer's specifications.

Table 4.3 Characterization of geosynthetic products used in FM2 project

Property	GGPP		GGPET		GT	
	Manufacturer Spec	Index Tests	Manufacturer Spec	Index Tests	Manufacturer Spec	Index Tests
Ultimate Tensile Strength, kN/m						
a. Machine Direction	12.4	24.6	29.2	22.0	70.0	?
b. Cross Machine Direction	19.0	18.6	29.2	57.9	70.0	
Initial Modulus (at 1% strain), kN/m						
a. Machine Direction	250	368	430	527	?	624
b. Cross Machine Direction	400	531	430	579		829
Tensile Modulus at 2% strain, kN/m						
a. Machine Direction	205	287	365	379	700	614
b. Cross Machine Direction	330	437	365	446	965	744
Tensile Modulus at 5% strain, kN/m						
a. Machine Direction	170	199	270	278	700	520
b. Cross Machine Direction	270	323	270	282	760	533
Tensile Modulus at 10% strain, kN/m						
a. Machine Direction	?	132	?	300	700	487
b. Cross Machine Direction		232		316	700	441
Tensile Modulus at Max Load, kN/m						
a. Machine Direction	?	97	?	289	?	440
b. Cross Machine Direction		226		366		363
Elongation at Break, %						
a. Machine Direction	?	14	?	12	?	19
b. Cross Machine Direction		10		13		20
Junction Strength (kN/m)						
a. Machine Direction	?	28.8	?	5.7	----	----
b. Cross Machine Direction		15.3		7.0		
Junction Efficiency, % of rib ultimate tensile strength	93 %	100 %	?	26 %	----	----
a. Machine Direction		82.6 %		12.2 %		
b. Cross Machine Direction						
Aperture Size, mm	25x33	25x33	25x25	25x33	0.6 (AOS)	----

4.3 PERFORMANCE MONITORING

Two main performance measures have been identified to be the most relevant in characterization of potential benefits from geosynthetic reinforcements. In particular, vertical deflection in the wheel path (rut depth) is identified as the main performance measure under traffic load and environmental longitudinal cracks were identified as the main distress type caused by the swelling and shrinkage of expansive subgrades due to environmental changes. Comparison of the performance of reinforced vs. control test sections with special focus on the two performance

measures can underline benefits and efficiency of the use of geosynthetic reinforcement in the field.

The monitoring program to evaluate the performance of the test sections under traffic loads and environmental conditions included:

- Nondestructive tests including Rolling Dynamic Deflectometer (RDD) and Falling Weight Deflectometer (FWD) to evaluate changes in the mechanical properties of pavement layers
- Installation of moisture sensors in horizontal and vertical arrays to study the moisture migration pattern under the pavement
- Monitoring environmental conditions including precipitation, humidity, and temperature at the site to investigate the effect of the environmental changes in the performance of the road sections
- Periodic condition surveys to identify and quantify the distresses involved in each section and determine the condition of the pavement surface

As a part of this project the results of the condition surveys in relation to traffic loads are evaluated. The condition surveys have been conducted in accordance with the instructions recommended in the TxDOT Pavement Management Information System, Rater's Manual. In particular, the distress data of the field test sections was collected and characterized in the following ten categories recommended by this manual for flexible pavements:

4.3.1 SHALLOW RUTTING AND DEEP RUTTING

Rutting was measured as the percentage of the section's total wheel paths area in different severity levels. While Shallow Rutting is defined as 0.25 to 0.49 inch (6 to 13 mm), Deep Rutting is determined as 0.5 to 0.99 inch (13 to 25 mm). Severe Rutting is referred to rutting as large as 1.0 to 1.99 inches (25 to 51 mm), and Failure Rutting is called to rutting equal to or greater than 2.0 inches (51mm). In this study, rutting of test sections is measured using a 6-foot straight edge and a steel ruler. An example of rutting measurement on FM2 road is illustrated in Figure 4.10.

Figure 4.10 Measurement of a significant rutting during condition survey of the FM2 pavement test sections

4.3.2 ALLIGATOR CRACKING AND BLOCK CRACKING

Alligator (or Fatigue) cracks are irregularly shaped interconnected cracks mainly developed in the wheel paths by the traffic load. Block Cracks are larger in dimensions and divide the pavement surface into almost rectangular shaped blocks. Unlike Alligator Cracking, Block Cracking is mainly caused by non-traffic associated reasons such as shrinkage of the asphalt layer or swelling and shrinkage of the base course layer. According to TxDOT PMIS Rater's Manual, Alligator Cracking should be measured as "the percentage of the rated lane's total wheel path area that is covered by alligator cracking" regardless of the crack width. This manual does not define any severity level for Alligator Cracking. Similar to Alligator Cracking, no severity level has been defined for Block Cracking in the Rater's Manual. Block Cracking should be measured in terms of the percentage of block cracking area out of the total lane's area.

4.3.3 LONGITUDINAL AND TRANSVERSE CRACKING

Since TxDOT PMIS Rater's Manual ignores longitudinal and transverse cracks with width less than 3mm, results presented in this study refer to cracks wider than 3mm. However, during the conditions surveys all cracks, even those cracks less than 3mm wide, have been recorded. This allowed us to better differentiate the performance of the sections and enabled tracking initiation and progress of cracks over time. The cracks are measured in terms of the linear foot of cracking per 100-ft stations, for longitudinal cracking, and the number of cracks per 100-ft stations, for transverse cracking.

4.3.4 PATCHING

Repairs made to cover distresses that appeared on the pavement surfaces are called patches. According to TxDOT PMIS Rater's Manual patching should be measured in terms of the percentage of the patches area with respect to the total area of the lane.

4.3.5 RAVELING AND FLUSHING

Disintegration of the material of the asphalt mix causes the aggregate particles to be exposed on the surface of the pavement. This distress is called Raveling and is measured as the percentage of the rated lane's total surface area that is covered by the raveling. On the other hand, exposure of bituminous material on the surface of the pavement is referred to as Flushing. This distress is measured as the percentage of flushing area out of the total surface area of the pavement.

4.3.6 FAILURES

Areas that are severely distressed are counted as failures. Failures may be caused by extreme rutting or widely opened cracks or even high severity alligator cracking.

4.4 PAVEMENT DISTRESS UNDER TRAFFIC LOADS

The field performance database is reduced to synthesize and evaluate the rut information in FM2 test sections. The rut depth is measured using a 6-ft long straight edge placed across the pavement surface on each wheel path. Then the distance between the straight edge and the pavement surface is measured at the deepest point using a steel ruler. The depth of rut is measured in both wheel paths and at multiple locations along each test section. The distance between rut measurement locations did not exceed 100 ft. In addition, locations with excessive rutting are also marked for careful monitoring.

The average depth of rut for each test section is then obtained by weighted average of the rut depths measured at all locations within that section. This calculation is conducted for the 32 test sections

in FM2 for all condition surveys. In particular, since the rut depth is found to be negligible for most sections before condition survey #14, the analysis presented in this chapter focuses on the data obtained after condition survey #14. Table 4.4 summarizes the rut depth values obtained for both wheel paths of the 32 sections calculated in condition surveys #14 to #21. The test sections are organized in eight design schemes. The last row in each group corresponds to the weighted average depth of rut for all test sections in that group.

The layout of the test sections in the field is presented in Figure 4.11. This figure also illustrates plasticity classes of the subgrade with color-coded mapping.

Table 4.4 Summary of rut depth for the 32 test sections in FM2

Design Scheme	Length	Section Number	AVG Rutting (mm) in White Line (W.L.) Wheel Path						AVG Rutting (mm) in Yellow Line (Y.L.) Wheel Path					
			Survey #14	Survey #16	Survey #17	Survey #18	Survey #19	Survey #21	Survey #14	Survey #16	Survey #17	Survey #18	Survey #19	Survey #21
Control	450	1	0.06	4.00	4.56	4.56	5.89	7.17	0.00	3.89	3.89	3.89	4.17	5.17
	150	10	5.00	11.00	13.33	13.33	14.17	16.00	0.00	9.33	9.33	9.33	9.83	11.00
	450	20	0.11	0.28	3.44	4.22	4.67	8.28	0.00	1.06	1.28	1.44	1.89	3.33
	450	26	16.00	19.33	20.44	21.83	21.97	33.07	7.11	9.22	9.22	10.11	11.61	14.22
	400	27	0.00	2.41	2.41	4.16	4.81	11.53	0.00	4.09	4.09	4.09	4.75	7.38
		AVG	4.22	6.97	8.30	9.18	9.84	15.18	1.68	4.95	5.01	5.26	5.96	7.80
LM	300	6	0.67	2.50	2.83	3.50	3.50	4.25	0.00	5.58	5.58	5.92	6.25	6.33
	450	13	1.19	3.69	3.69	3.69	3.69	4.67	0.00	2.17	2.17	2.17	2.17	3.75
	600	21	1.36	3.03	3.03	3.03	3.11	4.10	0.00	4.00	4.00	4.19	4.35	4.52
	450	31	0.64	2.67	2.67	2.67	2.67	5.78	1.07	5.87	8.79	8.96	9.65	13.83
		AVG	1.02	3.02	3.07	3.18	3.21	4.69	0.27	4.27	5.00	5.16	5.45	6.96
GG PP	450	2	0.83	2.67	2.67	2.67	3.50	6.89	0.00	4.00	4.44	4.44	4.56	8.67
	600	9	5.83	10.92	11.92	12.08	12.08	13.56	2.17	11.33	11.33	11.33	12.29	14.06
	450	17	0.00	0.00	0.00	0.00	0.42	3.26	0.00	0.00	0.00	0.47	0.47	3.13
	500	28	1.63	4.20	4.20	4.88	4.88	7.10	1.56	4.58	4.58	4.58	4.58	4.93
		AVG	2.34	4.93	5.23	5.44	5.73	8.13	1.04	5.44	5.54	5.65	5.96	8.10
GGPP+LM	550	7	1.50	3.27	4.45	4.45	4.45	4.73	0.47	4.82	4.82	4.95	4.95	5.23
	450	8	5.18	7.72	7.72	7.72	8.83	8.83	2.49	5.67	5.94	6.61	6.61	6.61
	450	14	0.22	3.06	3.06	3.06	3.06	3.67	0.00	3.11	3.11	3.11	3.94	4.83
	450	32	0.06	3.50	3.50	3.50	3.50	4.67	0.00	4.72	4.72	4.72	4.72	6.11
		AVG	1.73	4.33	4.67	4.67	4.93	5.43	0.73	4.59	4.66	4.86	5.05	5.67
GGPET	450	3	0.06	3.22	3.22	3.22	3.94	7.56	0.00	5.56	5.56	5.56	5.94	7.39
	350	11	3.21	6.88	7.23	8.28	9.38	14.80	1.44	4.95	5.13	5.13	8.35	9.55
	450	18	0.00	0.00	0.00	0.21	0.21	5.79	0.00	2.53	2.53	3.03	3.44	6.24
		AVG	0.92	3.09	3.18	3.55	4.12	8.95	0.40	4.30	4.35	4.53	5.72	7.58
GGPET+LM	500	5	1.25	3.25	3.25	3.35	4.25	4.95	1.69	5.28	5.28	5.28	6.28	8.20
	450	15	2.89	7.22	7.39	7.39	7.56	8.83	0.00	4.28	4.28	4.28	4.28	5.50
	450	29	1.06	3.11	3.11	4.56	4.56	8.67	0.00	5.78	5.78	6.44	7.11	8.44
		AVG	1.71	4.48	4.54	5.04	5.41	7.39	0.60	5.12	5.12	5.33	5.90	7.41
GT	450	4	0.11	4.50	4.50	5.28	6.17	7.22	0.00	3.33	3.33	3.33	3.78	5.06
	550	12	1.02	5.64	7.86	8.41	8.91	16.59	0.87	5.59	5.68	6.30	7.11	8.61
	450	19	0.00	1.56	4.53	4.81	4.86	9.06	0.00	2.67	3.11	5.42	5.53	10.47
	450	25	13.06	15.89	18.11	21.11	23.06	27.28	7.86	11.11	11.89	11.89	14.83	15.94
		AVG	3.41	6.83	8.70	9.82	10.65	15.12	2.11	5.67	5.99	6.71	7.78	9.95
GT+LM	450	16	0.25	5.36	5.44	5.44	6.11	6.36	0.00	5.31	5.31	5.81	5.81	9.61
	300	22	0.80	2.55	2.55	2.55	2.55	3.08	0.00	2.50	3.00	3.00	3.00	3.00
	300	23	0.00	2.25	2.25	2.25	2.25	3.17	0.00	1.75	2.00	2.00	2.00	2.00
	600	24	5.87	9.19	9.48	9.48	9.48	11.50	0.97	4.60	4.60	5.13	5.21	5.21
	450	30	0.00	2.39	2.39	2.39	2.39	3.28	0.00	5.42	5.42	5.42	5.42	5.86
		AVG	1.85	4.97	5.07	5.07	5.22	6.24	0.28	4.22	4.33	4.58	4.61	5.52

No Reinforcement
GGPP
GGPET
GT

High Expansive — Sections #5,8,9,21,24,25
Medium to High Expansive — Sections #7,10,22,23,26
Medium Expansive — Sections #3,4,6,14,15,16,19,20,30,31,32
Low to Medium Expansive — Sections #1,2,11,12,17,18,28
Low Expansive — Sections #13,27,29

High Expansive — Sections #5,8,9,21,24,25
Medium to High Expansive — Sections #7,10,22,23,26
Medium Expansive — Sections #3,4,6,14,15,16,19,20,30,31,32
Low to Medium Expansive — Sections #1,2,11,12,17,18,28
Low Expansive — Sections #13,27,29
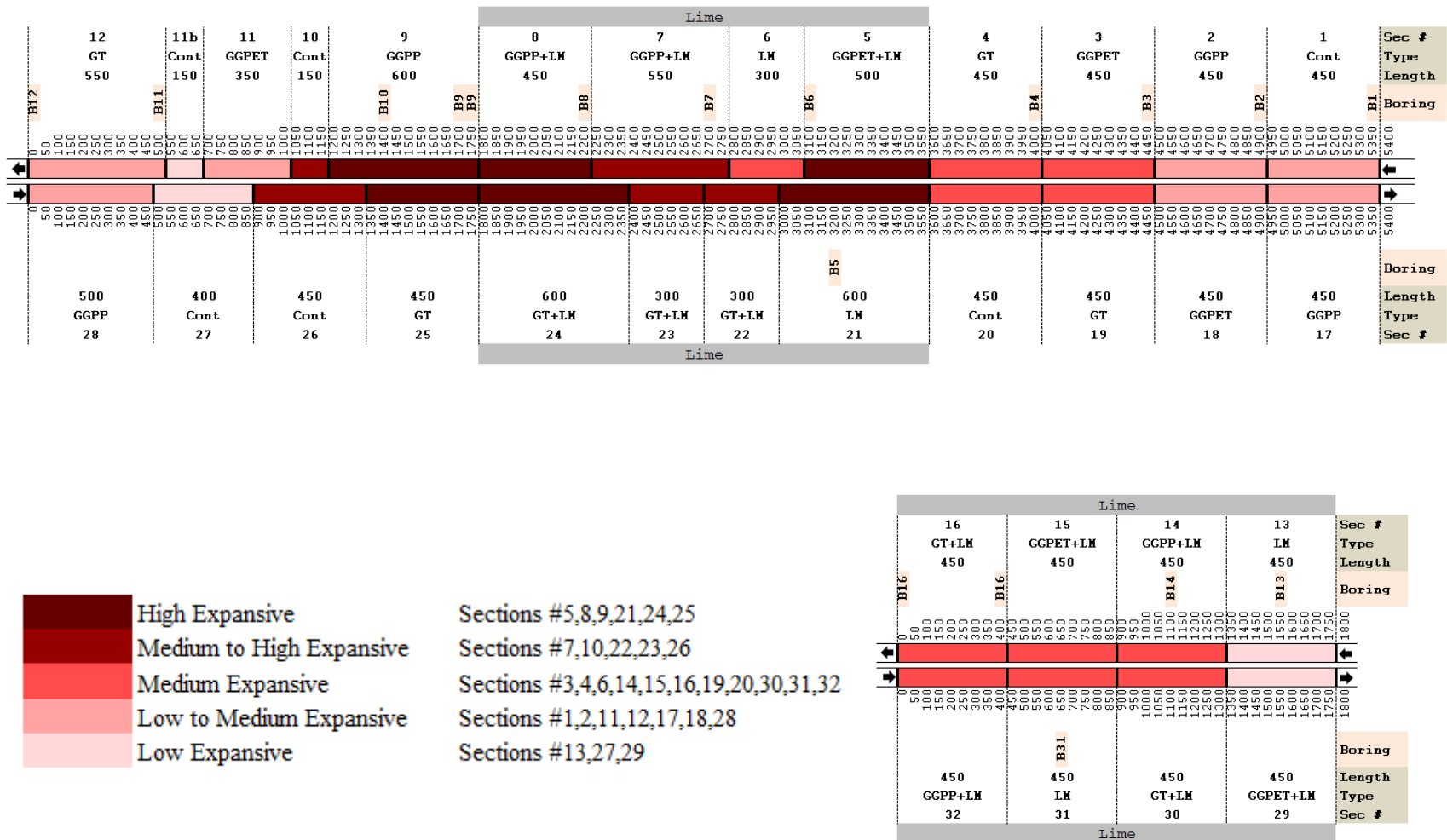
Figure 4.11 Layout of the test sections in FM2 along with color-coded plasticity classes

The development of the depth of rut is evaluated by plotting the rut values over time as illustrated in Figure 4.12 to Figure 4.20. The horizontal axis of these plots corresponds to the time, in days, which is also a representation of traffic volume. Since the rut depth was found to be small for most sections before Survey #14 (Day 1550) the horizontal axis starts slightly before this date. The vertical axis in all the figures corresponds to the depth of rut in mm. As identified in the figures, the rut depth is classified in three groups of shallow, deep, and severe rutting, which, according to TxDOT Rater's Manual, involve rut values below 0.5 inch, between 0.5 and 1 inch, and larger than 1 inch, respectively.

Figure 4.12 illustrates the rut data for individual sections in control and lime-treated design schemes. As listed in Table 4, control sections involve test sections #1, 10, 20, 26, and 27 and the test sections in lime-treated group include sections #6, 13, 21, and 31. Evaluation of the data presented in this figure indicates that while the depth of rut in all lime-treated sections remained in the shallow rut range, two control sections (i.e. Sections #10 and 26) exhibited excessively large rutting. Investigation of the location of these sections in the test section layout, presented in Figure 4.11, indicates that both sections are located in areas with Medium to High plastic subgrade soil adjacent to drainage channel routes. Therefore, the excessive rutting observed in the two sections may be partly caused by highly moist low-strength subgrade in that area.

| a) | Control sections | b) | Lime-treated sections |
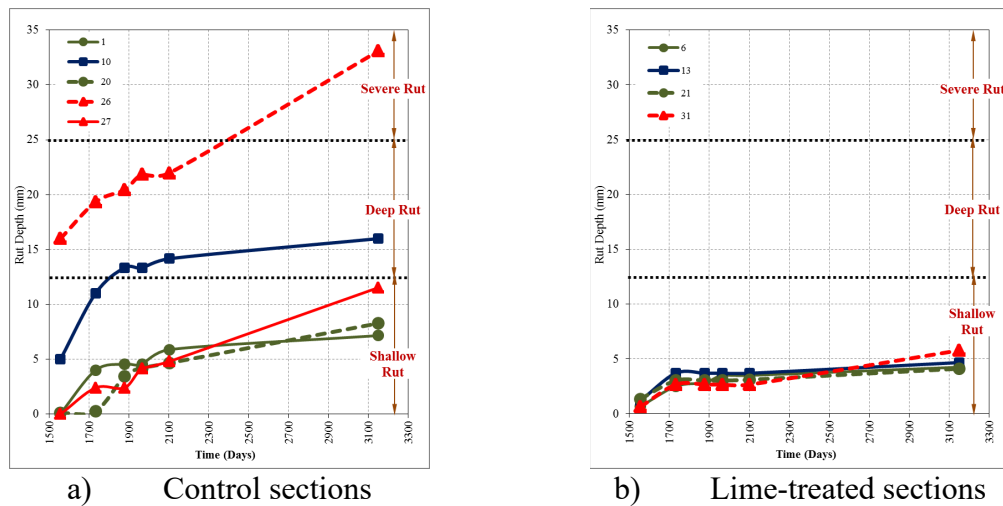
Figure 4.12 Evaluation of rut data for individual sections in control and lime-treated design

Change in the average rut depth over time for all sections in control and lime-treated design schemes are presented in Figure 4.13. The average depth of rut in lime-treated sections remained smaller than 5 mm, while the average rutting measured in control sections exceeded 15 mm, which is categorized as Deep Rut. Overall, it was found that control sections are more prone to excessive rutting than lime-treated sections, particularly in areas where plastic subgrade soil may be accompanied by high moisture content.

Figure 4.14 and Figure 4.15 summarize the rut data for sections designed with the three geosynthetic reinforcement. Comparison between the depths of rut measured for individual sections in each design scheme in Figure 4.14 indicates that, with the exception of one section in geotextile-reinforced group, the development of vertical deflection in the wheel paths was reasonably similar among all geosynthetic-reinforced sections.

46

a)   Control sections   b)   Lime-treated sections

Figure 4.13 Evaluation of the average rut depth for control and lime-treated design
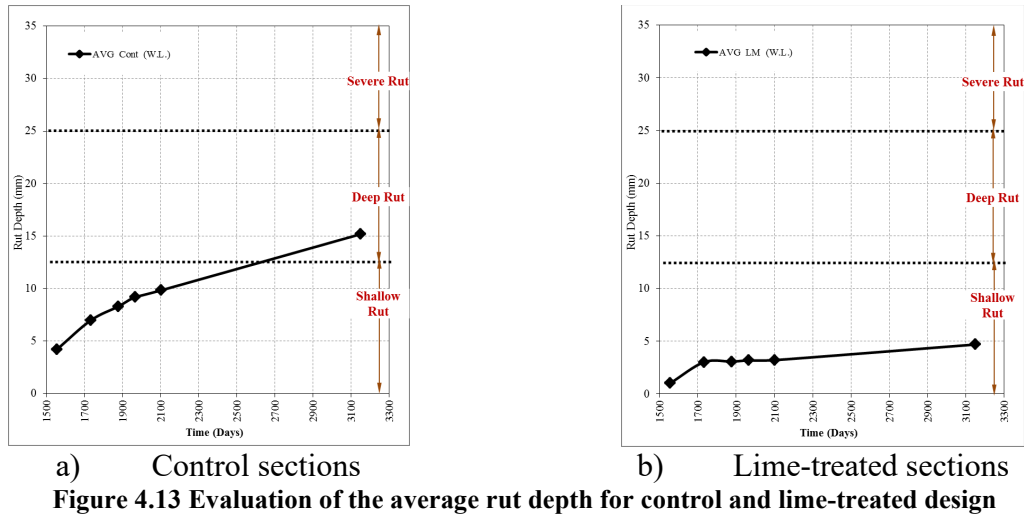
Rutting in most geosynthetic-reinforced sections remained smaller than 10 mm. However, three sections including Sections #9, 11, and 12, have exhibited deep rutting values exceeding 13 mm. Section #25 with geotextile-reinforced design was found to have excessively large rutting categorized as severe rut. Investigation of the location of this section on the layout presented in Figure 4.11 indicates that this section is located adjacent to the severely rutted area discussed for control sections on high plastic subgrade. Therefore, the severe rut measured in this section may also be partly attributed to the low strength subgrade that has been subjected to moisture increase. The poor performance of this geotextile-reinforced section may also be attributed to the deficiencies in construction practices. In particular, it is essential for geosynthetic reinforcement layers to be adequately stretched and be free of wrinkles or folds. Unlike geogrid reinforcements, geotextiles hold very low torsional rigidity that makes them to be particularly vulnerable to construction deficiencies such as wrinkles or folds.

a)   GGPP sections   b)   GGPET sections   c)   GT sections

Figure 4.14 Evaluation of rut data for individual sections in geosynthetic-reinforced design
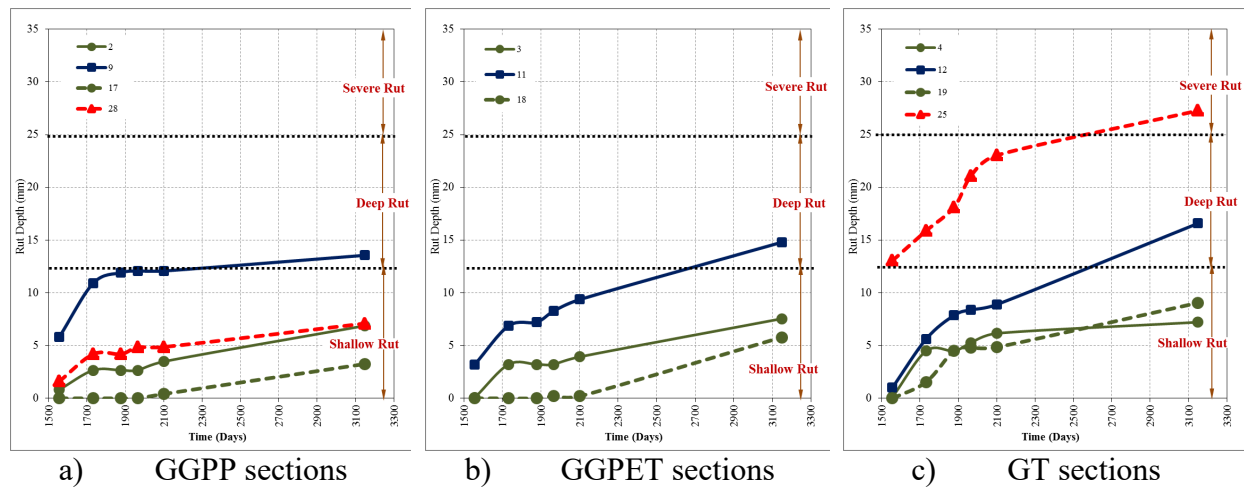
Figure 4.15 presents the average depth of rut for the three geosynthetic-reinforced design schemes. Overall, all three geosynthetics were found to be effective in maintaining the depth of rut reasonably low. The geogrid reinforcements were found to perform slightly better than the geotextile reinforcement in the performance under traffic loading.

47

| a) | GGPP sections | b) | GGPET sections | c) | GT sections |

Figure 4.15 Evaluation of the average rut depth for geosynthetic-reinforced design
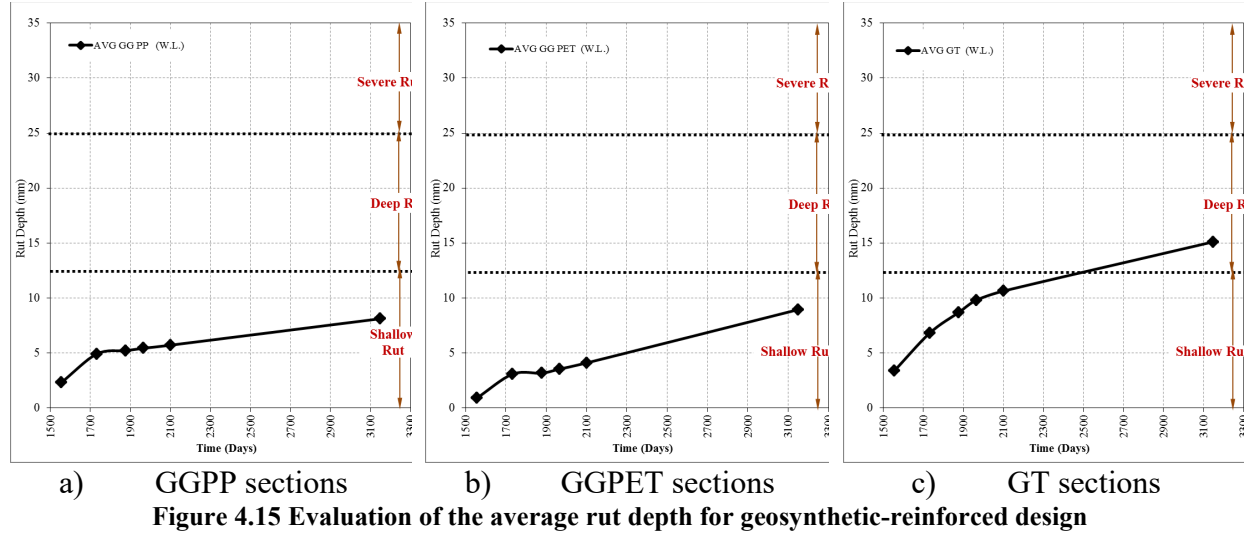
Figure 4.16 and Figure 4.17 present evaluation of the depth of rut for sections constructed with both geosynthetic reinforcement layer in the base course and lime-treatment in the subbase (i.e., GGPP+LM, GGPET+LM, and GT+LM sections). Figure 4.16 illustrates the data for individual sections in each group and Figure 4.17 summarizes the average rut in each group. Evaluation of the curves presented in these figures indicates that the combination of the two methods has been very effective in improving the performance under traffic loading.

| a) | GGPP+LM sections | b) | GGPET+LM sections | c) | GT+LM sections |

Figure 4.16 Evaluation of rut data for individual sections in geosynthetic-reinforced combined with lime-treated design

a)　　　GGPP+LM sections　　b)　　　GGPET+LM sections　　c)　　　GT+LM sections
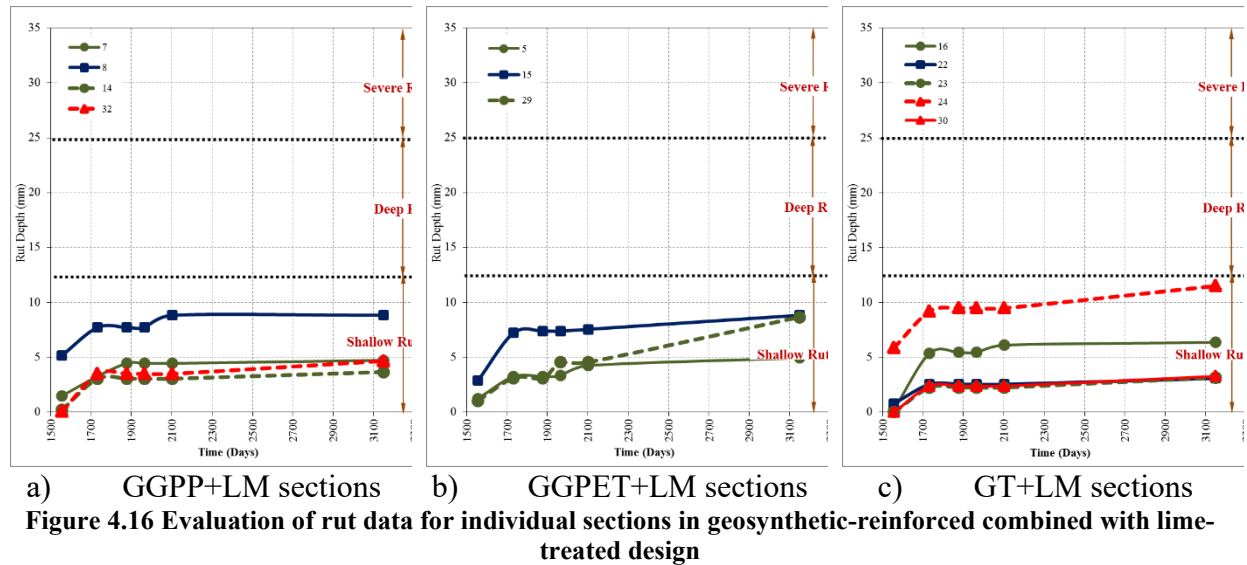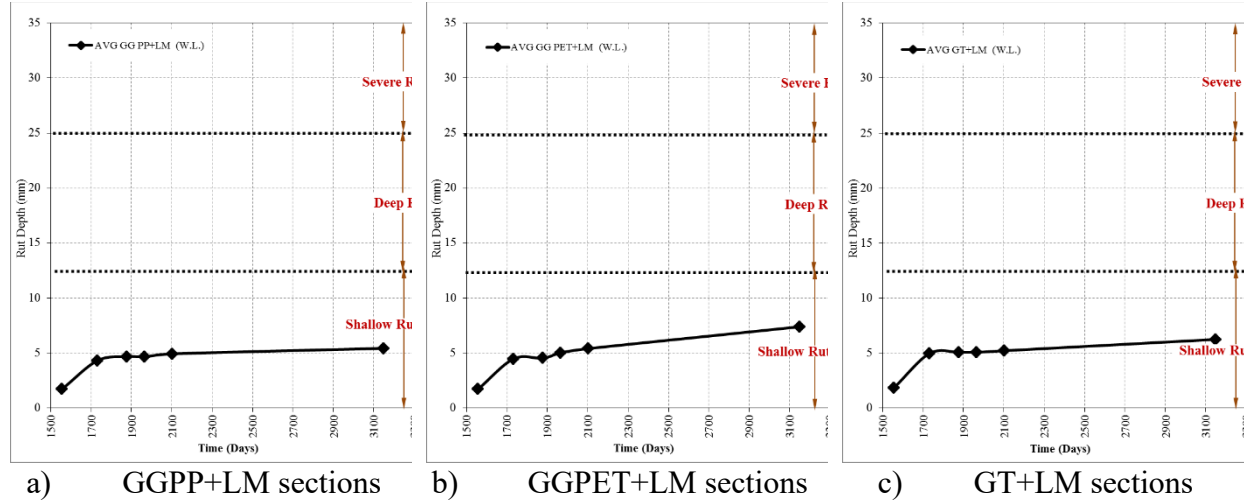
Figure 4.17 Evaluation of the average rut depth for geosynthetic-reinforced combined with lime-treated design

The average depth of rut for the eight design schemes are summarized and re-plotted in Figure 4.18 to Figure 4.20. Figure 4.18 compares the performance of geosynthetic-reinforced sections with control sections. On average, geogrid reinforcements were found to reduce the vertical deflections in the wheel path as compared to control sections. However, geotextile-reinforced sections were found to perform similar to control sections. As discussed before, this may be attributed to deficiencies in construction practices, which particularly affect performance of geotextile reinforcements.

Figure 4.19 and Figure 4.20 illustrate the impact of lime treatment in the subbase on the performance under traffic loading. Evaluation of the curves presented in Figure 4.19 underlines that lime-treated subbase was able to reduce the average depth of rut in the control and the geotextile-reinforced sections. While the average depth of rut exceeded 15 mm without the use of lime, this value did not exceed 7 mm when lime was added to subbase. Figure 4.20 exhibits the difference between the performance under traffic load of the geogrid-reinforced sections (GGPP and GGPET) and that of the geogrid-reinforced and lime-treated sections (GGPP+LM and GGPET+LM). It was found that geogrid reinforcement of base course and lime treatment of subbase are equally effective in maintaining small depth of rut in the wheel path.
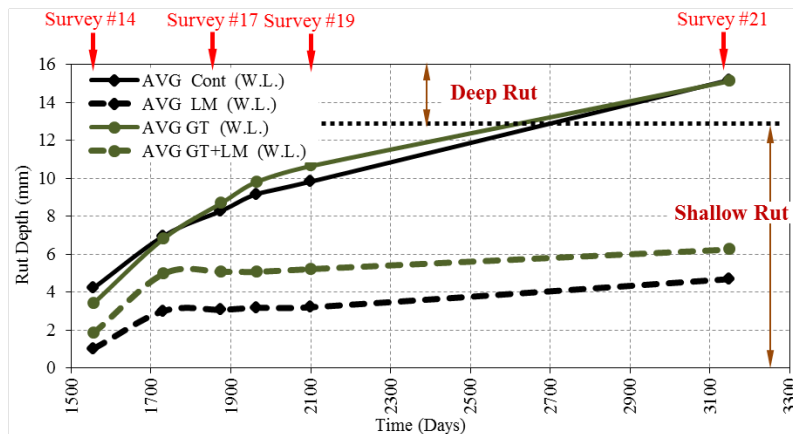
Figure 4.18 Impact of lime treatment on the average depth of rut in control and geotextile-reinforced sections

49
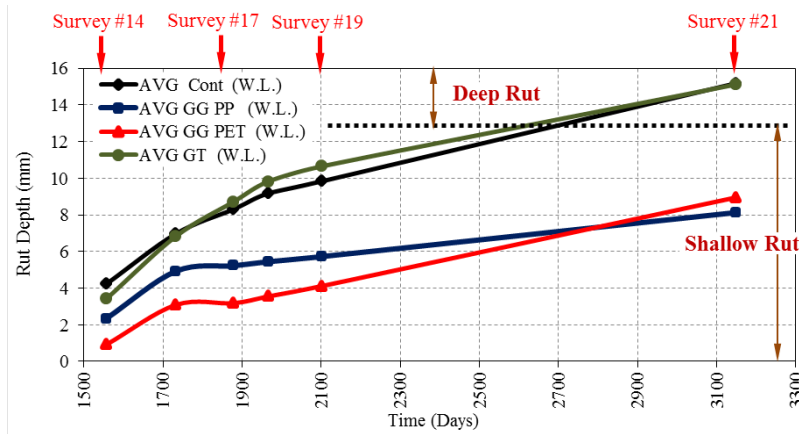
Figure 4.19 Impact of geosynthetic reinforcement on the average depth of rut
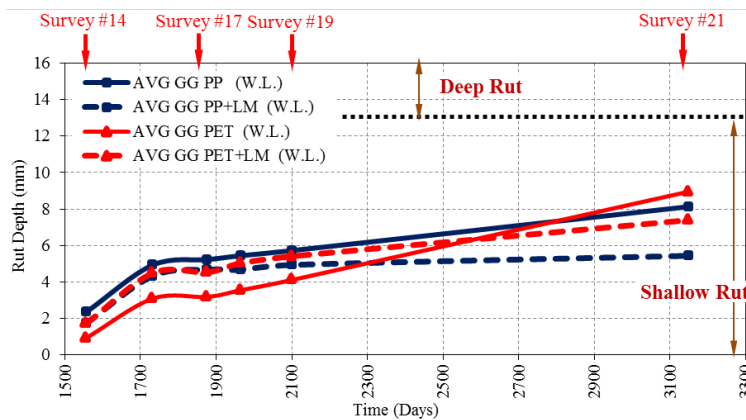
Figure 4.20 Impact of lime treatment on the average depth of rut in geogrid-reinforced sections

4.5 COMPARATIVE PERFORMANCE UNDER TRAFFIC LOADS

Performance of the geogrid-stabilized sections is compared with control sections using traffic benefit ratio (TBR) and rutting reduction ratio (RRR) parameters. The two ratios are obtained at various performance levels over time.

4.5.1 ESTIMATION OF EQUIVALENT SINGLE AXLE LOAD (ESAL)

Rut depths are measured over time during 21 condition surveys conducted from 2006 to 2015 as listed in Table 4.5. Raw rut depth data over time is presented in section 4.4 for condition surveys #14 to #21. In this section, the equivalent single axle load (ESAL) corresponding to the time of each survey is estimated. This estimation is obtained using the data available as part of TxDOT Pavement Management Information System (PMIS) database. Specifically, the data reported as "current-18kip-meas" is used. According to PMIS Data Dictionary Report, "current-18kip-meas" is defined as the ESAL value obtained from Texas road marker (TRM) for the data collection section. One 18-kip ESAL for each 18,000-pound equivalent traffic load projected over a twenty-year period. These values are stored in thousands.

Table 4.5 List of condition surveys conducted at FM2

	No.	Date	Life of the Project (Days)
	Opening of the Road		0
1	SURVEY 1	Aug-06	213
2	SURVEY 2	Nov-06	305
3	SURVEY 3	Feb-07	397
4	SURVEY 4	May-07	486
5	SURVEY 5	Nov-07	672
6	SURVEY 6	Apr-08	837
7	SURVEY 7	Aug-08	963
8	SURVEY 8	May-09	1221
9	SURVEY 9	Jun-09	1272
10	SURVEY 10	Aug-09	1332
11	SURVEY 11	Dec-09	1440
12	SURVEY 12	Mar-10	1525
13	SURVEY 13	Jun-10	1616
14	SURVEY 14	Nov-10	1769
15	SURVEY 15	Feb-11	1882
16	SURVEY 16	Apr-11	1945
17	SURVEY 17	Sep-11	2090
18	SURVEY 18	Dec-11	2179
19	SURVEY 19	May-12	2315
20	SURVEY 20	Nov-12	2519
21	SURVEY 21	Mar-15	3362

Table 4.6 presents the average ESAL values estimated at the location of the test sections at FM2 from 1996 to 2015 from PMIS database. As the reconstructed test sections opened in 2006, the cumulative ESAL values for the test sections were obtained by adding up the ESALs over time.

Figure 4.22 presents the relationship between time (in days) from opening of the experimental test sections to traffic and cumulative ESAL values on the road. Using this plot, the ESAL values correspond to the time of the condition surveys are identified and used in the analysis of the rut data.

The average rut depths measured for control and geogrid-stabilized test sections in condition Surveys #14 to #21 are then plotted versus the cumulative ESAL values correspond to that survey (Figure 3.2)

Table 4.6 Average ESAL values estimated at FM2 from TxDOT PMIS database

Year	ESAL (x 1000) Projected Over a 20-year Period	ESAL (x 1000) Per Year	Cumulative ESAL (x 1000)	Time (Day)
1996	116	5.80		
1997	116	5.80		
1998	111.5	5.58		
1999	61.5	3.08		
2000	84.5	4.23		
2001	84.5	4.23		
2002	185	9.25		
2003	97.5	4.88		
2004	195.5	9.78		
2005	228.5	11.43	0	0
2006	212.5	10.63	10.63	365
2007	155.5	7.78	18.40	730
2008	178	8.90	27.30	1095
2009	117.5	5.88	33.18	1460
2010	221.5	11.08	44.25	1825
2011	343.5	17.18	61.43	2190
2012	201.5	10.08	71.50	2555
2013	201.5	10.08	81.58	2920
2014	185	9.25	90.83	3285
2015	185	9.25	100.08	3650
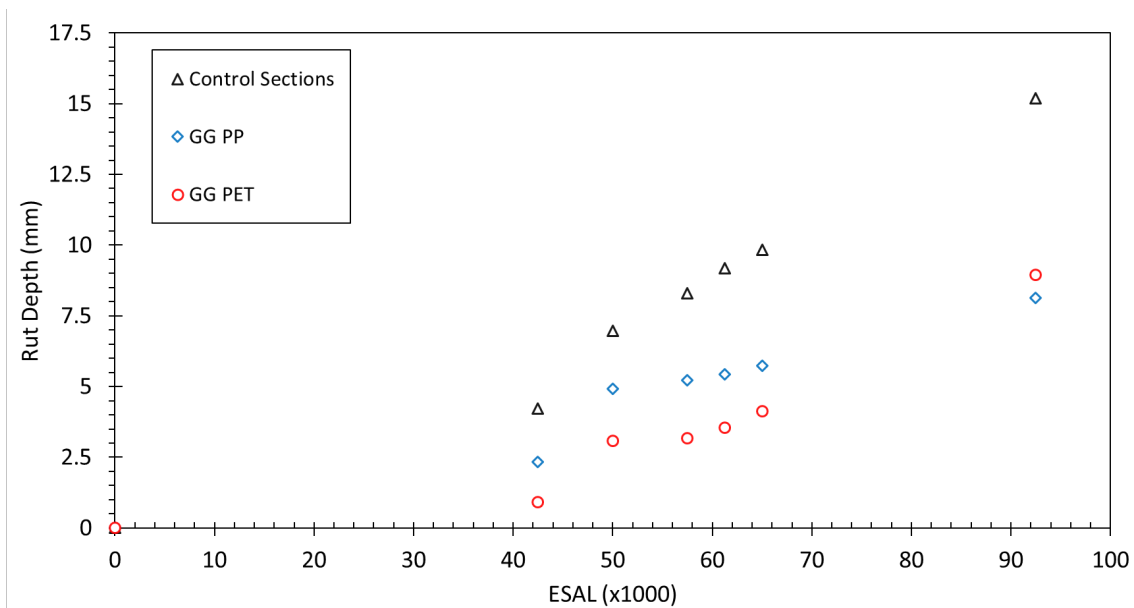
Figure 4.21 Rut depths measured in the test sections constructed at FM2
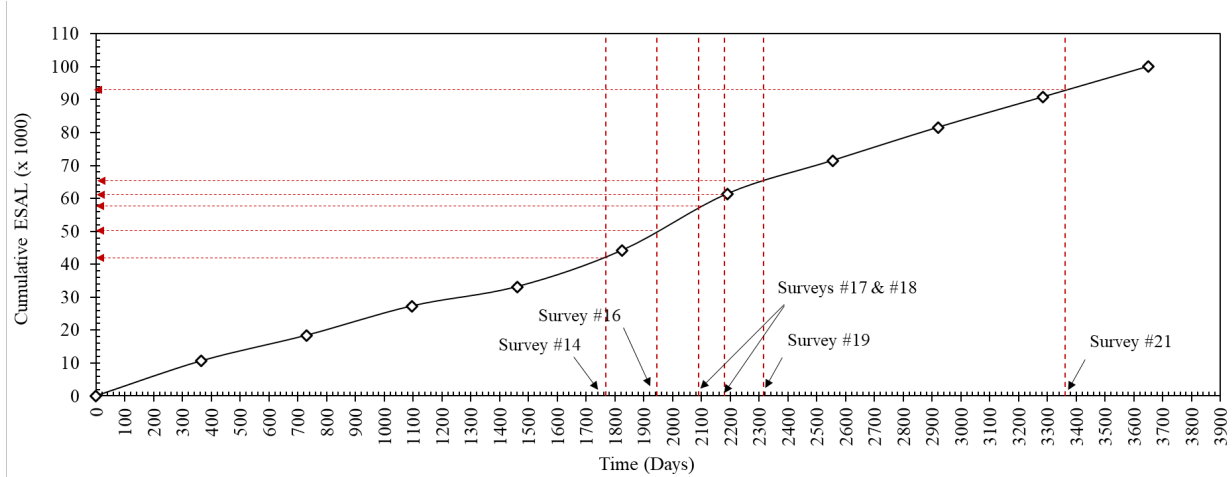
Figure 4.22 Estimation of ESAL values correspond to condition Surveys #14 to #21

4.5.2 COMPARISON OF PERFORMANCE USING TRAFFIC BENEFIT RATIO (TBR)

The traffic benefit ratio (TBR) is defined as a ratio between the number of load cycles in the geogrid-stabilized layer to reach a certain rut depth and the number of cycles in the un-stabilized layer needed to reach the same rut depth:

$$TBR = \frac{\#Cycles_{Geogrid-stabilized}}{\#Cycles_{Control}} (for\ a\ certain\ level\ of\ performance) \qquad (1)$$

TBR value is expected to be higher than one, which indicates that the stabilized section can withstand more ESALs than un-stabilized section.
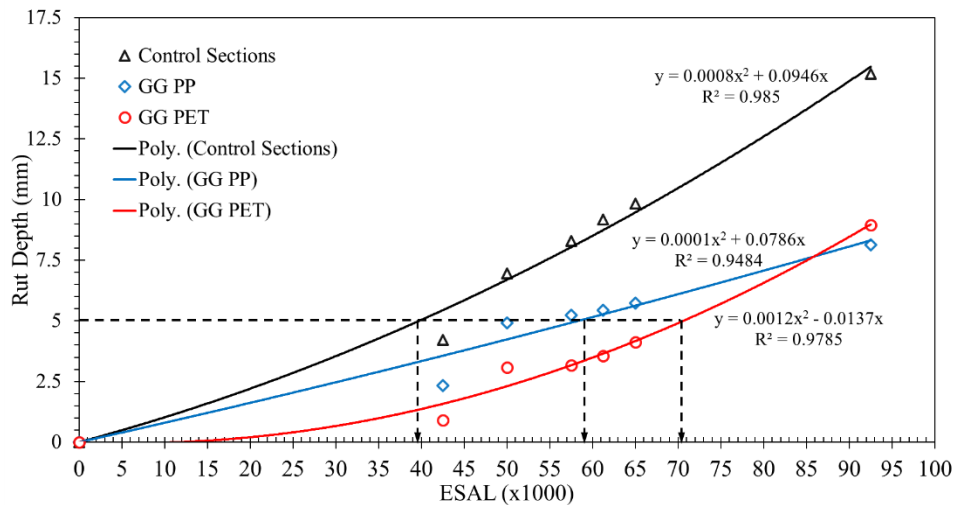
Figure 4.23 Quadratic relationships fitted to the experimental rut depth data and illustration of TBR calculation

53

In order to estimate TBR values at various rut depths, a second order (quadratic) function was fitted to the measured rut depth at FM2 test sections. The equations of the fitted functions are presented in Figure 4.23. It should be noted that since the thickness of the asphaltic surface layer was comparatively small, this layer was not expected to contribute to the structural capacity of the road. Furthermore, as the FM2 road was subjected to environmental loads induced by the expansive clay subgrade, the base layer was expected to degrade over time. Degradation of the base layer resulted from environmental loads, particularly during the drought occurred in 2011, expectedly led to increase in the rate of rutting over time (Figure 4.23).

Table 4.7 Estimation of TBR values for geogrid-stabilized sections at FM2

Rut Depth (mm)	ESAL (x 1000) (Control Sections)	ESAL (x 1000) (GG PP Sections)	ESAL (x 1000) (GG PET Sections)	TBR (GG PP Sections)	TBR (GG PET Sections)
2.5	22.2	30.6	51.7	1.4	2.3
5	39.6	59.2	70.5	1.5	1.8
7.5	54.3	86.0	85.0	1.6	1.6
10	67.3	111.4	97.2	1.7	1.4
12.5	79.2	135.6	107.9	1.7	1.4
15	90.0	158.8	117.7	1.8	1.3
17.5	100.2	181.0	126.6	1.8	1.3
20	109.7	202.4	134.9	1.8	1.2
22.5	118.7	223.0	142.8	1.9	1.2
25	127.3	243.0	150.2	1.9	1.2

As illustrated in Figure 4.23 for an example rut depth of 5 mm, TBR values for geogrid-stabilized sections (GG PP and GG PET) were obtained by the ratio between the ESAL values correspond to the rut depth in the geogrid-stabilized sections and the ESAL value corresponds to the same rut depth in the control sections. Results are presented in Table 4.7. The TBR values are estimated at rut depths ranging from 2.5 to 25 mm. The quadratic functions were used to project the ESAL values at rut depths higher than those measured in each section.

The TBR value was found to range from 1.4 to 1.9 in the test sections stabilized using GG PP and from 1.2 to 2.3 in the test sections stabilized using GG PET.

4.5.3 COMPARISON OF PERFORMANCE USING RUTTING REDUCTION RATIO

The rutting reduction ratio (RRR) is defined as a ratio between the rut depth in the geogrid-stabilized layer after a certain number of load cycles and the rut depth in the un-stabilized layer after the same number of cycles:

$$RRR = \frac{Rutting_{Geogrid-stabilized}}{Rutting_{Control}} (for\ a\ certain\ number\ of\ load\ cycles) \qquad (2)$$

As illustrated in Figure 4.24 for an example ESAL value of 50,000, RRR values for geogrid-stabilized sections (GG PP and GG PET) were obtained by the ratio between the rut depths correspond to the ESAL value in the geogrid-stabilized sections and the rut depth corresponds to

the same ESAL value in the control sections. Results are presented in Table 4.8. The RRR values are estimated at ESAL values ranging from 25,000 to 125,000.
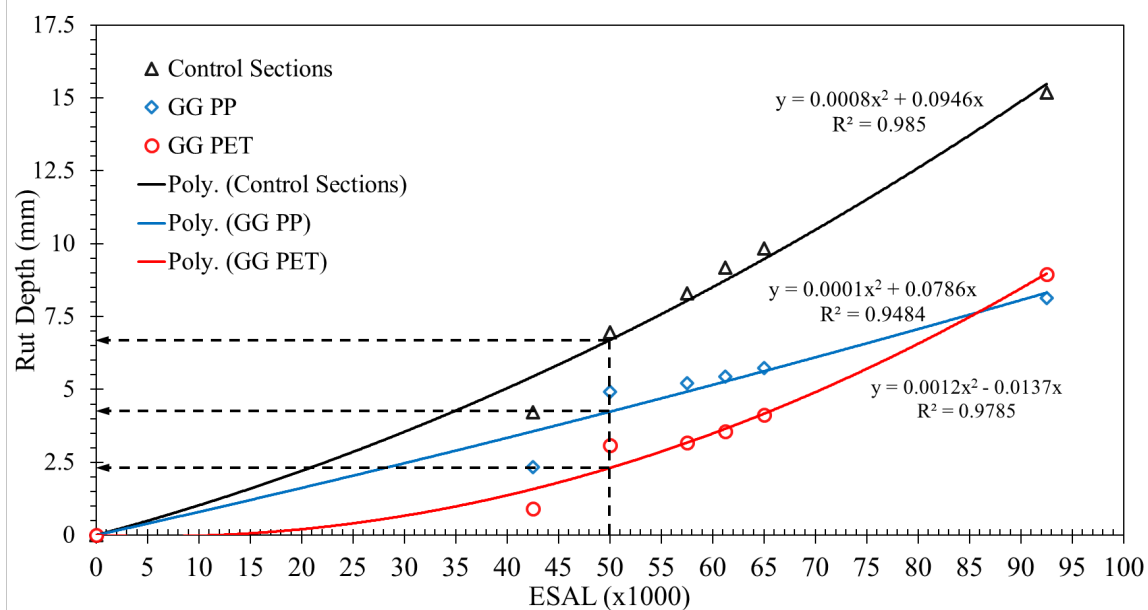
Figure 4.24 Illustration of RRR calculation

The RRR value was found to range from 0.48 to 0.71 in the test sections stabilized using GG PP and from 0.14 to 0.70 in the test sections stabilized using GG PET.

Table 4.8 Estimation of RRR values for geogrid-stabilized sections at FM2

ESAL (x1000)	Rut Depth (mm) (Control Sections)	Rut Depth (mm) (GG PP Sections)	Rut Depth (mm) (GG PET Sections)	RRR (GG PP Sections)	RRR (GG PET Sections)
25	2.9	2.0	0.4	0.71	0.14
50	6.7	4.2	2.3	0.62	0.34
75	11.6	6.5	5.7	0.56	0.49
100	17.5	8.9	10.6	0.51	0.61
125	24.3	11.4	17.0	0.47	0.70

4.6 COMPARATIVE PERFORMANCE UNDER ENVIRONMENTAL LOAD

Performance under environmental loads at the FM2 test sections is evaluated by analyzing longitudinal crack data collected as part of condition surveys. Results obtained are presented in Figure 3.5. The horizontal axis corresponds to the numbers assigned to the test sections and the vertical axis shows the percentage of environmental longitudinal cracks. The test sections were grouped in accordance with their design profiles in Control, GG PP, and GG PET groups. The last bar in each group presents the average percentage of longitudinal cracks for test sections in that group. Geogrid-stabilized sections were found to perform significantly better than the control sections. While the average percentage of longitudinal cracks were found to be below 30 % in the

geogrid-stabilized sections, the average percentage of longitudinal cracks in the control sections exceeded 85 %. On average, the test sections constructed using the two different geogrids (GG PP and GG PET) showed similar performance.
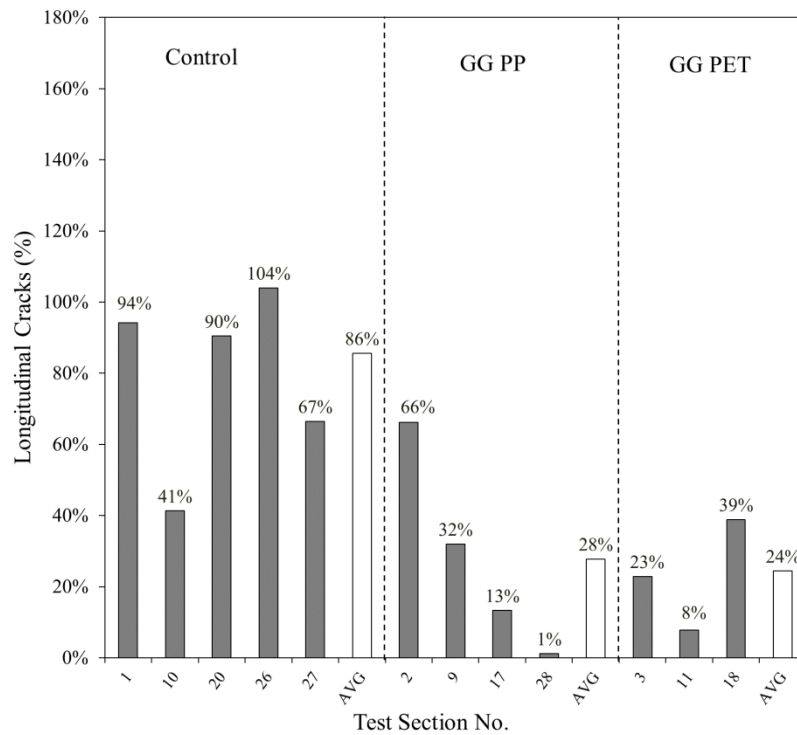
Figure 4.25 Percentage of environmental longitudinal cracks at FM2 test sections

5.   ACCELERATED PAVEMENT TESTING

The Accelerated Pavement Testing (APT) program devised as a part of this project is aimed at assessing the performance of geogrid-reinforced pavements (GRPs) under different conditions and design. This is done to understand the structural response of the GRPs under traffic loads on a reduced-scale, and determine the mechanisms associated with the enhancement of traffic performance by geogrid reinforcement. In order to achieve these goals 26 different test sections are constructed in various configurations and trafficked with the model mobile load simulator 3 (MMLS3) to assess their structural response. It is found that traffic performance enhancement facilitated by the presence of geogrid within the base layer is a function of numerous variables. The details of the findings are summarized in the following sections of this report.

5.1   MATERIAL CHARACTERIZATION

Asphaltic surface layer materials, base materials and subgrade materials used in the various test sections of the APT program are discussed in this section. Table 5.1 summarizes all the pavement materials that have been used in this project. Each material is identified by a unique codename as shown in the Table 5.1 and henceforth be referred to with the codename in this report.

Table 5.1 Summary of Codenames of Materials Used

Codename	Material
HMA Layer	
AC1	Thin Overlay Mix – Type A
AC2	Dense Graded Asphalt – Type D
AC3	Stone Matrix Asphalt – Type D
Base Layer	
BS1	River Washed Pea Gravel (conforming to AASHTO #8 Gradation)
BS2	Cemex Flex Base – Grade 2
Subgrade Layer	
SG1	Monterey Sand
SG2	Aquafoam
SG3	Steel
Geogrid	
GG1	Tensar BX1100
GG2	Tensar TX160
GG3	Enkagrid Colbond Max20
GG4	Mirafi BasXGrid 11
GG5	Synteen SF11
GG6	Huesker Fornit20
GG7	Naue Secugrid 30/30
GG8	Tensar TX130s
NGS	without geosynthetic

5.1.1 SURFACE LAYER (HMA LAYER)

The grain size distribution of the aggregates used in the various asphalt mixtures are shown in Figure 5.1 to Figure 5.2. The properties of the constituents and the mix are shown in Table 5.2.

Thin Overlay Mix – Type A (AC1)

Dense Graded Asphalt – Type D (AC2)

Stone Matrix Asphalt – Type D (AC3)
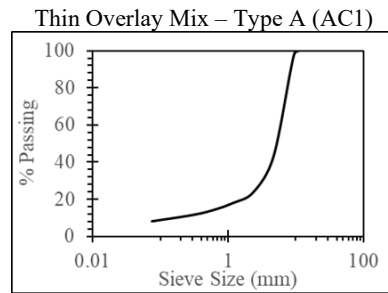
Figure 5.1 Grain Size Distribution in AC1
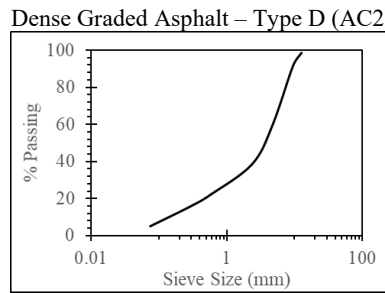
Figure 5.2 Grain Size Distribution in AC2
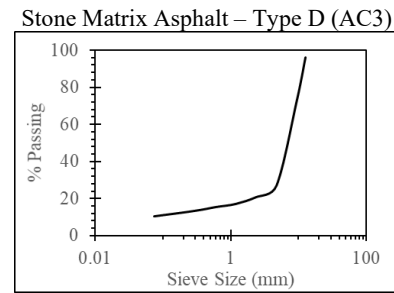
Figure 5.2 Grain Size Distribution of AC3

Table 5.2 Properties of ACs

	AC1	AC2	AC3
Aggregate			
Specific Gravity	2.232	2.346	2.272
Binder			
Grade	PG 76-22	PG 70-22	PG 76-22
Specific Gravity	1.04	1.037	1.041
Asphalt Mixture			
Binder Content	6.50%	5.30%	6.80%
Maximum Density	2.394	2.419	2.349

5.1.2 BASE LAYER (UNBOUND GRANULAR LAYER)

5.1.2.1 River-washed Pea Gravel (BS1)

The baseline base-course material to be used in the series of test section is the 3/8" clean river-washed pea gravel, which conforms to AASHTO #8 soil, from Martin Marietta (Location - Figure 5.3). The unconventional choice of a clean base arises from two prime reasons. Firstly, this material has been extensively tested alongside other geosynthetics and their interaction properties are well characterized. This means direct comparisons between the performance of different geosynthetics in the APT program and that from the pull-out experiments is possible. Secondly, the use of a clean base ensures consistent of the base layer in terms of its strength and stiffness across control section and sections reinforced with geosynthetics. This eliminates any error that creeps into the results as a consequence of variability of stiffness with compaction effort, moisture content, etc. Thus, despite the inherent shortcoming of using an unconventional base material is overcast by the potential crucial benefits essential for meeting the objectives of the project.
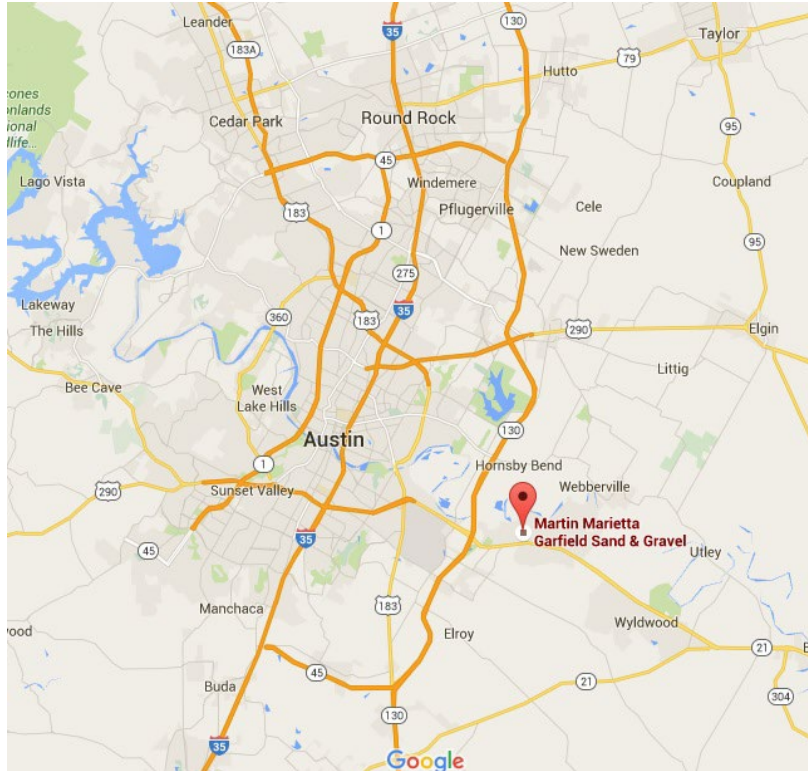
Figure 5.3. Location of Acquired River-washed Pea Gravel

Grain Size Distribution
Using the standard sieve analysis procedure, the River-washed Pea Gravel was used to determine the grain size distribution as shown in Figure 5.4. Values for D_{10}, D_{30}, and D60 in addition to the uniformity coefficient and the coefficient of gradation are shown in Table 5.3.

Specific Gravity
The average specific gravity (Gs) of the River-washed Pea Gravel was obtained as 2.65.

Atterberg Limits
Atterberg limits were not determined since the River-washed Pea Gravel had no fines.

Soil Classification
Based on the grain size distribution data presented in Table 5.3 and Figure 5.4. The values of Cc and Cu are calculated as shown in Table 5.3. As per ASTM D 2487, the River-washed Pea Gravel is classified as Poorly graded Gravel.

Maximum and Minimum Void Ratios
The minimum void ratio or maximum index density of the River-washed Pea Gravel was determined in accordance with ASTM D 4253. Also, the maximum void ratio or minimum index density of the River-washed Pea Gravel was determined in accordance with ASTM D 4254. The values of e_{min} and e_{max} are listed in Table 5.3.
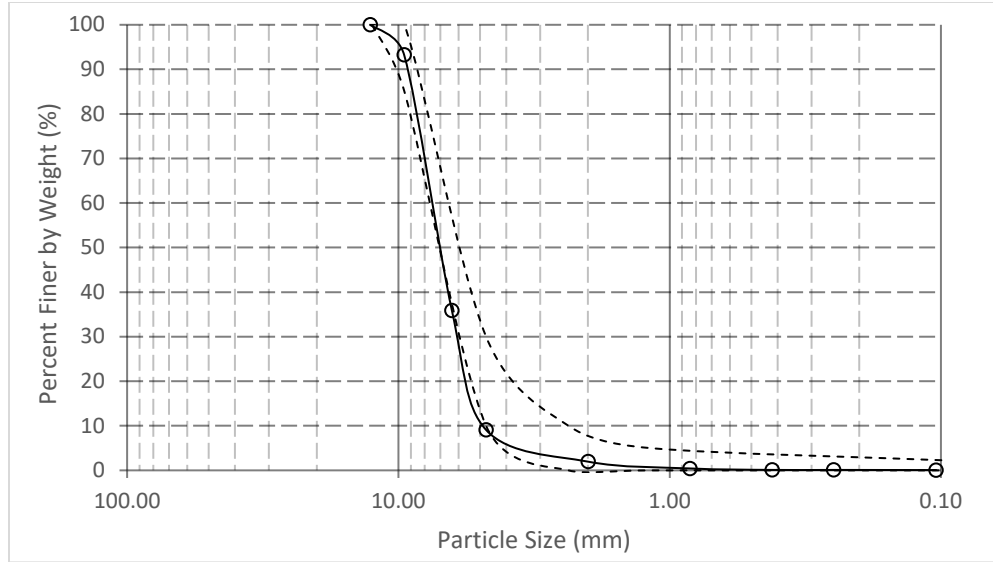
Figure 5.4. Grain Size Distribution of River-washed Pea Gravel

Table 5.3. Properties of River-washed Pea Gravel

Test	Index Parameter	Value	ASTM Standard
Soil Classification		GP	D 2487
Specific Gravity	Specific Gravity, G_s	2.65	D 854-14
Grain Size Distribution	D_{10} (mm)	4.8	D 422
	D_{30} (mm)	6.1	
	D_{60} (mm)	7.5	
	C_u	1.6	
	C_c	1.0	
Minimum Void Ratio	e_{min}	0.54	D 4253
Maximum Void Ratio	e_{max}	0.73	D 4254

Shear Strength
Results from the tri-axial tests conducted under different levels of confining pressure are used to determine the shear strength properties of BS1. The results are shown in Figure 5.5. From the results it is determined that the angle of internal friction of BS1 is 37^0 and apparent cohesion is negligible (~ 2 psi). The resulting stress-strain curves are modeled using the Duncan-Chang Hyperbole model. The modulus parameter, K = 425 psi and exponent parameter, n = 0.6123.

60
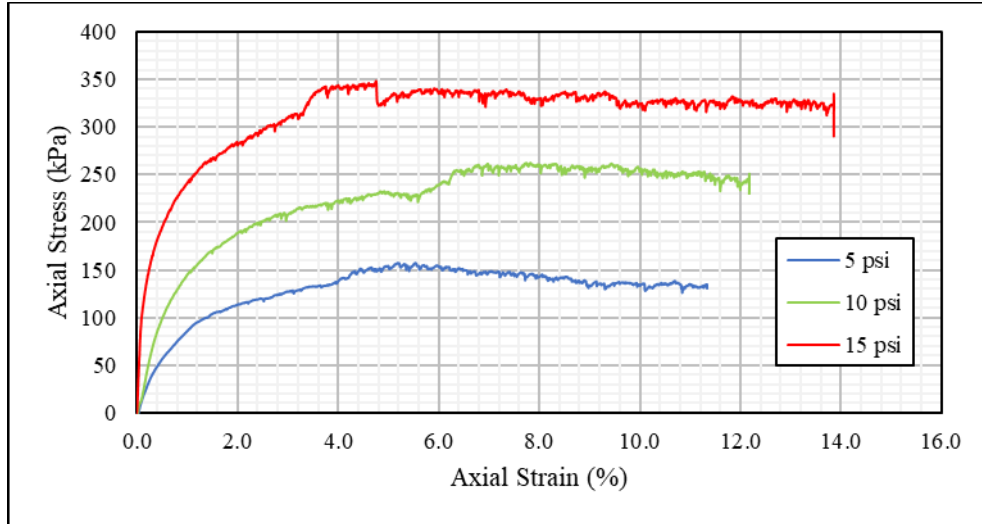
Figure 5.5 Results of Tri-axial Tests on BS1

5.1.2.2 Cemex Flex Base – Grade 2 (BS2)

The Cemex Flexible Base Gravel is a grade 2 Flexible Base gravel material available at the Balcones Quarry, just south of New Braunfels on Interstate 35 (Figure 5.6).
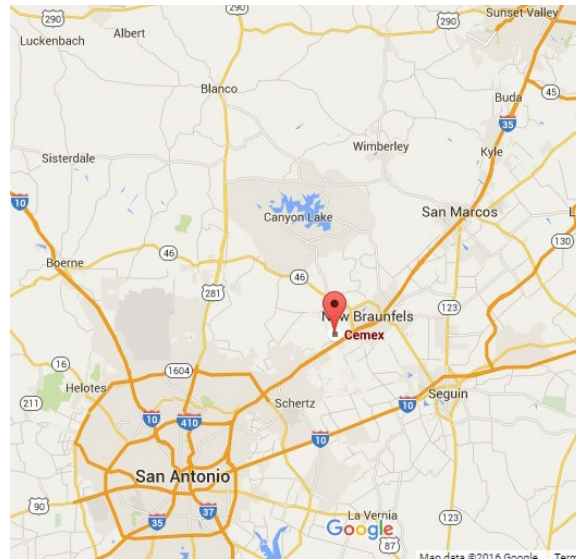
Figure 5.6. Location for Acquiring Cemex Flexible Base Gravel

Grain Size Distribution

Using the standard sieve analysis procedure, the Cemex Flexible Base Gravel was used to determine the grain size distribution as shown in Figure 5.7. Values for D_{10}, D_{30}, and D60 in addition to the uniformity coefficient and the coefficient of gradation are shown in Table 5.4.

Specific Gravity

The average specific gravity (G_s) of the Cemex Flexible Base Gravel was obtained as 2.65.

61

Atterberg Limits

Atterberg limits were determined according to ASTM D 4318 for the fines of the Cemex Flexible Base Gravel. The values for plastic limit, liquid limit and plasticity index are reported in Table 5.4.

Soil Classification

Based on the grain size distribution data presented in Table 5.4 and Figure 5.7, the values of C_c and C_u were calculated as shown in Table 5.4. As per ASTM D 2487, the Cemex Flexible Base Material is classified as Silty, Clayey Gravel (GC-GM).
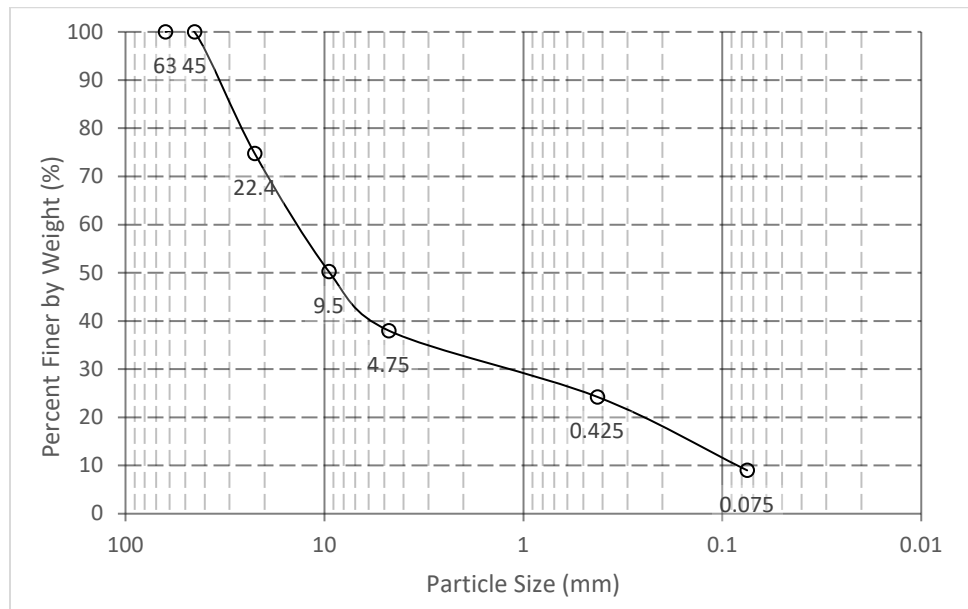
Figure 5.7. Grain Size Distribution of Cemex Gravel

Maximum Dry Density and Optimum Moisture Content

Standard Proctor compaction tests (ASTM D 698) were performed on the Cemex Flexible Base Gravel. The results obtained from the tests performed using the standard proctor procedure are summarized in Table 5.4. The curve corresponding to the procedure is plotted in Figure 5.8. The optimum moisture contents, in addition to maximum dry densities are presented in Table 5.4.
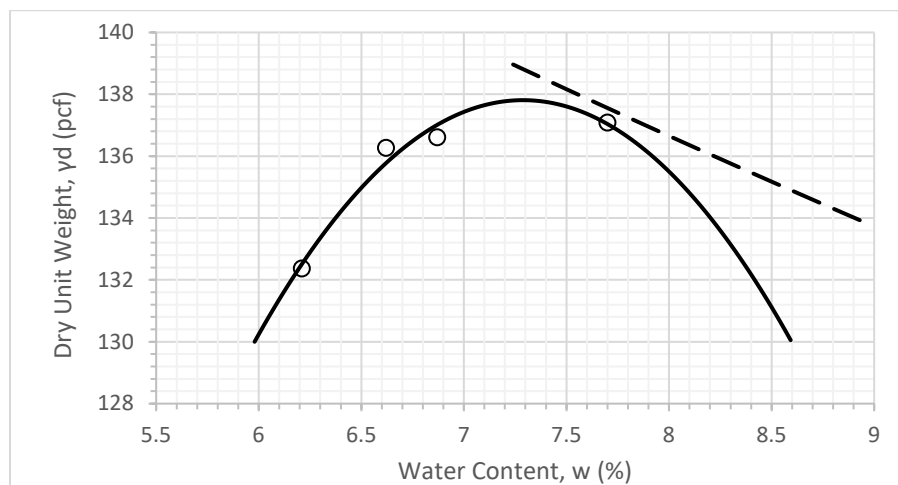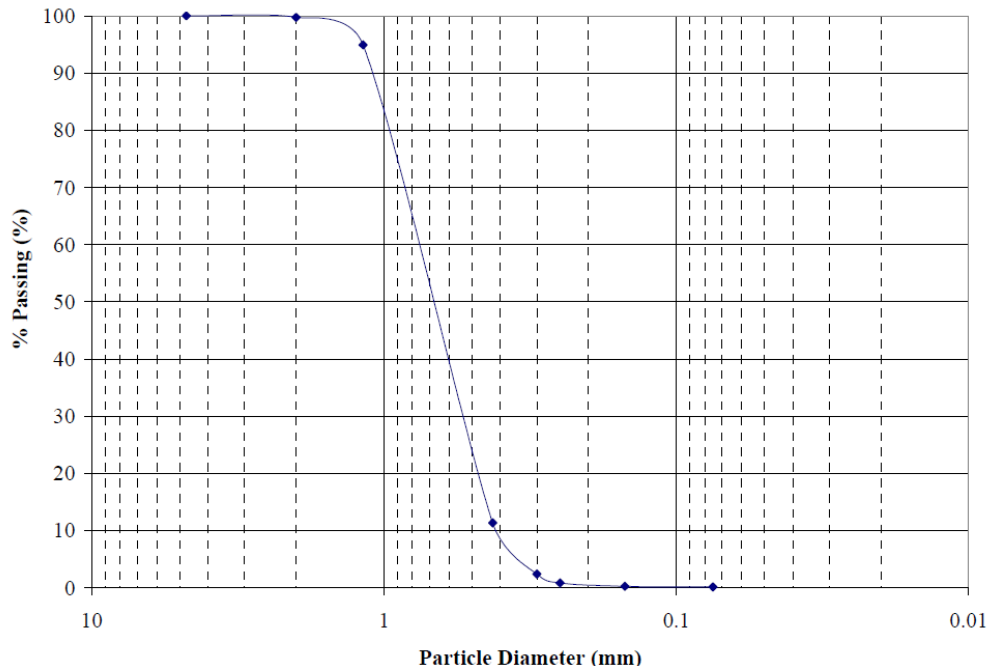
Figure 5.8. Compaction Characteristics of Cemex Gravel

62

Table 5.4. Properties of Cemex Gravel

Test	Index Parameter	Value	ASTM Standard
Soil Classification		GC-GM	D 2487
Specific Gravity	Specific Gravity, G_s	2.65	D 854-14
Grain Size Distribution	D_{10} (mm)	0.08	D 422
	D_{30} (mm)	1.3	
	D_{60} (mm)	14	
	Cu	175	
	Cc	1.51	
Atterberg Limits	Liquid Limit, LL (%)	20	D 4318
	Plastic Limit, PL (%)	15.5	
	Plasticity Index, PI (%)	4.5	
Standard Proctor Compaction	Optimum Moisture Content, OMC (%)	7.3	D 698
	Maximum Dry Density, γ_d (pcf)	137.8	

5.1.3 SUBGRADE LAYER

5.1.3.1 Monterey Sand (SG1)

SG1 is a clean uniformly graded sand, commercialized as Monterey No. 30 sand. It also classifies as SP according to the unified soil classification system. The sand particles are rounded to sub-rounded, consisting of mainly quartz with a small amount of fledspars and other minerals. The average diameter, D_{50}, is 0.7 mm and the specific gravity is 2.655. Based on the gradation curve, as shown in $\Leftrightarrow$, the coefficient of uniformity is 1.8 and the coefficient of curvature is approximately 1.0. The maximum and minimum void ratios are 0.76 and 0.56, respectively.
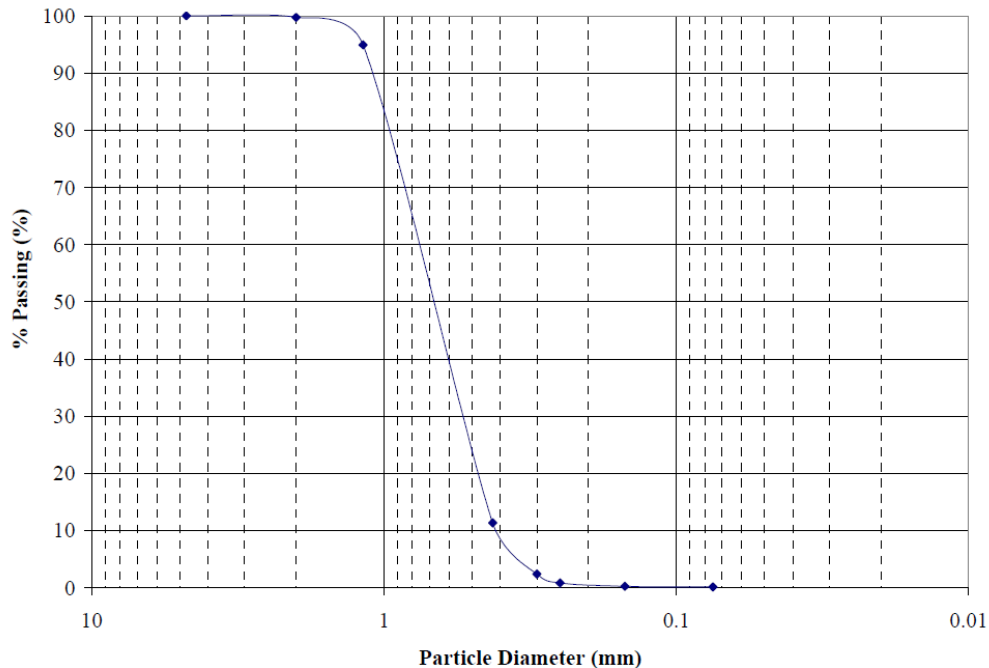
Figure 5.9 Grain Size Distribution of SG1

The results of large-scale triaxial tests (12" x 6") performed to study the shear strength of SG1 are available. The tests were conducted on specimens with relative densities of 48% and 65% (R_D used in the APT program). Figure 5.10 shows the stress-strain curve obtained from the triaxial tests. The test results show that the strain at peak deviatoric stress decreases with increasing relative density of soil. The stresses at large strain levels seem to converge to the same value, although the specimens may not have been tested to strains that are large enough to achieve critical state. The friction angles corresponding to relative densities of 48% and 65% are 31.6° and 35.2°, respectively. The residual friction angle is 31°. The mechanical properties are summarized in ◇.
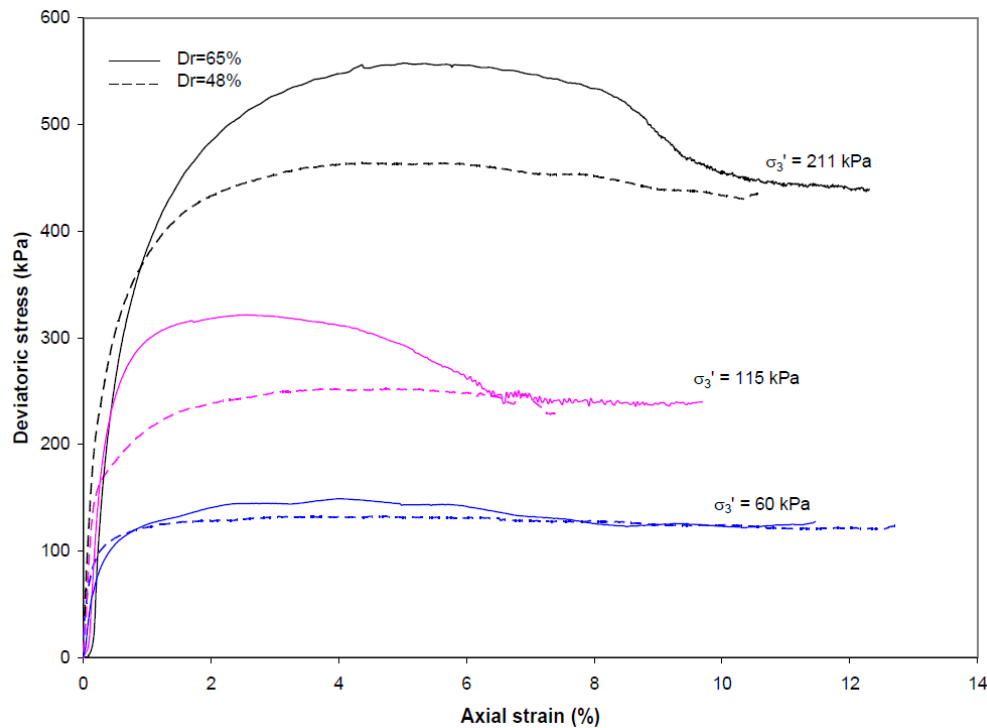
Figure 5.10 Stress-strain curves for SG1

Table 5.5 Properties of SG1

Dr (%)	48	65
γ_d (kN/m^3)	15.54	15.91
ϕ' (°)	31.6	35.2
c (kPa)	0	0

5.1.3.2 Aquafoam (SG2)
Aquafoam (Figure 5.11) is a synthetic foam made from phenol resins generally used in horticulture for their water retaining characteristics and porous structure. However, they are also highly plastic material that can conform and retain any plastic deformation that they are subjected to upon loading and unloading. This peculiar character and their porous nature make them a viable candidate for simulating soft clays. The key advantage is that since these are manufactured materials, their properties are likely to remain consistent across samples (better quality control). Since the material is not used for engineering applications, its mechanical properties have not been characterized so far.

64
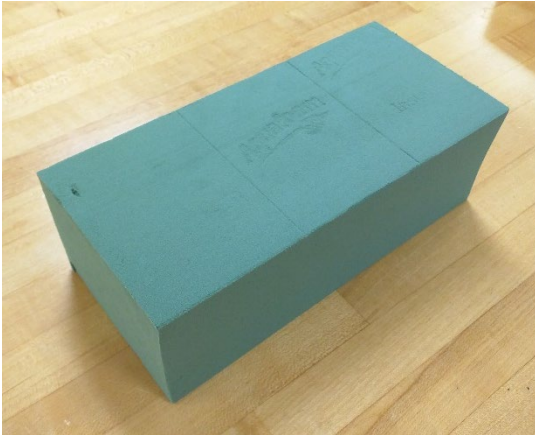
Figure 5.11. Aquafoam
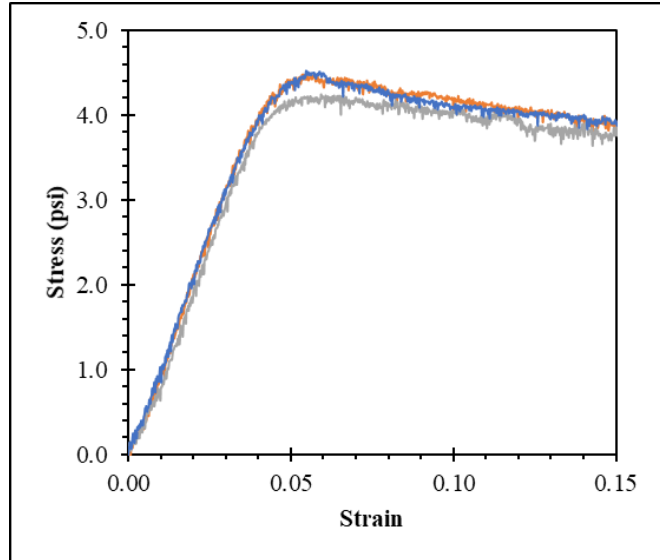
Figure 5.12 Stress-strain behavior of SG2

The stress-strain behavior of unconfined Aquafoam is shown in Figure 5.12. Three repeats of the test are conducted, and it is seen that results are highly repeatable, stemming from the fact that the product is factory manufactured and has very low variability. It is determined the modulus of the materials is 102.3 psi. The failure stress, under unconfined conditions, is 4.4 psi. Thus, the Aquafoam could be used to simulate very soft clay material (CBR < 1.0)

5.1.4 GEOGRIDS

5.1.4.1 Tensar BX1100 (GG1)

BX1100 is a biaxial polypropylene geogrid manufactured by Tensar Corporation (Figure 5.13). It has been very well characterized and has been used in a number of projects including TxDOT 0-4829, TxDOT 5-4829 and SH21 (Location 2). As a result of the immense familiarity the research team has with this product, BX1100 is be used as the baseline geogrid reinforcement in the project, TxDOT 0-6834.
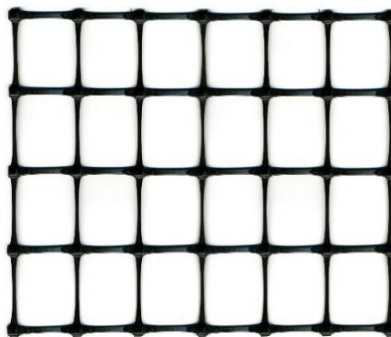
Figure 5.13. Tensar BX1100

Index Property Specifications:

Table 5.6. Index Properties of BX1100

Characteristics			Units	MD	CD
Mechanical Properties	**Tensile Strength - ASTM 6637 (Geogrids) - ASTM 4595 (Geotextiles)**	**@ 0.5% Strain**	**kN/m (lb./ft)**	-	-
		@ 2% Strain	**kN/m (lb./ft)**	4.1 (280)	6.6 (450)
		@ 5% Strain	**kN/m (lb./ft)**	8.5 (580)	13.4 (920)
		Ultimate	**kN/m (lb./ft)**	12.4 (850)	19.0 (1,300)
	Junction Efficiency (%)		**(%)**	93	-
	Flexural Stiffness		**mg-cm**	250,000	-
Geometric Properties	**Aperture Dimensions**		**mm (in)**	25 (1.0)	33 (1.3)
	Minimum Rib Thickness		**mm (in)**	0.76 (0.03)	0.76 (0.03)
	Rib Width		**mm (in)**	3.2 (.125)	3.2 (.125)
Polymer Type			Polypropylene		
Manufacturing Process			Integrally Formed Biaxial Geogrid		

Interaction Properties
(from small pullout test results)

Table 5.7. Stiffness of Soil-Geosynthetic Interaction for BX1100

Soil Type	Direction of Testing	Normal Pressure	
		3 psi	**5 psi**
3/8" Aggregate	**CD**	13.72	20.3
	MD	13.2	23.1

5.1.4.2 Tensar TX160 (GG2)

TX160 is manufactured from a punched polypropylene sheet, oriented in three substantially equilateral directions. This triaxial polypropylene geogrid is manufactured by Tensar Corporation. The interaction of a triaxial geogrid, as opposed to a biaxial geogrid, with the base material is expected to produce some interesting mechanisms which the research team intends to capture as part of TxDOT 0-6834. Hence the choice of TX160 as one of the alternative geogrids.
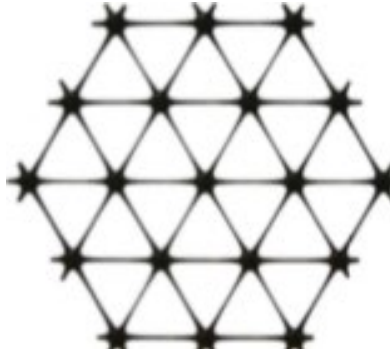
Figure 5.14. TriAx TX160

Index Property Specifications

Table 5.8. Index Properties of TX160

Characteristics		Units	Longitudinal	Diagonal	Transverse	General
Geometric Properties	**Rib Pitch**[1]	**mm (in)**	40 (1.60)	40 (1.60)	-	-
	Mid-Rib Depth[1]	**mm (in)**	-	1.6 (0.06)	1.4 (0.06)	-
	Mid-Rib Width[1]	**mm (in)**	-	1.0 (0.04)	1.2 (0.05)	-
	Aperture Shape	**-**	-	-	-	Triangular
Structural Integrity	**Junction Efficiency**	**%**	-	-	-	93
	Radial Stiffness @ 0.5% Strain[2]	**kN/m (lb./ft)**	-	-	-	300 (20,580)
Polymer Type		Polypropylene				
Manufacturing Process		Integrally Formed Triaxial Geogrid				

[1] Nominal Dimensions
[2] Radial Stiffness determined from tensile stiffness measured in any in-plane axis. Testing in accordance with ASTM D6637.

Interaction Properties
(from small pullout test results)

Table 5.9. Stiffness of Soil-Geosynthetic Interaction for TX160

Soil Type	Direction of Testing	Normal Pressure	
		3 psi	**5 psi**
3/8" Aggregate	**CD**	20.4	45.9
	MD	10.3	20.8

5.1.4.3 Enkagrid Colbond Max20 (GG3)

Enkagrid Max 20 is a biaxial polypropylene geogrid manufactured by Colbond. It has been used extensively in the field research project on FM 1774 by UT Austin with access to the research team of TxDOT 0-6834. Also, the interaction properties of Enkagrid Max 20 with soil has been studied in the pull-out box tests at UT Austin. Being a welded geogrid, the mechanistic behavior of these geogrids differs from the extruded and woven geogrids discussed earlier. This is observed as a part of the small pull-out box tests conducted.
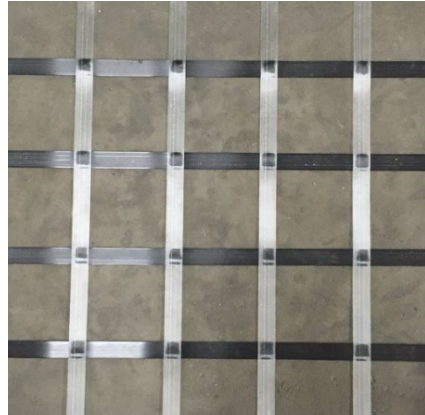
Figure 5.15. Enkagrid Max20

Index Property Specifications

Table 5.10. Index Properties of Enkagrid Max20

Characteristics			Units	MD	CD
Mechanical Properties	**Tensile Strength - ASTM 6637 (Geogrids) - ASTM 4595 (Geotextiles)**	**@ 1% Strain**	**kN/m (lb./ft)**	5.2 (356)	-
		@ 2% Strain	**kN/m (lb./ft)**	8.2 (563)	-
		@ 5% Strain	**kN/m (lb./ft)**	15.1 (1,031)	-
		Ultimate	**kN/m (lb./ft)**	24.2 (1,658)	-
	Junction Strength (Ultimate)		**kN (lbs)**	0.70 (157)	-
	Junction Strength (Ultimate)		**kN/m (lb./ft)**	14.0 (958)	-
Geometric Properties	**Aperture Dimensions**		**mm (in)**	41 (1.61)	41 (1.61)
	Minimum Rib Thickness		**mm (in)**	0.6 (0.02)	0.45 (0.02)
	Rib Width		**mm (in)**	8.9 (0.35)	9.1 (0.36)
Polymer Type			Polypropylene		
Manufacturing Process			Laser Welded Biaxial Geogrid		

Interaction Properties
(from small pullout test results)

Table 5.11. Stiffness of Soil-Geosynthetic Interaction for Enkagrid Max20

Soil Type	Direction of Testing	Normal Pressure	
		3 psi	**5 psi**
3/8" Aggregate	**CD**	9.61	15.9
	MD	4.9	10.0

5.1.4.4 Mirafi BasXGrid11 (GG4)

BasXGrid11 is composed of high molecular weight, high tenacity polyester multifilament yarns which are woven in tension and finished with a PVC coating. This renders the material inert to biological degradation and resistant to naturally encountered chemicals, alkalis, and acids. They are bi-axial geogrids with a load transfer mechanism of positive mechanical interlock. BasXGrid 11 is designed for base reinforcement and subgrade improvement.
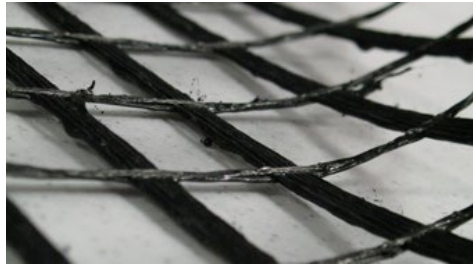
Figure 5.16 Mirafi-Tencate BasXGrid 11

Index Property Specifications

Table 5.12 Index Properties of BasXGrid 11

	Characteristics		Units	MD	CD
Mechanical Properties	**Tensile Strength - ASTM 6637 (Geogrids) - ASTM 4595 (Geotextiles)**	**@ 1% Strain**	**kN/m (lb./ft)**	4.4 (300)	4.4 (300)
		@ 2% Strain	**kN/m (lb./ft)**	7.3 (500)	7.3 (500)
		@ 5% Strain	**kN/m (lb./ft)**	13.4 (920)	13.4 (920)
		Ultimate	**kN/m (lb./ft)**	33.6 (2,300)	33.6 (2,300)
	FHWA Sum of Junctions - Efficiency		**%**	640	640
	Junction Strength (Ultimate)		**kN/junction (lb./junction)**	0.44 (30)	0.44 (30)
Geometric Properties	**Aperture Dimensions**		**mm (in)**	25 (1.0)	25 (1.0)

69

Polymer Type	Polyester
Manufacturing Process	Woven Polyester Yarns

Interaction Property
(from small pullout test results)

$$K_{SGI} = 14.5 \ (kN/m)^2/mm$$

@ 3 psi in Cross-machine Direction (CD)

5.1.4.5 Synteen SF11 (GG5)

The SF11 is a woven geogrid made of high molecular weight multifilament polyester. The yarns are woven into a stable network and placed under tension. The polyester yarns are PVC coated to help prevent degradation. This product is manufactured by Synteen Technical Fabrics, Inc.
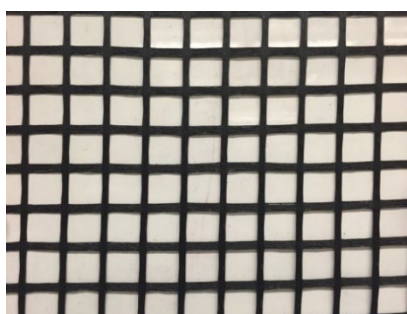
Figure 5.17. Synteen SF11

Index Property Specifications

Table 5.13. Index Properties of SF11

Characteristics			Units	MD	CD
Mechanical Properties	**Tensile Strength - ASTM 6637 (Geogrids) - ASTM 4595 (Geotextiles)**	**@ 1% Strain**	**kN/m (lb./ft)**	-	-
		@ 2% Strain	**kN/m (lb./ft)**	7.7 (526)	8.4 (578)
		@ 5% Strain	**kN/m (lb./ft)**	11.5 (792)	15.2 (1,042)
		Ultimate	**kN/m (lb./ft)**	34.9 (2,388)	56.5 (3,870)
	FHWA Sum of Junctions - Efficiency		**%**	201	100
	Junction Strength (Ultimate)		**kN/junction (lb./junction)**	0.87 (59.4)	0.69 (47.6)
Geometric Properties	**Aperture Dimensions**		**mm (in)**	25 (1.0)	25 (1.0)
	Minimum Rib Thickness		**mm (in)**	1.1 (0.04)	1.1 (0.04)
	Rib Width		**mm (in)**	5.4 (0.21)	6.6 (0.26)

Polymer Type	Polyester
Manufacturing Process	Woven Polyester Yarns

Interaction Properties
(from small pullout test results)

Table 5.14. Stiffness of Soil-Geosynthetic Interaction for SF11

Soil Type	Direction of Testing	Normal Pressure	
		3 psi	**5 psi**
3/8" Aggregate	**CD**	12.16	15.4
	MD	8.0	10.0

5.1.4.6 Huesker Fornit20

Fornit20 is comprised of polypropylene yarns, crafted into a stable, interlocking pattern and then coated for protection from installation damage. They are easy to install and resistant to freeze-thaw conditions, soil chemicals and ultra-violet exposure. Fornit 20 geogrid has been developed to stabilize poor soils by providing tensile reinforcement and soil separation. They confine and strengthen road base aggregate thereby reducing the required base thickness.

Figure 5.18 Fornit 20

Index Property Specifications

Table 5.15. Index Properties of SF11

Characteristics			Units	MD	CD
Mechanical Properties	**Tensile Strength - ASTM 6637 (Geogrids) - ASTM 4595 (Geotextiles)**	**@ 1% Strain**	**kN/m (lb./ft)**	-	-
		@ 2% Strain	**kN/m (lb./ft)**	5 (343)	7 (480)
		@ 5% Strain	**kN/m (lb./ft)**	9 (620)	14 (960)
		Ultimate	**kN/m (lb./ft)**	13 (900)	23.3 (1600)
	FHWA Sum of Junctions - Efficiency		**%**	-	-

		kN/junction	-	-
	Junction Strength (Ultimate)	**(lb./junction)**		
Geometric Properties	**Aperture Dimensions**	**mm**	15	15
		(in)	(0.6)	(0.6)
	Minimum Rib Thickness	**mm**	-	-
		(in)		
	Rib Width	**mm**	-	-
		(in)		
Polymer Type		Polypropylene		
Manufacturing Process		Woven Polypropylene Yarns		

Interaction Property
(from small pullout test results)

$$K_{SGI} = 15.57 \ (kN/m)^2/mm$$

@ 3 psi in Cross-machine Direction (CD)

5.1.4.7 Naue Secugrid 30/30

In Secugrid, the reinforcement element is a highly oriented polypropylene strap that is extruded and drawn to achieve high modulus and strength at low elongations. These straps are welded together to form the grid using vibratory welding technology.

Figure 5.19 Secugrid 30/30

Index Property Specifications

Table 5.16. Index Properties of SF11

	Characteristics		Units	MD	CD
Mechanical Properties	**Tensile Strength - ASTM 6637 (Geogrids) - ASTM 4595 (Geotextiles)**	**@ 1% Strain**	**kN/m**	6.6	6.6
			(lb./ft)	(453)	(453)
		@ 2% Strain	**kN/m**	10	10
			(lb./ft)	(686)	(686)
		@ 5% Strain	**kN/m**	21.5	21.5
			(lb./ft)	(1,475)	(1,475)
		Ultimate	**kN/m**	30	30
			(lb./ft)	(2,055)	(2,055)
	FHWA Sum of Junctions - Efficiency		**%**	285	285

	Junction Strength (Ultimate)	kN/junction	9	9
		(lb./junction)	(617)	(617)
Geometric Properties	Aperture Dimensions	mm	32	32
		(in)	(1.26)	(1.26)
	Minimum Rib Thickness	mm	-	-
		(in)		
	Rib Width	mm	-	-
		(in)		
Polymer Type		Polypropylene		
Manufacturing Process		Welded Polypropylene Straps		

Interaction Property
(from small pullout test results)

$$K_{SGI} = 16.87 \text{ (kN/m)}^2/\text{mm}$$

@ 3 psi in Cross-machine Direction (CD)

5.1.4.8 Tensar TX130s

TX160 is manufactured from a punched polypropylene sheet, oriented in three substantially equilateral directions. This triaxial polypropylene geogrid is manufactured by Tensar Corporation. The interaction of a triaxial geogrid, as opposed to a biaxial geogrid, with the base material is expected to produce some interesting mechanisms similar to TX160.
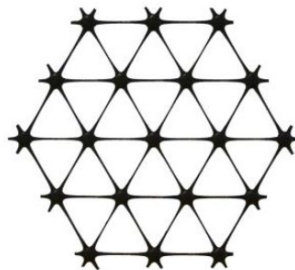
Figure 5.20 TX130s

Index Property Specifications

Table 5.17. Index Properties of TX160

	Characteristics	Units	Longitudinal	Diagonal	Transverse	General
Geometric Properties	**Rib Pitch**[1]	**mm**	33	33	-	-
		(in)	(1.30)	(1.30)		
	Mid-Rib Depth[1]	**mm**	-	2.0	1.8	-
		(in)		(0.08)	(0.07)	
	Mid-Rib Width[1]	**mm**	-	1.0	1.2	-
		(in)		(0.04)	(0.05)	
	Aperture Shape	**-**	-	-	-	Triangular

Structural Integrity	**Junction Efficiency**	%	-	-	-	93
	Radial Stiffness @ 0.5% Strain[2]	kN/m (lb./ft)	-	-	-	200 (13,708)
Polymer Type		Polypropylene				
Manufacturing Process		Integrally Formed Triaxial Geogrid				

[1] Nominal Dimensions

[2] Radial Stiffness determined from tensile stiffness measured in any in-plane axis. Testing in accordance with ASTM D6637.

Interaction Property
(from small pullout test results)

$$K_{SGI} = 18.79 \ (kN/m)^2/mm$$

@ 3 psi in Cross-machine Direction (CD)

5.2 INSTRUMENTATION USED

A comprehensive instrumentation design monitoring program has been developed as a part of this study to collect relevant data during the testing of the pavement sections. The data considered relevant with respect to the scope of the project are,

1. Rutting profiles
2. Displacement of the geogrids and within the base
3. Stresses within the pavement section

The Data Acquisition System is entirely handled by National Instruments Hardware and LabVIEW code, custom developed for this project. The actual sensors and instrumentation are obtained from various companies. The following instrumentation section is developed to address the same.

5.2.1 PROFILOMETER

A profilometer to quantify the rutting on the pavement surface was custom built at UT Austin. The device makes use of NEMA 23 Integrated Step SERVO Motor TSM23Q-2RG coupled with the Macron Dynamics PSC Actuator to act as the guide moving at a constant rate as slow as 0.5 mm/s. A laser distance meter (LDM) Leica Disto D8 is attached to the carriage on the actuator and samples every 1 second. The information regarding the position of the laser distance meter and the value recorded by it is transmitted to the computer. The actuator with the Step Servo motor is accurate to ±0.5 mm and the LDM is accurate to ±1 mm. This way the profile of the constructed test section is accurately determined. The pavement is painted white in order to improve the reflectivity of the laser to improve acquiring data.
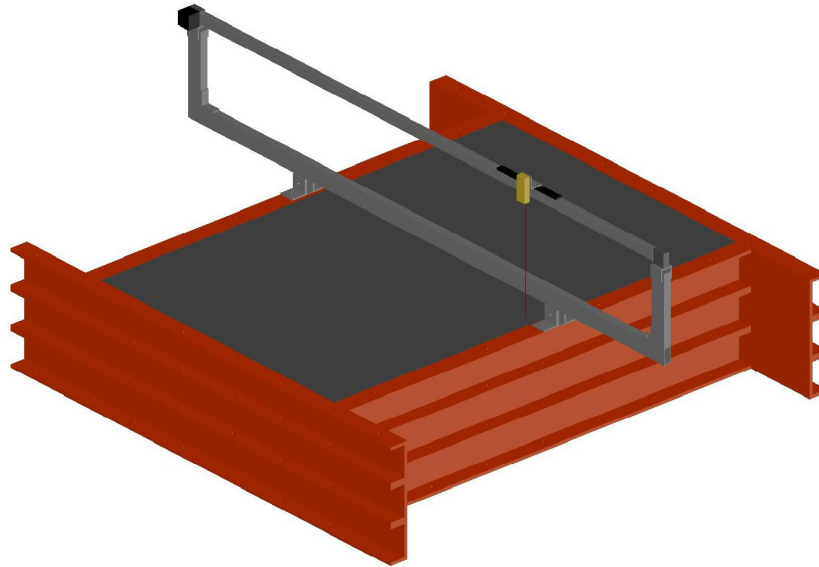
Figure 5.21. Schematic of Profilometer mounted on the section

Figure 5.22. Servomotor, Leica Laser Distance Meter, and Macron Actuator - Components of In-House Profilometer

5.2.2 LINEAR POTENTIOMETERS (LPS)

8 to 15 LPs are used in the test sections to measure the displacements within the base and of the geogrid nodes. In order to monitor the movement of particles within the base, the tell-tales are hooked to artificial gravel particles (nut and short bolt) embedded inside the base during construction. This setup with the LP and the tell-tales is together referred to as "tell-tale extensometer." The output from these sensors provides the position or displacement of the

particles/geogrid nodes within the base. The LPs used are Linear Position Transducers (LX-PA-2-N1N-NNN) from Unimeasure. They have an accuracy of ±0.01 mm.

Figure 5.23. LX-PA Series Linear Position Transducers from Unimeasure
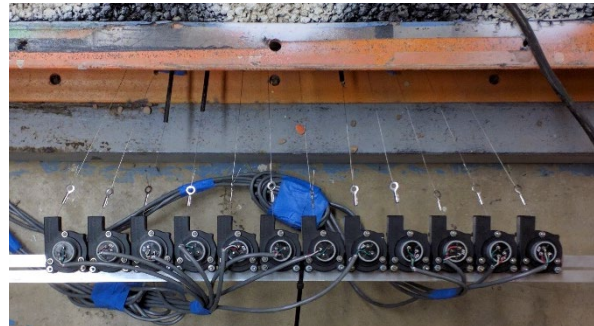
Figure 5.24. LPs used in Reduced-Scale APT Section
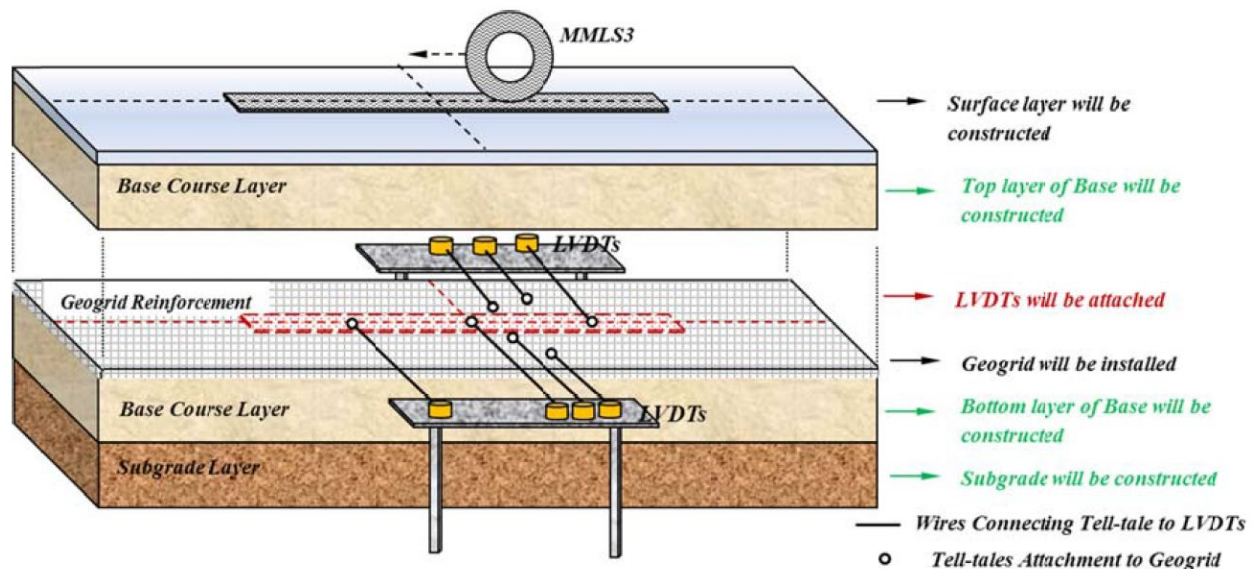
Figure 5.25. Schematic showing the use of tell-tales and LVDTs to measure geogrid displacements

5.2.3 FLEXIFORCE SENSORS

4 to 8 FlexiForce sensors (A301) from TekScan have been used to measure stresses acting within the pavement sections. Both static as well as dynamic stresses within the pavement under trafficking conditions are measured. Because these sensors are compact and cause minimal disturbance to the surrounding soil, they were of particular use in measuring the stresses on top of and within the subgrade. The positions of placement are as follows.

1. Directly under the wheel path at the interface of the base material and sub-grade material
2. Directly under the wheel path within the subgrade material
3. 12" away from the wheel path at the interface of the base material and sub-grade material
4. 12" away from the wheel path within the subgrade material
5. Repeat of FF Sensors 1 to 4.

76

5.3 TEST SECTIONS AND PERFORMANCE

26 test sections are constructed and trafficked as a part of this APT program. The 26 tests conducted are categorized into eight structure categories as originally proposed in Exhibit B (TxDOT 0-6834). Each test configuration is uniquely identified by a series of codenames identified in Table 5.1. For instance, AC1-BS1-SG1-GG1 refers to a test section constructed with TOM-A mix as the HMA Layer, Pea Gravel as Base, Monterey Sand as Subgrade and BX1100 as reinforced in the baseline configuration. The baseline configuration is shown in Table 5.18. If there are no numbers next to the codenames in square brackets [ ], it refers to the base configuration. Any number within those square brackets would refer to the modified thickness/position of the material. For instance, AC1-BS1-SG1-GG1[1] refers to the baseline configuration except with the geogrid at 1 inch below the asphalt-base interface instead of the usual 2 inches.

Of the numerous data collected and processed, three key parameters are reported in this technical memorandum,

1. Rutting Vs. Number of Cycles of the Various Sections (performance data)
2. Soil-Geogrid mobilization data (instrumentation results)
3. Density data (auxiliary test results)

Table 5.18. Baseline Configuration

Material	Thickness
HMA Layer	1"
Base Layer	5"
Subgrade Layer	6" - Monterey Sand 3" - Aquafoam Steel Channels
Geogrid Position	2" below the Asphalt-Base Interface
Width of the Box	**6'**

Rutting is measured using an in-house laser profilometer at three transverse locations of the pavement section. A typical rutting profile is shown in Figure 5.26. From this profile, the rut depth is calculated as RD = a + d. For any test section, the profiling is done at three transverse locations for any N cycles. From the three profiles, three rut depth values are calculated, and the average is reported for any N cycles in this technical memorandum. The complete data, including all the profiles taken, is too comprehensive to be presented in a technical memorandum. The database developed will be handed over at the end of the project to the funding agency.
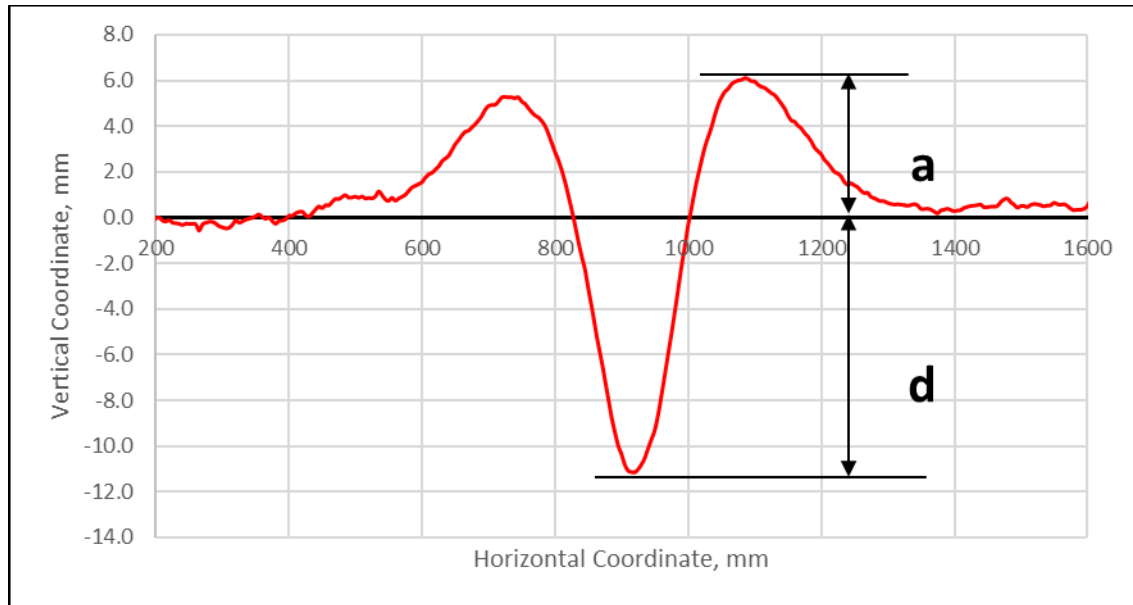
Figure 5.26. Typical Rutting Profile from Laser Profilometer

The soil-geogrid mobilization data will be presented in the form of horizontal soil particle / geogrid movement for any N cycles

The density data will be reported as the average measured from a number of measurements. This serves purely as a quality control measure.

5.3.1 CONTROL SERIES

This series of tests is conducted with unreinforced pavement bases overlying low to high stiffness subgrades. These establish a baseline to evaluate the benefits of geogrid. There are 8 tests conducted as part of this series, namely

5.3.1.1 AC3-BS1[4.75]-SG3-NGS-3'

Rutting

Figure 5.27 Rut Depth Vs. No of Cycles - AC3-BS1[4.75]-SG3-NGS-3'

Soil Mobilization Data

Not Available

Density Data

Table 5.19 Density of Pavement Layers – AC3-BS1[4.75]-SG3-NGS-3'

Layer	Density	Unit
HMA	2176	kg/m^3
Base Layer	1654	kg/m^3

5.3.1.2 AC3-BS1-SG3-NGS-3'

Rutting

Figure 5.28 Rut Depth Vs. No of Cycles - AC3-BS1-SG3-NGS-3'

Soil Mobilization Data

Not Available

Density Data

Table 5.20 Density of Pavement Layers – AC3-BS1-SG3-NGS-3'

Layer	Density	Unit
HMA	2154	kg/m^3
Base Layer	1654.7	kg/m^3

5.3.1.3 AC3-BS1-SG2-NGS-3'

Rutting

Figure 5.29 Rut Depth Vs. No of Cycles - AC3-BS1-SG2-NGS-3'

Soil Mobilization Data

Not Available

Density Data

Table 5.21 Density of Pavement Layers – AC3-BS1-SG2-NGS-3'

Layer	Density	Unit
HMA	2147	kg/m^3
Base Layer	1653.6	kg/m^3

5.3.1.4 AC1-BS1[2]-SG2-NGS

Rutting
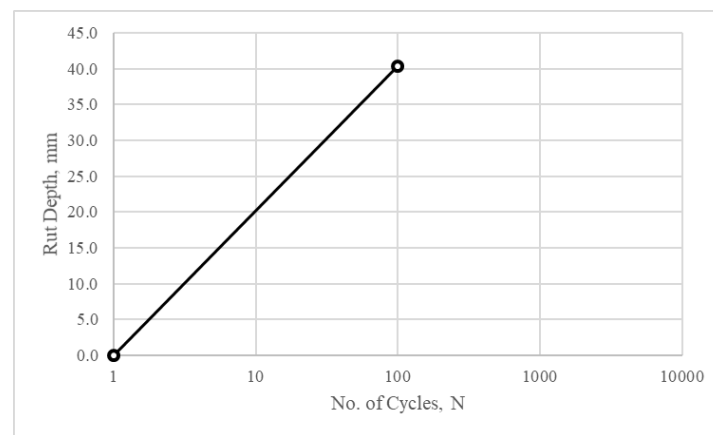
Figure 5.30 Rut Depth Vs. No of Cycles – AC1-BS1[2]-SG2-NGS

Soil Mobilization Data

Not Available

Density Data

Table 5.22 Density of Pavement Layers - AC1-BS1[2]-SG2-NGS

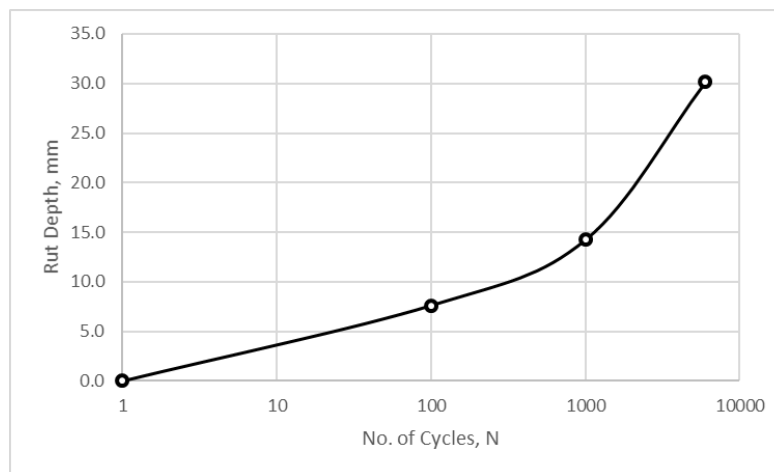| Layer	Density	Unit
HMA	2116	kg/m^3
Base Layer	1649	kg/m^3

5.3.1.5 AC1-BS1-SG3-NGS
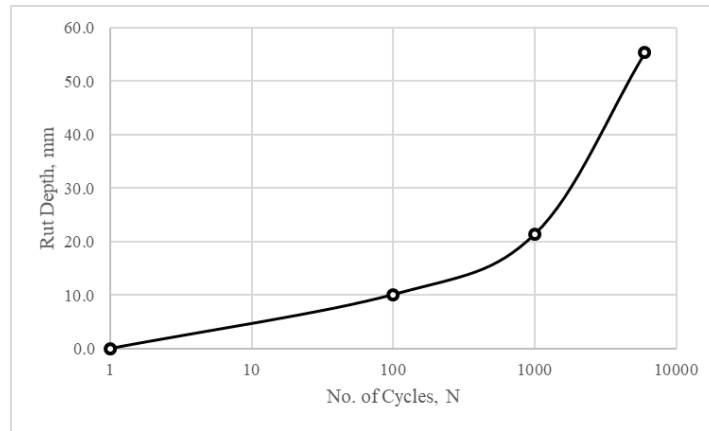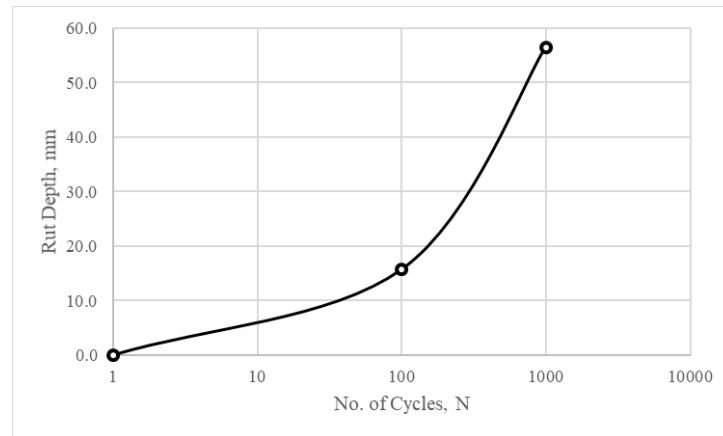
Rutting
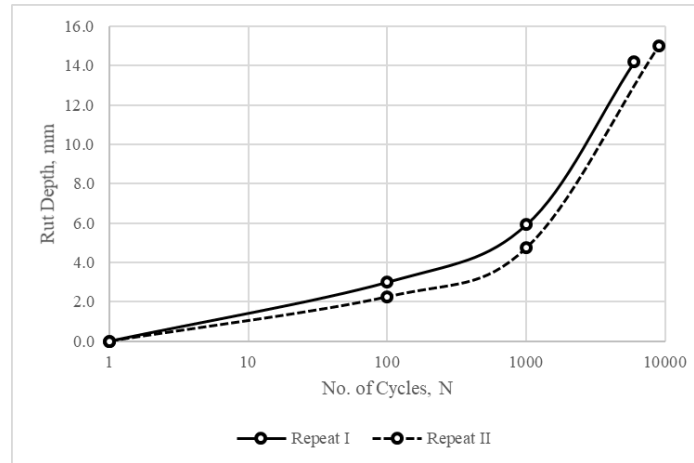
Figure 5.31 Rut Depth Vs. No of Cycles – AC1-BS1-SG3-NGS

Soil Mobilization Data

Not Available

Density Data

Table 5.23 Density of Pavement Layers - AC1-BS1-SG3-NGS

Layer	Density I	Density II	Unit
HMA	2111	2123	kg/m^3
Base Layer	1651	1657	kg/m^3

5.3.1.6 AC1-BS1-SG1-NGS (I,II)

Rutting

Figure 5.32 Rut Depth Vs. No of Cycles – AC1-BS1-SG1-NGS

Soil Mobilization Data
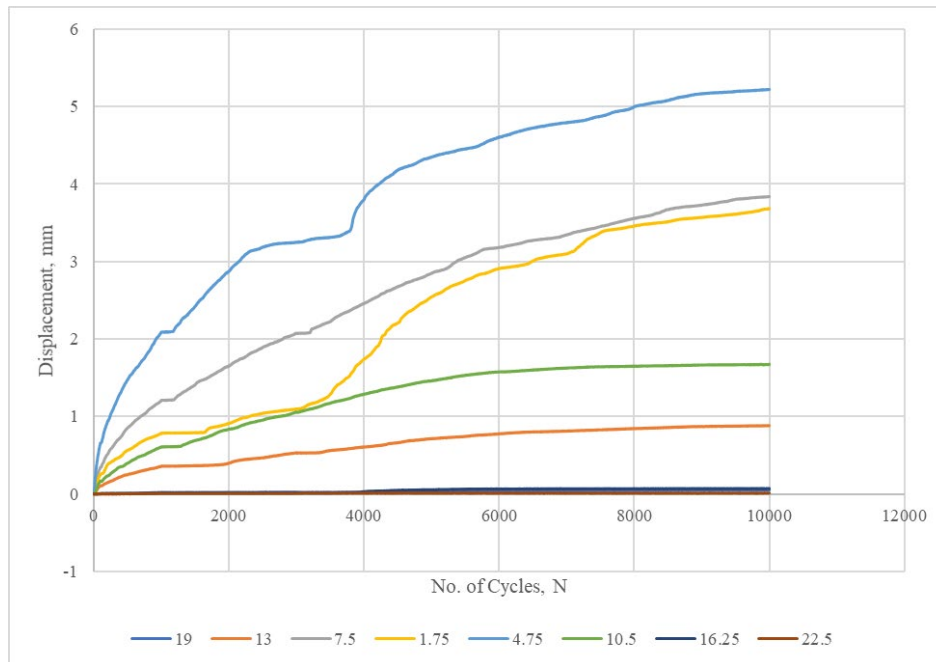
Figure 5.33 LP Displacements with No. of Cycles - AC1-BS1-SG1-NGS

legend: the distance in inches from the center of the wheel path at 2" below the AC-BS interface

Positive value denotes movement away from the center of the wheel path.

Density Test Data

Table 5.24 Density of Pavement Layers - AC1-BS1-SG1-NGS

Layer	Density	Unit
HMA	2120	kg/m^3
Base Layer	1738	kg/m^3
Subgrade Layer	1559	kg/m^3

5.3.1.7 AC1-BS2-SG1-NGS
Rutting

Figure 5.34 Rut Depth Vs. No of Cycles – AC1-BS2-SG1-NGS

Soil Mobilization Data
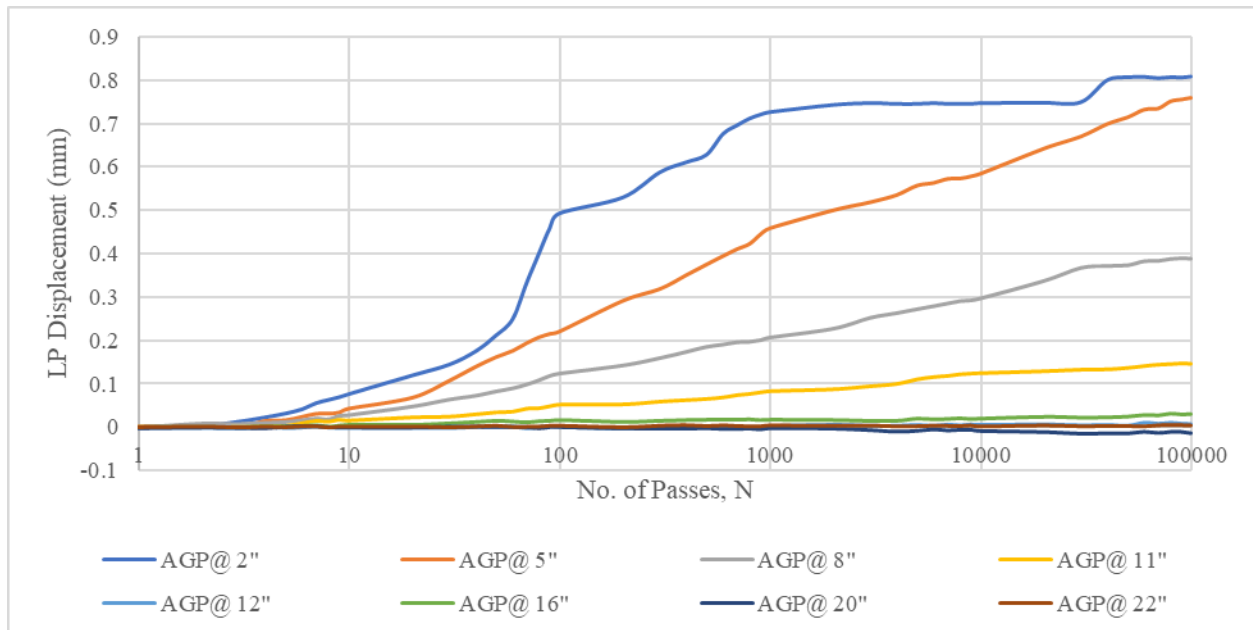
Figure 5.35 LP Displacements with No. of Cycles - AC1-BS2-SG1-NGS

Density Data

Table 5.25 Density of Pavement Layers - AC1-BS2-SG1-NGS

Layer	Density I	Unit
HMA	2116	kg/m^3
Base Layer	2210	kg/m^3
Subgrade Layer	1559	kg/m^3

5.3.2 BASELINE SERIES (AC1-BS1-SG1-GG1 (I,II))

The testing configuration selected for this series is considered "baseline" condition as the results are used as reference for comparison with the performance of each of the other pavement test sections. In order to assess repeatability, two sections are constructed in the baseline configuration and their results are discussed below.

Rutting
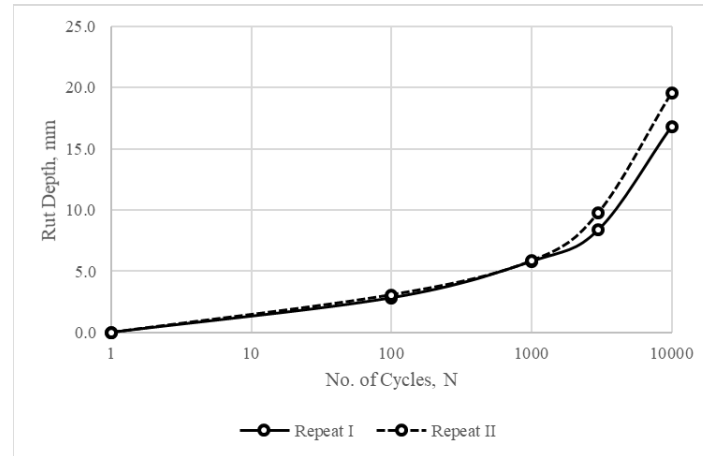
Figure 5.36 Rut Depth Vs. No of Cycles – AC1-BS1-SG1-GG1

Soil-Geogrid Mobilization Data
Repeat II
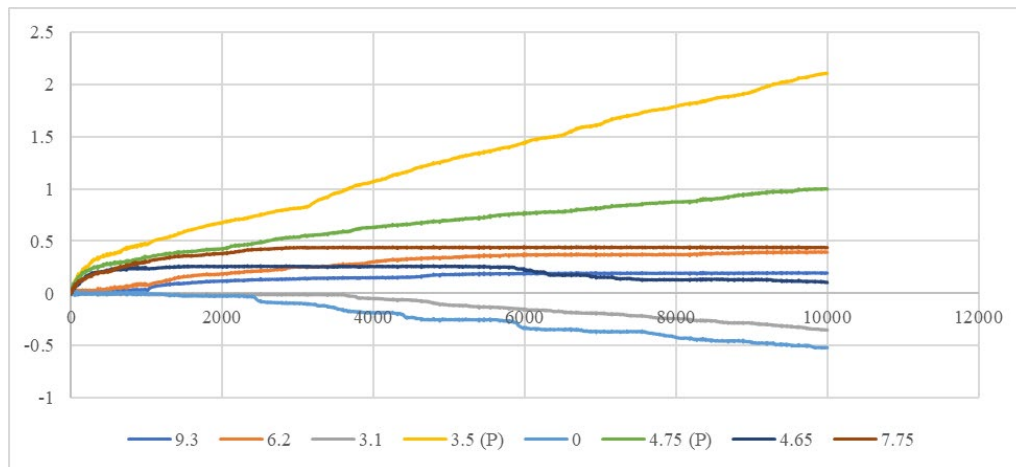
Figure 5.37 LP Displacements with No. of Cycles - AC1-BS1-SG1-GG1

where (P) denotes particle movement, while others are geogrid nodal displacements

Density Data

Table 5.26 Density of Pavement Layers - AC1-BS1-SG1-GG1

Layer	Density I	Density II	Unit
HMA	2110	2116	kg/m^3
Base Layer	1731	1736	kg/m^3
Subgrade Layer	1568	1568	kg/m^3

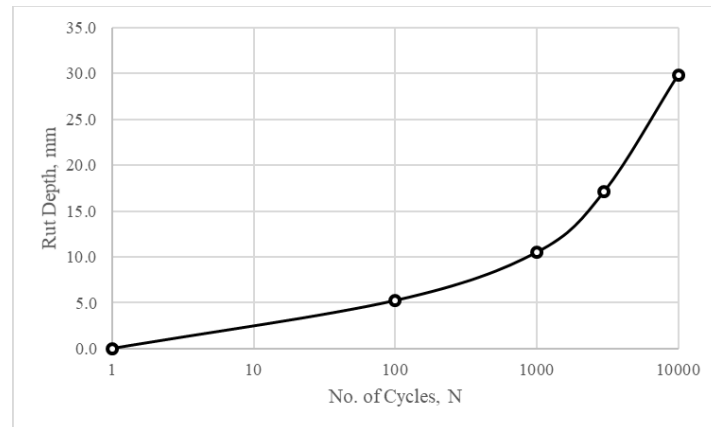### 5.3.3 BASE MATERIAL SERIES (AC1-BS2-SG1-GG1)
Rutting

Figure 5.38 Rut Depth Vs. No of Cycles – AC1-BS2-SG1-GG1

Soil Mobilization Data
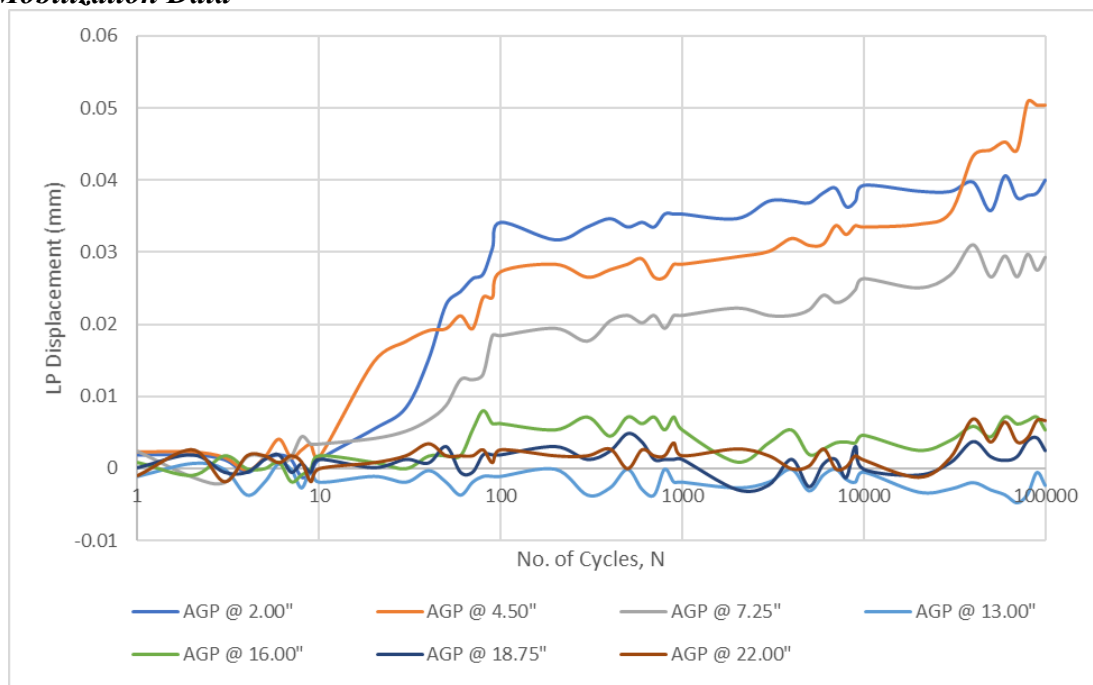
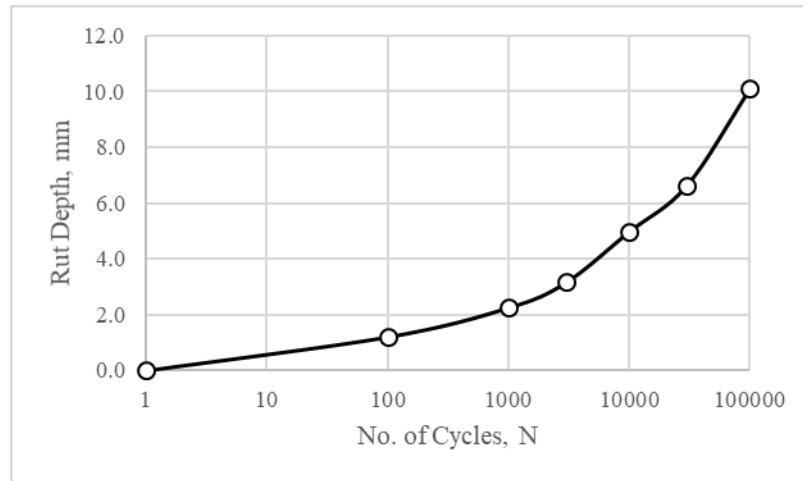**Figure 5.39 LP Displacements with No. of Cycles - AC1-BS2-SG1-GG1**

As seen from Figure 5.38 and Figure 5.39, use of real base materials results in very stiff pavement sections when reinforced. This in turn results in negligible rutting within the error of repeatability. Therefore, no meaningful interpretation of evaluation of benefits of geosynthetic reinforcement is possible. Hence, tests in this series to be conducted with alternate real base materials are suspended.

Density Data

Table 5.27 Density of Pavement Layers - AC1-BS2-SG1-NGS

Layer	Density I	Unit
HMA	2125	kg/m^3
Base Layer	2290	kg/m^3
Subgrade Layer	1575	kg/m^3

5.3.4 BASE THICKNESS SERIES

This series is carried out with the baseline configuration but with varying thickness of the base layer. Since the baseline configuration is already discussed in 2.2. The results of the test sections with two different thicknesses are summarized here.

5.3.4.1 AC1-BS1[4]-SG1[7]-GG1

Rutting

Figure 5.40 Rut Depth Vs. No of Cycles – AC1-BS1[4]-SG1[7]-GG1

Soil Mobilization Data

Figure 5.41 LP Displacements with No. of Cycles - AC1-BS1[4]-SG1[7]-GG1

The data represents soil particle movement in the plane of the geogrid i.e., 2 inches below the AC-BS interface

Density Data

Table 5.28 Density of Pavement Layers - AC1-BS1[4]-SG1[7]-GG1

| Layer	Density I	Unit
HMA	2125	kg/m^3
Base Layer	1736	kg/m^3
Subgrade Layer	1570	kg/m^3

5.3.4.2 AC1-BS1[2.5]-SG[8.5]-GG1

Rutting
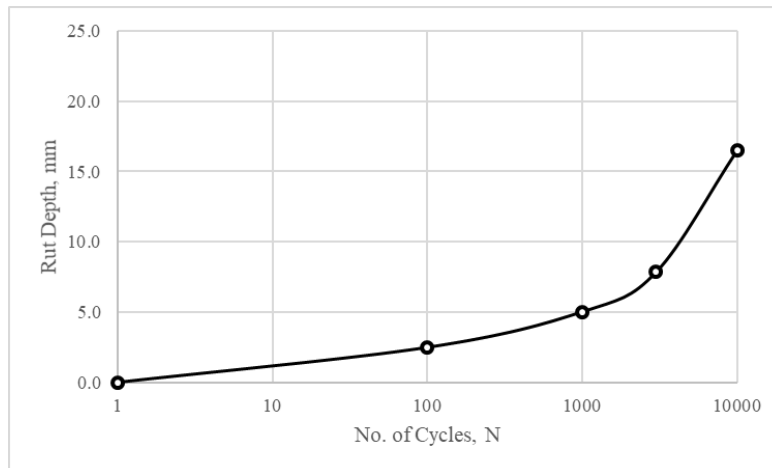
Figure 5.42 Rut Depth Vs. No of Cycles – AC1-BS1[2.5]-SG1[8.5]-GG1
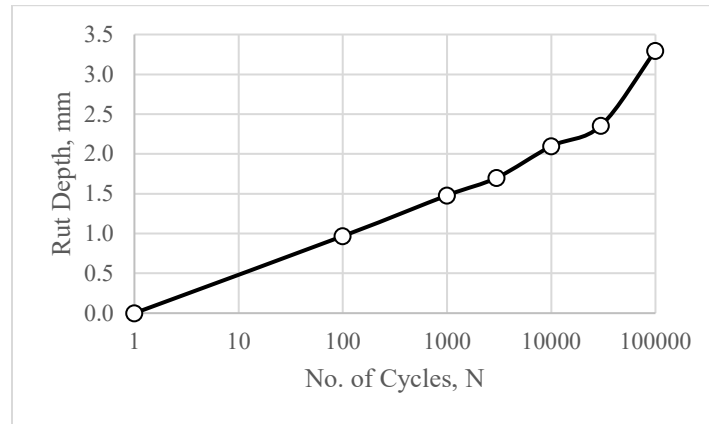
Soil Mobilization Data
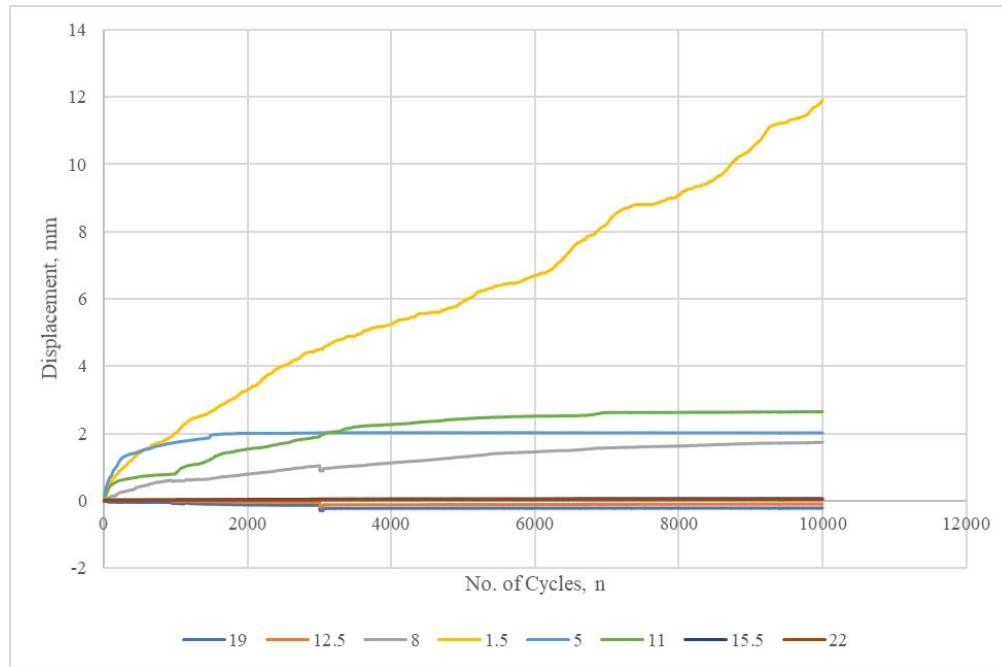
Figure 5.43 LP Displacements with No. of Cycles - AC1-BS1[2.5]-SG1[8.5]-GG1

The data represents soil particle movement in the plane of the geogrid i.e., 2 inches below the AC-BS interface

Density Data

Table 5.29 Density of Pavement Layers - AC1-BS1[2.5]-SG1[8.5]-GG1

Layer	Density I	Unit
HMA	2135	kg/m^3
Base Layer	1740	kg/m^3
Subgrade Layer	1570	kg/m^3

5.3.5 BASE STIFFNESS SERIES

This series is to be originally completed by repeating the baseline section with the base material at two different moisture contents, thereby changing their stiffness. Since the baseline base material is without fines, and as seen in TM III has a very narrow void ratio, a reasonable repeatable variation in stiffness is not achievable by moisture variation or by density variation.

For this purpose, the research team proposed the use of real base material as the baseline configuration for this series alone. However, as seen earlier, use of real base materials results in very high stiffness pavement sections. This in turn resulted in negligible rutting within the error of repeatability. Therefore, no meaningful interpretation of evaluation of benefits of geosynthetic reinforcement is possible. Hence, tests in this series to be conducted with base materials at different moisture contents were suspended.

5.3.6 SUBGRADE STIFFNESS SERIES

This series comprises of running the baseline configuration with two additional subgrade stiffnesses. This is achieved by replacing the medium stiff Monterey sand subgrade with less stiff Aquafoam and very high stiff steel channels.
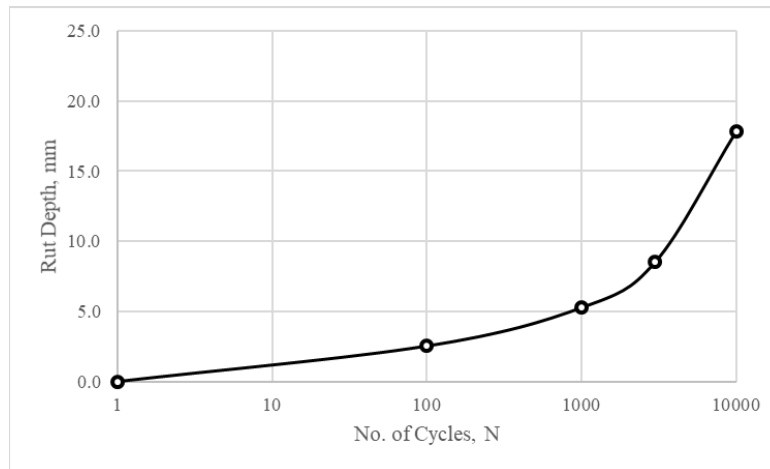
5.3.6.1 AC1-BS1-SG2-GG1

Rutting
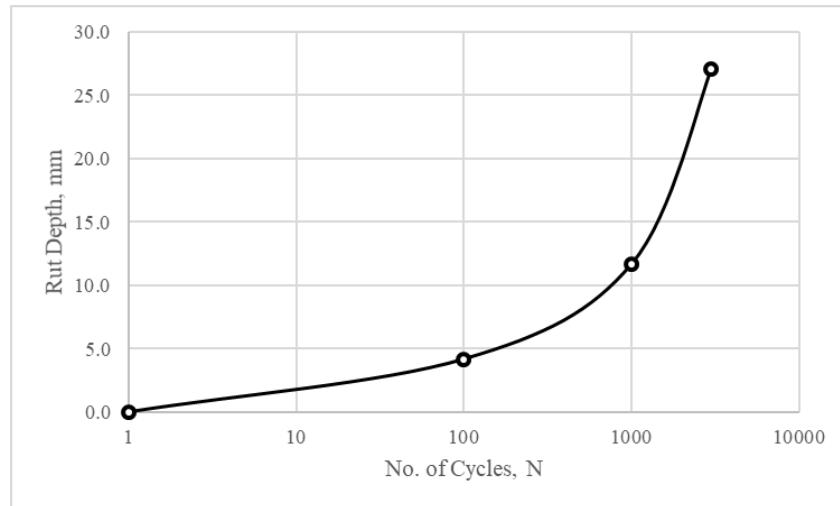
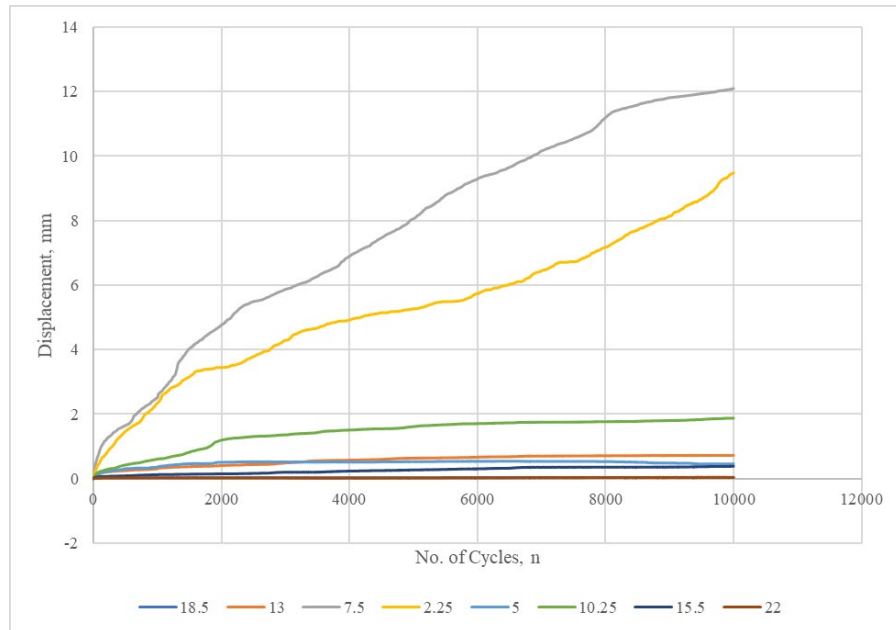**Figure 5.44 Rut Depth Vs. No of Cycles – AC1-BS1-SG2-GG1**

Soil Mobilization Data
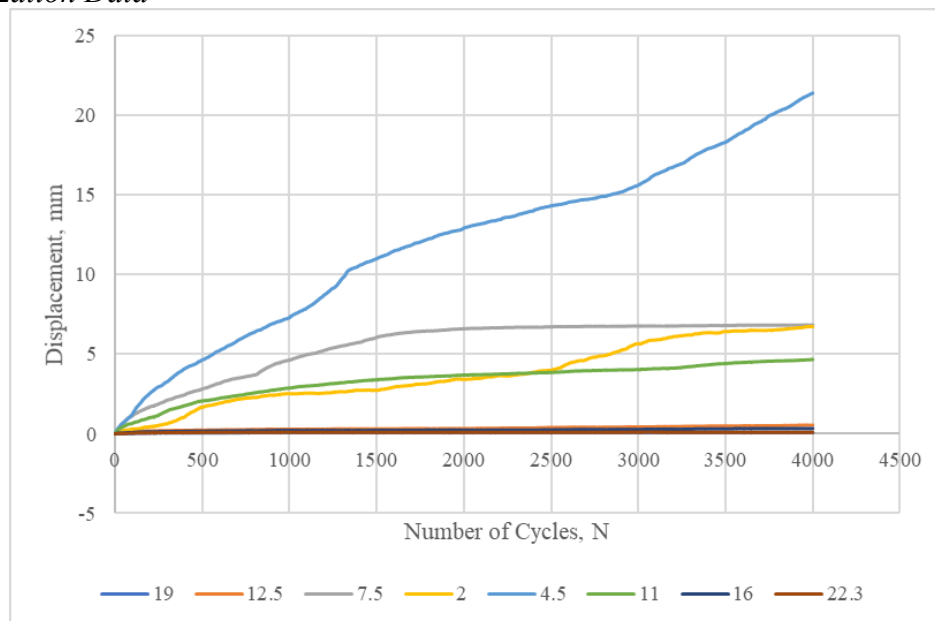
Figure 5.45 LP Displacements with No. of Cycles - AC1-BS1-SG2-GG1

The data represents soil particle movement in the plane of the geogrid i.e., 2 inches below the AC-BS interface

89

Density Data

Table 5.30 Density of Pavement Layers - AC1-BS1-SG2-GG1

Layer	Density I	Unit
HMA	2112	kg/m^3
Base Layer	1732	kg/m^3

5.3.6.2 AC1-BS1-SG3-GG1

Rutting
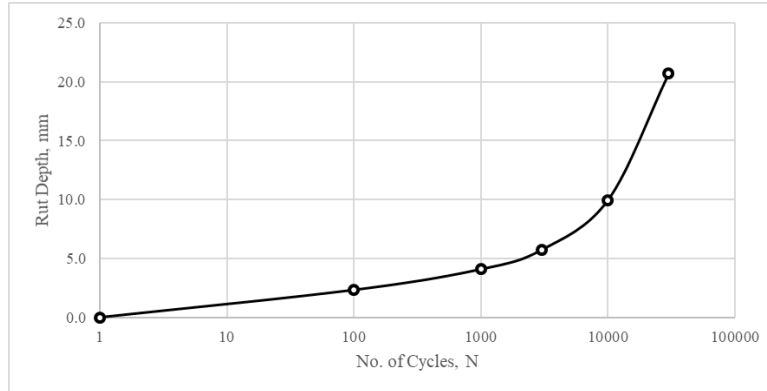
Figure 5.46 Rut Depth Vs. No of Cycles – AC1-BS1-SG3-GG1

Geogrid Mobilization Data

Not Available – Negligible Geogrid Displacements observed.

Density Data

Table 5.31 Density of Pavement Layers - AC1-BS1-SG3-GG1

Layer	Density I	Unit
HMA	2116	kg/m^3
Base Layer	1735	kg/m^3

5.3.7 GEOGRID TYPE SERIES

This series is conducted by repeating the baseline series sections with four additional different geogrid products. This makes up for 8 different products used in total.

5.3.7.1 AC1-BS1-SG1-GG2

Rutting

Figure 5.47 Rut Depth Vs. No of Cycles – AC1-BS1-SG1-GG2

Geogrid Mobilization Data
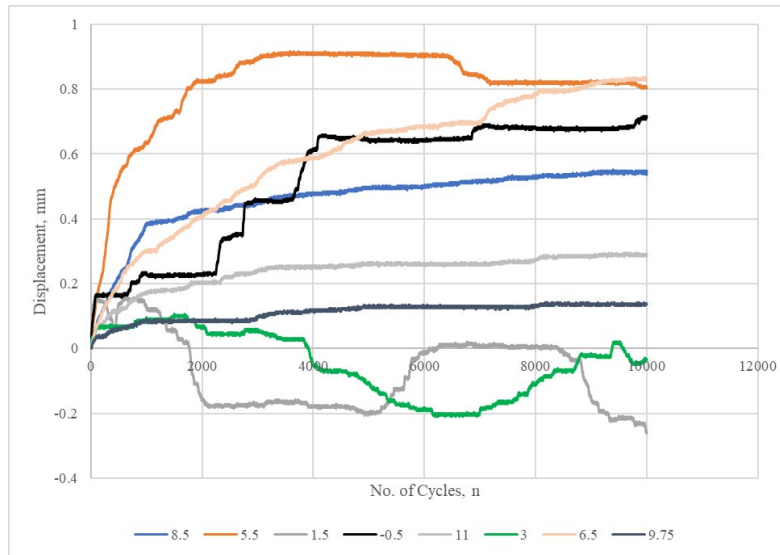
Figure 5.48 LP Displacements with No. of Cycles - AC1-BS1-SG1-GG2

The values represent the nodal displacements of the geogrid with positive values denoting movement away from the wheel path.

Density Data

Table 5.32 Density of Pavement Layers - AC1-BS1-SG1-GG2

Layer	Density	Unit
HMA	2123	kg/m^3
Base Layer	1738	kg/m^3
Subgrade Layer	1564	kg/m^3

5.3.7.2 AC1-BS1-SG1-GG3

Rutting

Figure 5.49 Rut Depth Vs. No of Cycles – AC1-BS1-SG1-GG3

Geogrid Mobilization Data
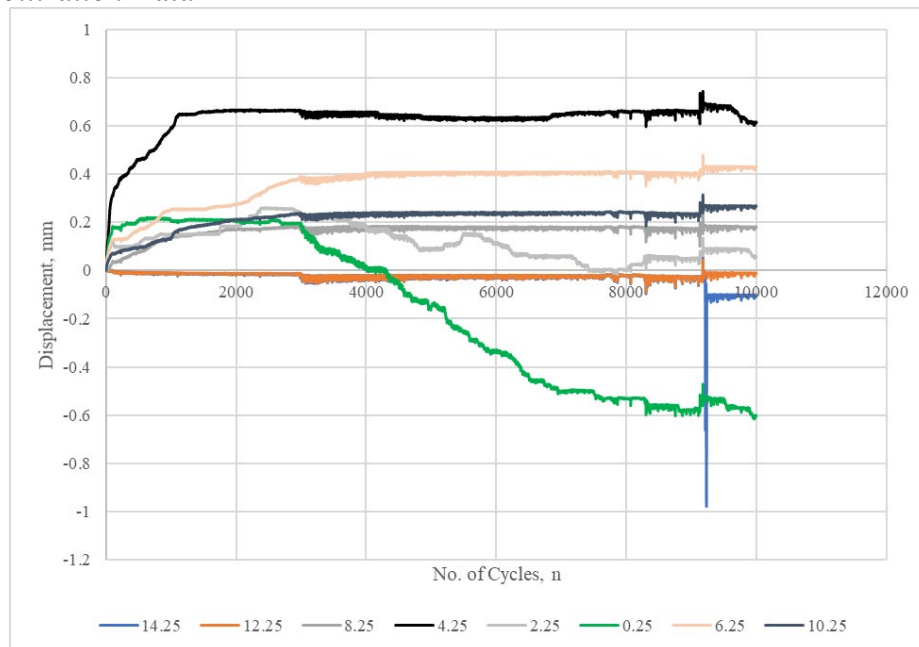
Figure 5.50 LP Displacements with No. of Cycles - AC1-BS1-SG1-GG3

The values represent the nodal displacements of the geogrid with positive values denoting movement away from the wheel path.

Density Data

Table 5.33 Density of Pavement Layers - AC1-BS1-SG1-GG3

Layer	Density	Unit
HMA	2112	kg/m^3
Base Layer	1739	kg/m^3
Subgrade Layer	1566	kg/m^3

5.3.7.3 AC1-BS1-SG1-GG4

Rutting

Figure 5.51 Rut Depth Vs. No of Cycles – AC1-BS1-SG1-GG4

Soil-Geogrid Mobilization Data
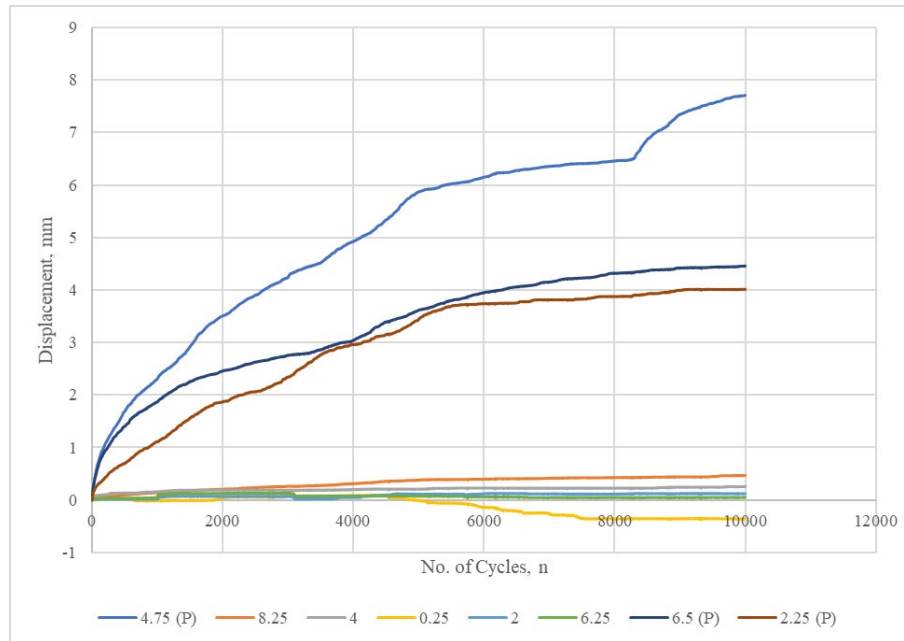
Figure 5.52 LP Displacements with No. of Cycles - AC1-BS1-SG1-GG4

where points with (P) represent soil particle movement whereas the others represent Geogrid Nodal Displacements

Density Data

Table 5.34 Density of Pavement Layers - AC1-BS1-SG1-GG4

| Layer	Density	Unit
HMA	2129	kg/m^3
Base Layer	1725	kg/m^3
Subgrade Layer	1575	kg/m^3

5.3.7.4 AC1-BS1-SG1-GG5
Rutting

Figure 5.53 Rut Depth Vs. No of Cycles – AC1-BS1-SG1-GG5

Soil-Geogrid Mobilization Data
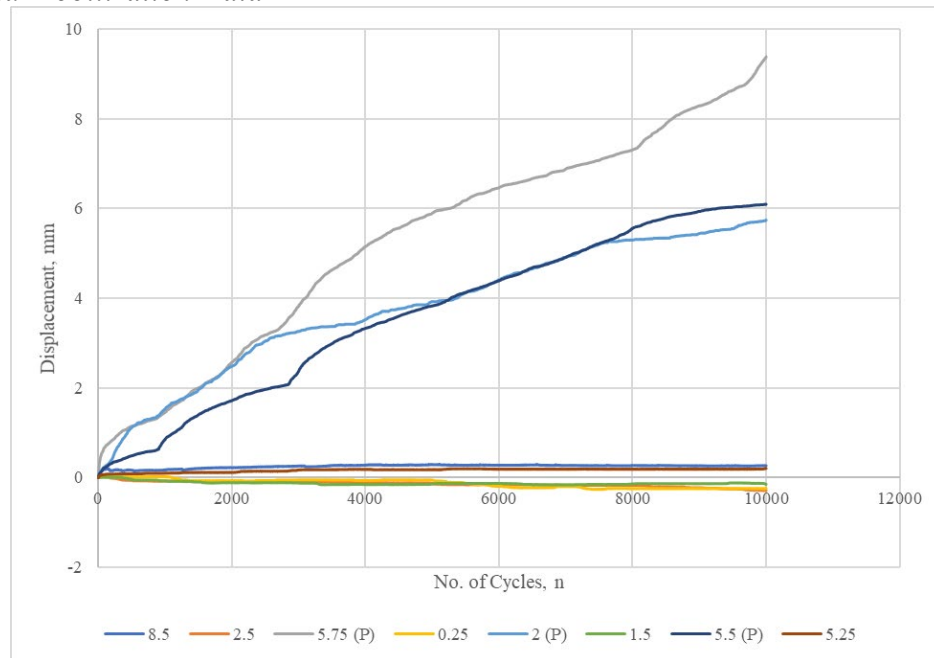
Figure 5.54 LP Displacements with No. of Cycles - AC1-BS1-SG1-GG5

where points with (P) represent soil particle movement whereas the others represent Geogrid Nodal Displacements

Density Data

Table 5.35 Density of Pavement Layers - AC1-BS1-SG1-GG5

Layer	Density	Unit
HMA	2115	kg/m^3
Base Layer	1726	kg/m^3
Subgrade Layer	1572	kg/m^3

5.3.7.5 AC1-BS1-SG1-GG6
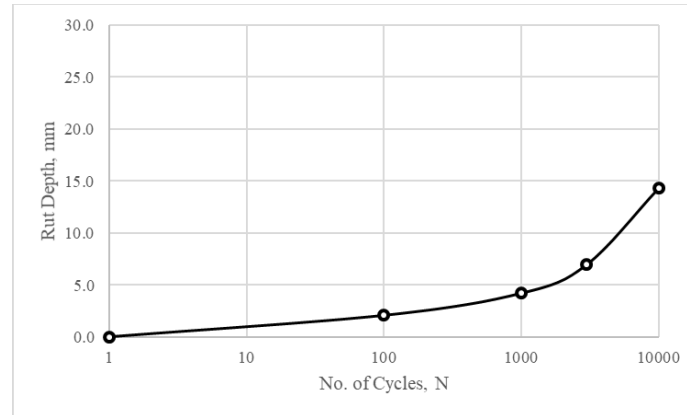
Rutting
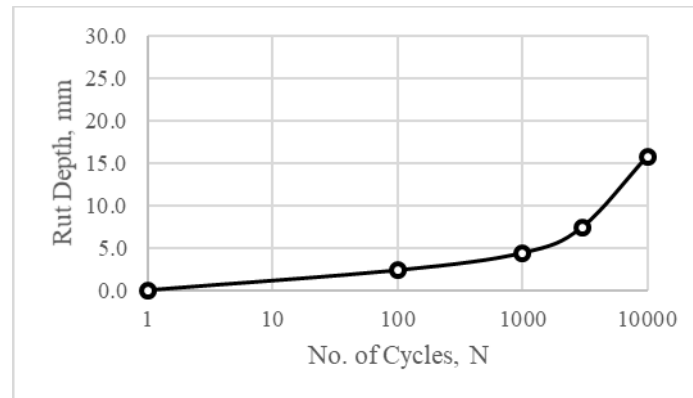
Figure 5.55 Rut Depth Vs. No of Cycles – AC1-BS1-SG1-GG6

Soil Mobilization Data
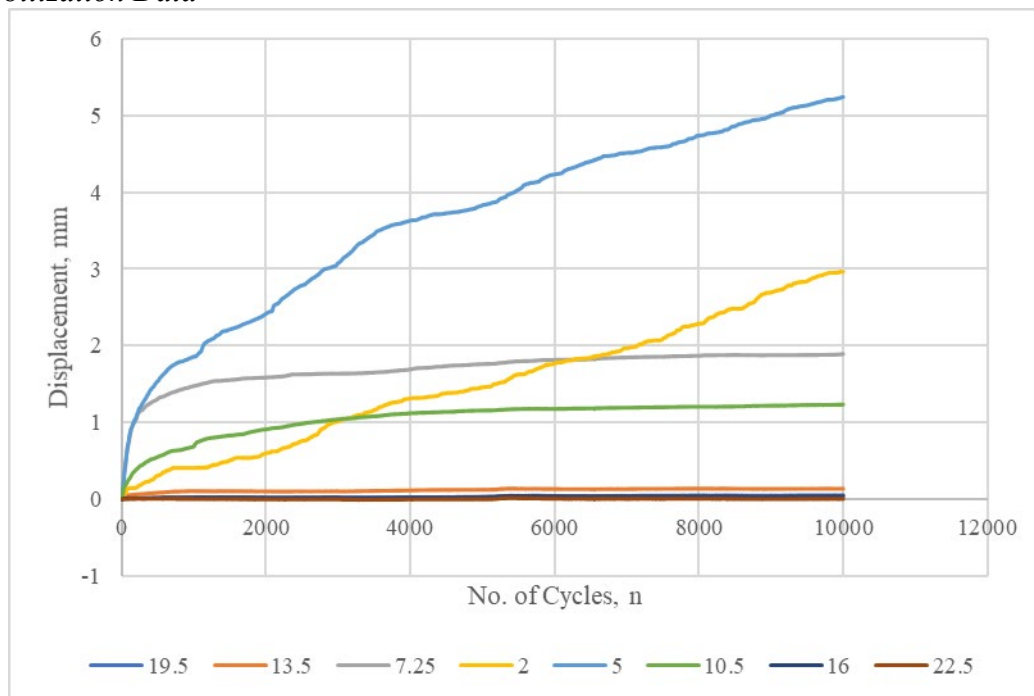
Figure 5.56 LP Displacements with No. of Cycles - AC1-BS1-SG1-GG6

Density Data

Table 5.36 Density of Pavement Layers - AC1-BS1-SG1-GG6

Layer	Density	Unit
HMA	2115	kg/m^3
Base Layer	1726	kg/m^3
Subgrade Layer	1572	kg/m^3

5.3.7.6 AC1-BS1-SG1-GG7

Rutting
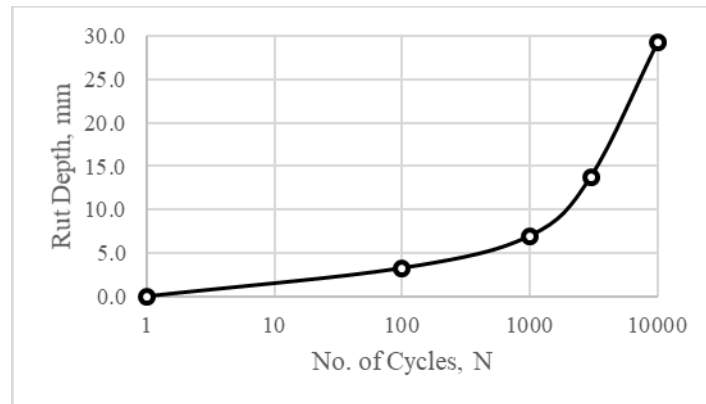
Figure 5.57 Rut Depth Vs. No of Cycles – AC1-BS1-SG1-GG7

Soil Mobilization Data

Data – Not Available

Density Data

Table 5.37 Density of Pavement Layers - AC1-BS1-SG1-GG7

Layer	Density	Unit
HMA	2112	kg/m^3
Base Layer	1715	kg/m^3
Subgrade Layer	1561	kg/m^3

5.3.7.7 AC1-BS1-SG1-GG8

Rutting
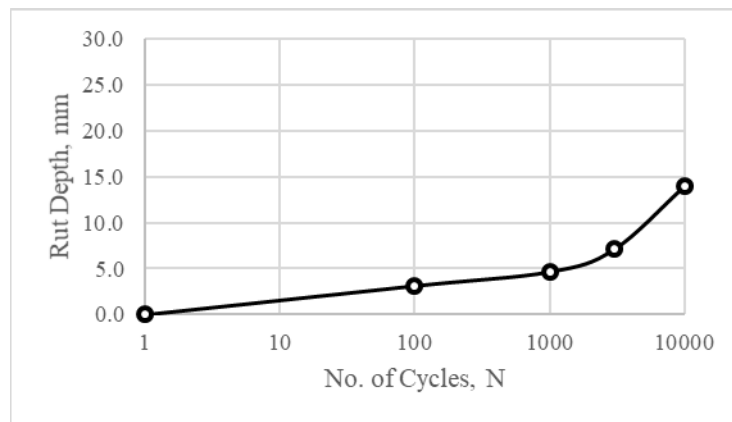
Figure 5.58 Rut Depth Vs. No of Cycles – AC1-BS1-SG1-GG7

Soil Mobilization Data

Data – Not Available

Density Data

Table 5.38 Density of Pavement Layers - AC1-BS1-SG1-GG7

Layer	Density	Unit
HMA	2120	kg/m^3
Base Layer	1730	kg/m^3
Subgrade Layer	1570	kg/m^3

5.3.8 GEOGRID LOCATION SERIES

This series comprises of tests conducted by the alteration of the location of the geogrid in the baseline configuration. Two additional tests have been performed for this series with the geogrid at different distances from the AC-BS interface against the baseline configuration.

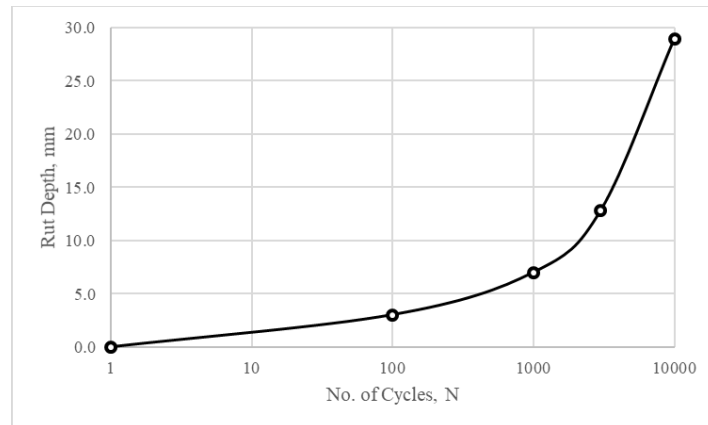### 5.3.8.1 AC1-BS1-SG1-GG1[1]

Rutting
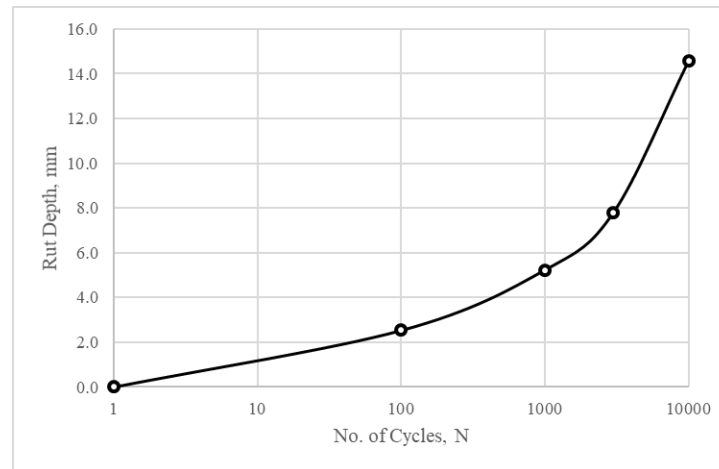
Figure 5.59 Rut Depth Vs. No of Cycles – AC1-BS1-SG1-GG1[1]

Soil-Geogrid Mobilization
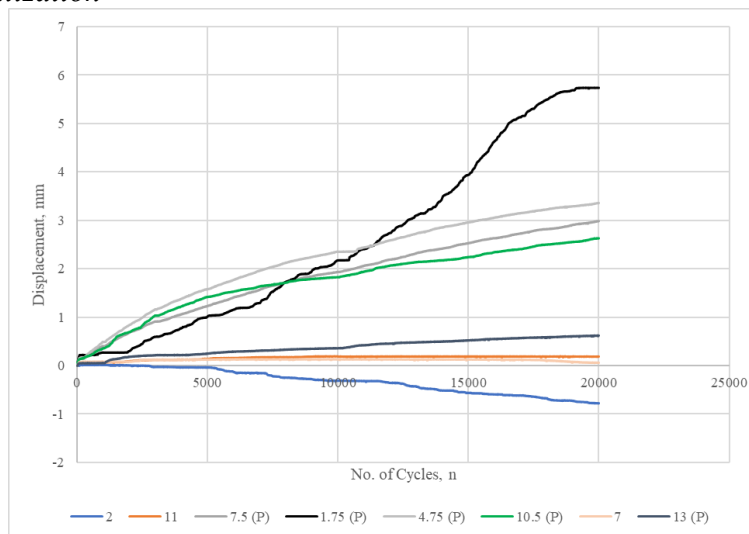
Figure 5.60 LP Displacements with No. of Cycles - AC1-BS1-SG1-GG1[1]

97

where (P) represents soil particle movements and others represent geogrid nodal displacements

Density Data

Table 5.39 Density of Pavement Layers - AC1-BS1-SG1-GG1[1]

Layer	Density	Unit
HMA	2113	kg/m^3
Base Layer	1738	kg/m^3
Subgrade Layer	1554	kg/m^3

5.3.8.2 AC1-BS1-SG1-GG1[3]

Rutting
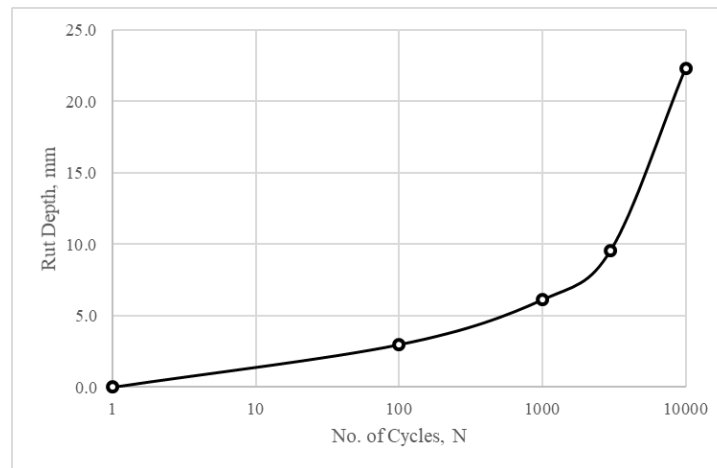
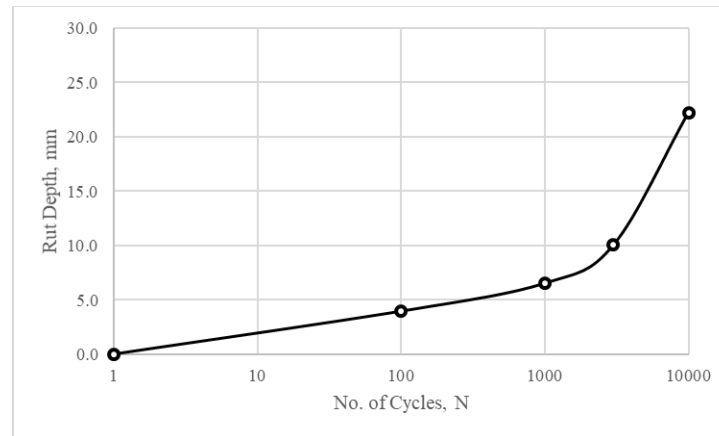**Figure 5.61 Rut Depth Vs. No of Cycles – AC1-BS1-SG1-GG1[3]**

Geogrid Mobilization
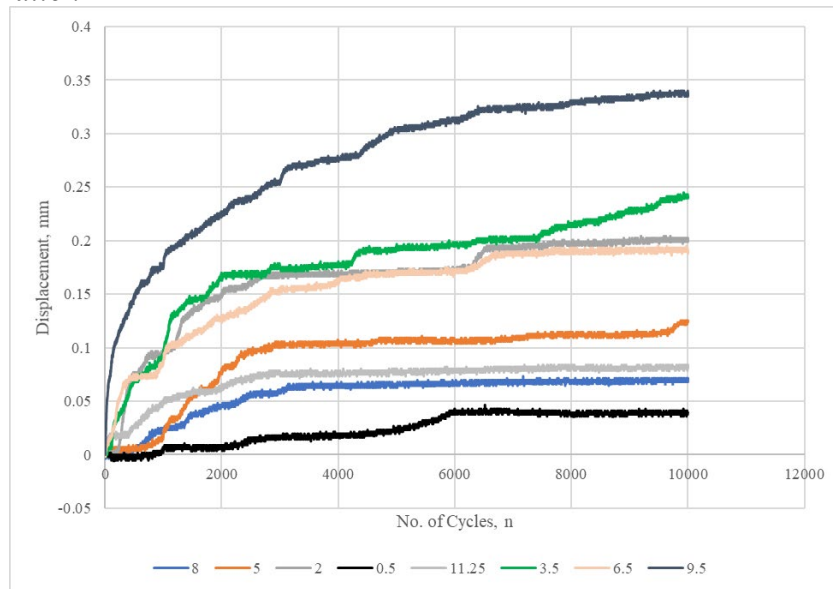
Figure 5.62 LP Displacements with No. of Cycles - AC1-BS1-SG1-GG1[3]

The data represents the horizontal nodal displacements of the geogrid.

Table 5.40 Density of Pavement Layers - AC1-BS1-SG1-GG1[3]

Layer	Density	Unit
HMA	2115	kg/m^3
Base Layer	1726	kg/m^3
Subgrade Layer	1570	kg/m^3

5.3.9 MISCELLANEOUS TESTS

One of the important objectives of the project is to determine the underlying mechanism by which incorporation of geogrids in the base layer improve the pavement performance. In the process of deciphering this mechanism(s), the research team focused on a particular decoupling process. For this reason, additional tests are conducted with thin base layer and a very stiff steel subgrade. The results of these tests are as follows.

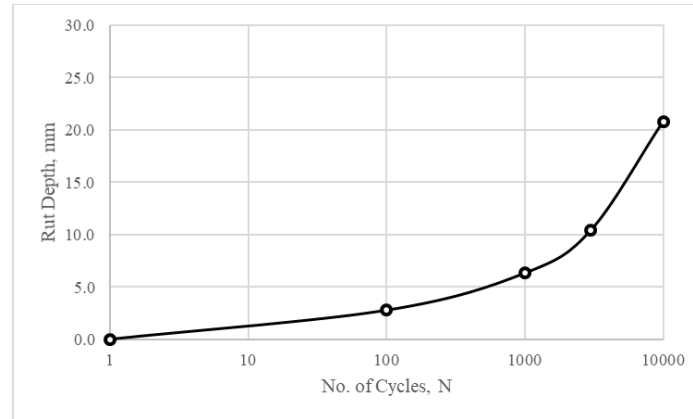### 5.3.9.1 AC1-BS1[2]-SG3-GG1[1.5]-4'

Rutting
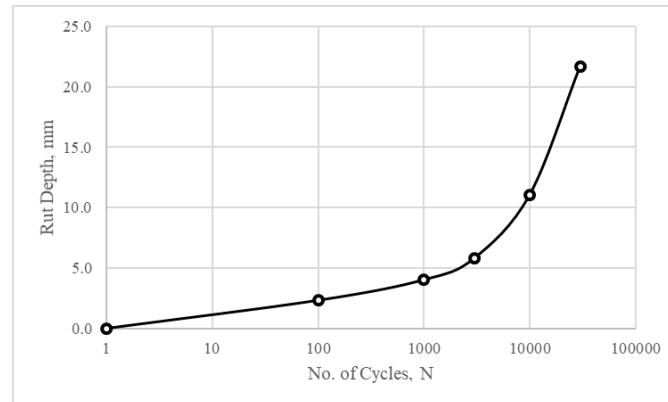
Figure 5.63 Rut Depth Vs. No of Cycles – AC1-BS1[2]-SG3-GG1[1.5]-4'

Geogrid Mobilization Data
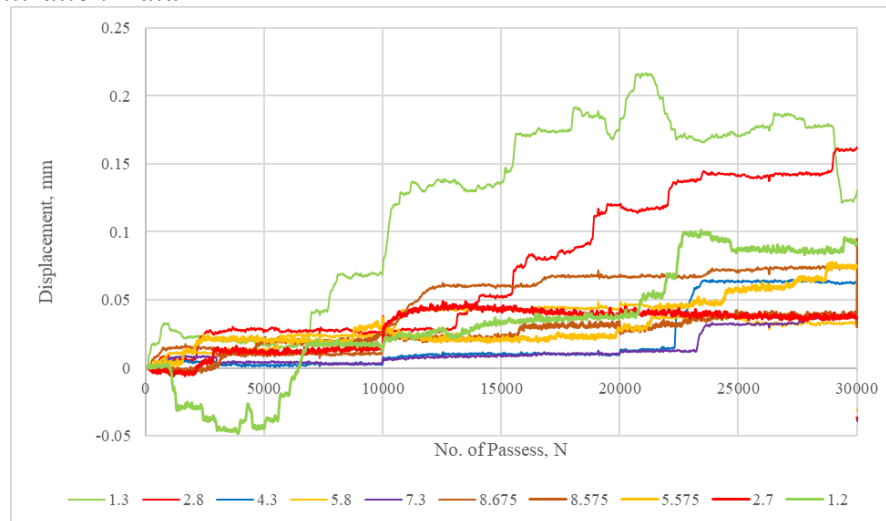
Figure 5.64 LP Displacements with No. of Cycles - AC1-BS1[2]-SG3-GG1[1.5]-4'

Density Data

Table 5.41 Density of Pavement Layers - AC1-BS1[2]-SG3-GG1[1.5]-4'

Layer	Density	Unit
HMA	2117	kg/m^3
Base Layer	1728	kg/m^3
Subgrade Layer	1570	kg/m^3

5.3.9.2 AC1-BS1[2]-SG3*-GG1[1.5]-4'-Mylar Backing

Rutting
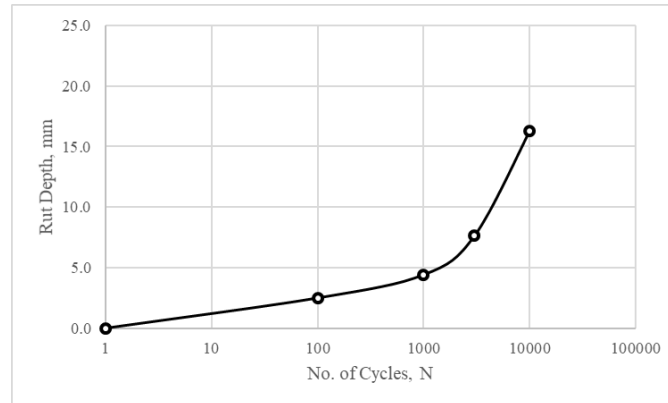
Figure 5.65 Rut Depth Vs. No of Cycles – AC1-BS1[2]-SG3*-GG1[1.5]-4'

Geogrid Mobilization Data
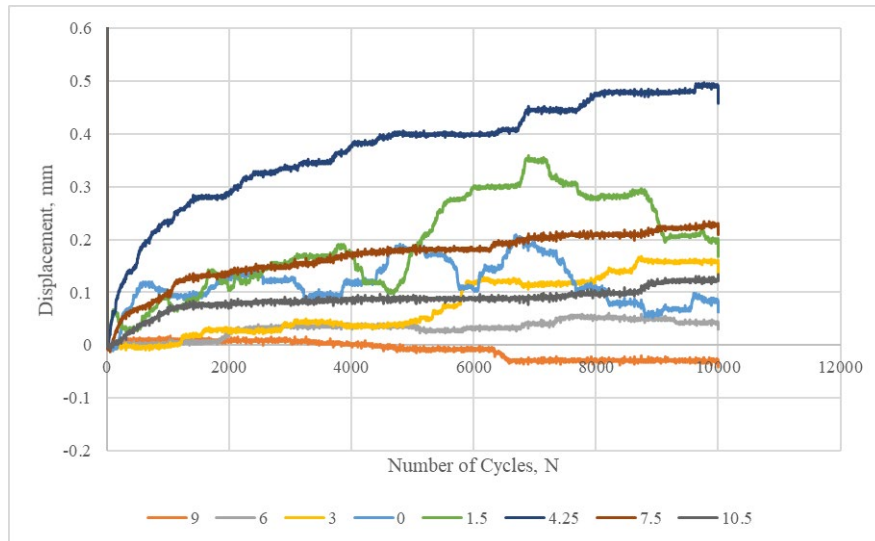
Figure 5.66 LP Displacements with No. of Cycles - AC1-BS1[2]-SG3*-GG1[1.5]-4'

Density Data

Table 5.42 Density of Pavement Layers - AC1-BS1[2]-SG3*-GG1[1.5]-4'

Layer	Density	Unit
HMA	2114	kg/m^3
Base Layer	1734	kg/m^3
Subgrade Layer	1561	kg/m^3

6. PERFORMANCE OF GEOGRID-REINFORCED PAVEMENTS UNDER REDUCED-SCALE APT

The quantification of the benefits of geogrid reinforcements in improving the performance of flexible pavements is summarized in this chapter. Since the focus is on the performance of pavements, rutting criteria is evaluated in both control and reinforced sections under various configurations in the reduced-scale APT Program Traffic Benefit Ratios (TBRs) and Rutting Reduction Ratios (RRRs)

The evaluation of the benefits of geogrids in pavement test sections is conducted in five categories, namely,

- Baseline Series
- Base Thickness Series
- Subgrade Stiffness Series
- Geogrid Type Series
- Geogrid Location Series

Since the performance is evaluated in terms of TBRs and RRRs, measurement of rutting is crucial to this quantification of benefits of geogrid reinforcement. The rut depth is evaluated for the various test sections for every N pass of trafficking.

Once the rut depth is determined as a function of the number of cycles N, the TBR at any rut depth and the RRR at any number of cycles is evaluated as follows.

$$TBR = \frac{N_{Geogrid\ Stabilized}}{N_{Control}} \ (for\ certain\ level\ of\ rutting)$$

$$RRR = \frac{RD_{Geogrid\ Stabilized}}{RD_{Control}} \ (for\ certain\ no.\ of\ cycles)$$

6.1 BASELINE SERIES

The baseline series comprises of two test sections with identical configuration stated in Table 6.1.

Table 6.1 Baseline Series Section Configuration

Material	Thickness
HMA Layer	1" of AC1
Base Layer	5" of BS1
Subgrade Layer	6" of SG1
Geogrid	GG1 at 2" below AC-BS Interface
Width of the Box	**6'**

6.1.1 TRAFFIC BENEFIT RATIO
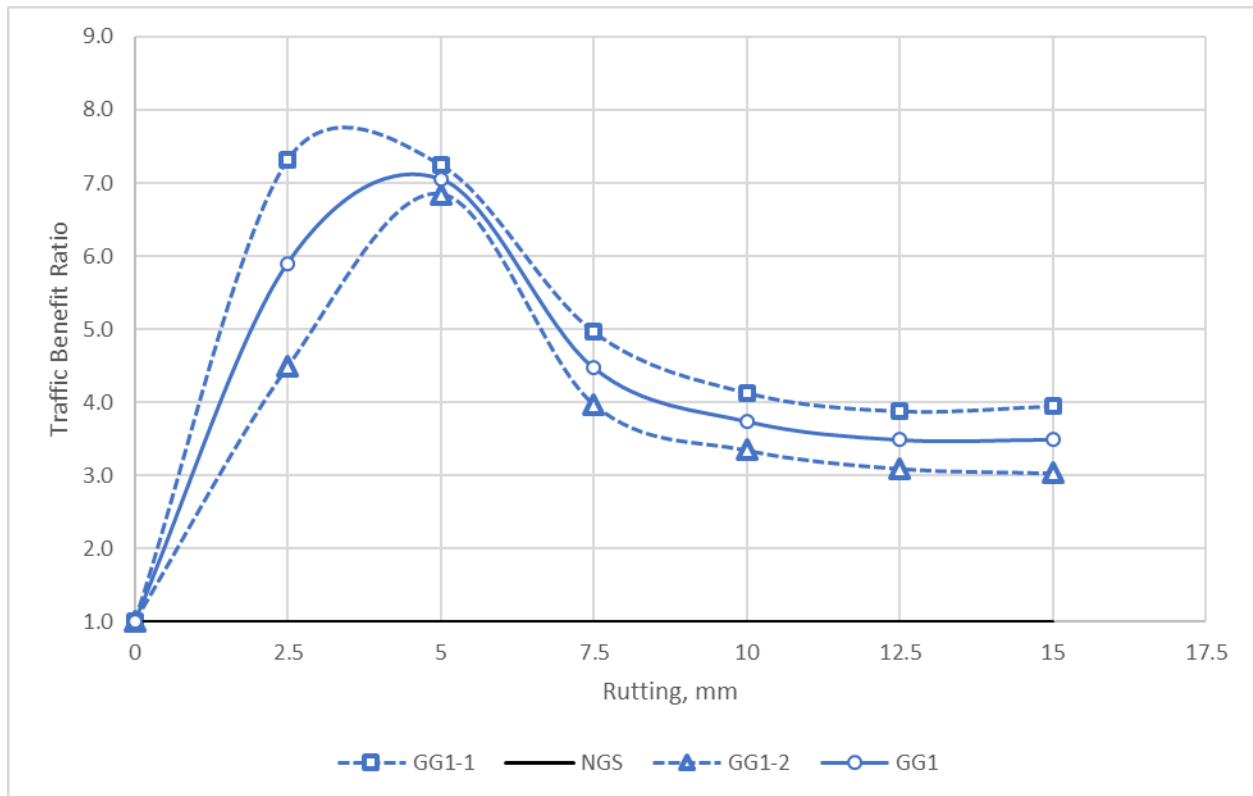
Figure 6.1 Traffic Benefit Ratio of Baseline Series

Figure 6.1 shows the TBR as a function of Rut Depth for the two repeats of the baseline series (in dashed blue lines) and their average in solid blue line. It is worth noting that the TBR is not constant throughout the degree of deformation of the pavement. It is smaller in the beginning of the pavement trafficking and increases with increase in rut depth until a point (around 4 mm, in this case), and then decreases to asymptote to a constant value at higher values of Rut Depth (around 12.5 mm = 0.5 inch). This behavior has been observed in literature as well. Thus, depending on the failure criteria for performance, the TBR may be vastly different.

6.1.2 RUTTING REDUCTION RATIO
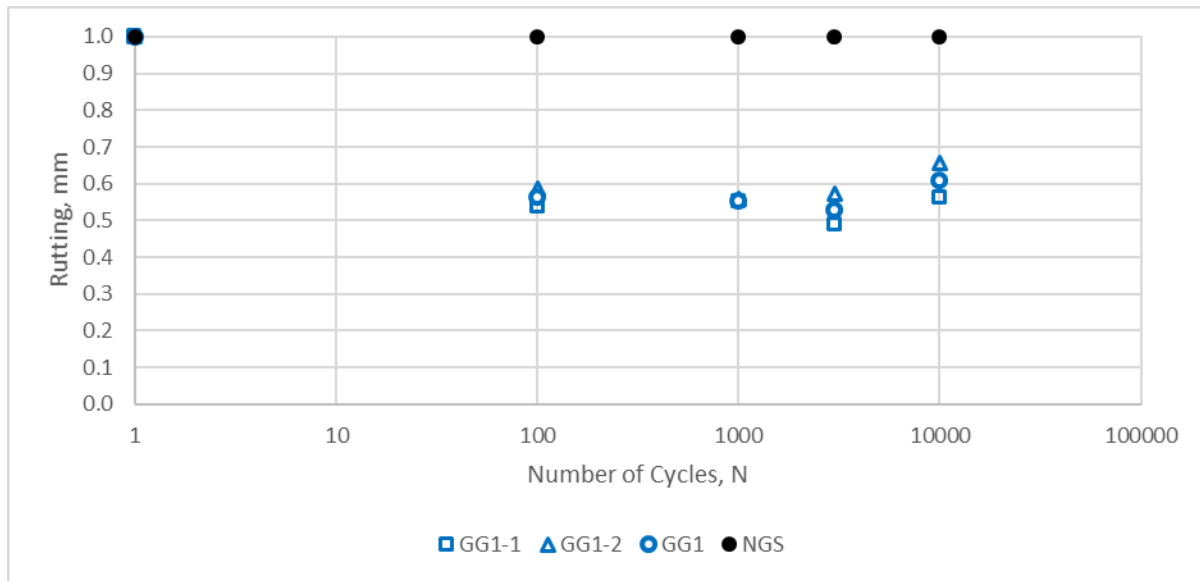
Figure 6.2 Rutting Reduction Ratio of Baseline Series

The RRR appears to decrease at the beginning, then flattens out and even decreases towards the end. This is the inverse effect observed with the TBR trend and is compatible with what was observed in the case of TBR vs. Rut Depth.

6.1.3 SOIL-GEOGRID MOBILIZATION
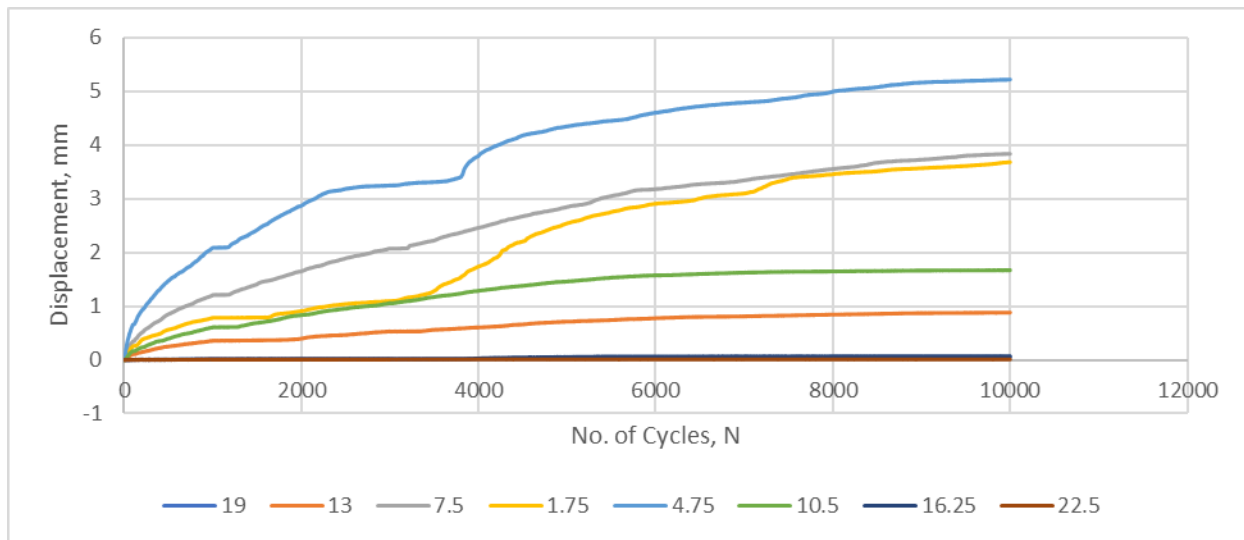
Figure 6.3 Soil Particle Displacement in Control Section
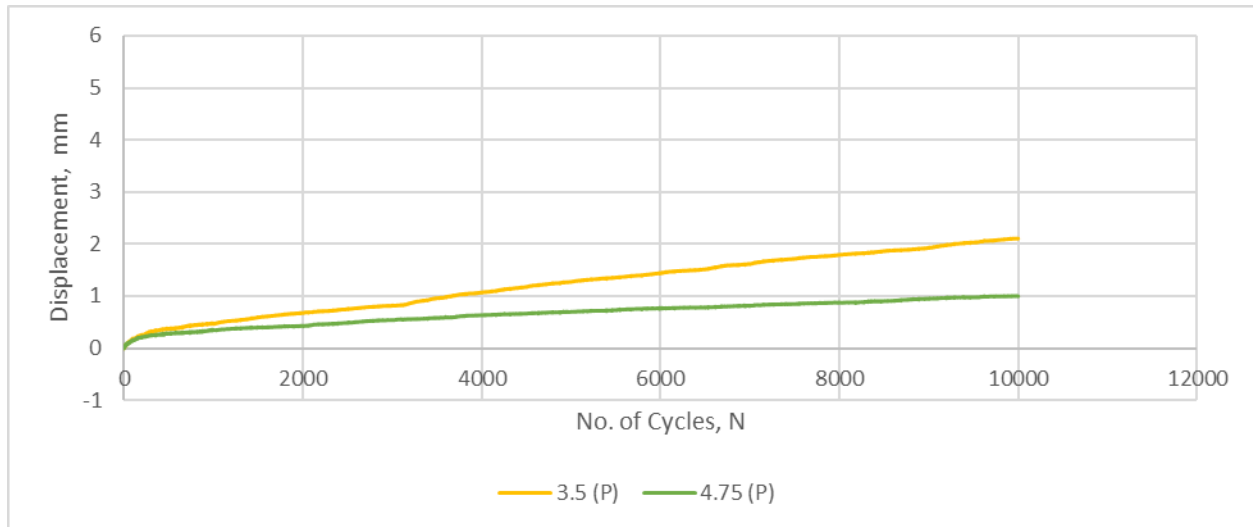
Figure 6.4 Soil Particle Displacement in Baseline Section

From Figure 6.3 and Figure 6.4 it can be seen that the particle movement (all curves in Figure 6.3 and (P) curves in Figure 6.4) in the reinforced baseline section is significantly smaller than in the control section. This shows that the reinforcement offers lateral restraint against the horizontal movement of particles from under the wheel path, thereby mitigating the reduction in confinement under the wheel, resulting in increased resilient modulus and better performance of the reinforced pavement under traffic loads.

6.2 BASE THICKNESS SERIES

The base thickness series comprises of the baseline configuration and two additional tests with different base thicknesses which are identical to the baseline section in all other aspects. The details are listed in Table 6.2

Table 6.2 Base Thickness Series Section Configuration

Material	Baseline Section	Section 1	Section 2
HMA Layer		1" of AC1	
Base Layer	5" of BS1	4" of BS1	2.5" of BS1
Subgrade Layer	6" of SG1	7" of SG1	8.5" of SG1
Geogrid		GG1	
GG Position		2" below AC-BS Interface	
Width of Box		**6'**	

6.2.1 Traffic Benefit Ratio
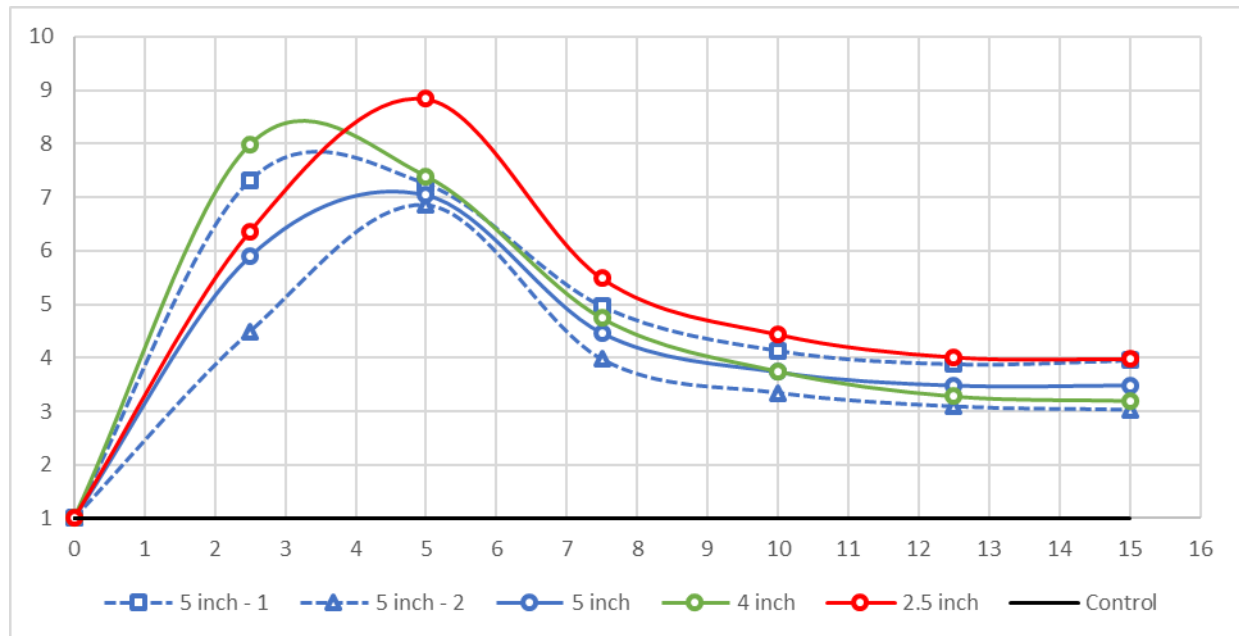
Figure 6.5 Traffic Benefit Ratio of Base Thickness Series

It can be seen from Figure 6.5, that the change in the thickness of the base layer has little to no influence on the TBR. Rather they are within the errors of repeatability (the blue lines). This may be attributed to the fact that the location of the geogrid does not change across all test sections. Therefore, the stabilization provided by the geogrid on all test sections in this series is more or less equal.

6.2.2 Rutting Reduction Ratio
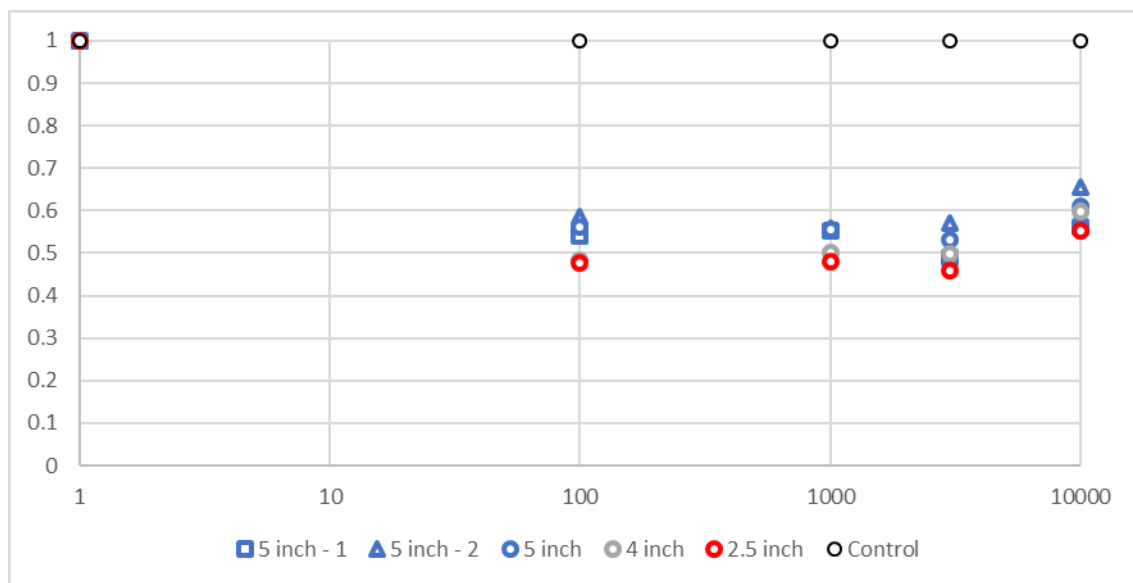
Figure 6.6 Rutting Reduction Ratio of the Base Thickness Series

It appears that the RRR of reduced thickness sections are lower than the full thickness section. This may be counter intuitive but is still compatible with what was observed in the TBR curves and also variation is so small that it is within the error of repeatability.

6.3 SUBGRADE STIFFNESS SERIES

This series comprises of the baseline configuration section and two additional sections with modified subgrades. The configurations are detailed in Table 6.3.

Table 6.3 Subgrade Stiffness Series Section Configuration

Material	Baseline Section	Section 1	Section 2
HMA Layer		1" of AC1	
Base Layer		5" of BS1	
Subgrade Layer	6" of SG1	3" of SG2	SG3
Geogrid		GG1	
GG Position		2" below AC-BS Interface	
Width of Box		**6'**	

6.3.1 TRAFFIC BENEFIT RATIO
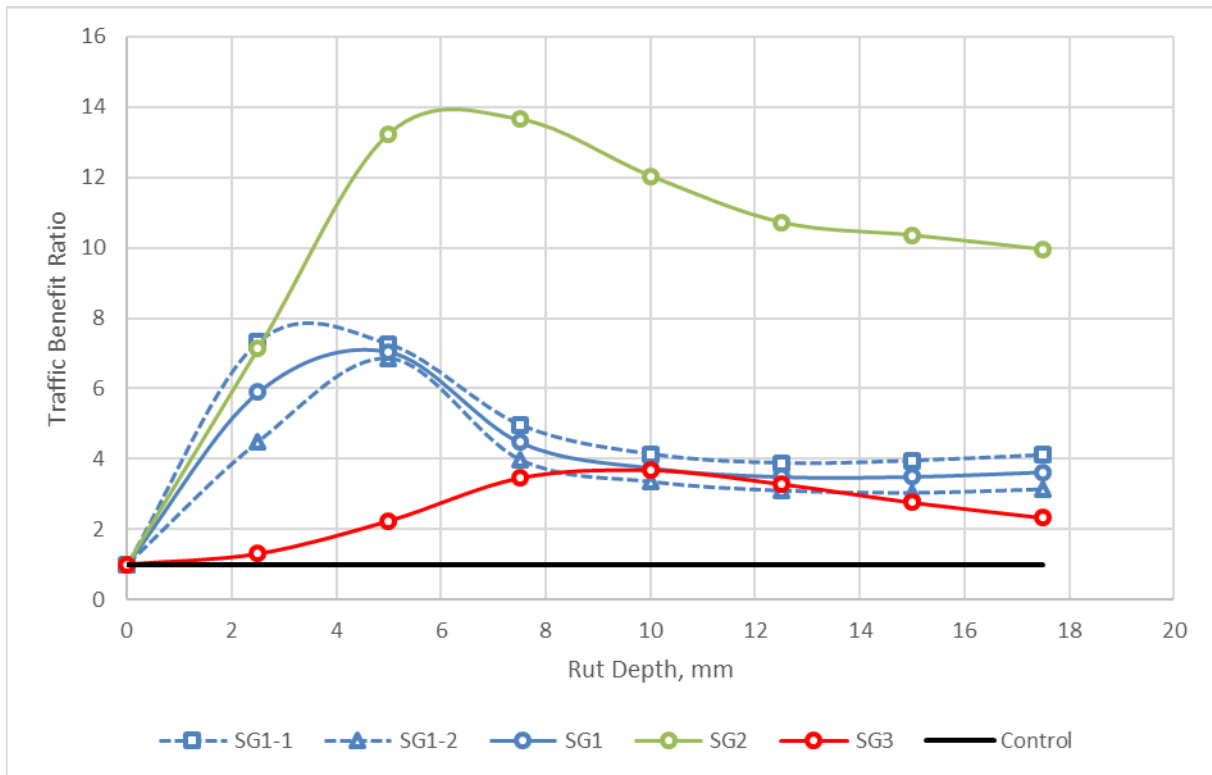
Figure 6.7 Traffic Benefit Ratio of Subgrade Stiffness Series

It can be seen from Figure 6.7, the softer the subgrade (SG2<SG1<SG3 in terms of stiffness), the greater is the traffic benefit ratio. It is noted that the TBR is calculated as ratios of No. of Cycles of respective reinforced and control section configurations.

106

6.3.2 RUTTING REDUCTION RATIO

Since the various configurations are tested through variable no. of cycles (100s, 1000s and 10,000s of cycles), a rutting reduction ratio curve representative of the pavement sections is not available.

6.4 GEOGRID TYPE SERIES

This series comprises of the baseline section and four additional identical sections but with different geogrids. The details of the configurations are as in Table 6.4.

Table 6.4 Geogrid Type Series Section Configurations

Material	Baseline	Section 1	Section 2	Section 3	Section 4
HMA Layer	1" of AC1	1" of AC1	1" of AC1	1" of AC1	1" of AC1
Base Layer	5" of BS1	5" of BS1	5" of BS1	5" of BS1	5" of BS1
Subgrade Layer	6" of SG1	6" of SG1	6" of SG1	6" of SG1	6" of SG1
Geogrid	GG1	GG2	GG3	GG4	GG1
GG Position	2" below AC-BS Interface				
Width of Box	**6'**	**6'**	**6'**	**6'**	**6'**

6.4.1 TRAFFIC BENEFIT RATIO
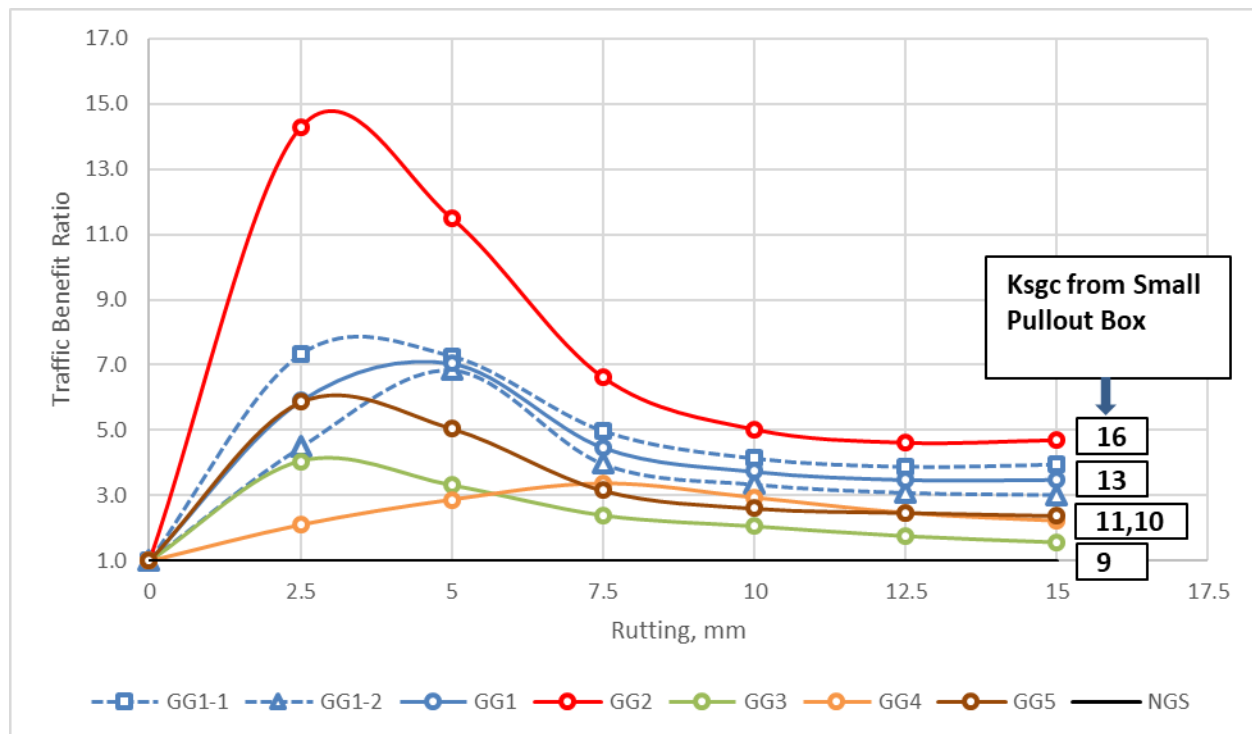
Figure 6.8 Traffic Benefit Ratio of Geogrid Type Series along with K_{SGI} Values of the Geogrids

As seen in Figure 6.8, the terminal TBR values for the various geogrids can be ranked with a direct correlation to the K_{SGI} values of the geogrid with the river washed pea gravel at 3 psi in the small pullout box tests. This result reaffirms the use of K_{SGI} from small pullout box tests as a valid parameter for the evaluation of the performance of geogrid reinforced pavements.

6.4.2 RUTTING REDUCTION RATIO
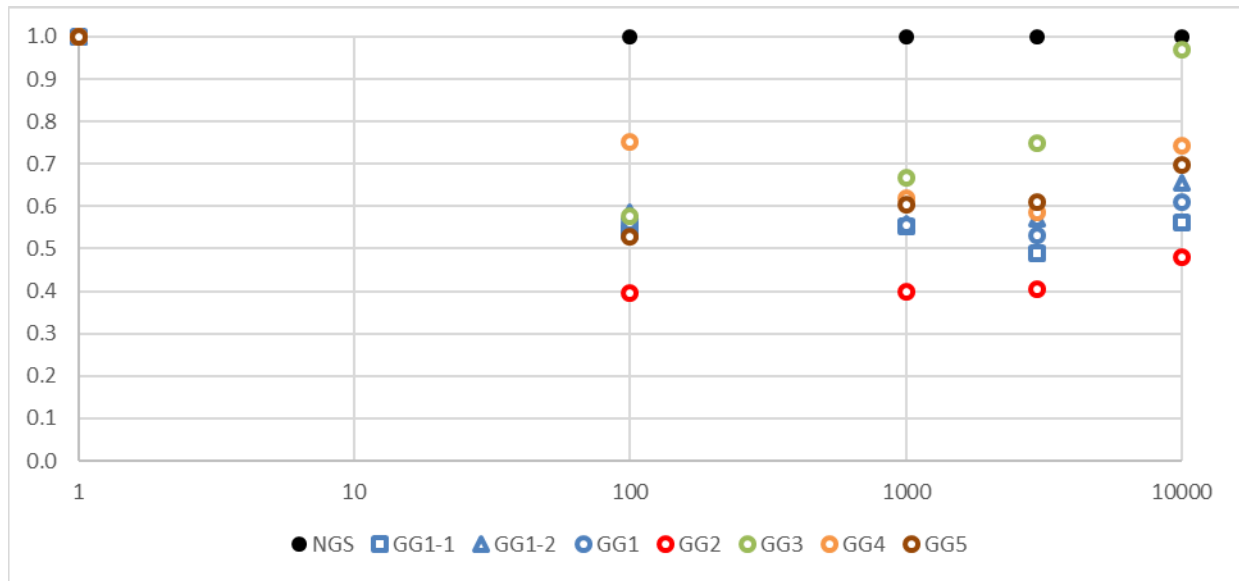
Figure 6.9 Rutting Reduction Ratio of Geogrid Type Series

From Figure 6.9, it is inferred that the benefit from the presence of a geogrid is not indefinite for all geogrids, in that, given enough number of cycles, the Rutting Reduction Ratio maybe reduced to 1.0 like in the case of GG3. For every configuration, there lies an optimum number of cycles in which the benefit from the geogrid is maximum. Therefore, it becomes important to choose that configuration in which the optimum number of cycles from RRR curve is equivalent to the design life of the pavement. This procedure aims at maximizing the benefits of using geogrids in pavement design.

6.5 GEOGRID LOCATION SERIES

This series consists of the baseline section and two additional sections similar to the baseline section except in the location of the geogrid from the Asphalt Concrete – Base Layer interface (AC-BS interface). The details of the configuration used in this section are outlined in Table 6.5.

Table 6.5 Geogrid Location Series Section Configuration

Material	Baseline Section	Section 1	Section 2
HMA Layer	1" of AC1	1" of AC1	1" of AC1
Base Layer	5" of BS1	5" of BS1	5" of BS1
Subgrade Layer	6" of SG1	6" of SG1	6" of SG1
Geogrid	GG1	GG1	GG1
GG Position	2" below AC-BS Interface	1" below AC-BS Interface	3" below AC-BS Interface
Width of Box	**6'**	**6'**	**6'**

6.5.1 TRAFFIC BENEFIT RATIO
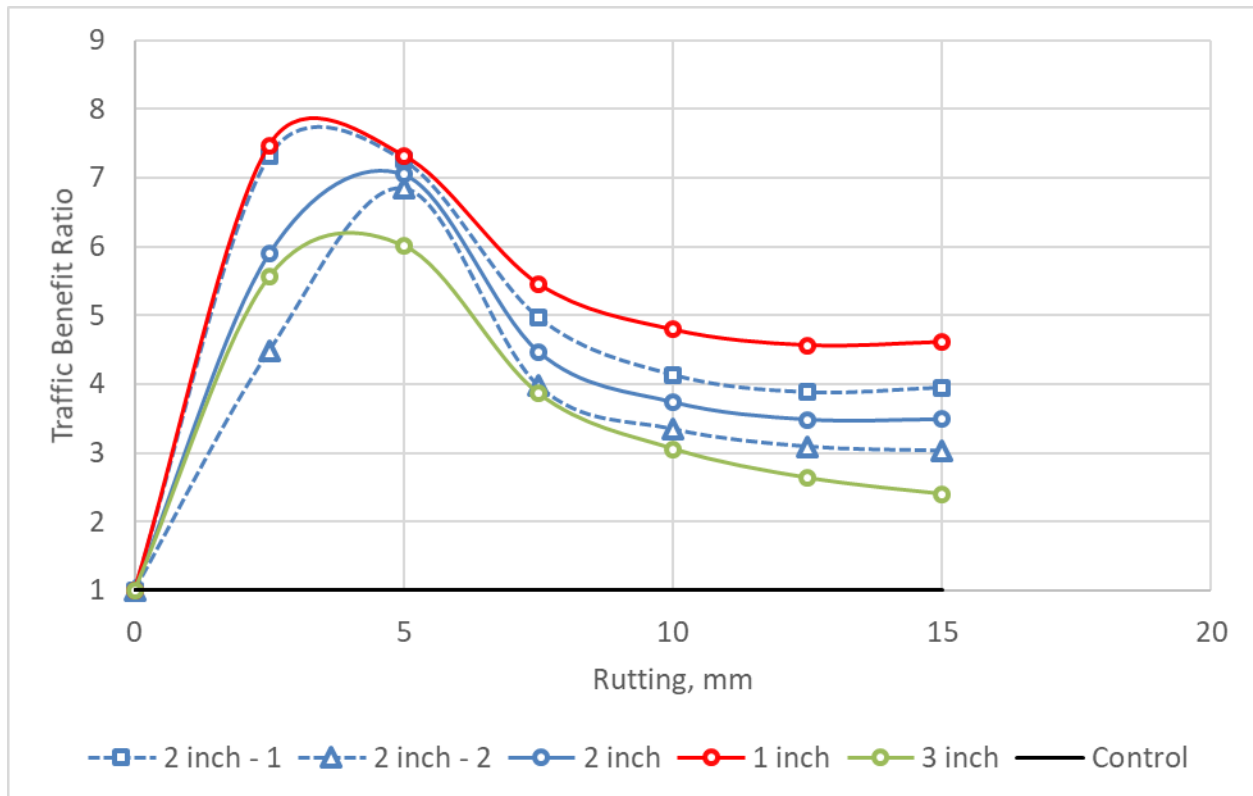
Figure 6.10 Traffic Benefit Ratio of Geogrid Location Series

From Figure 6.10 it is seen that as the geogrid is moved towards the surface of the pavement, the TBR increases, thereby increasing the benefit of the reinforcement. However, existing literature suggests that the geogrid be placed at one-third depth or middle of the base layer for maximizing the benefits and practical limitations in constructability dictates that the geogrid be placed at the base-subgrade interface. Also, it is noted that the trend observed is specific to the configuration in which the sections are built. The research team does not advise the generalization of the observed trend without further testing with different configurations. It is reasoned that the higher the geogrid in the system, the earlier the mobilization of the lateral restraint effect and greater the membrane effects from the reinforcement adding additional structural capacity to the pavement system.

6.5.2 RUTTING REDUCTION RATIO
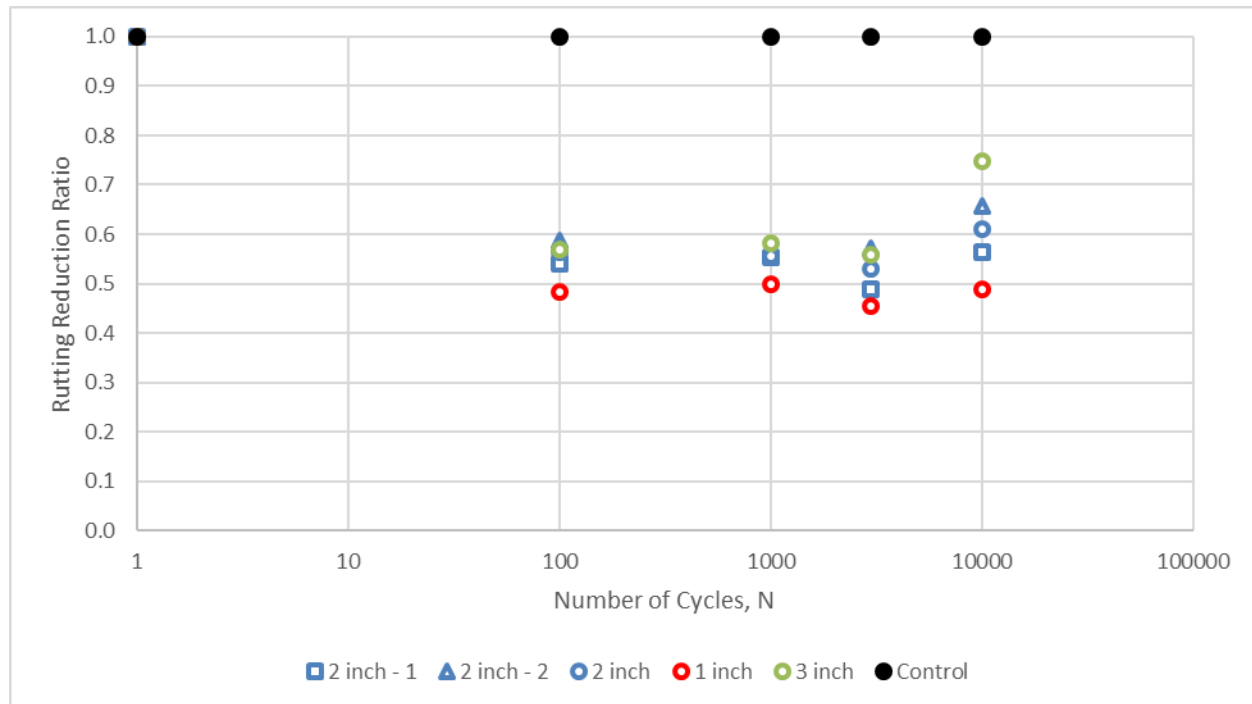
Figure 6.11 Rutting Reduction Ratio of Geogrid Location Series

The higher the geogrid within the pavement structure, the longer the influence of the reinforcement in the structural capacity of the pavement structure. The pavement section with the geogrids placed at deeper depths show minimal improvement in performance in terms of magnitude and in terms of life span. Towards the end of the life, RRR increases significantly for the section with geogrid at 3 inches below the AC-BS interface than it does for the section with the geogrid at 1 inch.

6.6 SUMMARY

The results from the APT program show certain key features, namely,

- The presence of geogrids within the base layer of the pavement section improves the rutting performance of the pavement structure under trafficking.
- The traffic benefit ratio initially increases with increase in deformation up to an optimum deformation. Then it gradually reduces and asymptotes to a constant value.
- The rutting reduction ratio follows a reverse trend with the number of cycles. It initially decreases from 1.0, reaches an optimum minimum and then increases. In some cases, RRR could be very close to 1.0 towards the end. RRR curve did not asymptote to a constant value in the scope of this APT Program.
- Change in thickness of the base layer did not have an accompanied change in performance. This is attributed to the near similar stiffness of the base layer and subgrade utilized.
- The TBR increases and RRR decreases, in general, with decrease in subgrade stiffness
- The type of geogrid utilized affects the performance of the pavement section and ranking of the performance of the different geogrids is the same as the ranking based on their Ksgc from small pullout box tests.

- The closer the geogrid is to the surface, the better the performance of the pavement structure.

It must be noted that some of these observations are also observed in the field program. Some of the key differences being, in the field, the value of TBR recorded is somewhat lower than those observed in the laboratory. This is attributed to the long-term relaxation effects on the stresses in the geogrid (ergo, confining pressure in the base material). There is also consideration for the difference in configuration of the pavement section. This is one of the major challenges in the development of design procedures. These concerns will be addressed in the upcoming chapter.

7.   DESIGN OF GRPS – TOOLS AND APPROACHES

One of primary objectives of the project is the development of approaches to modify FPS-21 (procedure for design of flexible pavements) to enable the design of geogrid reinforced bases in flexible pavements. This chapter explains the approach adopted in this regard. The use of the SGI test results and the parameter K_{SGI} is validated as a selection criterion in the geogrids to be used as reinforcement for Base Layers to mitigate traffic induced pavement distresses.

7.1   PERFORMANCE EQUATION – FPS-21

Flexible Pavement Design System 21 (FPS-21), used by TxDOT, is a mechanistic-empirical approach to the design of flexible pavements. In this approach, the pavement design is carried out by utilizing a performance equation that establishes the balance between design, traffic, environmental and performance variables. The development of design tools for Geogrid Reinforced Pavements (GRPs) and subsequent recommendation for the design procedure involved direct or indirect modification of the variables used in the performance equation of FPS-21. In this section, the performance equation is discussed, and the variable(s) of interest is identified. The tests carried out as part of TxDOT 0-6834 are reduced scale tests. Hence the validity of scaling results obtained from these tests to full-scale field sections are considered.

7.1.1   PERFORMANCE EQUATION FOR APTS

The performance equation used in FPS-21 was first introduced in TTI Research Report 32-11. It includes two terms, one representing the traffic associated serviceability loss and another representing the environmental damage associated serviceability loss (swelling clay and differential foundation movements). The equation takes the form takes the form shown below.

$$Q_2 = \frac{0.134(N_k - N_{k-1})S_c^2}{\bar{\alpha}} + Q_2'\left(1 - e^{-b_k(t_k - t_{k-1})}\right) \quad (3)$$

$$\text{Traffic Induced} \quad + \quad \text{Environmental Induced}$$

where Q   = Serviceability Loss Function at time, $t = \sqrt{5 - P} - \sqrt{5 - P_1}$

Q_2 = Q at P = P_2

Q_2'   = $\sqrt{5 - P_2'} - \sqrt{5 - P_1}$

P   = Pavement Serviceability Index at time, t

P_1 = Expected Max. Pavement Serviceability Index after initial or overlay construction

P_2 = Pavement Serviceability Index at the end of the considered performance period

P_2'   = P at t = ∞ in the absence of traffic ($0 \leq P_2' \leq P_1$)

t   = time (in years) since original construction

t_k = time at the end of the kth performance period i.e., $t_0 = 0$ years

b_k = a swelling clay parameter applying to the kth performance period

N   = number of 18-kip ESALs

N_k = N at the end of the kth performance period i.e., $N_0 = 0$ ESALs

α = a daily temperature constant = $\frac{1}{2}$ (max. daily temp. + min. daily temp.) $- 32^0$ F

$\bar{\alpha}$ = the effective value of α for a typical year in a given locality (harmonic mean)

S_c = Corrected Surface Curvature Index under a dual wheel load

In the case of accelerated pavement tests (APTs) conducted on reduced scale test sections inside controlled-environment laboratory, the serviceability loss associated with environmental loads is zero for all practical purposes. Thus, the performance equation for the APTs consists of only the traffic load associated serviceability losses as follows.

$$Q_2 = \frac{0.134(N_k - N_{k-1})S_c^2}{\bar{\alpha}} \tag{4}$$

The loss in serviceability of the test section can be quantified from monitoring the pavement distresses observed as it is trafficked. In the APTs conducted as a part of TxDOT 0-6834, it is observed that the only type of pavement distress observed under accelerated trafficking is the rutting of the pavement section.

• If the performance of the various test sections is evaluated between the same levels of rutting, the serviceability loss function Q_2 in equation (4) will remain a constant. In this study, all test sections have been evaluated between the following rut levels.

Initial Rut Depth = 0 mm (0") and Final Rut Depth = 12.5 mm (0.5")

• Since the tests are all conducted under a controlled environment (72^0 F), the effective temperature constant will remain the same between tests.
• There is only one performance period between rut depths of 0 mm to 12.5 mm.

Therefore equation (4) can be rewritten as,

$$NS_c^2 = constant \tag{5}$$

where N = No. of Passes to 12.5 mm of Rut Depth

S_c = Corrected Surface Curvature Index under dual wheel load

constant = remains a constant across all test sections

Equation (5) represents the performance equation for Accelerated Pavement Test sections evaluated in this study.

7.1.2 CALCULATION OF SURFACE CURVATURE INDEX
In the original performance equation (3), the surface curvature index of the design pavement section is determined by conducting a dual wheel load test using Multi-Layer Linear Elastic Analysis (LEA). The modulus values used in this analysis is those obtained from back-calculation from Falling Weight Deflectometer (FWD) tests conducted on existing pavements section with similar materials. The surface curvature index obtained from Multi-Layer LEA, is then corrected for FWD to Truck Wheel loading and Truck Speed. Thus

$$S_c = 1.16(1 + F)S \tag{6}$$

113

where 1.16 = Correction from FWD moduli to Truck Wheel Loading moduli

(1 + F) = Truck Speed Correction

S = Surface Curvature Index from LEA

Since the type of wheel load and the speed, are the same across various test sections, equation (5) can be rewritten as,

$$NS^2 = constant \qquad (7)$$

where NS^2 should remain constant across all APT test sections.

Since the APT sections are reduced scale test sections, the standard full-scale dual-wheel load cannot be used to determine the surface curvature index of the various test sections. As an alternative, a reduced-scale dual wheel load is adopted.

Figure 7.1 shows the full-scale dual wheel load used for LEA in FPS-21 and the reduced-scale dual wheel load used as a part of this study.
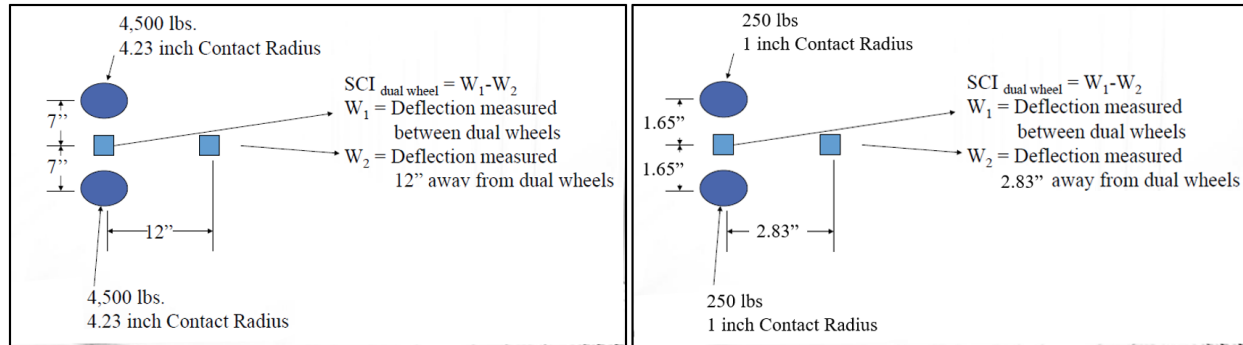
Figure 7.1. Dual Wheel Load (a) Full-scale (b) Reduced Scale

The following parameters are assumed in the LEA.

- Full-scale Standard Dual-wheel load = 18 kips / 2 = 9000 lbs
- MMLS-scale Single-wheel load = 500 lbs
- Tire Pressure in both cases = 80 psi
- Therefore, Ratio of Loads = Ratio of Areas = 18
- For similitude, scaling factor = $\sqrt{18}$ = 4.24

Therefore, all linear dimensions are reduced by a factor of 4.24 and all loads are reduced by a factor of 18 to obtain the reduced-scale dual wheel load. It is to be noted that since the surface curvature index has the dimension of length, the calculated reduced-scale SCI must be multiplied by 4.24 to obtain the full-scale value. However, since this multiplier is a constant across the test sections, this may be ignored in further analysis and equation (7) is valid for the reduced-scale test sections as well.

7.1.3 CALCULATION OF MODULUS OF MATERIAL LAYERS

The elastic modulus of material layers used in test sections (Cemex Flex Base, River-washed Pea Gravel, Monterey Sand and Aquafoam) is determined by conducting tri-axial tests at various confining pressures. The relative density/relative compaction used to determine the modulus are

114

the same as those used in the actual test sections. The resulting stress-strain curves are used to calibrate a Duncan-Chang hyperbolic model. This model is then used to determine the modulus of the various materials at different levels of confinement. Since the modulus depends on the level of confinement, the confinement on the state of stress and the state of stress on the modulus, an iterative procedure is employed to determine the modulus of the various layers. An illustration of the procedure employed is demonstrated below using Monterey Sand.
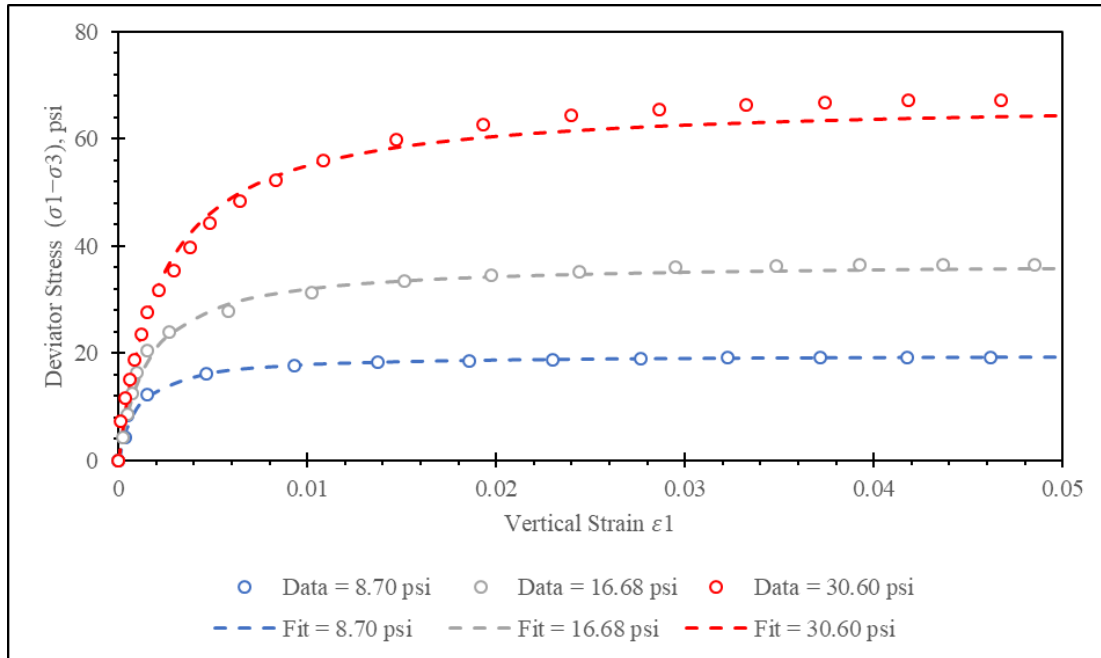
Figure 7.2. Stress-Strain Curves - Monterey Sand

Figure 7.2 shows the stress-strain relationship obtained from tri-axial tests conducted on Monterey Sand at different confining pressures. The data points obtained from the test are shown in open circles. The dashed line through the data points represents the fit obtained from Duncan-Chang Hyperbolic Model defined by

$$\sigma_1 - \sigma_3 = \frac{\varepsilon_1}{a + b\varepsilon_1} \tag{8}$$

where E_i $\qquad$ = Initial Modulus = 1/a

$\quad (\sigma_1 - \sigma_3)_u$ $\quad$ = Deviatoric Stress at Failure = 1/b

$\quad \varepsilon_1$ $\qquad$ = Vertical Strain

Thus, the parameters (E_i , ($\sigma_1 - \sigma_3)_u$) are obtained for each level of confinement. The results for Monterey Sand are tabulated in Table 7.1.

Table 7.1. Duncan Chang Hyperbolic Model Parameters

Confinement (psi) σ_3	Initial Modulus (psi) E_i	Deviator Stress at Failure (psi) $(\sigma_1 - \sigma_3)_u$
8.70	19320	19.7

| 16.68 | 23838 | 36.9 |
| 30.60 | 30357 | 67.3 |

These parameters are then fitted with appropriate equations to determine the modulus and shear strength of the materials under various levels of confinement. These equations are as follows.

$$E_i = Kp_a \left(\frac{\sigma_3}{p_a}\right)^n \tag{9}$$

$$(\sigma_1 - \sigma_3)_u = (M - 1)\sigma_3 \tag{10}$$

where K, n, and M   = Dimensionless Constants for Fitting

    p_a = Atmospheric Pressure = 14.696 psi

The fitted curves are shown in Figure 7.3 and Figure 7.4.
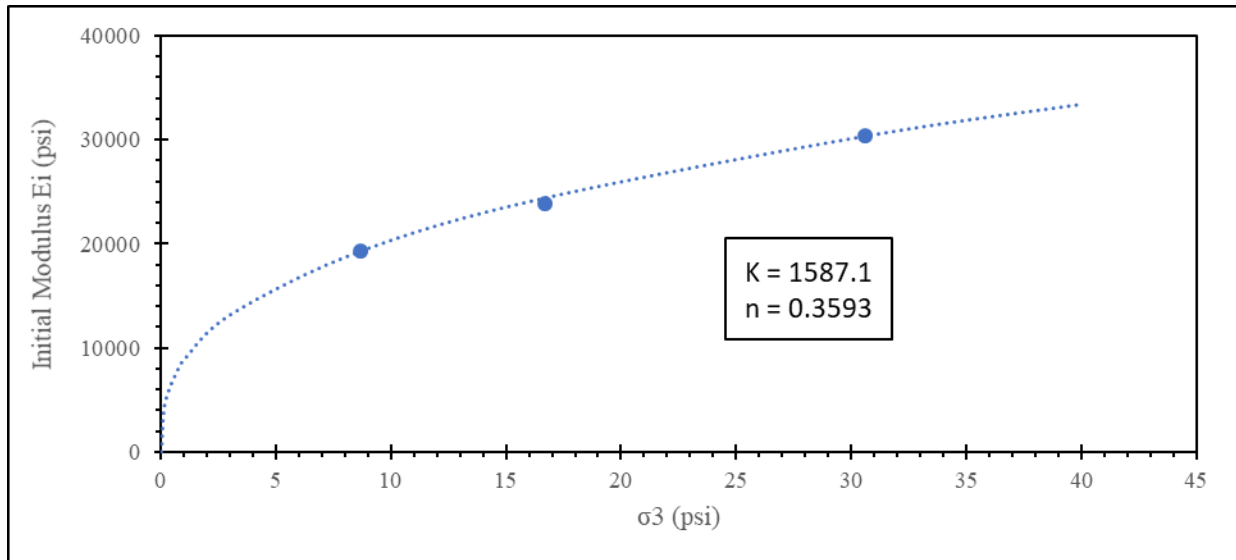
Figure 7.3. Duncan-Chang - Initial Modulus

116
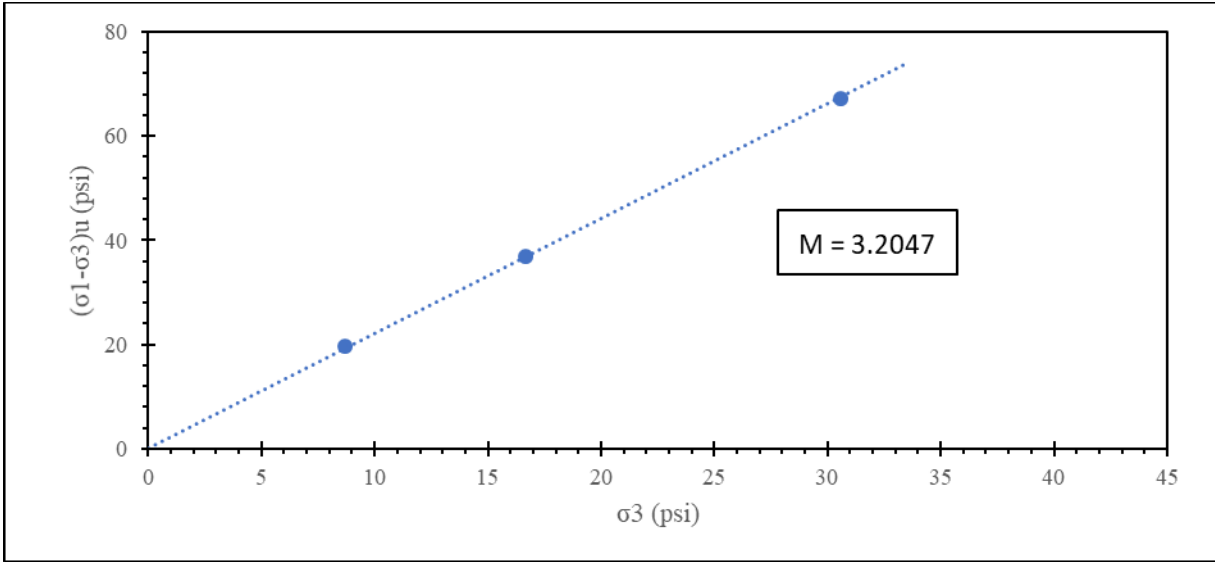
Figure 7.4. Duncan-Chang - Deviator Stress at Failure

Equation (9) can be used to determine the modulus of the material under any level of confinement. The modulus of the material in the pavement structure is determined from iterative LEA such that the state of stress, modulus of the material and level of confinement under the single-wheel load are compatible with each other. Once an equilibrium is reached within the iterations, the single-wheel load is replaced with the reduced-scale dual wheel load and the surface curvature index is determined as described in Section 7.1.2.

It must be noted that ideally the modulus calculated from laboratory tests and LEA iterations must be corrected for wheel type and wheel speed. However, it is assumed that these corrections are the same across the various test sections and thus equation (7) can be used with the surface curvature index obtained from LEA section having modulus that is calculated from laboratory tests and LEA iterations without additional corrections.

7.1.4 SUMMARY

The performance equation used in the design of flexible pavements by FPS-21 is a serviceability loss function. This function contains two components: traffic induced serviceability loss and environment induced serviceability loss. For the accelerated pavement tests, environment induced serviceability is irrelevant as the experiment is conducted under a controlled environment and expansive soils are not used. Thus, the performance equation reduces loss in serviceability with traffic only. Since the only type of pavement distress observed in the test sections is rutting, the loss in serviceability is simply a function of rutting. By considering the performance of all test sections between the same levels of rutting (0 mm to 12.5 mm), it is possible to equate the performance equations of all test sections to each other, as each section has suffered the same loss in serviceability. It is seen that the relative performance between the various test sections depends on the number of passes to the end of the performance period and the surface curvature index (SCI) of the section determined from LEA.

SCI is determined in FPS-21 by evaluating the full-scale design pavement section under a full-scale dual-wheel load in LEA. However, since the test sections are a reduced-scale model, a full-scale dual-wheel load on the reduced-scale model would be unrealistic. For this purpose, a

117

reduced-scale dual wheel model, with a similitude ratio of 4.24:1 for length is used for calculating SCI on reduced-scale pavement test sections.

To determine the SCI of the reduced-scale pavement section, the test section must be modeled in a multi-layer elastic system. For this purpose, the modulus of the various materials used must be determined. This is facilitated by conducting laboratory tri-axial tests on the materials under various levels of confinement. The confinement-dependent modulus is then used with LEA, iteratively, to determine the modulus of the material in the pavement system under the single-wheel load from MMLS. This modulus is then used to evaluate the surface curvature index of the reduced-scale test section under the reduced-scale dual-wheel load.

7.2 SGI TEST RESULTS AND APT

The Soil-Geosynthetic interaction (SGI) test, formerly Small Pull-out Box (SPB) test, is used to assess the pull-out resistance of a geosynthetic inside the soil under confinement. Recent developments from TxDOT Project 5-4829 indicated that another parameter, namely, the soil-geosynthetic interface stiffness, K_{SGI} can be measured in an SGI test. It was summarized that K_{SGI} can be used as a geogrid selection criterion for base-reinforcement to mitigate loss in serviceability due to environmental loads. However, it was hypothesized that K_{SGI} can also be used as a geogrid selection criterion to mitigate loss in serviceability due to traffic loads.

7.2.1 DATA COLLECTED FROM APT SECTIONS

TBR as a function of Rut Depth is determined for each configuration of pavement test section, for which both control and reinforced sections are trafficked. A typical TBR Vs. Rut Depth curve looks like Figure 7.5. The TBR value increases with rut depth initially, reaches a peak and then asymptotes out to a constant value. In this study, the asymptotic TBR value at 12.5 mm of rutting is taken as representative of the improvement in performance of the pavement section (i.e., TBR = 3.5 in the case of BX1100 in Baseline Configuration). Thus, TBR values for all sections are calculated at 12.5 mm rut depth after the TBR vs Rut Depth function has become a constant.
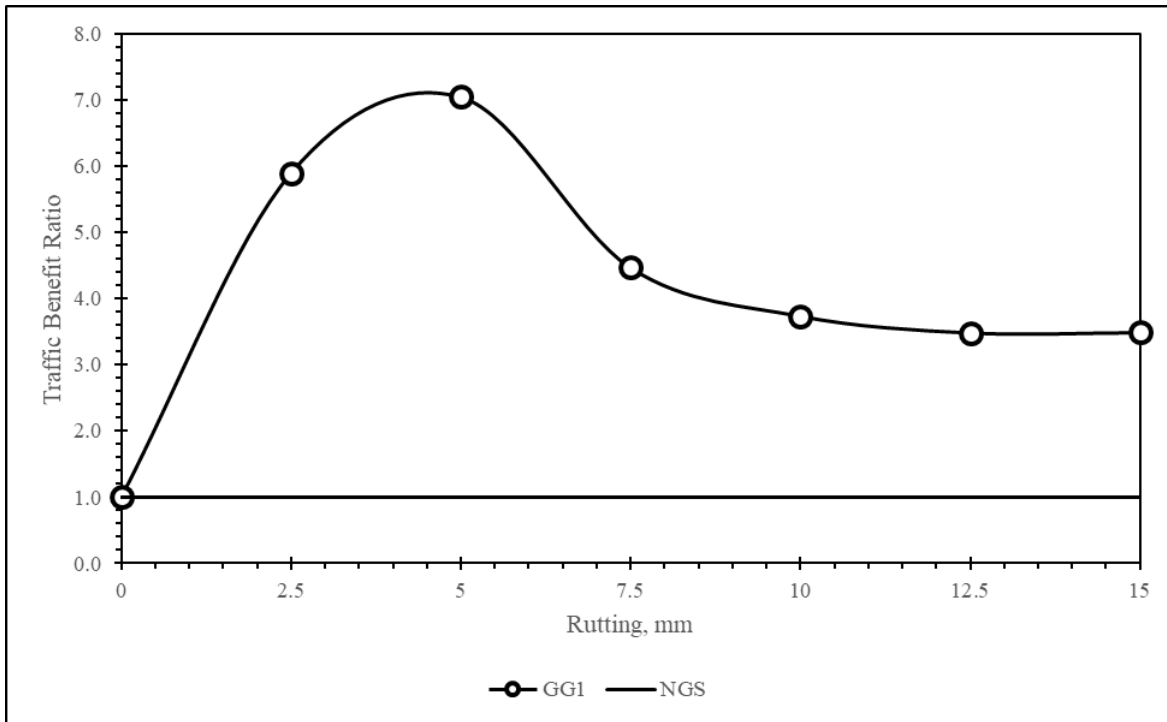
Figure 7.5. TBR as a function of Rut Depth for GG1 in Baseline Section

The above exercise is repeated for 7 different geogrid products in Baseline configuration and the results along with their K_{SGI} value as determined from the SGI test are shown in Table 7.2.

Table 7.2. TBR and K_{SGI} of different geogrids

Product Code	Product Name	TBR Baseline Configuration	K_{SGI} $(kN/m)^2/mm$
GG1	Tensar BX 1100	3.5	13.7
GG2	Tensar TX 160	4.6	16.0
GG3	Enkagrid Colbond Max 20	1.8	9.6
GG4	Mirafi BasXGrid 11	2.5	11.0
GG5	Synteen SF 11	2.5	12.2
GG6	Huesker Fornit 20	4.4	15.6
GG7	Tensar TX 130	5.7	18.8

7.2.2 VALIDATION OF USE OF K_{SGI} AS GEOGRID SELECTION CRITERION

The TBR Vs. K_{SGI} data is plotted in Figure 7.6. It can be seen from the plot that the TBR of any reinforced section in baseline configuration is linearly correlated with the K_{SGI} of the geogrid used as reinforcement in the section.
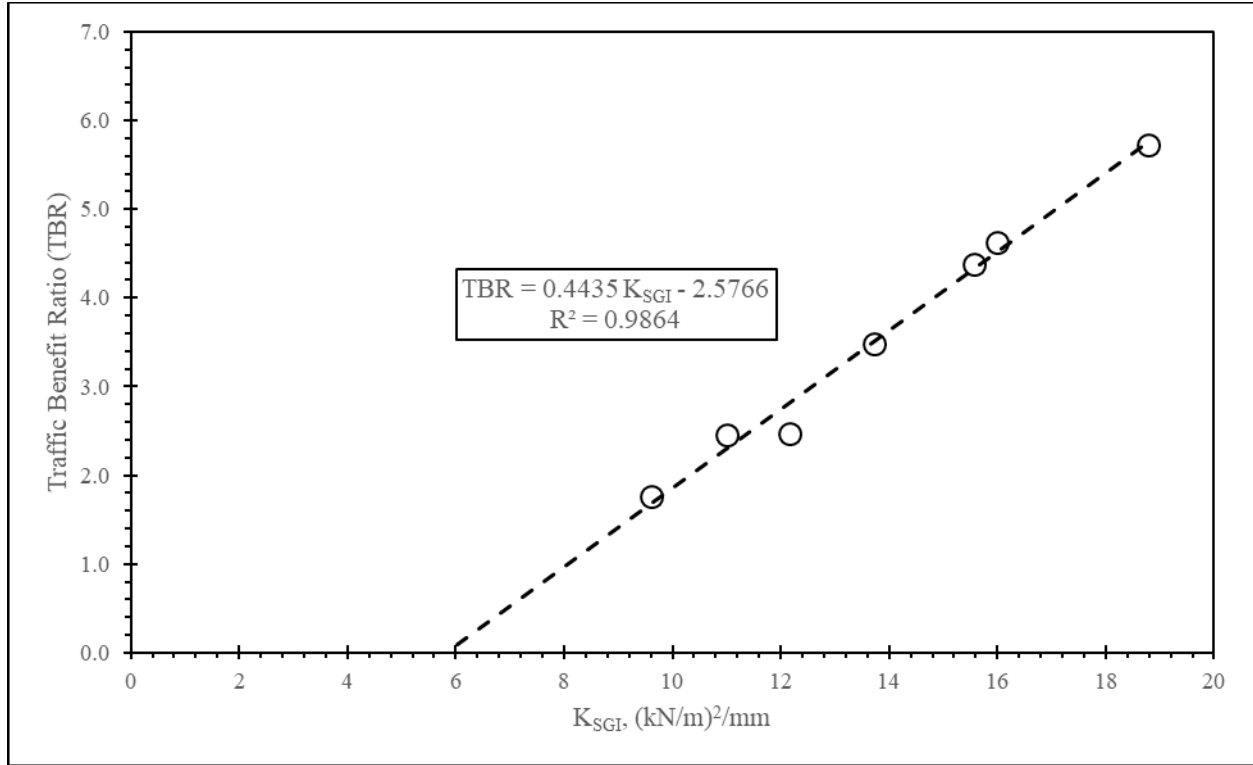
Figure 7.6. TBR (baseline config.) Vs. K$_{SGI}$

This high degree (R^2 = 0.9864) of linear correlation between TBR and K$_{SGI}$ values is a strong justification for the use of K$_{SGI}$ as a critical parameter in the selection of geogrids to be used as base reinforcement for mitigation of pavement distress due to traffic loads.

It must also be noted that the particle and geogrid displacements are measured as the test section is trafficked. It is found that the order of displacement of the particles with respect to the geogrid at 12.5 mm of rut depth (0.1 to 1 mm) at surface is comparable to the levels of displacements (0.2 mm) at which K$_{SGI}$ is measured in the SGI tests. This further shows how closely the two variables are related.

7.3 MODIFICATION OF FPS-21

FPS-21 provides for a mechanistic-empirical approach to the design of flexible pavement systems using conventional pavement materials. It does not accommodate the design of Geogrid Reinforced Pavement Structures (GRPS). GRPS includes flexible pavement structures with geogrid reinforcement in the asphalt layer, base layer, sub-base layer or on top of sub-grade. This study focusses primarily on GRPS with geogrid reinforcement placed within the base layer. To facilitate the design of GRPS with base reinforcement, the design procedure built into FPS-21 must be modified. In this chapter, the various means of modifying the design procedure in FPS-21 are considered.

7.3.1 MODIFYING THE SURFACE CURVATURE INDEX

In this procedure, the design surface curvature index used in the conventional performance equation (3), is corrected for the inclusion of the geogrid. From equation (7),

120

$$N_U S_U^2 = N_R S_R^2 = constant \tag{11}$$

where subscripts U and R stand for Unreinforced and Reinforced, respectively. Therefore,

$$TBR = \frac{N_R}{N_U} = \frac{S_U^2}{S_R^2} \tag{12}$$

The Surface Curvature Index of the Reinforced Section can be expressed as,

$$S_R = \frac{1}{\sqrt{TBR}} \times S_U \tag{13}$$

From TM 6, it is found that the TBR value of the reinforced section depends on

- Type of Geogrid
- Position of Geogrid
- Stiffness of Subgrade

It is noted that the TBR, which is a function of K_{SGI} could also depend on the type and stiffness of the base material. However, the correction factor that is suggested for the type of geogrid is likely to account for this. This idea will be dealt with in detail when the correction factor for the type of geogrid is discussed.

7.3.1.1 Correction Factor for Type of Geogrid
It is seen from section 7.2.2 that the TBR of a reinforced test section is linearly correlated to the K_{SGI} of the geogrid used as reinforcement. This relationship is given by the equation,

$$TBR = 0.4435 K_{SGI} - 2.5766 \tag{14}$$

Substituting (14) in (13),

$$S_R = \frac{1}{\sqrt{0.4435 K_{SGI} - 2.5766}} \times S_U \tag{15}$$

Therefore, the correction factor for type of geogrid,

$$C_T = \frac{1}{\sqrt{0.4435 K_{SGI} - 2.5766}} \tag{16}$$

7.3.1.2 Correction Factor for Type of Base Material
The soil used as base layer in the test sections of the APT program 0-6834 is the same standard soil that is used to determine the K_{SGI} in TxDOT Project 5-4829. Thus, if a different material is used as the base layer, it is suggested to conduct an SGI test with the different base material and type of geogrid chosen, to determine the K_{SGI} value, instead of using the K_{SGI} value of the geogrid with the standard soil. By doing this, the effect of the type of base material on the correction factor is also determined in equation (16).

7.3.1.3 Correction Factor for Position of Geogrid
It is determined that the optimum location for placing the geogrid reinforcement is at that depth within the base layer, where the horizontal tensile strain is maximum under the wheel path.

Keeping this in mind a correction equation is developed represented by the plot shown in Figure 7.7.
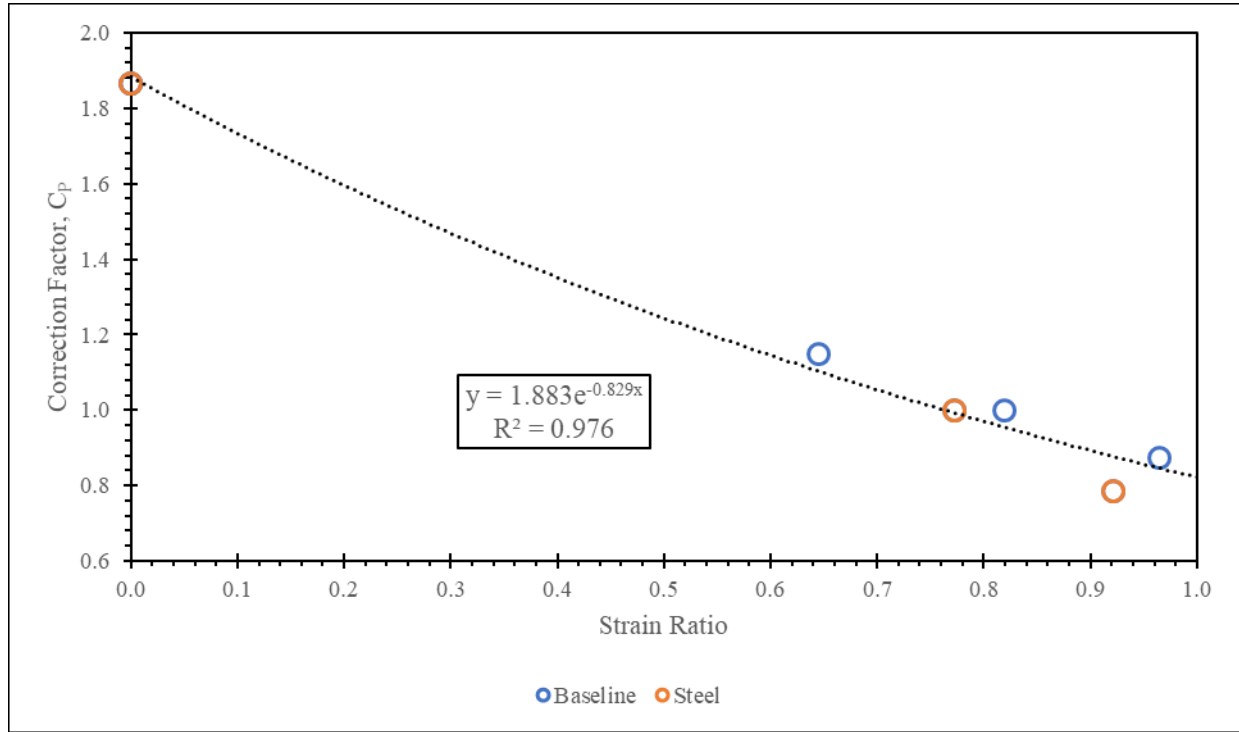
Figure 7.7. Correction Factor for Position of Geogrid

Thus, the correction factor for the position of geogrid is given by

$$C_P = 1.883e^{-0.829R} \tag{17}$$

where R $= \dfrac{Horizontal\ Tensile\ Strain\ at\ the\ location\ of\ Geogrid}{Maximum\ Horizontal\ Strain\ in\ Base\ Layer}$

Note:

1.   at R = 1.0, C_P = 0.822 ($\neq$1.0)
2.   the maximum recommended depth of embedment of geogrid = 6 inches below the HMA-Base Layer interface, at which point R is assumed to be equal to 1.0

7.3.1.4 Correction Factor for Stiffness of Subgrade

The control section and baseline section configurations are repeated with three different values of subgrade stiffness (275 psi, 14000 psi and 29000000 psi) to simulate soft soil, stiff soil, and bedrock conditions. Keeping all other aspects of the test a constant and the 14000 psi as the baseline, the correction factors for the other two cases of subgrade stiffness are determined from the TBR calculated. The results are shown in Figure 7.8.

122
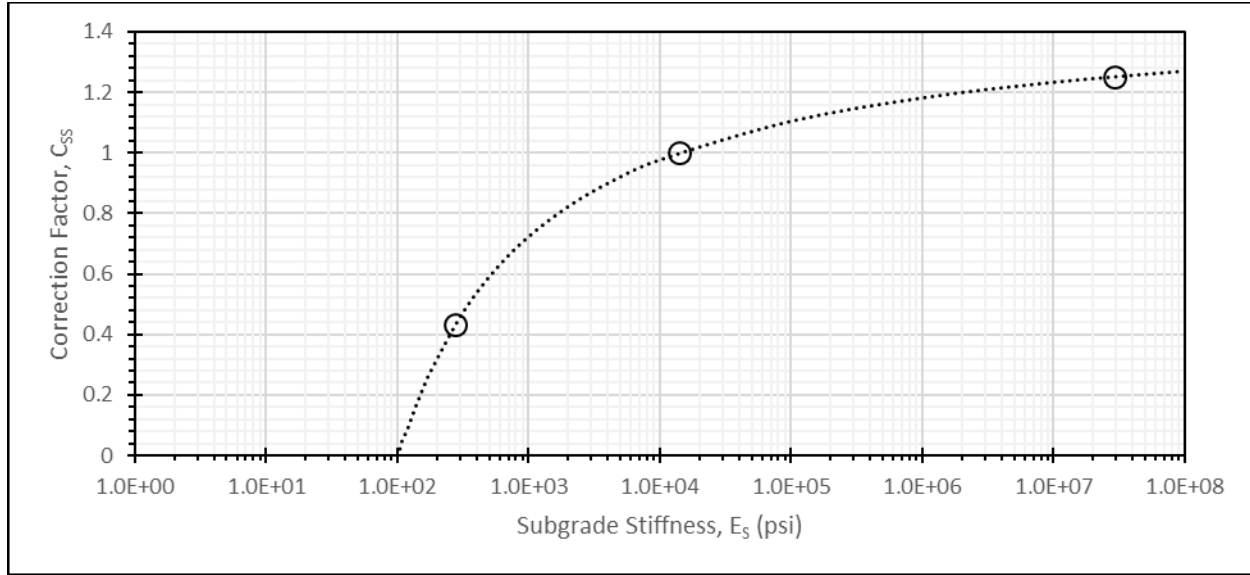
Figure 7.8. Correction Factor for Subgrade Stiffness

The correction factor for subgrade stiffness is given by,

$$C_{SS} = \frac{log_{10}\left(\frac{E_s}{100}\right)}{0.7056 + 0.6699 \, log_{10}\left(\frac{E_s}{100}\right)} \tag{18}$$

where E_S = Stiffness of the Subgrade Layer in psi.

7.3.1.5 Corrected Surface Curvature Index of GRPS

The corrected surface curvature index of the reinforced pavement structure is given by

$$S_R = C_T \times C_P \times C_{SS} \times S_U \tag{19}$$

where C_T, C_P and C_{SS} are correction factors obtained from equations (16), (17), and (18).

7.3.2 MODIFYING THE MODULUS OF THE BASE LAYER

In this procedure the modulus of the reinforced layer is modified by use of a correction factor. It is assumed that the presence of a reinforcement affects the modulus of the base layer 6 inches above and 2 inches below the reinforcement. Thus, the correction factors proposed here should only be used for modification of the base layer in the proposed 6 + 2 inches. This is illustrated in Figure 7.9 and is henceforth referred to as the zone of influence of the geogrid.

By modifying the modulus of the base layer in the zone of influence, the surface curvature index determined from LEA is modified. The modulus of the zone of influence is modified such that the surface curvature index of the modified section as determined from LEA is consistent with the expected surface curvature index for a reinforced section as determined in equation (13).

Three corrections factors are proposed for

- Type of geogrid and base material
- Position of geogrid

123

- Stiffness of Subgrade
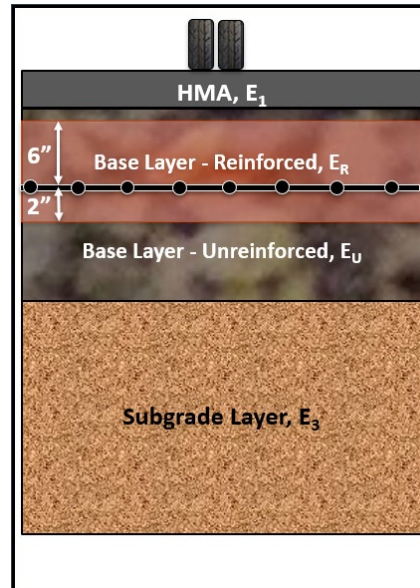
Figure 7.9. Zone of Influence

7.3.2.1 Correction Factor for Type of GeoGrid and Base Material

The modulus of the zone of influence is modified such that the SCI of the modified section is equal to the expected SCI of the reinforced section. The results of this modification are presented in Table 7.3. Figure 7.10 shows the plot of the modulus correction factor, C_T Vs. the K_{SGI} of the soil-geosynthetic composite in baseline configuration. The correction factor is linearly correlated to the K_{SGI} of the soil-geosynthetic composite. Thus, the correction factor for soil-geosynthetic composite stiffness is given by

$$C_T = C_{SGI} = 0.6833\,K_{SGI} - 4.1617 \tag{20}$$

Table 7.3. Modified Modulus of Zone of Influence with Type of Geogrid and Base Material

Modified Modulus (psi)	SCI LEA	SCI Expected	GG Product	Correction Factor, C_T	K_{SGI} $(kN/m)^2/mm$
2200	4.07E-03	4.07E-03	Control	1.00	NA
11650	2.18E-03	2.18E-03	GG1	5.30	13.7
15400	1.89E-03	1.89E-03	GG2	7.00	16.0
5250	3.07E-03	3.07E-03	GG3	2.39	9.6
7900	2.60E-03	2.60E-03	GG4	3.59	11.0
8000	2.59E-03	2.59E-03	GG5	3.64	12.2
14700	1.94E-03	1.94E-03	GG6	6.68	15.6
18600	1.70E-03	1.70E-03	GG8	8.45	18.8
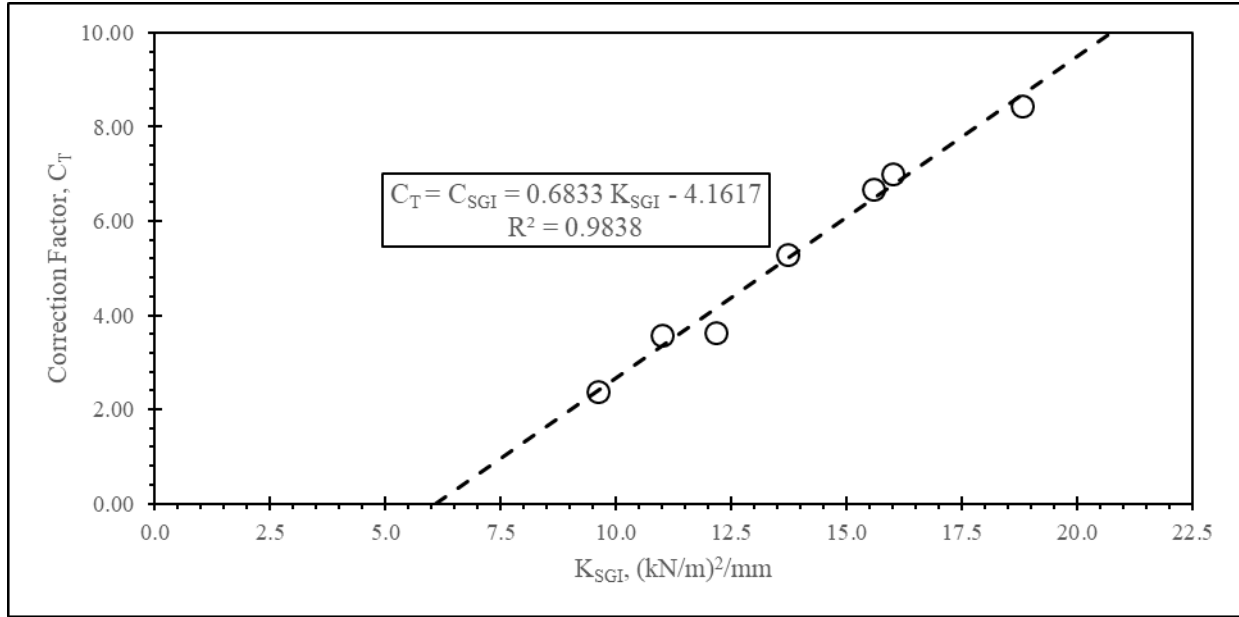
Figure 7.10. Correction Factor for Soil-Geosynthetic Interaction Stiffness

7.3.2.2 Correction Factor for Position of Geogrid

The most efficient location to place the geogrid inside the base layer is at that location where the horizontal tensile strain is the maximum. If it is not practical to place the geogrid at that location, then the benefits from the geogrid are reduced and hence the modified modulus of the zone of influence must be corrected for the position of geogrid. From the series of tests, in which everything except the location of the geogrid is identical, the following correction factor for the position of geogrid is proposed.

$$C_P = 0.1158 \, e^{2.6797R} \qquad\qquad\qquad (21)$$

where $R = \dfrac{Horizontal\ Tensile\ Strain\ at\ the\ location\ of\ Geogrid}{Maximum\ Horizontal\ Strain\ in\ Base\ Layer}$

The data from which this expression is derived is shown in Figure 7.11.

125
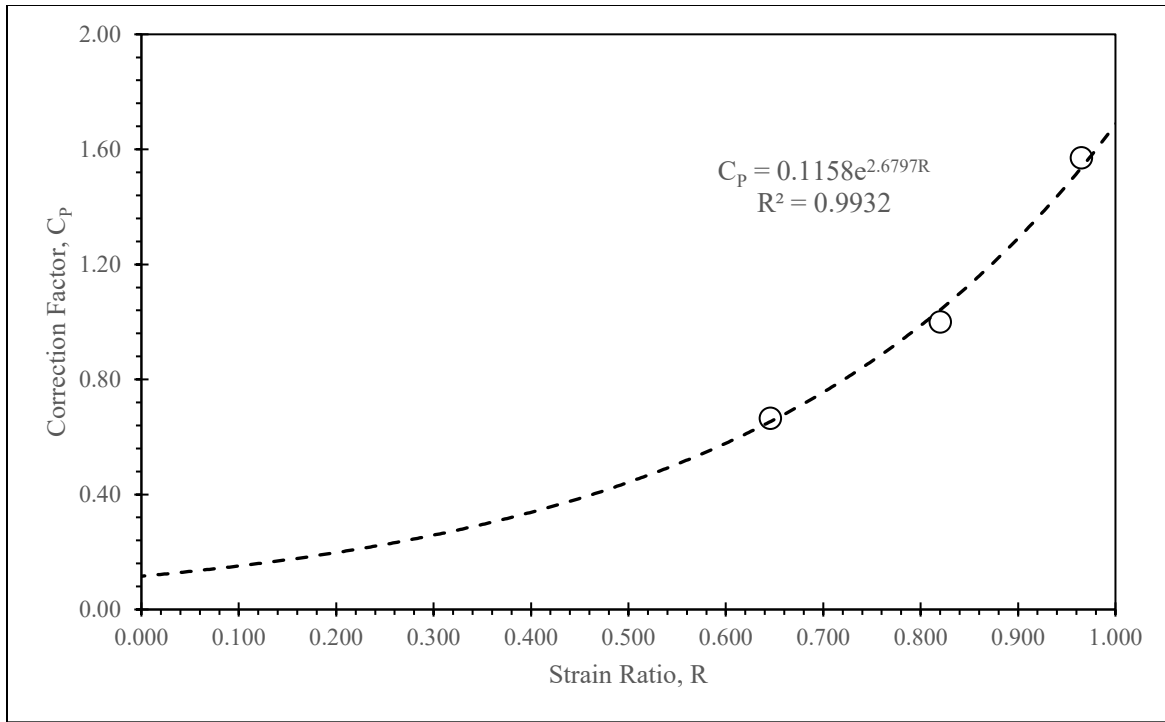
Figure 7.11. Correction Factor for Position of Geogrid

Note:

1.   at R = 1.0, C_P = 1.688 ($\neq$1.0)
2.   the maximum recommended depth of embedment of geogrid = 6 inches below the HMA-Base Layer interface, at which point R is assumed to be equal to 1.0

7.3.2.3 Correction Factor for Stiffness of Subgrade
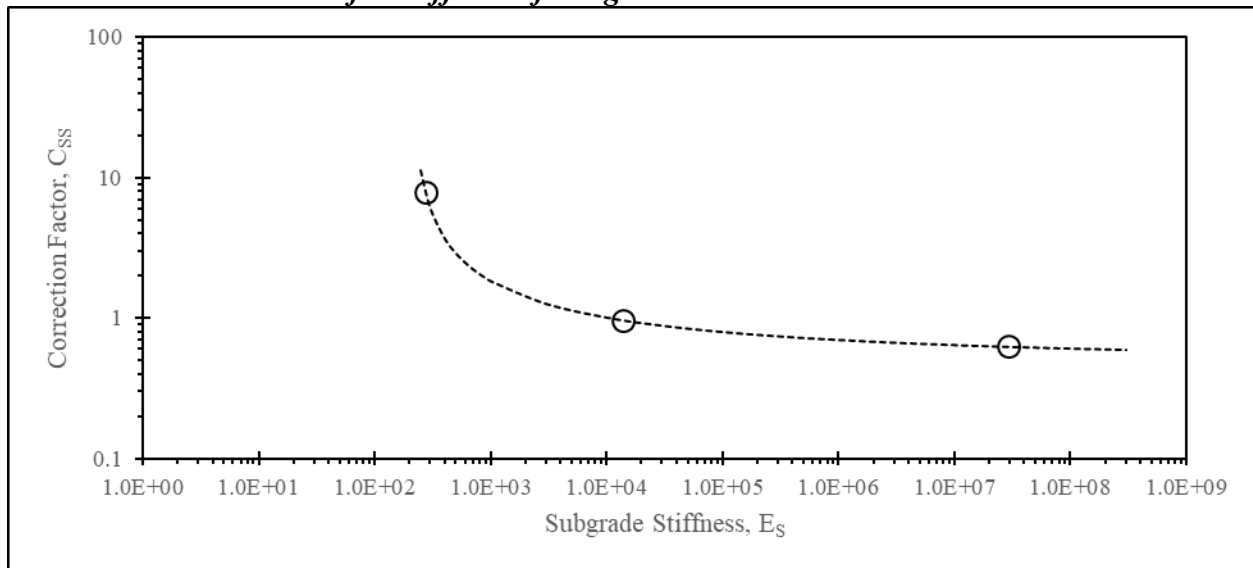
Figure 7.12. Correction Factor for Stiffness of Subgrade

The control section and baseline section configurations are repeated with three different values of subgrade stiffness (275 psi, 14000 psi and 29000000 psi) to simulate soft soil, stiff soil, and bedrock conditions. Keeping all other aspects of the test a constant and the 14000 psi as the baseline, the correction factors for the other two cases of subgrade stiffness are determined in similar procedure as the one illustrated above. The results of these tests are illustrated in Figure 7.12. The correction factor for the change in subgrade stiffness is given by

$$C_{SS} = \frac{0.9633 + 0.4310 \, log_{10} \frac{E_s}{200}}{log_{10} \frac{E_s}{200}} \tag{22}$$

where E_S = Subgrade Stiffness in psi

7.3.2.4 Corrected Modulus of Zone of Influence
Therefore, the corrected modulus of the zone of influence is given by

$$E_{ZoI} = C_{SGI} \times C_P \times C_{SS} \times E_B \tag{23}$$

where C_{SGI}, C_P, and C_{SS} are correction factors as defined by equations (20),(21), and (22)

E_B is the modulus of the base material in the pavement section

7.4 SUMMARY
The design approach used in FPS-21 is modified to enable the use of the program to design geogrid reinforcement base-layers in flexible pavements. Two approaches are considered for the modification, namely modification of surface curvature index and modification of base layer moduli in a zone of influence. A third approach, namely modification of base layer thickness, is not considered owing to the inverted base effect discussed in section 2.2 of TM 6.

The first approach, modification of surface curvature index, involves the modification of the surface curvature index determined for an unreinforced section using LEA by a correction factor that is function of the type of geogrid, type of base material, position of geogrid and subgrade stiffness. The scalability of this method of modification from reduced-scale APT sections to full-scale field sections is debatable. While all other parameters are scalable, the geogrid is a laminar layer and is not necessarily scalable. Therefore, the influence of geogrid, is not scalable linearly. Therefore, this approach to the modification of FPS-21 is not recommended by the research team.

The second approach, modification of the modulus of the zone of influence, involves the modification of the modulus over a specific region around the geogrid. The correction factor used for this modification is a function of the geogrid type, base material type, location of geogrid and subgrade stiffness. This approach is superior to the first approach in that it is assumed that the zone of influence is not scaled between the reduced-scale and full-scale sections. This is because the geogrid is a laminar layer and hence its influence is not scaled with the scaling of the model. Since the second approach accounts for non-scalability of the laminar geogrid layer, this approach is recommended by the research team for the modification of FPS-21.

8. PATH FORWARD - FULL-SCALE APT

With the approach to modify FPS-21, to enable the design of flexible pavements with geogrid-reinforced base, ascertained, the next logical step is to determine the validity of the empirical equations for a full-scale pavement section. This is to be achieved in two separate ways with one complimenting the other. Namely, a field evaluation of GRPs with emphasis on traffic loads (IH10 San Antonio Project) and a full-scale APT program to facilitate accelerated and controlled testing of GRPs

8.1 GOALS OF FULL-SCALE APT PROGRAM

To facilitate the implementation of the design of Geogrid Reinforced Pavements (GRPs) using FPS-21 is the major underlying goal of the full-scale APT program. The data collected from the full-scale APT program, supplemented with the results of the evaluations in the soil-geosynthetic interactions test (5-4829-03), reduced-scale APT of geogrid reinforced pavements (0-6834) and actual field GRPs will help complete the understanding of the behavior of GRPs.

To validate the design procedure (modification of FPS-21) developed as a part of the reduced-scale APT Program (0-6834) is a key objective. The scalability of the empirical correlations developed as a part of the reduced-scale APT Program to aid in the design of GRPs must be verified to implement any design procedure with credibility. Thus, the full-scale program will aid validating the scalability of the empirical equations or establishing a correlation between the reduced-scale and full-scale empirical equations.

Material Properties
- Dynamic Modulus Test (HMA)
- Resilient Modulus Test (Granular Base, Subbase, Subgrade)
- Soil-Geogrid Interaction Test (GG Reinforced Base)

Reduced-Scale APT
- Validation of design procedure for traditional flexible pavements
- Identification of mechanisms of behavior of GRPs
- Development of design procedure for GRPs

Full-Scale APT
- Validation of design procedures for GRPs
- Validation of scalability of results or Development of Correlations of results
- Heavily Instrumented Section for Robust Data Collection without Environmental Variables

Field Section
- Implementation of design procedure for GRPs
- Check for influence of non-traffic induced damage on traffic induced distresses such as rutting, fatigue cracking, etc.

Figure 8.1. The missing link in the development of design algorithm for GRPs

To measure the elastic response of the pavement structure under traffic loads. One of the key issues faced in the instrumentation of the reduced-scale section is the measurement of the elastic response. Since the scale of the test section is reduced, so is the elastic response, thus requiring a high degree of precision in measurement of the response. This not only drives up the instrumentation cost, thus reducing the total number of sensors implemented, but also in some cases, sensors of required precision are not available. A full-scale section will enable the measurement of such crucial responses, completing the understanding of behavior of GRPs.

To measure the plastic response of the pavement structure under traffic loads. One concern in the measurement of plastic response in reduced-scale section is the precision required in the placement of the sensors. Since the scale is smaller, a slight error in the position of the sensor resulted in larger errors in measurement, especially in the case of tell-tale extensometers used to measure the position of particles within the pavements layers. Another example would be when traditional earth pressure cells are used. The size of these sensors (with protection) relative to the thickness of the pavement layers becomes large resulting in non-representative measurements. These concerns are better addressed in a full-scale section.

8.2   FULL-SCALE PAVEMENT TEST SECTIONS

This chapter details the various full-scale pavement sections to be considered as part of the final APT program. The performance of these pavement sections has been predicted from the results of the reduced-scale APT Program.

8.2.1   RECOMMENDED TEST SECTIONS
The test section alternatives that may be considered for the final APT Program are as follows.

Control Section

Figure 8.2. Control Section of Full-Scale APT Program

The control section forms the most basic configuration of all test sections. Every other test section will have one of the variables of this control section changed (except in the case of alternative subgrade material and base material test sections). For the full-scale APT Program, the control section shown in Figure 8.2 is recommended. This recommendation is because the control section established must reflect as much as possible a true field section, in terms of behavior. However, it is also considered that the time to failure cannot be the same as that of a field section, which would take several years (although APT would reduce that to a couple of years). This configuration was chosen so that it behaves similar to traditional full-scale field pavement sections, while at the same

time would reach failure rutting in a maximum period of 4 months (assuming 10,000 passes per day and 5 days per week).

Baseline Section
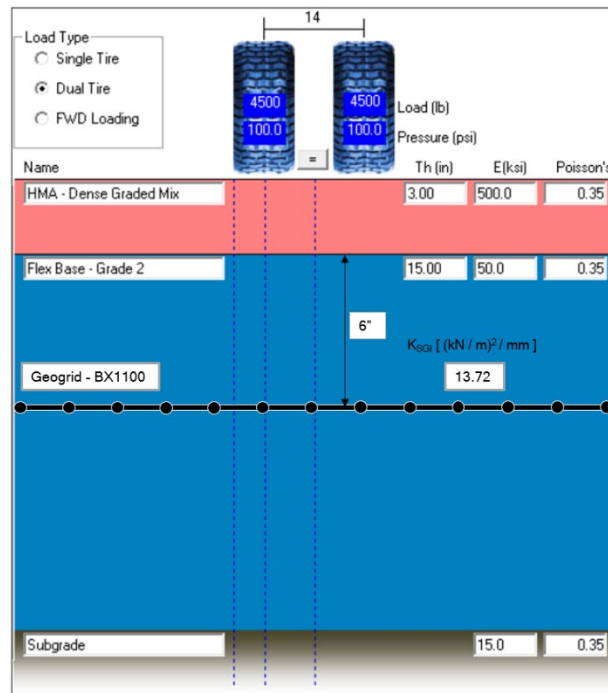
Figure 8.3. Baseline Section of Full-Scale APT Program

The baseline section is essentially the control section, except the baseline geogrid reinforcement placed inside the base layer at 6" below the HMA Layer – Base Layer interface. Although preliminary analysis indicated that the best location for placement of the geogrid is at 2" below the interface, the research team believes this may be too close to the surface and hence recommends 6", which is maximum recommended value from the reduced-scale sections. However, to confirm this assumption, one of test sections in the section 0 has the control section with geogrid at 2" below the interface. It is recommended that one baseline section and one repeat of the same are constructed.

Type of Geogrid

To establish the linear correlation between traffic benefit ratio (TBR) and the soil-geogrid interaction stiffness (K_{SGI}), similar to the reduced-scale APT Program, 3 additional sections with different geogrid (different K_{SGI} values) are chosen. The widest range possible is chosen to ensure wider applicability of the data in the future.

Table 8.1. Types of Geogrids used

Geogrid Name	K_{SGI}
GG3	9.61
GG1 (Baseline)	13.72
GG2	24.02
GG8	32.67

130

Figure 8.4. Location of Geogrid variant in Full-Scale APT Program

To determine the optimum location of the geogrid, 2 additional sections apart from the baseline section will be considered. The geogrid is placed at 2" and 10" below the interface in these additional sections. These sections are shown in Figure 8.4.

Stiffness of Subgrade Variant
From the reduced-scale APT Program, it is noted that the stiffness of subgrade plays a vital role in the modification of the TBR. Thus, to investigate this effect of the stiffness of subgrade, the baseline section is to be rebuilt with two different subgrade moduli (7 psi and 30 psi). However, to calculate the TBR of these modified sections, corresponding unreinforced sections must be built. Thus, a total of 4 additional sections are to be built to investigate this effect. Figure 8.6 shows the layout of the configuration of the unreinforced and reinforced sections with modified subgrade.

Type of Base Material Variant
In the reduced-scale APT Program, the effect of change in base material on the TBR of the reinforced section, could not be investigated successfully. This is due to the highly rigid nature of the conventional base material, that the sections built with them did not undergo significant rutting till failure. Therefore, an unreinforced and reinforced section built with the same configuration of the control and baseline sections but with an alternate base material would be a welcome addition to the full-scale APT Program. This adds two additional sections to the program.

Reduction in Thickness of Base Layer
Another aspect that could not be investigated in the reduced-scale section is the determination of equivalent thickness of the reinforced base layer to an unreinforced base layer. This is because the

131

test sections in the reduced-scale section are inverted base structure. Therefore, one additional test

Figure 8.5. Stiffness of Subgrade Variant, E$_S$ = 30.0 psi
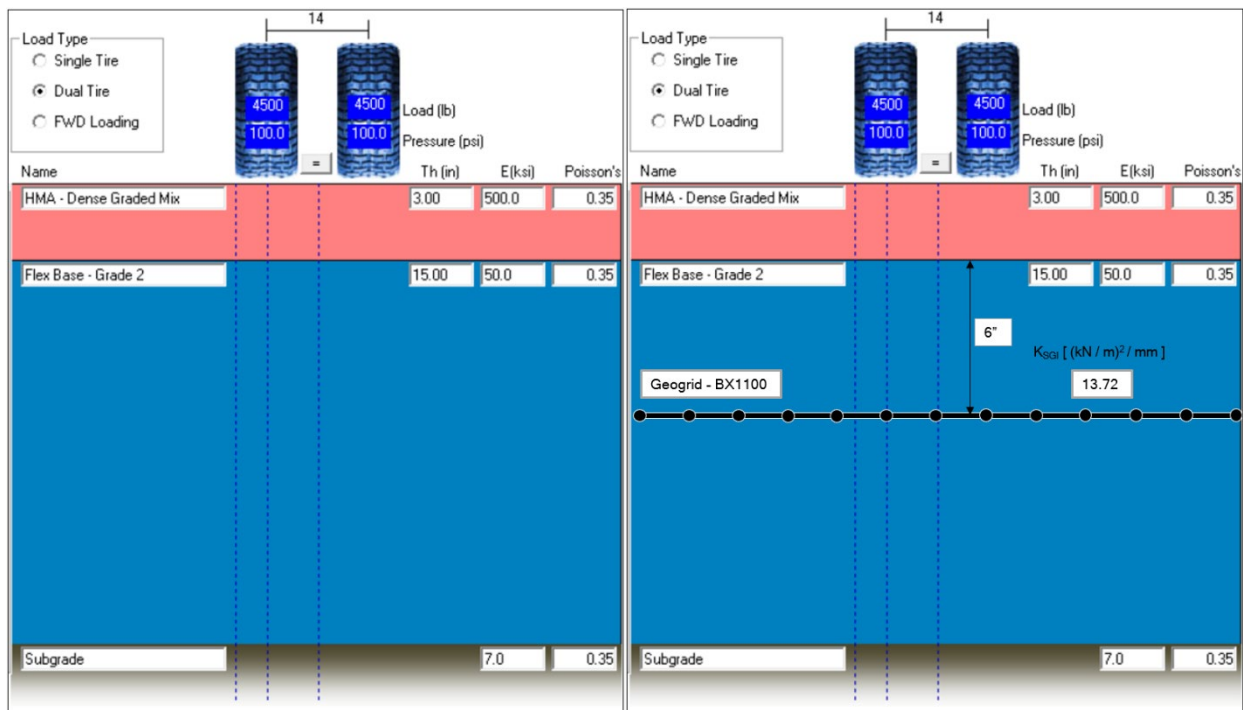
Figure 8.6. Stiffness of Subgrade Variant, E$_S$ = 7.0 psi

section with the base thickness reduced to 10" is recommended.

8.2.2 PREDICTED PERFORMANCE OF FULL-SCALE TEST SECTIONS

The following assumptions are made to determine the performance of the full-scale test sections.

- Initial Serviceability Index $P_1 = 4.5$
- Failure Rut Depth, RD = 0.5 inches
- Initial Cracking and Patching, $C_1 = 0$
- Final Cracking and Patching, $C_2 = 0$ (APT does not allow age related cracking)

The serviceability index of any full-scale pavement section is related to the pavement distress by the following equation.

$$P = 5.03 - 1.91 log_{10}(1 + SV) - 1.38\, RD^2 - 0.01C^{0.5} \tag{24}$$

where P   = Serviceability Index

SV   = Slope Variance

C   = Cracking and Patching (in ft^2 per 1000 ft^2)

RD   = Rut Depth (in inches)

At the end of construction of the test section, from equation (3)

$$4.5 = 5.03 - 1.91 log_{10}(1 + SV) - 1.38\,(0)^2 - 0.01(0^{0.5})$$

$$5.03 - 1.91 log_{10}(1 + SV) = 4.5 \tag{25}$$

At the end of trafficking of the test section, the rut depth at failure, RD = 0.5 inches. From equation (3),

$$P_2 = 4.5 - 1.38\,(0.5)^2 \tag{26}$$

Therefore, pavement serviceability index at the failure rut depth of 0.5 inches is

$$P_2 = 4.15$$

From the performance equation built into FPS-21, considering, there are no environment induced damage,

$$\sqrt{5 - P_2} - \sqrt{5 - P_1} = \frac{0.134NS_c^2}{\bar{\alpha}} \tag{27}$$

Substitute P_1, P_2 and $\bar{\alpha} = 31$ (for Austin) in equation (27). Rewriting the equation after substitution,

$$N = \frac{\left(\sqrt{5 - 4.15} - \sqrt{5 - 4.5}\right) \times 31}{0.134 \times S_c^2}$$

Solving,

$$N = \frac{49.70}{S_c^2} \tag{28}$$

Also,

$$S_C = 1.16 * \left(1 + \frac{4(h) - 5}{100}\right) S = 1.16 * \left(1 + \frac{4(3) - 5}{100}\right) S$$

$$S_C = 1.2413\ S \tag{29}$$

Substituting (29) into (28),

$$N = \frac{32.26}{S^2} \tag{30}$$

The above equation is used to determine the number of passes required till failure. The results for the various sections considered are tabulated in Table 8.2.

Table 8.2. Predicted Performances of Full-Scale Sections

Type of Section	No. of Passes, N	TBR
Control	1,282,555	1.0
Baseline	5,618,079	4.4
Type of Geogrid – GG3	2,330,165	1.8
Type of Geogrid – GG2	15,968,503	12.4
Type of Geogrid – GG8	25,891,660	20.2
Location of Geogrid – 2 inches	2,384,802	1.9
Location of Geogrid – 10 inches	2,893,871	2.2
Stiffness of Subgrade – 7 ksi – Unreinforced	1,063,479	1.0
Stiffness of Subgrade – 7 ksi – Reinforced	2,979,093	2.0
Stiffness of Subgrade – 30 ksi – Unreinforced	1,515,969	1.0
Stiffness of Subgrade – 30 ksi - Reinforced	10,719,030	7.1
Type of Base Material – 80 ksi – Unreinforced	2,622,553	1.0
Type of Base Material – 80 ksi - Reinforced	10,320,139	3.9
Reduction of Base Thickness – 10 inches	3,653,026	2.8

The number of passes to failure as seen from Table 8.2 is on the higher end possible values. Within FPS-21 this value is reduced depending on the level of reliability required of the design.

Also, TBR values of the order of 10 and 20 are unrealistic. Hence, it must be assumed at this stage that the Base Modulus Correction Factor, $C_{SGI} - K_{SGI}$ correlation for the full-scale section must be a fraction of that of the reduced-scale section.

Table 8.2 shows the need for a full-scale APT Program to validate the findings from the reduced-scale APT Program. The most reliable value in the table is that of the number of passes to failure on the control section and other unreinforced sections. These values are roughly of the order to 1.5 ESALs, which means these sections are likely to survive up to a 1 million ESALs before failure by rutting.

Reducing the asphalt layer thickness can help accelerate the rate of failure. However, this may contribute to the section being unrealistic with respect to the field pavement sections.

8.2.3 PRIORITY OF TEST SECTIONS TO BE BUILT

The total number of test sections listed is 15. This makes performing all the test sections proposed a significantly expensive project. Therefore, the research team would like to prioritize the test sections from the most important to least important as follows

Table 8.3. Priority of Test Sections

Ranking	Description	No. of Test Sections	Comments
1	Control	1	
2	Baseline	1	
3	Type of Geogrid	2	If possible, 3
4	Position of Geogrid	2	
5	Type of Base Material	2	
6	Stiffness of Subgrade	2	If possible, 4
7	Reduction in Base Thickness	1	

The research team feels that test sections ranked 1 through 4 are highly crucial for the development of a design procedure for GRPs. Test sections ranked 5 through 7 will greatly help in supplementing the design method developed. Thus, the full-scale APT program will consist of a minimum of 6 test sections to as high as 15 sections.

8.3 PROTOCOLS AND CAPABILITIES OF TEST FACILITY

8.3.1 TRAFFICKING WHEEL LOAD

- The testing facility must have the capability of applying tracking wheel loads along a specified length of the test section.
- The tracking wheel used should be a full-scale dual-wheel or a full-scale standard axle with two dual-wheels.
- For a single full-scale dual wheel used to traffic the pavement test section, the magnitude of the load should be half the standard axle load (18 kips), i.e., 9000 lbs.
- For the standard axle used as the trafficking device, the full standard axle load of 18 kips must be applied to the pavement section.
- The tire pressure in the wheel in either case must be 100 psi.
- Speed of Trafficking can be between 15 mph to 30 mph. The reduced speed of trafficking must help reduce the modulus of the HMA layer, thereby accelerating distresses in the pavement.
- The number of passes per hour of operation of the trafficking device = min. 6000 passes per hour.
- Maximum number of passes per section = 1 to 2 million passes.
- Estimated time of completion of one test section = 3 to 6 weeks. This is assuming 12 hours per day and 5 days per week.
- No. of test sections per year = 10 to 15 test sections per year.

8.4 FALLING WEIGHT DEFLECTOMETER

A Falling Weight Deflectometer (FWD) must be used to characterize the modulus of the various layers of the pavement structure before, during and after trafficking. This allows us to recalibrate the performance equation build into FPS-21 to accommodate the design of geogrid reinforced pavement structures and collect relevant data regarding changes in modulus of the various layers with time. One FWD test must be performed near the wheel path and another away from the wheel path on all occasions. During testing, the FWD tests should be conducted every log cycle of the number of passes (0, 100, 1000, 3000, 10000, 30000, 100000, 300000, 1000000, 2000000).

8.5 DATA COLLECTION

The following data should be collected at every log cycle of number of passes.

i.e., at N = (0, 100, 1000, 3000, 10000, 30000, 100000, 300000, 1000000 and 2000000)

> 5 Transverse Profiles
>
> 1 Longitudinal Profiles
>
> Dynamic Response of Pavement Structure under Trafficking Wheel Loads at 50 Hz
>
>> Tell-tale displacements (tracking particle and geogrid displacements with LPs)
>>
>> Earth Pressure measurements
>>
>> LVDT surface profile measurements
>>
>> Settlement Plate measurements (LVDTs)

The following data must be collected at every 2 wheel passes up to 100,000 cycles and every 20-wheel pass over 100,000 cycles

> Plastic Response of Pavement Structure with number of passes
>
>> Tell-tale displacements (tracking particle and geogrid displacements with LPs)
>>
>> Locked in stresses due to pavement deformations
>>
>> Surface Profile deformation (LVDTs)
>>
>> Settlement Plate measurements (LVDTs)
>>
>> Soil Strains (Soil Extensometers)

8.6 DATA MANAGEMENT

Automated codes should be developed,

> to handle the large volume of data generated from each section.
>
> To process and condition the signals obtained from the various sensors and instrumentation.
>
> To archive the raw data from the instrumentation network so as ensure backup and security.

REFERENCES

American Society for Testing and Materials. (1995). ASTM Standards on Geosynthetics. Sponsored by ASTM Committee D-35 on Geosynthetics, 4th edition, 178p.

ASTM D4339 – 15a, *"Standard Terminology of Geosynthetics."* American Society of Testing Materials, West Conshohocken, PA.

Alabaster, D., G. Arnold, and B. Steven, *"The Equivalent Standard Axle Approach and Flexible Thin Surfaced Pavements,"* Proceedings of the 2nd International Conference on Accelerated Pavement Testing, Minneapolis, Minn., Sep. 26–29, 2004a.

Alabaster, D., G. Arnold, and B. Steven, and L. Sleath, *"Do We Really Know How Thin Surfaced Granular Pavements Behave Under Higher Axle Loads?"* Proceedings 8th International Symposium on Heavy Vehicle Weights and Dimensions, Johannesburg, South Africa, Mar. 14–18, 2004b.

Archer S. and Wayne M. H. (2012). *"Relevancy of Material Properties in Predicting the Performance of Geogrid-Stabilized Roadway."* Proc. of the conference GeoFrontiers, Advances in Geotechnical Engineering, ASCE, Oakland, California, pp.1320-1329

Austin, R. A., and A. J. T. Gilchrist. *"Enhanced performance of asphalt pavements using geocomposites."* Geotextiles and Geomembranes 14.3 (1996): 175-186.

Brandon, T., Al-Qadi, I., Lacina, B. and Bhutta, S. (1996). *"Construction and instrumentation of geosynthetically stabilized secondary road test sections."* Transportation Research Record: Journal of the Transportation Research Board 1534: 50-57

Bender, D. A., & Barenberg, E. J. (1978). Design and behavior of soil-fabric-aggregate systems. *Transportation Research Record*, (671).

Berg, R. (2000). *"Geosynthetic reinforcement of the aggregate base/subbase courses of pavement structures."* Geosynthetic Materials Association

Brown, R., B. Powell, R. West, and D. Timm, *"Update on NCAT Test Track,"* Proceedings of the 2nd International Conference on Accelerated Pavement Testing, Minneapolis, Minn., Sep. 26–29, 2004

Brown, S.F., Kwan, J., Thom, N.H. (2007). *"Identifying the Key Parameters that Influence Geogrid Reinforcement of Railway Ballast."* Geotextile and Geomembranes, v.25, pp. 326- 335.

Brown, S.F., Thom, N.H., Kwan, J., and McDowell, G.R. (2008*). "Improving the Performance of Railway Track through Geogrid Reinforcement of Ballast."* Proceedings of the 4th European Geosynthetics Conference (EuroGeo 4), Edinburg, Scotland, Paper Number 31, 8p.

Christopher, B. R., Cuelho, E. V., & Perkins, S. W. (2008). Development of geogrid junction strength requirements for reinforced roadway base design. In *Proceedings of GeoAmericas 2008 Conference, Cancun, Mexico* (pp. 1003-1012).

Chehab, G. R., Palomino, A. M., and Tang, X. (2007*). "Laboratory evaluation and specification development for geogrids for highway engineering applications."* Report No. FHWA-PA-2007-009-050110

De Beer, M., C. Fisher, and L. Kannemeyer, *"Towards the Application of Stress-In-Motion (SIM) Results in Pavement Design and Infrastructure Protection,"* Proceedings 8th International Symposium on Heavy Vehicle Weights and Dimensions, Johannesburg, South Africa, Mar. 14–18, 2004.

Epps, A. L., Ahmed, T., Little, D. C. and Hugo, F. (2001). *"Performance Prediction with the MMLS3 at WesTrack."* Report FHWA/TX-01/2134-1, Texas Transportation Institute, the Texas A&M University System, College Station, Texas

Fetten, C. P. and Humphrey, D. N. (1998). *"Instrumentation and performance of geosynthetics beneath flexible pavements in Winterport and Frankfort, Maine."* Maine DOT No. ME 97-14,

Holtz, R. D., Christopher, B. R., & Berg, R. R. (1998). Geosynthetic Design & Construction Guidelines, Publication No. FHWA-HI-95-038.

Hugo, F., & Epps, A. L. (2004). NCHRP synthesis 325: *significant findings from full-scale accelerated pavement testing.* National Cooperative Highway Research Program.

Hugo, F., & Martin, A. E. (2004). *Significant findings from full-scale accelerated pavement testing* (Vol. 325). Transportation Research Board.

Janoo, V., Irwin, L., Knuth, K., Dawson, A. & Eaton, R. (1999). *Use of inductive coils to measure dynamic and permanent pavement strains.* Proceedings of the International Conference on Accelerated Pavement Testing, Reno, NV.

Kerkhoven, R. E., & Dormon, G. M. (1953). *Some considerations on the California bearing ratio method for the design of flexible pavements.* Shell Petroleum Company.

Kuo, C. M., & Hsu, T. R. (2003). *Traffic induced reflective cracking on pavements with geogrid-reinforced asphalt concrete overlay.* In Proceedings of the 82nd Annual Meeting at the Transportation Research Board.

Liu, W., & Scullion, T. (2001). *Flexible Pavement Design System FPS 19W: User's Manual* (No. FHWA/TX-02/1869-1).

Liu, W., & Scullion, T. (2011). Flexible pavement design system FPS 21: User's manual. *Texas Dept. of Transportation, Austin, TX.*

Lytton, Robert L. *"Use of geotextiles for reinforcement and strain relief in asphalt concrete."* Geotextiles and Geomembranes 8.3 (1989): 217-237.

Machemehl, R.B., F. Wang, and J.A. Prozzi, *"Analytical Study of Effects of Truck Tire Pressure on Pavements Using Measured Tire-Pavement Contact Stress Data,"* Transportation Research Record: Journal of the Transportation Research Board, No. 1919, Transportation Research Board of the National Academies, Washington, D.C., 2005, pp. 111–120.

Metcalf, J. B. (1996). Synthesis of Highway Practice 235: *Application of Full-Scale Accelerated Pavement Testing.* NCHRP Synthesis, 235.

Núñez, W. P., Ceratti, J. A., Gehling W. Y., and Oliveira J. A. (2008). *"Twelve Years of Accelerated Pavement Testing in Southern Brazil; Challenges, Achievements and Lessons*

Learned.'' Proc. of the 3rd International Conference on Accelerated Pavement Testing, Madrid, 2008.

Øiseth, E., Thakur, V., and Watn, A. (2008*). "Application of geosynthetics reinforcement in freezing thawing roads: A case study from Norway."* Proc. f the 2nd International Workshop on Geotechnics of Soft Soils, Glasgow, Scotland, pp. 411-416

Perkins, S. W. (2002). *"Evaluation of geosynthetic reinforced flexible pavement systems using two pavement test facilities."* Helena, MT: Montana Department of Transportation. Report Number FHWA/MT-02-008/20040

Perkins, S. W., Christopher, B. R., Cuelho, E. L., Eiksund, G. R., Schwartz, C. S., & Svanø, G. (2009). A mechanistic–empirical model for base-reinforced flexible pavements. *International Journal of Pavement Engineering*, *10*(2), 101-114.

Perkins, S. W. and Cortez, E. R. (2005). *"Evaluation of base-reinforced pavements using a heavy vehicle simulator."* Geosynthetics International 12, no. 2 (2005): 86-98

Prozzi, J.A. and R. Luo, *"Quantification of the Joint Effect of Wheel Load and Tire Inflation Pressure on Pavement Response,"* Transportation Research Record: Journal of the Transportation Research Board, No. 1919, Transportation Research Board of the National Academies, Washington, D.C., 2005, pp. 134–141.

Saal, R. N. J., & Pell, P. S. (1960). Fatigue of bituminous road mixes. *Kolloid-Zeitschrift*, *171*(1), 61-71.

Sargand, S. M., Green, R. and Khoury, I. (1997). *"Instrumenting Ohio test pavement."* Transportation Research Record: Journal of the Transportation Research Board 1596: 23-30

Selig, E. T., Zhang, J. & Ebersöhn, W. (1997). *Evaluation of dynamic earth pressure cells for subgrade.* Transportation Research Record 1596, pp. 1–6.

Smit, A. d. F., Hugo, F., and Epps, A. L. (1999). "*Report on The First Jacksboro MMLS Tests."* Report 1814-2, Center for Transportation Research, Bureau of Engineering Research, the University of Texas at Austin

Smit, A. d. F., Hugo, F., Rand, D., and Powell, B. (2003). *"Model Mobile Load Simulator Testing at National Centre for Asphalt Technology Test Track."* Transportation Research Record, Journal of the Transportation Research Board, Washington, D. C., USA

Smith, T., T. Brandon, I. Al-Qadi, B. Lacina, S. Bhutta, and S. Hoffman. *Laboratory Behavior of Geogrid and Geotextile Stabilized Flexible Pavements.* Final Report. Virginia Polytechnic Institute and University Blacksburg, 1995, 94 pp.

Steyn, W. J. (2012). NCHRP synthesis of highway practice 433: *Significant findings from full-scale accelerated pavement testing.*

Tang X., Chehab G. R., and Palomino A. (2008*). "Evaluation of geogrids for stabilizing weak pavement subgrade."* International Journal of Pavement Engineering, Vol 9, No. 6, pp413-429

Texas Department of Transportation (TxDOT) (2011). *"Pavement Design Guide."* 428p.

Texas Department of Transportation (TxDOT) (2010). *"Geogrid for Base/Embankment Reinforcement."* Department of Material Specification. DMS-6240

Tingle, J. S. and Jersey, S. R. (2009). *"Full-Scale Evaluation of Geosynthetic-Reinforced Aggregate Roads."* In Transportation Research Record: Journal of the Transportation Research Board, No. 2116, Transportation Research Board of the National Academies, Washington, D.C., pp.96-107.

Tingle, J. S. and Webster, S. L. (2005). *"Corps of Engineers Design of Geosynthetic-Reinforced Unpaved Roads."* In Transportation Research Record: Journal of the Transportation Research Board, No. 1849, Transportation Research Board of the National Academies, Washington, D.C., pp. 193-201.

Walubita, L. F., Hugo, F. and Epps, A. L. (2000). *"Performance of Rehabilitated Lightweight Aggregate Asphalt Concrete Pavements under Wet and Heated Model Mobile Load Simulator Trafficking: A Comparative Study with the TxMLS."* Report 1814-3, Center for Transportation Research, Bureau of Engineering Research, the University of Texas at Austin

Wang, F. and R.B. Machemehl, *"Development of Quick Solutions for Prediction of Critical Asphalt Pavement Responses Due to Measured Tire–Pavement Contact Stresses,"* Preprint CD, prepared for the 85th Annual Meeting of the Transportation Research Board, Washington, D.C., Jan. 22–26, 2006a.

Wang, F. and R.B. Machemehl, *"Mechanistic–Empirical Study of Effects of Truck Tire Pressure on Pavement Using Measured Tire–Pavement Contact Stress Data,"* Transportation Research Record: Journal of the Transportation Research Board, No. 1919, Transportation Research Board of the National Academies, Washington, D.C., 2006b, pp. 136–145.

Warren, K. A. & Howard, I. L. (2007). *Sensor selection, installation, and survivability in a geosynthetic-reinforced flexible pavement.* Geosynthetics International, 14, No. 5, 298-315

Warren, K., Brooks, J. A. and Howard, I. L. (2006). *"Foil strain gauge attachment techniques for geotextile and geogrid."* Proc. of Geo Congress 2006

Watn, A., Eiksund, G., Jenner, C., and Rathmayer, H. (2005). *"Geosynthetic Reinforcement for Pavement Systems - European Perspectives."* ASCE Proceeding of International Perspectives on Soil Reinforcement Applications

Weinmann, T., *"Pavement Sensors Used at Accelerated Pavement Test Facilities,"* Proceedings of the 2nd International Conference on Accelerated Pavement Testing, Minneapolis, Minn., Sep. 26–29, 2004.

Zornberg, J. C., & Christopher, B. R. (2000). Advances in Transportation and Geoenvironmental systems using geosynthetics.

Zornberg, J. G., & Christopher, B. R. (2007). Chapter 37: Geosynthetics. *The Handbook of Groundwater Engineering, 2nd Edition, Jacques W. Delleur (Editor-in-Chief), CRC Press, Taylor & Francis Group, Boca Raton, Florida*, *2*.

Zornberg, J. G. and Gupta, R. (2010). *"Geosynthetics in pavements: North American contributions."* Proc. of the 9th International Conference on Geosynthetics, Brazil, 2010. pp.379-398.

Zornberg, J.G., Ferreira, J.A.Z., and Roodi, G.H. (2013). *"Geosynthetic-Reinforced Unbound Base Courses: Quantification of the Reinforcement Benefits."* Report No. FHWA/TX-13/5-4829-01-2

Zornberg, J.G., Ferreira, J.A.Z., Gupta, R., Joshi, R. V., Roodi, G.H. (2012). *"Geosynthetic-Reinforced Unbound Base Courses: Quantification of the Reinforcement Benefits."* Report No. FHWA/TX-10/5-4829-01-1

Zornberg, J.G., Prozzi, J., Gupta, R., Luo, R., McCartney, J. S., Ferreira, J. Z. and Nogueira, C. (2008). *"Validating Mechanisms in Geosynthetic Reinforced Pavements."* Report No. FHWA/TX-08/0-4829-1